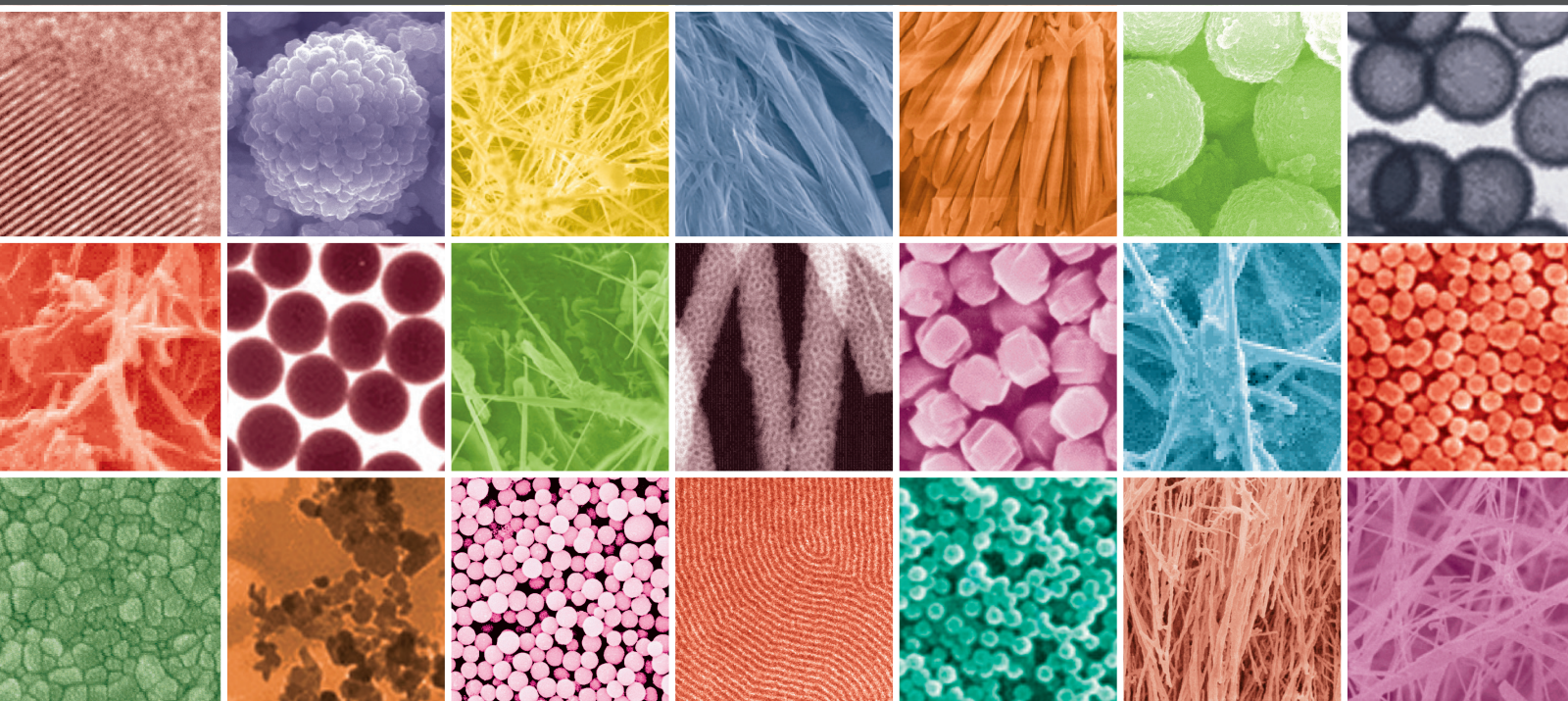


Biocompatibility and Toxicity of Nanobiomaterials 2014

Guest Editors: Xiaoming Li, Sang Cheon Lee, Shuming Zhang,
and Tsukasa Akasaka





Biocompatibility and Toxicity of Nanobiomaterials 2014

Biocompatibility and Toxicity of Nanobiomaterials 2014

Guest Editors: Xiaoming Li, Sang Cheon Lee, Shuming Zhang,
and Tsukasa Akasaka



Copyright © 2015 Hindawi Publishing Corporation. All rights reserved.

This is a special issue published in “Journal of Nanomaterials.” All articles are open access articles distributed under the Creative Commons Attribution License, which permits unrestricted use, distribution, and reproduction in any medium, provided the original work is properly cited.

Editorial Board

Katerina Aifantis, Greece
Nageh K. Allam, USA
Margarida Amaral, Portugal
Xuedong Bai, China
Enrico Bergamaschi, Italy
Theodorian Borca-Tasciuc, USA
C. Jeffrey Brinker, USA
Christian Brosseau, France
Xuebo Cao, China
Sang-Hee Cho, Republic of Korea
Shafiu Chowdhury, USA
Cui ChunXiang, China
Miguel A. Correa-Duarte, Spain
Shadi A. Dayeh, USA
Ali Eftekhari, USA
Claude Estournes, France
Alan Fuchs, USA
Lian Gao, China
Russell E. Gorga, USA
Hongchen Chen Gu, China
Mustafa O. Guler, Turkey
John Zhanhu Guo, USA
Smrati Gupta, Germany
Michael Harris, USA
Zhongkui Hong, USA
Michael Z. Hu, USA
David Hui, USA
Y.-K. Jeong, Republic of Korea
Sheng-Rui Jian, Taiwan
Wanqin Jin, China
Rakesh K. Joshi, India
Zhenhui Kang, China

Fathallah Karimzadeh, Iran
Do Kyung Kim, Republic of Korea
Kin Tak Lau, Australia
Burtrand Lee, USA
Benxia Li, China
Jun Li, Singapore
Shijun Liao, China
Gong Ru Lin, Taiwan
J.-Y. Liu, USA
Jun Liu, USA
Tianxi Liu, China
Songwei Lu, USA
Daniel Lu, China
Jue Lu, USA
Ed Ma, USA
Gaurav Mago, USA
Sanjay R. Mathur, Germany
Nobuhiro Matsushita, Japan
A. McCormick, USA
Vikas Mittal, UAE
Weihai Ni, Germany
Sherine Obare, USA
Edward Andrew Payzant, USA
Kui-Qing Peng, China
Anukorn Phuruangrat, Thailand
Ugur Serincan, Turkey
Huaiyu Shao, Japan
Donglu Shi, USA
Suprakas Sinha Ray, South Africa
Vladimir Sivakov, Germany
Marinella Striccoli, Italy
Bohua Sun, South Africa

Saikat Talapatra, USA
Nairong Tao, China
Titipun Thongtem, Thailand
Somchai Thongtem, Thailand
Valeri P. Tolstoy, Russia
Tsung-Yen Tsai, Taiwan
Takuya Tsuzuki, Australia
Raquel Verdejo, Spain
Mat U. Wahit, Malaysia
Shiren Wang, USA
Yong Wang, USA
Cheng Wang, China
Zhenbo Wang, China
Jinquan Wei, China
Ching Ping Wong, USA
Xingcai Wu, China
Guodong Xia, Hong Kong
Zhi Li Xiao, USA
Ping Xiao, UK
Shuangxi Xing, China
Yangchuan Xing, USA
N. Xu, China
Doron Yadlovker, Israel
Ying-Kui Yang, China
Khaled Youssef, USA
Kui Yu, Canada
Haibo Zeng, China
Tianyou Zhai, Japan
Renyun Zhang, Sweden
Yanbao Zhao, China
Lianxi Zheng, Singapore
Chunyi Zhi, Japan

Contents

Biocompatibility and Toxicity of Nanobiomaterials 2014, Xiaoming Li, Sang Cheon Lee, Shuming Zhang, and Tsukasa Akasaka

Volume 2015, Article ID 259264, 2 pages

Evaluation of Samarium Doped Hydroxyapatite, Ceramics for Medical Application: Antimicrobial Activity, C. S. Ciobanu, S. L. Iconaru, C. L. Popa, M. Motelica-Heino, and D. Predoi

Volume 2015, Article ID 849216, 11 pages

***In Vivo* Osteogenesis of Vancomycin Loaded Nanohydroxyapatite/Collagen/Calcium Sulfate Composite for Treating Infectious Bone Defect Induced by Chronic Osteomyelitis**, Xiaojie Lian, Kezheng Mao, Xi Liu, Xiumei Wang, and Fuzhai Cui

Volume 2015, Article ID 261492, 8 pages

The Effects of Surface Properties of Nanostructured Bone Repair Materials on Their Performances, Feng Zhao, Jian Wang, Hongjuan Guo, Shaojun Liu, and Wei He

Volume 2015, Article ID 893545, 11 pages

Effects of Carboxylated Multiwalled Carbon Nanotubes on the Function of Macrophages, Xia Dong, Lanxia Liu, Dunwan Zhu, Hailing Zhang, Yingxin Li, and Xigang Leng

Volume 2015, Article ID 638760, 8 pages

Synthesis of Luminescent Ag Nanoclusters with Antibacterial Activity, Ying-Fan Liu, Lei Wang, Chun-Po Bu, Guo-Qing Wang, Yan-Hui Zhang, Shao-Ming Fang, and Wan-Zhen Shi

Volume 2015, Article ID 792095, 8 pages

Targeted *In Vivo* Imaging of Mouse Hindlimb Ischemia Using Fluorescent Gelatin Nanoparticles, Ju Zhang, Gang Wang, Duo Mao, Aitian Han, Nannan Xiao, Xin Qi, Dan Ding, and Deling Kong

Volume 2015, Article ID 704817, 7 pages

Clinical Use of the Nanohydroxyapatite/Polyamide Mesh Cage in Anterior Cervical Corpectomy and Fusion Surgery, Hui Xu, Xiaofeng Ren, Dawei Wang, Yongfei Zhao, Yan Wang, Geng Cui, Songhua Xiao, and Xuesong Zhang

Volume 2015, Article ID 217585, 6 pages

The Preparation and *In Vitro* Evaluations of a Nanoscaled Injectable Bone Repair Material, Xinhui Liu, Chao Zhu, Yijiong Li, Yueling Yan, Chuanyong Hou, Hua Wang, Yelin Yang, Guoping Guan, and Qingling Feng

Volume 2015, Article ID 858493, 8 pages

Investigations into the Biocompatibility of Nanohydroxyapatite Coated Magnetic Nanoparticles under Magnetic Situation, Qing Li, Gang Zhou, Tong Wang, Yongzhao Hou, Xuliang Deng, and Yan Wei

Volume 2015, Article ID 835604, 10 pages

The Transport and Deposition of Nanoparticles in Respiratory System by Inhalation, Huiting Qiao, Wenyong Liu, Hongyu Gu, Daifa Wang, and Yu Wang

Volume 2015, Article ID 394507, 8 pages

Clinical Effects of Novel Nanoscaled Core Decompression Rods Combined with Umbilical Cord Mesenchymal Stem Cells on the Treatment of Early Osteonecrosis of the Femoral Head, Hongyang Gao, Guoping Zhang, Jian Wang, Feng Zhao, Yuchen Zhang, Wei Wang, and Yang You

Volume 2015, Article ID 902836, 6 pages



Current Development of Silver Nanoparticle Preparation, Investigation, and Application in the Field of Medicine, Maxwell Murphy, Kang Ting, Xinli Zhang, Chia Soo, and Zhong Zheng
Volume 2015, Article ID 696918, 12 pages

Recent Applications of Nanomaterials in Prosthodontics, Wei Wang, Susan Liao, Yuhe Zhu, Ming Liu, Qian Zhao, and Yating Fu
Volume 2015, Article ID 408643, 11 pages

Editorial

Biocompatibility and Toxicity of Nanobiomaterials 2014

Xiaoming Li,¹ Sang Cheon Lee,² Shuming Zhang,³ and Tsukasa Akasaka⁴

¹Key Laboratory for Biomechanics and Mechanobiology of Ministry of Education, School of Biological Science and Medical Engineering, Beihang University, Beijing 100191, China

²Department of Maxillofacial Biomedical Engineering, School of Dentistry, Kyung Hee University, Seoul 130-701, Republic of Korea

³Department of Materials Science and Engineering, Johns Hopkins University, Baltimore, MD 21218, USA

⁴Department of Biomedical Materials and Engineering, Hokkaido University, Sapporo 060-8586, Japan

Correspondence should be addressed to Xiaoming Li; x.m.li@hotmail.com

Received 21 April 2015; Accepted 21 April 2015

Copyright © 2015 Xiaoming Li et al. This is an open access article distributed under the Creative Commons Attribution License, which permits unrestricted use, distribution, and reproduction in any medium, provided the original work is properly cited.

It is well known that nanomaterials have developed rapidly over the past few decades. Based on their unique physicochemical properties and special mechanical properties, nanomaterials have provided application possibility in many different fields. Currently, as nanobiomaterials, they are widely used in various biomedical applications, such as drug delivery systems, tissue engineering, dental/bone implant, and biosensors. For example, nanobiomaterials have been used in tissue engineering because of their satisfactory bioactivity, high mechanical properties, and large surface area to adsorb specific proteins. Many kinds of nanobiomaterials are used to prepare composite scaffolds to get better biocompatibility and higher ability in repairing specific tissues. Several antibacterial metallic nanobiomaterials are used to coat implant surfaces to improve the speed of healing fractures. In addition, lots of nanobiomaterials have the potential to break the limitations of the traditional delivery systems. They can load larger amount of drugs and provide stable drug release for long time at the targeted sites, such as tumors. Moreover, they can combine with polymers to furnish simultaneous drug delivery systems with the controllable release rate. Besides these applications, more and more nanobiomaterials show great potential to be applied as highly sensitive biosensors because they have higher ability in loading firmly or interacting completely with recognition aptamers.

Although, due to their special properties, nanobiomaterials have been applied into many aspects of the biomedical field, their biocompatibility and toxicity are very important

issues, which is really the concern of more and more people. For example, the nanobiomaterials that are used to deliver drugs to targeted cells can normally traverse the cell membranes purposefully and have ineluctable interactions with intracellular substances. So, the safety of the used nanobiomaterials is fatal indeed, which directly determines the success rate of the drug delivery. Moreover, many implants containing nanomaterials undergo biodegradation *in vivo* and unavoidably release nanoparticles, whose effects on the cells and tissue in the physiological environment should be obviously investigated. Only when the related research findings have confirmed that the nanomaterials are safe enough for the interacted cells and surrounding tissues, can adapt to organism reciprocally, and cannot be excluded by the immune system do these nanobiomaterials have the qualification to be really used for the related biomedical purposes.

Currently, a series of *in vitro* and *in vivo* research have been launched on the biocompatibility and toxicity of nanobiomaterials. Usually, the *in vitro* investigations are firstly conducted to show if the materials affect the normal morphology of the cultured cells or the mixed cells with microscopies and their bioactive functions, including proliferation, differentiation, mineralization, and so forth, by studying both the genes and proteins of the cells with various biochemical analyses. After the studies *in vitro*, the nanobiomaterials are normally implanted into animal body, such as dorsal muscle pouch, to see if they have significant effect on the normal functions of the surrounding

tissues and the main organs by histological, histopathological, and immunohistochemical studies. Though there have been some methods to test the biocompatibility and toxicity of nanobiomaterials, they are not enough. More appropriate methods both *in vitro* and *in vivo* to evaluate and comprehend the biocompatibility and cytotoxicity of nanobiomaterials are necessary. Most importantly, the current measurement accuracy of biocompatibility and toxicity needs further improvements. Furthermore, it is urgent to find new methods to reduce the cytotoxicity and improve the biocompatibility of nanobiomaterials.

In this special issue, several articles are devoted to show the effects of some specific nanobiomaterials on their biocompatibility and toxicity and to find out their mechanisms. For example, the investigations into the biocompatibility of nanohydroxyapatite coated magnetic nanoparticles under magnetic situation, the effects of surface properties of nanostructured bone repair materials on their performances, and the transport and deposition of nanoparticles in respiratory system by inhalation also have been studied. Deep investigations into the applications of nanobiomaterials have been carried out, such as their recent applications in prosthodontics. In addition, accurate data and updated reviews about the preparation, synthesis, properties, and evaluations of nanobiomaterials have been presented. For instance, the preparation and *in vitro* evaluations of a nanoscaled injectable bone repair material and the synthesis of luminescent Ag nanoclusters with antibacterial activity have been studied. What is more, some researches focused on the clinical effects of nanobiomaterials. For example, the clinical use of the nanohydroxyapatite/polyamide mesh cage in anterior cervical corpectomy and fusion surgery and the clinical effects of novel nanoscaled core decompression rods combined with umbilical cord mesenchymal stem cells on the treatment of early osteonecrosis of the femoral head have been investigated. This is a successful issue to cover many aspects of evaluating the biocompatibility and toxicity of nanobiomaterials *in vitro* and *in vivo*. However, further researches on this subject are still needed, such as investigations into the effects of size, shape, and surface of nanobiomaterials on their biocompatibility and toxicity and more deep analytical approaches to animal experiments and much more convincing mechanisms of the corresponding researches.

Xiaoming Li
Sang Cheon Lee
Shuming Zhang
Tsukasa Akasaka

Research Article

Evaluation of Samarium Doped Hydroxyapatite, Ceramics for Medical Application: Antimicrobial Activity

C. S. Ciobanu,^{1,2} S. L. Iconaru,¹ C. L. Popa,¹ M. Motelica-Heino,³ and D. Predoi¹

¹National Institute for Materials Physics, P.O. Box MG 07, Bucharest, 077125 Magurele, Romania

²Department of Science and Engineering of Oxide Materials and Nanomaterials, Faculty of Applied Chemistry and Materials Science, University POLITEHNICA of Bucharest, 1-7 Polizu Street, P.O. Box 12-134, 011061 Bucharest, Romania

³ISTO, UMR 7327, CNRS-Université d'Orléans, 1A rue de la Férollerie, 45071 Orléans Cedex 2, France

Correspondence should be addressed to D. Predoi; dpredoi@gmail.com

Received 25 September 2014; Revised 20 December 2014; Accepted 21 December 2014

Academic Editor: Xiaoming Li

Copyright © 2015 C. S. Ciobanu et al. This is an open access article distributed under the Creative Commons Attribution License, which permits unrestricted use, distribution, and reproduction in any medium, provided the original work is properly cited.

Samarium doped hydroxyapatite (Sm:HAp), $\text{Ca}_{10-x}\text{Sm}_x(\text{PO}_4)_6(\text{OH})_2$ (HAp), bionanoparticles with different x_{Sm} have been successfully synthesized by coprecipitation method. Detailed characterization of samarium doped hydroxyapatite nanoparticles (Sm:HAp-NPs) was carried out using X-ray diffraction (XRD), scanning electron microscopy (SEM), transmission electron microscopy (TEM), and Fourier transform infrared spectroscopy (FTIR). The biocompatibility of samarium doped hydroxyapatite was assessed by cell viability. The antibacterial activity of the Sm:HAp-NPs was tested against Gram-negative bacteria (*Pseudomonas aeruginosa* and *Escherichia coli*) and Gram-positive bacteria (*Enterococcus faecalis* and *Staphylococcus aureus*). A linear increase of antimicrobial activity of *P. aeruginosa* has been observed when concentrations of Sm:HAp-NPs in the samples with $x_{\text{Sm}} = 0.02$ were higher than 0.125 mg/mL. For Sm:HAp-NPs with $x_{\text{Sm}} = 0.05$ a significant increase of antibacterial activity on *E. coli* was observed in the range 0.5–1 mg/mL. For low concentrations of Sm:HAp-NPs ($x_{\text{Sm}} = 0.05$) from 0.031 to 0.125 mg/mL a high antibacterial activity on *Enterococcus faecalis* has been noticed. A growth of the inhibitory effect on *S. aureus* was observed for all concentrations of Sm:HAp-NPs with $x_{\text{Sm}} = 0.02$.

1. Introduction

Nowadays, the development of new nanoscale materials has reached such complexity that engineered particles have the potential to be used for applications in various areas ranging from medicine to environment and electronics. The most studied engineered particles are the inorganic ones and mostly the ones that exhibit biological properties [1–3].

Hydroxyapatite, $\text{Ca}_{10}(\text{PO}_4)_6(\text{OH})_2$ (HAp), is a calcium phosphate ceramic material and also the major inorganic component in bones and teeth of animals and humans [4]. Due to its excellent biocompatibility, bioactivity, and osteoconductivity, HAp is widely investigated and promoted in all biomaterial related research areas [5–8].

Apatites, especially HAp, have a strong affinity to ion substitution and a real potential for being used as structural matrices for materials design. Due to the tendency of

substituting Ca^{2+} ions with other divalent elements, mostly metals such as Ag^+ , Cu^{2+} , and Zn^{2+} , hydroxyapatite is widely used to develop new compounds with exquisite properties. In the last years, the attention has been focused on the family of rare-earth elements as substituents of Ca^{2+} in the HAp structure [9–12]. Hydroxyapatite doped with rare-earth ions is of interest in the area of biomaterials for bone related applications [13]. Lanthanides, also called rare-earth elements, are the family of elements between lanthanum and lutetium. These elements exhibit a pronounced biological activity, and they are able to replace Ca^{2+} ions in structured molecules [14–16]. One of the most important representative elements from the lanthanides family is samarium. Sm^{3+} ions are one of the most interesting ions to be analyzed due to their use in high-density optical storage, exquisite optical properties, and antibacterial properties [17, 18].

Recently [19], the primary tests concerning the adherence of *Enterococcus faecalis* ATCC 29212 (Gram-positive bacteria) to samarium doped hydroxyapatite showed high antibacterial activity against *Enterococcus faecalis* ATCC 29212. Here, we have synthesized the samarium doped hydroxyapatite bionanoparticles (Sm:HAp-NPs), with other concentrations of samarium ($x_{\text{Sm}} = 0$, $x_{\text{Sm}} = 0.02$, and $x_{\text{Sm}} = 0.05$) by a quick and cheap method of synthesis. The present paper is mainly focused on the antibacterial activity of samarium doped hydroxyapatite bionanoparticles (Sm:HAp-NPs). The structural and morphological studies have confirmed the formation of Sm:HAp-NPs with the characteristics of pure apatite with good crystal structure. The particle sizes were measured by transmission electron microscopy (TEM) and using dynamic light scattering (DLS). The biocompatibility of the Sm:HAp-NPs was evaluated using *in vitro* assays, consisting in the quantification of hFOB 1.19 osteoblasts cells viability. The antibacterial activity of Sm:HAp-NPs with $x_{\text{Sm}} = 0$, $x_{\text{Sm}} = 0.02$, and $x_{\text{Sm}} = 0.05$ was tested against Gram-negative bacteria (*Pseudomonas aeruginosa* and *Escherichia coli*) and Gram-positive bacteria (*Enterococcus faecalis* and *Staphylococcus aureus*).

2. Materials and Methods

2.1. Materials. All the reagents used for the synthesis, ammonium dihydrogen phosphate $[(\text{NH}_4)_2\text{HPO}_4]$, calcium nitrate tetrahydrate $[\text{Ca}(\text{NO}_3)_2 \cdot 4\text{H}_2\text{O}]$, Samarium(III) nitrate hexahydrate $[\text{Sm}(\text{NO}_3)_3 \cdot 6\text{H}_2\text{O}]$, and ammonia (NH_3), were purchased from Sigma-Aldrich and used without further purification.

2.2. Synthesis of Samarium Doped Hydroxyapatite. Nanocrystalline hydroxyapatite doped with Sm, $\text{Ca}_{10-x}\text{Sm}_x(\text{PO}_4)_6(\text{OH})_2$, with $x_{\text{Sm}} = 0$, $x_{\text{Sm}} = 0.02$, and $x_{\text{Sm}} = 0.05$, was obtained by setting the atomic ratio of $\text{Sm}/[\text{Sm} + \text{Ca}]$ from 0% to 5% and $[\text{Ca} + \text{Sm}]/\text{P}$ as 1.67. The $\text{Sm}(\text{NO}_3)_3 \cdot 6\text{H}_2\text{O}$ and $\text{Ca}(\text{NO}_3)_2 \cdot 4\text{H}_2\text{O}$ were dissolved in 300 mL deionised water. On the other hand, the $(\text{NH}_4)_2\text{HPO}_4$ was dissolved in 300 mL deionised water. The $[\text{Ca} + \text{Sm}]$ solution was put into a Berzelius and stirred at 100°C for 30 minutes. The $(\text{NH}_4)_2\text{HPO}_4$ solution was added drop by drop into the $[\text{Ca} + \text{Sm}]$ solution and stirred for 2 h. The pH was adjusted to 10 with NH_3 and stirred continuously for 30 minutes. After the reaction, the deposited mixtures were washed several times with deionised water. The resulting material (Sm:HAp) was dried at 100°C .

2.3. Characterisation. The X-ray diffraction measurements for Sm:HAp samples were recorded using a Bruker D8 Advance diffractometer, with nickel filtered $\text{Cu K}\alpha$ ($\lambda = 1.5418 \text{ \AA}$) radiation, and a high efficiency one-dimensional detector (Lynx Eye type) operated in integration mode. The diffraction patterns were collected in the 2θ range between 15° and 90° , with a step of 0.02° and 34 s measuring time per step. The particle size was measured by the SZ-100 Nanoparticle Analyzer (Horiba) using dynamic light scattering (DLS). The signal obtained from the scattered light is fed into a

multichannel correlator that generates a function used to determine the translational diffusion coefficient of the particles analyzed. The Stokes-Einstein equation is then used to calculate the particle size. The scanning electron microscopy (SEM) study was performed on a HITACHI S2600N-type microscope equipped with an energy dispersive X-ray attachment (EDAX/2001 device). Energy dispersive X-ray analysis, referred to as EDS or EDAX, was used to identify the elemental composition of materials. The functional groups present in samarium doped hydroxyapatite nanopowders were identified by Fourier transform infrared spectroscopy, FTIR, using a Spectrum BX spectrometer. The spectra were recorded on 10 mm diameter tablets containing 1% KBr and 99% samarium doped hydroxyapatite nanopowder in the range of 500 to 4000 cm^{-1} with a resolution of 4 cm^{-1} .

2.4. Cell Cultures and Conditions. The hFOB 1.19 osteoblasts cells lines were purchased from American Type Culture Collection (ATCC CCL-12, Rockville, MD, USA). The cells were routinely maintained in Dulbecco's modified Eagle's medium (Sigma-Aldrich) supplemented with 10% fetal bovine serum (Sigma-Aldrich) and 1% antibiotic antimycotic solution (including 10,000 units penicillin, 10 mg streptomycin, and $25 \mu\text{g}$ amphotericin B per mL, Sigma-Aldrich) at 37°C in a humidified atmosphere of 5% CO_2 . The cultured cells were loaded on samarium doped hydroxyapatite discs at a seeding density of $5 \times 10^4 \text{ cells/cm}^2$ in 24-well plates. Cells cultured in 24-well plates at the same seeding density were used as control.

2.5. In Vitro Cytotoxicity Assay. Biocompatibility test of the samarium doped hydroxyapatite ($x_{\text{Sm}} = 0$, $x_{\text{Sm}} = 0.02$, and $x_{\text{Sm}} = 0.05$) discs has been made using primary osteoblast cell line. After osteoblast culture achievement, the cells were treated with trypsin 0.05% and spitted in 35/35 mm Petri dish. Cells were seeded at a density of 105 cells/mL in a Petri dish and incubated with samarium doped hydroxyapatite ($x_{\text{Sm}} = 0$, $x_{\text{Sm}} = 0.02$, and $x_{\text{Sm}} = 0.05$) for 4, 12, and 24 hours. The cell viability was determined by MTT (3-(4,5-dimethylthiazol-2-yl)-2,5-diphenyltetrazolium bromide) reduction test. The cells were incubated (5% CO_2 atmosphere, $T = 37^\circ\text{C}$) for 4 h with MTT (0.1 mg/mL). The optical density at 595 nm, for each well, was then determined using a Tecan multiplate reader (Tecan GENios, Grödic, Germany). The absorbance from the wells of cells cultured in the absence of ceramic discs was used as the 100% viability value.

2.6. Antimicrobial Studies. The antibacterial activity of Sm:HAp-NPs was assessed by the Kirby-Bauer disc diffusion technique against Gram-negative bacteria (*Pseudomonas aeruginosa* and *Escherichia coli*) and Gram-positive bacteria (*Enterococcus faecalis* and *Staphylococcus aureus*). The 5 mg of the Sm:HAp-NPs ($x_{\text{Sm}} = 0$, $x_{\text{Sm}} = 0.02$, and $x_{\text{Sm}} = 0.05$) was put in Sterile Whatman filter paper discs of 5 mm diameter. Finally, the sterile Whatman filter paper was placed on nutrient agar plates inoculated with bacterial cultures and incubated at 37°C for 24 h. The zone of inhibition was measured by using antibiotic zone scale (Hi media) [20].

The effect of Sm:HAp-NPs on different phases of bacterial growth was evaluated by adding various concentration of Sm:HAp-NPs with $x_{\text{Sm}} = 0$, $x_{\text{Sm}} = 0.02$, and $x_{\text{Sm}} = 0.05$ (40 mg/mL) to overnight culture of Gram-negative bacteria (*Pseudomonas aeruginosa* and *Escherichia coli*) and Gram-positive bacteria (*Enterococcus faecalis* and *Staphylococcus aureus*) in a 500 mL culture flask and kept in an incubator shaker at 27°C for 24 h. The absorbance of the bacterial culture was measured at 620 nm at various concentrations (1, 0.5, 0.25, 0.125, 0.62, and 0.031 mg/mL).

3. Results and Discussion

Hydroxyapatite doped with metal ions can play a key role in the development of modern chemotherapy on humans and animals. The hydroxyapatite doped with samarium ions with the molar compositions $\text{Ca}_{10-x}\text{Sm}(\text{PO}_4)_6(\text{OH})_2$, where $x_{\text{Sm}} = 0$, $x_{\text{Sm}} = 0.02$, and $x_{\text{Sm}} = 0.05$, was synthesized by coprecipitation method. The structure, composition, and the qualitative analysis of chemical bonds of the samarium doped hydroxyapatite nanoparticles are discussed. Furthermore, the antimicrobial evaluation of Sm:HAp was performed, too.

The XRD patterns of Sm:HAp ($x_{\text{Sm}} = 0$, $x_{\text{Sm}} = 0.02$, and $x_{\text{Sm}} = 0.05$) and the standard data for the hexagonal hydroxyapatite are shown in Figure 1. For all values of x_{Sm} the diffraction peaks can be well indexed to the hexagonal $\text{Ca}_{10}(\text{PO}_4)_6(\text{OH})_2$ in $P6_3m$ space group (ICDD-PDF number 9-432). In the XRD analysis of Sm:HAp, peaks for any new phase or impurity were not observed.

In good agreement with previous studies on Sm:HAp [21–24], the XRD of Sm:HAp ($x_{\text{Sm}} = 0$, $x_{\text{Sm}} = 0.02$, and $x_{\text{Sm}} = 0.05$) have also shown that samples with samarium doped hydroxyapatite exhibit the characteristics of pure apatite with good crystal structure.

The diffraction peak intensities of the Sm:HAp powders in the XRD spectra were reduced and the peak shapes were broadened when the Sm concentration increased. In good agreement with previous studies [25], the broadened peaks when Sm concentration increased in the Sm:HAp samples are attributed to the decrease of particle size.

In agreement with previous studies proposed by Ravindran et al. [24] and Shirkhanzadeh et al. [26], these results demonstrate that the Sm^{3+} ions have successfully substituted Ca^{2+} ions without affecting the crystal structure of the hydroxyapatite.

TEM images of Sm:HAp ($x_{\text{Sm}} = 0$, $x_{\text{Sm}} = 0.02$, and $x_{\text{Sm}} = 0.05$) at low resolution are presented in Figure 2. The samples of samarium doped hydroxyapatite have a similar shape and maintain the morphology of pure HAp ($x_{\text{Sm}} = 0$). We can see that the Sm:HAp nanoparticles were relatively uniform in shape for all the concentrations of samarium. The size of the Sm:HAp samples decreases when the samarium concentration increases. The synthesized Sm:HAp nanoparticles have ellipsoidal shape with regular surface and smoother edges.

The selected area electron diffraction (SAED) pattern recorded from an area containing a large number of nanoparticles is presented in Figure 2(d). The rings can be indexed as (002), (210), (211), (310), (222), (213), (004), and (304)

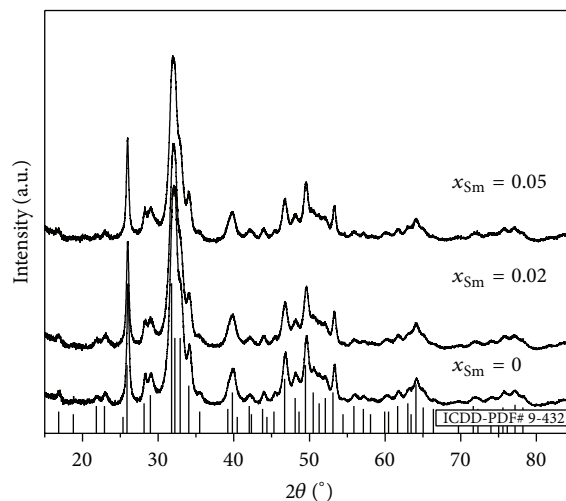


FIGURE 1: Comparative representation of the experimental XRD patterns of the Sm:HAp samples with $x_{\text{Sm}} = 0$, $x_{\text{Sm}} = 0.02$, and $x_{\text{Sm}} = 0.05$ and the characteristic lines of hydroxyapatite according to the ICDD-PDF number 9-432.

reflections of the hexagonal HAp. Because other reflections are not observed we can conclude that the results are in good agreement with the XRD results which indicated that the nanoparticles have a good crystal structure.

In Figure 3 the mean average size of samarium doped hydroxyapatite obtained by dynamic light scattering (DLS) measurements is presented. We can see that the diameter of the particles is similar to the TEM size. This result shows that the Sm:HAp nanoparticles in suspension are unagglomerated. On the other hand, the Sm:HAp nanoparticles are monodisperse in water.

The elemental composition of the Sm:HAp samples was highlighted by energy dispersive X-ray (EDX) analysis (Figure 4). The EDX spectrum of $\text{Ca}_{10-x}\text{Sm}_x(\text{PO}_4)_6(\text{OH})_2$ confirmed the presence of calcium (Ca), phosphorus (P), oxygen (O), and samarium (Sm) in the samples with $x_{\text{Sm}} = 0.02$ and $x_{\text{Sm}} = 0.05$. The EDX spectrum of Sm:HAp sample with $x_{\text{Sm}} = 0.02$ is shown in Figure 4. The EDX Mapping of Sm:HAp with $x_{\text{Sm}} = 0.02$ is also presented in Figure 4. EDX Mapping (element distribution images) provides in addition to the conventional SEM image a meaningful picture of the element distribution at the surface of $\text{Ca}_{10-x}\text{Sm}_x(\text{PO}_4)_6(\text{OH})_2$ samples. The uniform distributions of calcium (Ca), phosphorus (P), oxygen (O), and samarium (Sm) in the samples have been confirmed.

The FTIR spectra of Sm:HAp (with $x_{\text{Sm}} = 0$, $x_{\text{Sm}} = 0.02$, and $x_{\text{Sm}} = 0.05$) samples synthesized by adapted coprecipitation method at 100°C are shown in Figure 5. The FTIR spectra of Sm:HAp samples for $x_{\text{Sm}} = 0$, $x_{\text{Sm}} = 0.02$, and $x_{\text{Sm}} = 0.05$ of samarium concentration are shown. The spectra of Sm:HAp samples with concentrations of samarium $x_{\text{Sm}} = 0$, $x_{\text{Sm}} = 0.02$, and $x_{\text{Sm}} = 0.05$ exhibited all vibrational modes corresponding to phosphate and hydroxyl groups present in HAp [27, 28]. The peak at 473 cm^{-1} is attributed to double degenerated bending mode of the O–P–O bond while

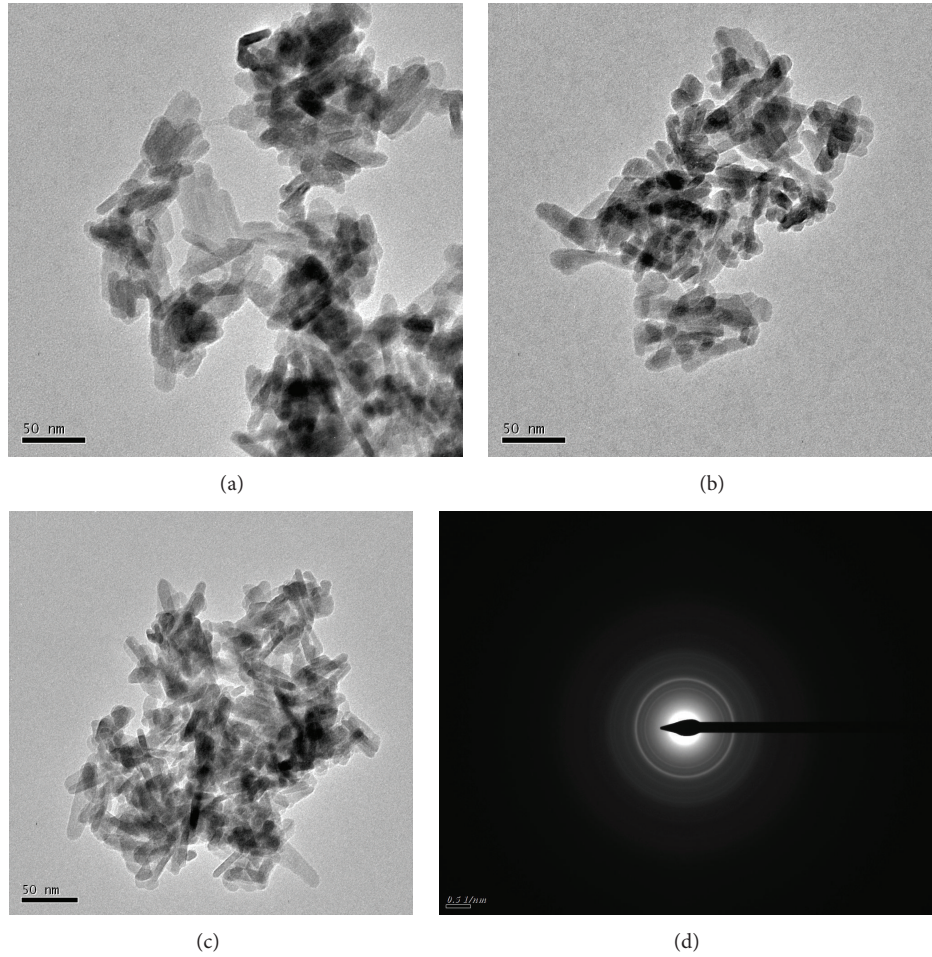


FIGURE 2: The TEM images at low resolution of Sm:HAp with $x_{\text{Sm}} = 0$ (a), $x_{\text{Sm}} = 0.02$ (b), and $x_{\text{Sm}} = 0.05$ (c). The SAED analysis of Sm:HAp with $x_{\text{Sm}} = 0.02$ (d).

the peaks at $1030\text{--}1100\text{ cm}^{-1}$ are attributed to triply degenerate asymmetric stretching mode of the P–O bond. On the other hand, nondegenerated symmetric stretching mode of the P–O bond is observed at 962 cm^{-1} [29]. The peaks at 563 cm^{-1} and 603 cm^{-1} are characteristic to ν_4 vibration of PO_4 . The bands at 872 cm^{-1} are attributed to CO_3^{2-} ions and indicate B-type substitution, where CO_3^{2-} substitutes the phosphate positions in the hydroxyapatite lattice [30, 31]. According to Nelson and Featherstone [32] and Barralet et al. [33] the B-type substitution is predominant in hydroxyapatite synthesized from precipitation reactions.

According to Predoi et al. [5, 34, 35] the absorption peak in the region of $1600\text{--}1700\text{ cm}^{-1}$ is characteristic to O–H bending mode and it is evidence of the presence of absorbed water in the synthesized samples. In recent studies on samarium doped hydroxyapatite nanoparticles (Sm:HAp-NPs), Han et al. [29] attributed the weak band in the region $3200\text{--}3600\text{ cm}^{-1}$ to the stretching vibration of structural OH bond. When the concentration of samarium increases in the samples, the hydroxyl vibration band in the region $3200\text{--}3600\text{ cm}^{-1}$ decreases in intensity. According to Barralet et al. [36] a decrease of the hydroxyl vibration peak intensity in

the region $3200\text{--}3600\text{ cm}^{-1}$ and PO_4^{3-} stretching mode at 960 cm^{-1} indicates an increase in the crystallinity of the particles. This decrease in crystallinity of the particles is consistent with the XRD results discussed before.

MTT assay is an assay which measures changes in colour for measuring cellular proliferation. It is used to determine cytotoxicity of potential medicinal agents and other toxic materials. The 3-(4,5-dimethylthiazol-2-yl)-2,5-diphenyltetrazolium bromide is reduced to purple formazan in the mitochondria of living cells. To dissolve the insoluble purple formazan product into a coloured solution a solubilization solution is added. The hFOB 1.19 osteoblasts cells were permanently monitored to detect any possible influence due to samarium doped hydroxyapatite ($x_{\text{Sm}} = 0$, $x_{\text{Sm}} = 0.02$, and $x_{\text{Sm}} = 0.05$) that might alter the cell growth, viability, and proliferation.

hFOB 1.19 osteoblast cells incubated with the samarium doped hydroxyapatite ($x_{\text{Sm}} = 0$, $x_{\text{Sm}} = 0.02$, and $x_{\text{Sm}} = 0.05$) for 4, 12, and 24 hours presented a growth inhibition and the decrease of viability, relating to control (100%). After 4 hours of exposure with Sm:HAp and diminish in proliferation of the osteoblast cells at 68.92% (Sm:HAp with $x_{\text{Sm}} = 0$),

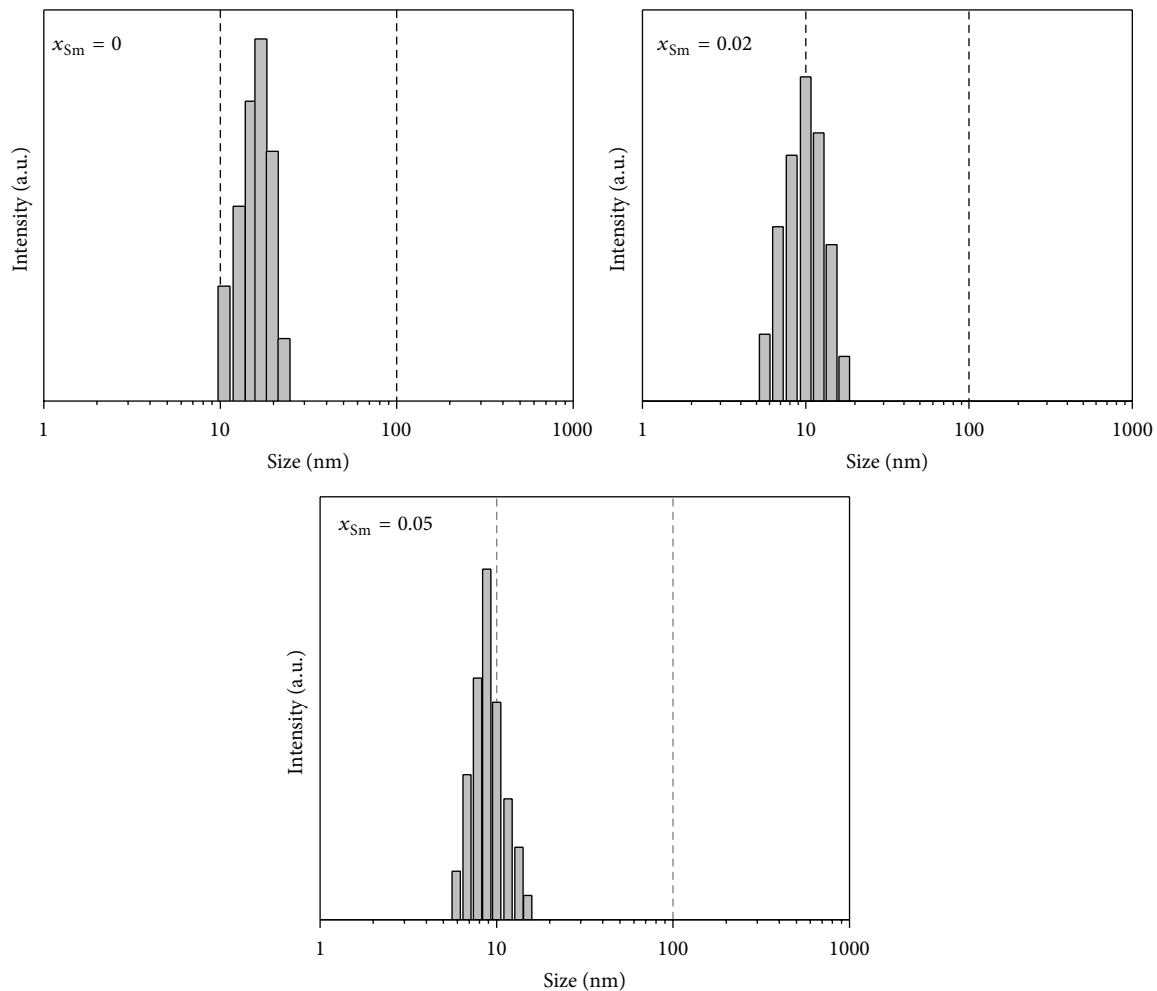


FIGURE 3: DLS showing mean average size of samarium doped hydroxyapatite.

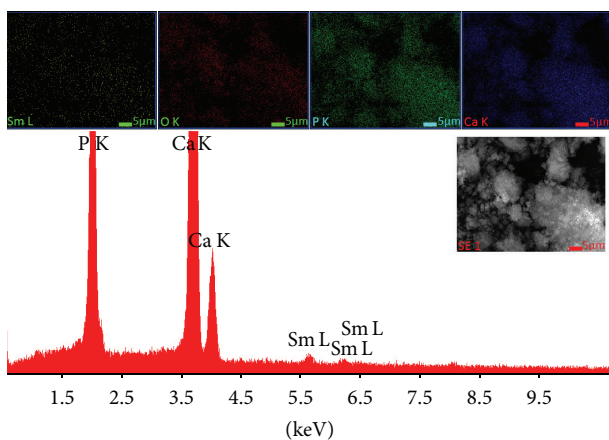


FIGURE 4: EDAX spectrum of the Sm:HAp ($x_{\text{Sm}} = 0.02$) samples and simultaneous distributions of individual elements based on selected region of the sample.

68.56% (Sm:HAp with $x_{\text{Sm}} = 0.02$), and 68.12% (Sm:HAp with $x_{\text{Sm}} = 0.05$) a tendency of linear increase of viability and

proliferation after 12 and 24 hours was observed. The increase of viability and proliferation of the osteoblast cells after 24 hours at around 100% relating to control was observed for all the samples (Figure 6).

Studies on the antimicrobial properties of these nanoparticles were also performed. The antimicrobial activity of Sm:HAp-NPs against Gram-negative (*Pseudomonas aeruginosa* and *Escherichia coli*) and Gram-positive (*Enterococcus faecalis* and *Staphylococcus aureus*) bacteria was evaluated.

Gram-negative bacteria can cause infections of surgical site or wound, bloodstream infections, pneumonia, and even meningitis. The Gram-negative bacteria have a unique structure of the outer membrane which gives them the ability to find new ways to be drug-resistant. The most common Gram-negative infections include those caused by *Pseudomonas aeruginosa*, *Escherichia coli*, *Acinetobacter*, and *Klebsiella*. According to Poole [37], one of the most worrisome characteristics of *P. aeruginosa* is its low antibiotic susceptibility. On the other hand, *P. aeruginosa* can easily develop resistance to antibiotics by mutation in chromosomally encoded genes. *Escherichia coli* is known for virulence in urinary tract infections and neonatal meningitis. It is known

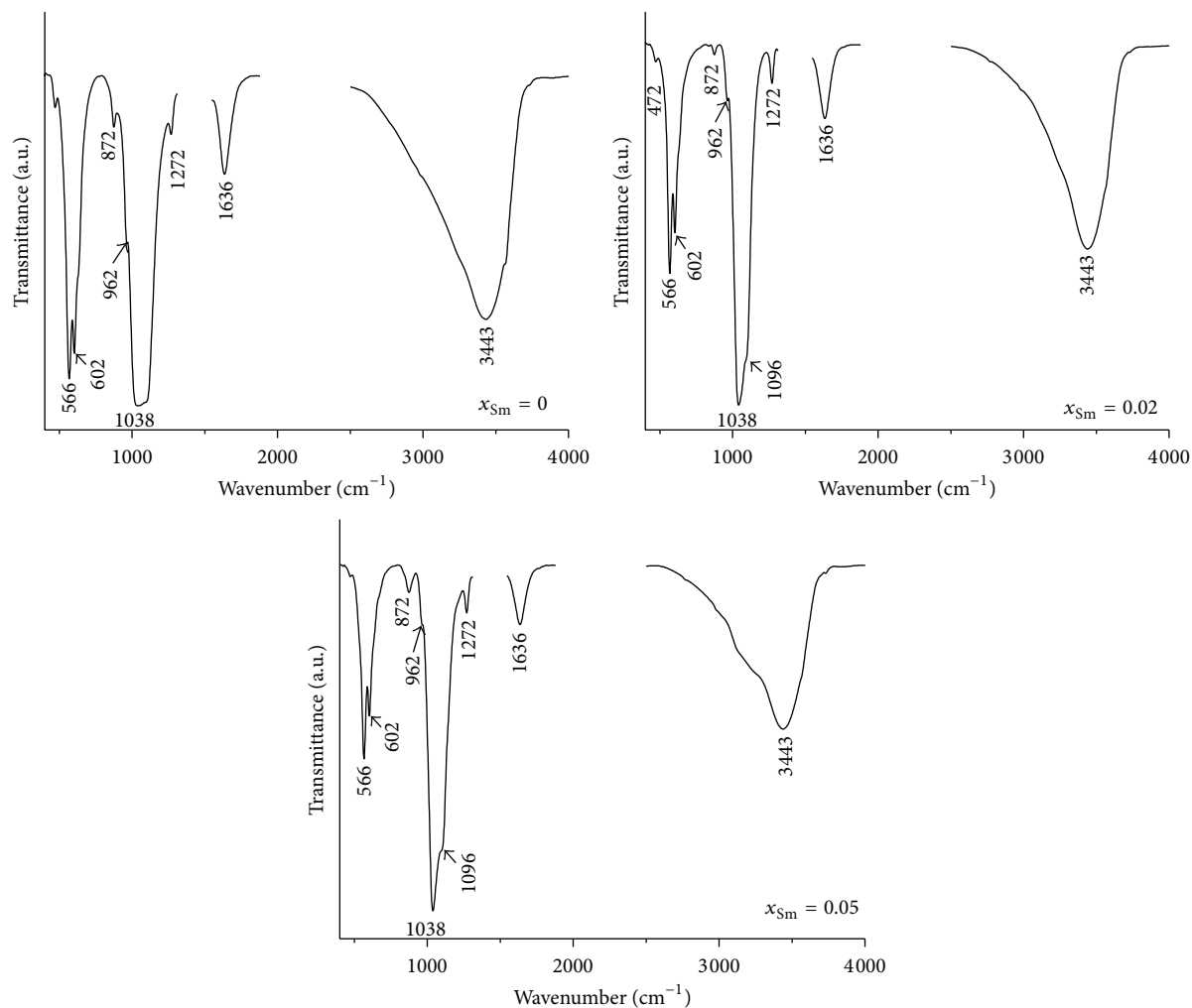


FIGURE 5: Infrared spectra in transmission mode of the Sm:HAp samples synthesized with $x_{\text{Sm}} = 0$, $x_{\text{Sm}} = 0.02$, and $x_{\text{Sm}} = 0.05$.

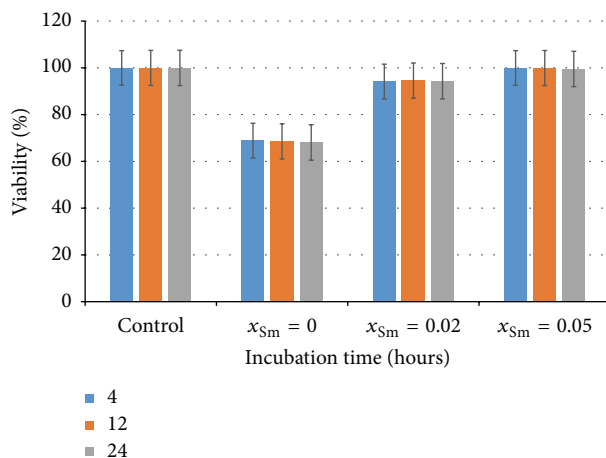


FIGURE 6: MTT assay in hFOB 1.19 osteoblast cells incubated on Sm:HAp ($x_{\text{Sm}} = 0$, $x_{\text{Sm}} = 0.02$, and $x_{\text{Sm}} = 0.05$).

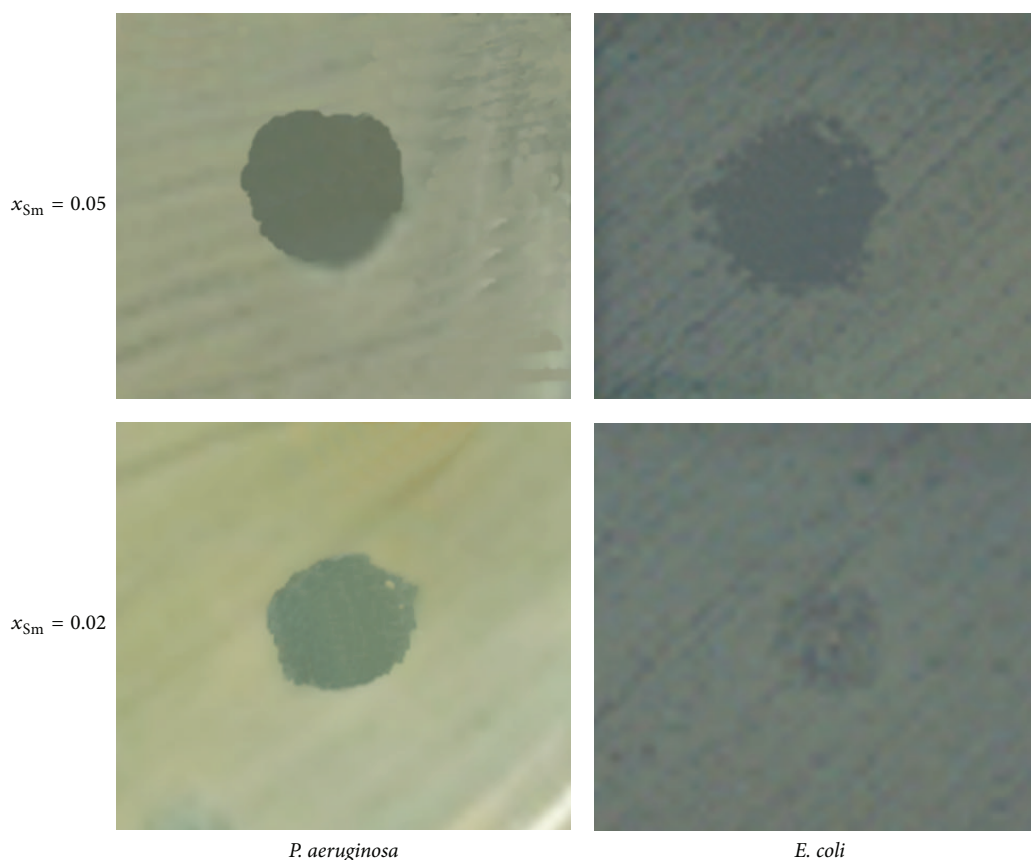


FIGURE 7: Qualitative antibacterial activity evaluation of Sm:HAp-NPs ($x_{Sm} = 0.02$ and $x_{Sm} = 0.05$) on *Pseudomonas aeruginosa* and *Escherichia coli* Gram-negative bacteria.

that it is one of the main causes of urinary tract infections [38].

The results of qualitative antibacterial activity evaluation of Sm:HAp-NPs ($x_{Sm} = 0.02$ and $x_{Sm} = 0.05$) on Gram-negative and Gram-positive bacteria are shown in Figures 7 and 8.

The antibacterial activity of Sm:HAp-NPs ($x_{Sm} = 0.02$ and $x_{Sm} = 0.05$) was evaluated. For the Sm:HAp-NPs with $x_{Sm} = 0$ no activity against the *Pseudomonas aeruginosa*, *Escherichia coli*, *Enterococcus faecalis*, and *Staphylococcus aureus* was observed. On the other hand, the interactions of Sm:HAp-NPs ($x_{Sm} = 0.02$ and $x_{Sm} = 0.05$) with Gram-negative and Gram-positive tested bacteria were different. The different interaction between our compounds and microbial strains tested could be due to differences occurring in the microbial wall structures. The qualitative antibacterial activity evaluation on Sm:HAp-NPs was revealed by a clear zone of inhibition when the concentrations were $x_{Sm} = 0.02$ and $x_{Sm} = 0.05$. A significant antibacterial activity was observed on Sm:HAp-NPs with $x_{Sm} = 0.02$ for all of the bacteria used.

In Figure 9 the antibacterial activity of Sm:HAp-NPs ($x_{Sm} = 0$, $x_{Sm} = 0.02$, and $x_{Sm} = 0.05$) on Gram-negative bacteria (*Pseudomonas aeruginosa* and *Escherichia coli*) is shown. We can see that the *P. aeruginosa* was inhibited when concentrations of Sm:HAp-NPs in the samples with $x_{Sm} = 0.02$ and $x_{Sm} = 0.05$ were higher than 0.125 mg/mL.

When concentrations of Sm:HAp-NPs in the samples with $x_{Sm} = 0.02$ and $x_{Sm} = 0.05$ were lower than 0.125 mg/mL, an increase in microbial activity for the sample with $x_{Sm} = 0.02$ was observed, while for the samples with $x_{Sm} = 0.05$ the values obtained are comparable to the control sample (M^+). A linear increase of antimicrobial activity of *P. aeruginosa* has been observed when concentrations of Sm:HAp-NPs in the samples with $x_{Sm} = 0.02$ were higher than 0.125 mg/mL. A linear increase in the antimicrobial activity is also observed for concentrations of Sm:HAp-NPs with $x_{Sm} = 0.05$ in the range 0.25–0.5 mg/mL. When the concentration of Sm:HAp-NPs in the samples with $x_{Sm} = 0.05$ is equal to 1, the antibacterial effect is maximum, and we can say that the *P. aeruginosa* was completely killed. For all the concentrations of Sm:HAp-NPs in the samples with $x_{Sm} = 0$ an increase in microbial activity was observed compared with that of the control (M^+). The antibacterial activity of Sm:HAp-NPs ($x_{Sm} = 0$, $x_{Sm} = 0.02$, and $x_{Sm} = 0.05$) on *E. coli* can be seen in Figure 9(b). The antibacterial activity of Sm:HAp-NPs on *E. coli* is observed for concentrations of Sm:HAp-NPs with $x_{Sm} = 0.05$ in the range 0.031–1.0 mg/mL. For this sample (Sm:HAp-NPs with $x_{Sm} = 0.05$) a significant increase of antibacterial activity of *E. coli* was observed in the range 0.5–1 mg/mL. An increase in microbial activity compared with that of the control (M^+) was observed in the region of 0.031–0.5 mg/mL for concentration of Sm:HAp-NPs with $x_{Sm} = 0.02$

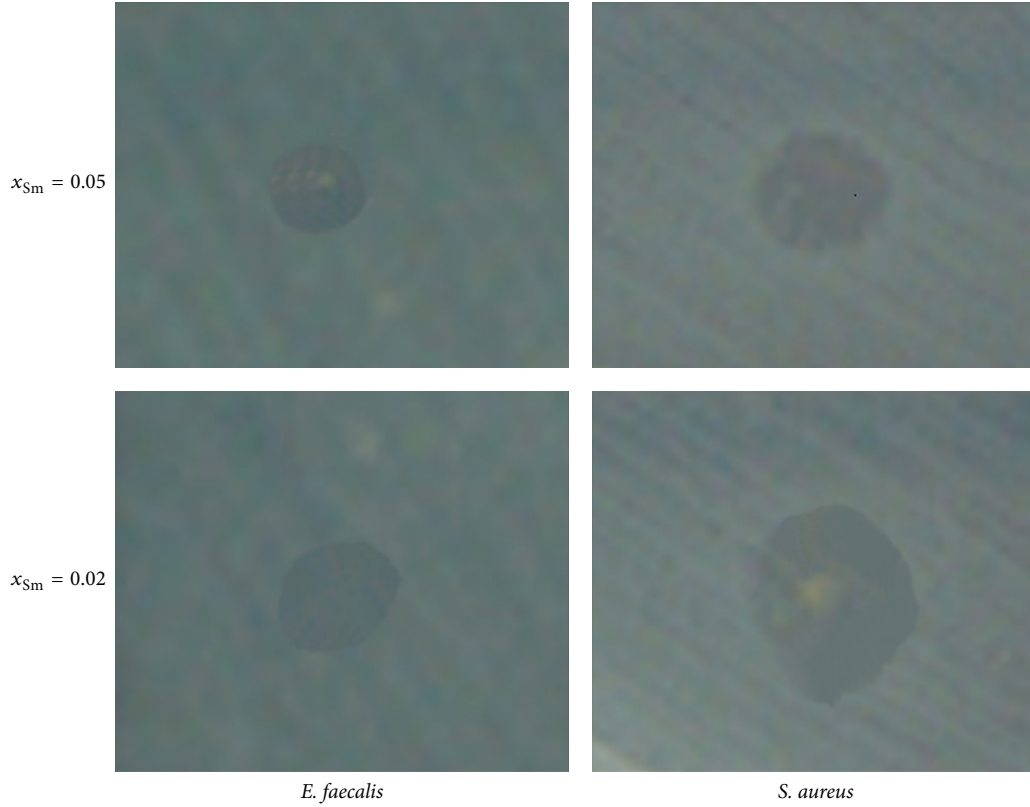


FIGURE 8: Qualitative antibacterial activity evaluation of Sm:HAp-NPs ($x_{sm} = 0.02$ and $x_{sm} = 0.05$) against *Enterococcus faecalis* and *Staphylococcus aureus* Gram-positive bacteria.

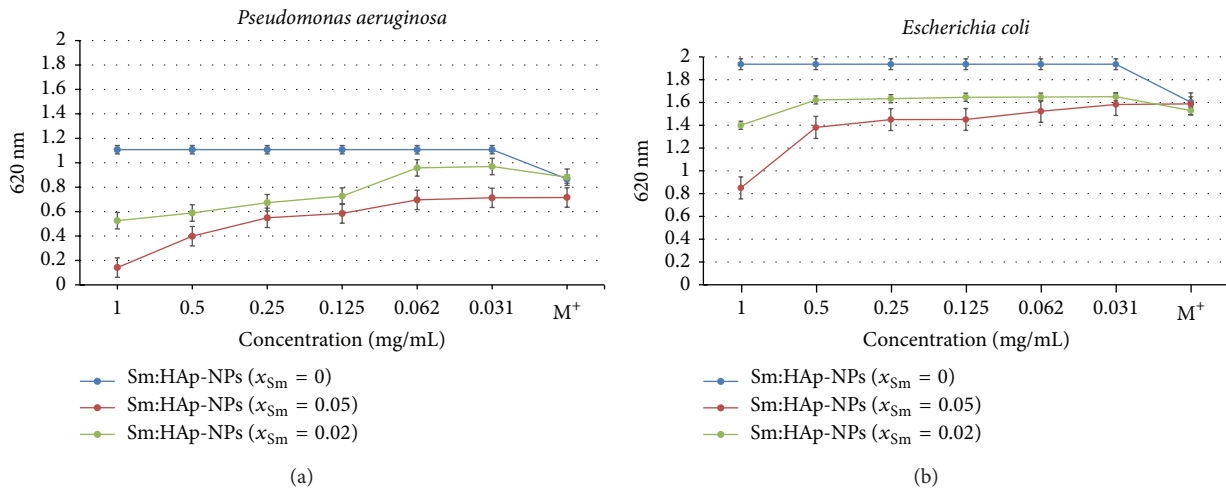


FIGURE 9: The antibacterial activity of Sm:HAp-NPs ($x_{sm} = 0$, $x_{sm} = 0.02$, and $x_{sm} = 0.05$) on *Pseudomonas aeruginosa* (a) and *Escherichia coli* (b) after 24 h.

and $x_{sm} = 0$. In the region 0.5–1 mg/mL, the microbial activity remains constant compared with the microbial activity in the region 0.031–0.5 mg/mL for the concentration of Sm:HAp-NPs with $x_{sm} = 0$, while, for concentration of Sm:HAp-NPs with $x_{sm} = 0.02$, a significant decrease is observed.

The antibacterial activity of Sm:HAp-NPs ($x_{sm} = 0$, $x_{sm} = 0.02$, and $x_{sm} = 0.05$) on Gram-positive bacteria

(*Enterococcus faecalis* and *Staphylococcus aureus*) is shown in Figure 10. Gram-positive and Gram-negative bacteria have similar internal structures while the external structure is very different. The most common Gram-positive bacteria such as *Enterococcus*, *Staphylococcus*, and *Streptococcus* are responsible for a large number of serious infections worldwide. Based on the recent update from the National Healthcare Safety

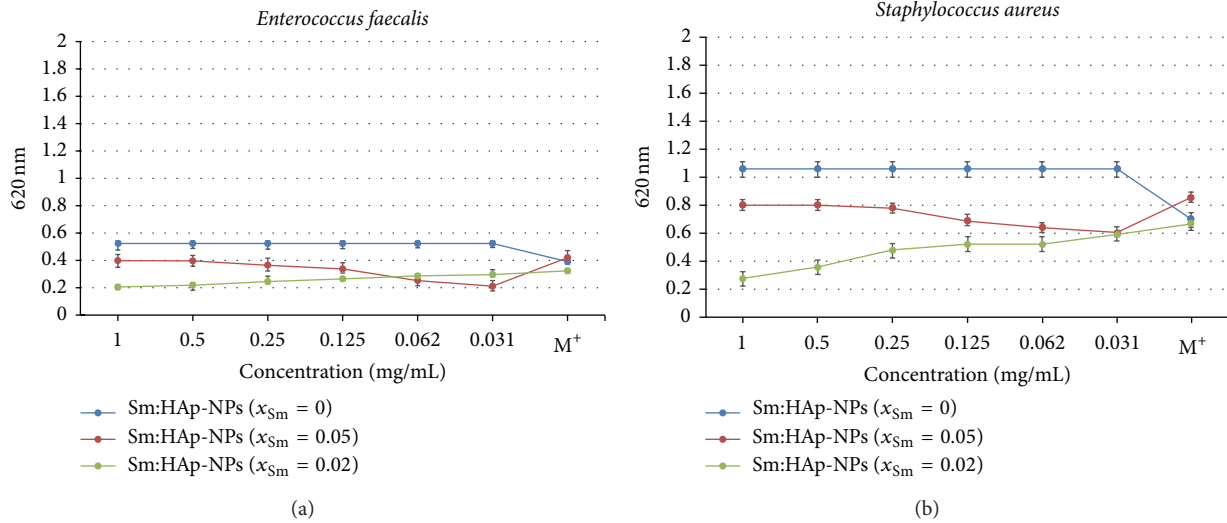


FIGURE 10: The antibacterial activity of Sm:HAp-NPs ($x_{Sm} = 0$, $x_{Sm} = 0.02$, and $x_{Sm} = 0.05$) on *Enterococcus faecalis* (a) and *Staphylococcus aureus* (b) after 24 h.

Network (NHSN) for surveillance of antimicrobial-resistant pathogens [39], *S. aureus* and *Enterococcus faecalis* are the most frequently isolated organisms. On the other hand, *S. aureus* and *Enterococcus faecalis* are the most commonly present organisms in hospitals in Europe [40].

Figure 10(a) displays the antibacterial performance against Gram-positive, *Enterococcus faecalis*, bacteria obtained for the Sm:HAp-NPs ($x_{Sm} = 0$, $x_{Sm} = 0.02$, and $x_{Sm} = 0.05$). The antimicrobial test showed that Sm:HAp-NPs with $x_{Sm} = 0$ caused an increase in the microbial activity of *Enterococcus faecalis* compared to that of the control (M^+). Antibacterial activity of Sm:HAp-NPs samples with $x_{Sm} = 0.02$ increased with an increase of the Sm:HAp-NPs concentration from 0.031 to 1 mg/mL. The Sm:HAp-NPs samples with $x_{Sm} = 0.05$ showed a weak antibacterial activity for high concentrations of Sm:HAp-NPs from 0.125 to 1 mg/mL. For low concentrations of Sm:HAp-NPs ($x_{Sm} = 0.05$) from 0.031 to 0.125 mg/mL a high antibacterial activity of *Enterococcus faecalis* has been noticed. In Figure 10(b) the antibacterial activity of Sm:HAp-NPs at various concentrations from 0.031 to 1 mg/mL on *Staphylococcus aureus* is shown when $x_{Sm} = 0$, 0.02, and 0.05. When $x_{Sm} = 0$ the microbial activity is higher compared to that of the control (M^+) for all tested concentrations. At low concentrations from 0.031 to 0.125 mg/mL, the antibacterial activity of Sm:HAp-NPs ($x_{Sm} = 0.05$) is high, while, for higher concentrations of 0.25 mg/mL, the antibacterial activity decreases reaching values close to that of the control (M^+). A growth of the inhibitory effect on *S. aureus* was observed for all concentrations of Sm:HAp-NPs with $x_{Sm} = 0.02$. For the concentrations from 0.5 to 1 mg/mL of Sm:HAp-NPs ($x_{Sm} = 0.02$) a very good antibacterial activity was noticed.

A growing proportion of Gram-negative and Gram-positive organisms display reduced susceptibility to antibiotics in communities and hospitals [41, 42]. According to

Woodford and Livermore [43] the resistant bacteria have a significant impact on overall healthcare utilization and costs. As a result of the increased antibiotic resistance of the various microorganisms like bacteria, molds, viruses, and so forth, new antimicrobial agents that could be used to prevent infections are made. For the first time, this study has examined the synthesis of samarium doped hydroxyapatite at low temperature by coprecipitation method and its antibacterial activity. It could be concluded that the Sm:HAp-NPs have the antibacterial potential for treating wounds or even for covering medical instruments.

4. Conclusions

Samarium doped hydroxyapatite nanoparticles were successfully synthesized by coprecipitation method. hFOB 1.19 osteoblast cells incubated with the samarium doped hydroxyapatite ($x_{Sm} = 0$, $x_{Sm} = 0.02$, and $x_{Sm} = 0.05$) exhibit an increase of viability and proliferation after 24 hours at around 100% relating to control for all the samples.

The Sm:HAp-NPs were tested for their antibacterial activity. The Sm:HAp-NPs with $x_{Sm} = 0$, 0.02, and 0.05 have antimicrobial property against the Gram-negative and Gram-positive bacteria depending on the concentration of samarium. The bioproperties of Sm:HAp-NPs can be controlled by varying the samarium in hydroxyapatite. The antibacterial properties of Sm:HAp-NPs can lead to increasing their applicability in medical or environmental area.

Conflict of Interests

The authors declare that there is no conflict of interests regarding the publication of this paper.

Acknowledgments

The work has been funded by the Sectoral Operational Programme Human Resources Development 2007–2013 of the Ministry of European Funds through the Financial Agreement POSDRU/159/1.5/S/134398. The authors are grateful to Professor M. C. Chifiriuc (University of Bucharest, Faculty of Biology), for performing antimicrobial studies and their helpful discussions.

References

- [1] M. G. Albu, D. M. Suflet, G. C. Chitanu, P. Budrugaec, I. Titorencu, and V. Trandafir, "Biocomposites based on collagen and phosphorylated dextran for bone regeneration," *Journal of Materials Research*, vol. 27, no. 7, pp. 1086–1096, 2012.
- [2] A. Fica, E. Andronescu, D. Fica, M. Sonmez, M. G. Albu, and G. Voicu, "Mimicking the morphology of long bone," *Central European Journal of Chemistry*, vol. 10, no. 6, pp. 1949–1953, 2012.
- [3] A. Groza, A. Surmeian, C. Diplasu, M. Ganciu, P. Chapon, and I. I. Popescu, "Spectral investigations of the processes observed at polydimethylsiloxane polymer-substrate interface during its polymerization process in negative and positive corona discharges," *Journal of Optoelectronics and Advanced Materials*, vol. 12, no. 11, pp. 2311–2314, 2010.
- [4] S. R. Ramanan and R. Venkatesh, "A study of hydroxyapatite fibers prepared via sol-gel route," *Materials Letters*, vol. 58, no. 26, pp. 3320–3323, 2004.
- [5] A. Costescu, C. S. Ciobanu, S. L. Iconaru et al., "Fabrication, characterization, and antimicrobial activity, evaluation of low silver concentrations in silver-doped hydroxyapatite nanoparticles," *Journal of Nanomaterials*, vol. 2013, Article ID 194854, 9 pages, 2013.
- [6] C. S. Ciobanu, F. Massuyeau, L. V. Constantin, and D. Predoi, "Structural and physical properties of antibacterial Ag-doped nano-hydroxyapatite synthesized at 100°C," *Nanoscale Research Letters*, vol. 6, article 613, 2011.
- [7] A. Fica, M. G. Albu, M. Birsan et al., "Collagen hydrolysate based collagen/hydroxyapatite composite materials," *Journal of Molecular Structure*, vol. 1037, pp. 154–159, 2013.
- [8] A. Groza, "Review of the processes identified during the polymerization of organic and organosilicon liquid films in atmospheric pressure air corona discharges," *Romanian Reports in Physics*, vol. 64, no. 4, pp. 1227–1242, 2012.
- [9] G. Blasse, "Influence of local charge compensation on site occupation and luminescence of apatites," *Journal of Solid State Chemistry*, vol. 14, no. 2, pp. 181–184, 1975.
- [10] S. A. Payne, L. D. DeLoach, L. K. Smith et al., "Ytterbium-doped apatite-structure crystals: a new class of laser materials," *Journal of Applied Physics*, vol. 76, no. 1, pp. 497–503, 1994.
- [11] W. Suchanek and M. Yoshimura, "Processing and properties of hydroxyapatite-based biomaterials for use as hard tissue replacement implants," *Journal of Materials Research*, vol. 13, no. 1, pp. 94–117, 1998.
- [12] J. Rakovan, R. J. Reeder, E. J. Elzinga, D. J. Cherniak, C. D. Tait, and D. E. Morris, "Structural characterization of U(VI) in apatite by X-ray absorption spectroscopy," *Environmental Science & Technology*, vol. 36, no. 14, pp. 3114–3117, 2002.
- [13] A. Aissa, M. Debbabi, M. Gruselle et al., "Sorption of tartrate ions to lanthanum (III)-modified calcium fluor- and hydroxyapatite," *Journal of Colloid and Interface Science*, vol. 330, no. 1, pp. 20–28, 2009.
- [14] S. P. Fricker, "The therapeutic application of lanthanides," *Chemical Society Reviews*, vol. 35, no. 6, pp. 524–533, 2006.
- [15] T. Matsuda, C. Yamanaka, and M. Ikeya, "ESR study of Gd³⁺ and Mn²⁺ ions sorbed on hydroxyapatite," *Applied Radiation and Isotopes*, vol. 62, no. 2, pp. 353–357, 2005.
- [16] J. Coelho, N. S. Hussain, P. S. Gomes et al., "Development and characterization of lanthanides doped hydroxyapatite composites for bone tissue application," in *Current Trends on Glass and Ceramic Materials*, pp. 87–115, 2012.
- [17] V. Venkatramu, P. Babu, C. K. Jayasankar, T. Tröster, W. Sievers, and G. Wortmann, "Optical spectroscopy of Sm³⁺ ions in phosphate and fluorophosphate glasses," *Optical Materials*, vol. 29, no. 11, pp. 1429–1439, 2007.
- [18] M. S. Refat, F. M. Al-Azab, H. M. A. Al-Maydama, R. R. Amin, and Y. M. S. Jamil, "Synthesis and in vitro microbial evaluation of La(III), Ce(III), Sm(III) and Y(III) metal complexes of vitamin B6 drug," *Spectrochimica Acta Part A: Molecular and Biomolecular Spectroscopy*, vol. 127, pp. 196–215, 2014.
- [19] C. S. Ciobanu, C. L. Popa, and D. Predoi, "Sm:HA nanopowders present antibacterial activity against *Enterococcus faecalis*," *Journal of Nanomaterials*, vol. 2014, Article ID 780686, 9 pages, 2014.
- [20] M. G. Cormican, W. W. Wilke, M. S. Barrett, M. A. Pfaller, and R. N. Jones, "Phenotypic detection of mec A-positive staphylococcal blood stream isolates: high accuracy of simple disk diffusion tests," *Diagnostic Microbiology and Infectious Disease*, vol. 25, no. 3, pp. 107–112, 1996.
- [21] C. L. Popa, C. S. Ciobanu, S. L. Iconaru et al., "Systematic investigation and in vitro biocompatibility studies on mesoporous europium doped hydroxyapatite," *Central European Journal of Chemistry*, vol. 12, no. 10, pp. 1032–1046, 2014.
- [22] C. S. Ciobanu, S. L. Iconaru, P. Le Coustumer, L. V. Constantin, and D. Predoi, "Antibacterial activity of silver-doped hydroxyapatite nanoparticles against gram-positive and gram-negative bacteria," *Nanoscale Research Letters*, vol. 7, article 324, 2012.
- [23] C. S. Ciobanu, S. L. Iconaru, M. C. Chifiriuc, A. Costescu, P. Le Coustumer, and D. Predoi, "Synthesis and antimicrobial activity of silver-doped hydroxyapatite nanoparticles," *BioMed Research International*, vol. 2013, Article ID 916218, 10 pages, 2013.
- [24] A. Ravindran, A. Singh, A. M. Raichur, N. Chandrasekaran, and A. Mukherjee, "Studies on interaction of colloidal Ag nanoparticles with Bovine Serum Albumin (BSA)," *Colloids and Surfaces B: Biointerfaces*, vol. 76, no. 1, pp. 32–37, 2010.
- [25] S.-L. Iconaru, M. Motelica-Heino, and D. Predoi, "Study on europium-doped hydroxyapatite nanoparticles by fourier transform infrared spectroscopy and their antimicrobial properties," *Journal of Spectroscopy*, vol. 2013, Article ID 284285, 10 pages, 2013.
- [26] M. Shirkhanzadeh, M. Azadegan, and G. Q. Liu, "Bioactive delivery systems for the slow release of antibiotics: incorporation of Ag⁺ ions into micro-porous hydroxyapatite coatings," *Materials Letters*, vol. 24, no. 1–3, pp. 7–12, 1995.
- [27] C. S. Ciobanu, S. L. Iconaru, F. Massuyeau, L. V. Constantin, A. Costescu, and D. Predoi, "Synthesis, structure, and luminescent properties of europium-doped hydroxyapatite nanocrystalline powders," *Journal of Nanomaterials*, vol. 2012, Article ID 942801, 9 pages, 2012.

- [28] C. S. Ciobanu, S. L. Iconaru, P. Le Coustumer, and D. Predoi, "Vibrational investigations of silver-doped hydroxyapatite with antibacterial properties," *Journal of Spectroscopy*, vol. 2013, Article ID 471061, 5 pages, 2013.
- [29] Y. J. Han, S. C. J. Loo, N. T. Phung, F. Boey, and J. Ma, "Controlled size and morphology of EDTMP-doped hydroxyapatite nanoparticles as model for ¹⁵³Samarium-EDTMP doping," *Journal of Materials Science: Materials in Medicine*, vol. 19, no. 9, pp. 2993–3003, 2008.
- [30] W. H. Emerson and E. E. Fischer, "The infrared absorption spectra of carbonate in calcified tissues," *Archives of Oral Biology*, vol. 7, no. 6, pp. 671–683, 1962.
- [31] V. Jokanović, D. Izvonar, M. D. Dramićanin et al., "Hydrothermal synthesis and nanostructure of carbonated calcium hydroxyapatite," *Journal of Materials Science: Materials in Medicine*, vol. 17, no. 6, pp. 539–546, 2006.
- [32] D. G. A. Nelson and J. D. B. Featherstone, "Preparation, analysis, and characterization of carbonated apatites," *Calcified Tissue International*, vol. 34, supplement 2, pp. S69–S81, 1982.
- [33] J. Barralet, S. Best, and W. Bonfield, "Carbonate substitution in precipitated hydroxyapatite: an investigation into the effects of reaction temperature and bicarbonate ion concentration," *Journal of Biomedical Materials Research*, vol. 41, no. 1, pp. 79–86, 1998.
- [34] D. Predoi, R. V. Ghita, F. Ungureanu, C. C. Negrila, R. A. Vataşescu-Balcan, and M. Costache, "Characteristics of hydroxyapatite thin films," *Journal of Optoelectronics and Advanced Materials*, vol. 9, no. 12, pp. 3827–3831, 2007.
- [35] A. Groza, A. Surmeian, M. Ganciu, and I. I. Popescu, "Infrared spectral investigation of the linseed oil polymerization in a corona discharge in air at atmospheric pressure," *Europhysics Letters*, vol. 68, no. 5, pp. 652–657, 2004.
- [36] J. Barralet, J. C. Knowles, S. Best, and W. Bonfield, "Thermal decomposition of synthesised carbonate hydroxyapatite," *Journal of Materials Science: Materials in Medicine*, vol. 13, no. 6, pp. 529–533, 2002.
- [37] K. Poole, "Efflux-mediated multiresistance in gram-negative bacteria," *Clinical Microbiology and Infection*, vol. 10, no. 1, pp. 12–26, 2004.
- [38] D. W. Hilbert, *Uropathogenic Escherichia coli: The Pre-Eminent Urinary Tract Infection Pathogen*, Nova Publishers, 2013.
- [39] D. M. Sievert, P. Ricks, J. R. Edwards et al., "Antimicrobial-resistant pathogens associated with healthcare-associated infections: Summary of data reported to the national healthcare safety network at the centers for disease control and prevention, 2009–2010," *Infection Control and Hospital Epidemiology*, vol. 34, no. 1, pp. 1–14, 2013.
- [40] J.-L. Vincent, J. Rello, J. Marshall et al., "International study of the prevalence and outcomes of infection in intensive care units," *The Journal of the American Medical Association*, vol. 302, no. 21, pp. 2323–2329, 2009.
- [41] S. E. Cosgrove, Y. Qi, K. S. Kaye, S. Harbarth, A. W. Karchmer, and Y. Carmeli, "The impact of methicillin resistance in *Staphylococcus aureus* bacteremia on patient outcomes: mortality, length of stay, and hospital charges," *Infection Control and Hospital Epidemiology*, vol. 26, no. 2, pp. 166–174, 2005.
- [42] J. M. Rybak, K. E. Barber, and M. J. Rybak, "Current and prospective treatments for multidrug-resistant gram-positive infections," *Expert Opinion on Pharmacotherapy*, vol. 14, no. 14, pp. 1919–1932, 2013.
- [43] N. Woodford and D. M. Livermore, "Infections caused by Gram-positive bacteria: a review of the global challenge," *Journal of Infection*, vol. 59, supplement 1, pp. S4–S16, 2009.

Research Article

In Vivo Osteogenesis of Vancomycin Loaded Nanohydroxyapatite/Collagen/Calcium Sulfate Composite for Treating Infectious Bone Defect Induced by Chronic Osteomyelitis

Xiaojie Lian,¹ Kezheng Mao,² Xi Liu,^{3,4} Xiumei Wang,⁴ and Fuzhai Cui⁴

¹College of Mechanics, Taiyuan University of Technology, Taiyuan 030024, China

²Zhengzhou Orthopedics Hospital, Zhengzhou 450052, China

³National Engineering Laboratory for Modern Silk, College of Textile and Clothing Engineering, Soochow University, Suzhou 215123, China

⁴State Key Laboratory of New Ceramics and Fine Processing, Department of Materials Science and Engineering, Tsinghua University, Beijing 100084, China

Correspondence should be addressed to Xiaojie Lian; yuhalian@126.com

Received 31 August 2014; Accepted 24 October 2014

Academic Editor: Xiaoming Li

Copyright © 2015 Xiaojie Lian et al. This is an open access article distributed under the Creative Commons Attribution License, which permits unrestricted use, distribution, and reproduction in any medium, provided the original work is properly cited.

A novel antibacterial bone graft substitute was developed to repair bone defects and to inhibit related infections simultaneously. This bone composite was prepared by introducing vancomycin (VCM) to nanohydroxyapatite/collagen/calcium sulphate hemihydrate (nHAC/CSH). XRD, SEM, and CCK-8 tests were used to characterize the structure and morphology and to investigate the adhesion and proliferation of murine osteoblastic MC3T3-E1 cell on VCM/nHAC/CSH composite. The effectiveness in restoring infectious bone defects was evaluated *in vivo* using a rabbit model of chronic osteomyelitis. Our *in vivo* results implied that the VCM/nHAC/CSH composite performed well both in antibacterial ability and in bone regeneration. This novel bone graft substitute should be very promising for the treatment of bone defect-related infection in orthopedic surgeries.

1. Introduction

Bone defect-related infections especially chronic osteomyelitis are quite common in open fracture and trauma in clinical treatment, which continues to be very difficult to treat and brings challenges to clinicians. It is difficult to make effective bone repair and inhibit infection at the same time. Vancomycin hydrochloride (VCM) is an antibiotic drug that is specifically used against *Staphylococcus aureus* in the treatment of bone-related infections. However, systemically administered antibiotics have been associated with a number of difficulties including toxic side effects if the drug level is too high or may fail to exert the proper therapeutic effect if the drug level is too low at the site of need. These disadvantages could be markedly reduced if the antibiotic is applied locally at the site of infection by incorporating it into, or onto,

implantable skeletal delivery scaffold, and it may also improve efficacy by delivering valid and safe drug concentrations to the infected bone.

Therefore, it is critical to select an appropriate scaffold for constructing drug delivery system, in which the scaffold should be biocompatible, osteogenic, operable, biodegradable, and antibacterial. Primarily, the scaffold should possess suitable ingredients and structure for cell attachment, proliferation, and osteogenic differentiation. Li et al. did some related studies [1–3].

PMMA is often incorporated with antibiotics such as gentamicin as one of the most widely used bone materials in clinical applications. However, the inherent biological inertia of PMMA leads to poor osseointegration between bone tissue and cement interface, apart from other shortcomings such as nonabsorbability, impermeability to antibiotic, monomer

toxicity, and high polymerization temperature [4–8]. Because of these drawbacks, several absorbable, osteoconductive, and low reaction temperature antibiotic carriers have been developed for inhibiting infection as well as avoiding a second surgery [9–14].

Calcium sulfate hemihydrate (CSH) itself has a long clinical history as a bone graft substitute, known for its bioresorption, satisfactory handling properties, or self-setting ability *in situ* after filling the defect. After mixing, CSH form a viscous moldable paste, which in some instances can be injected during surgery using minimally invasive procedures. Moreover, the setting reaction of CSH is not obviously exothermic as PMMA, which are widely used in orthopedic surgery, especially for arthroplasty fixation and vertebroplasty. Therefore, the incorporation of different drugs and biological molecules makes them good candidates for drug delivery applications in bone tissue engineering [15]. However, there are also some drawbacks with the calcium sulfate material including its insufficient ability to stimulate bone regeneration. CSH cement cannot form a chemical bond with bone tissue at the early stage of therapy because of its poor bioactivity [16–19]. Ideal antibiotic carriers should be able to promote early mineralization and support new bone formation and simultaneously control the release of drug.

To optimize the performance of bone regeneration of CSH, some previous studies in our group suggested that nanohydroxyapatite/collagen (nHAC) could be incorporated, which was prepared from mineralizing type I collagen with excellent osteoconductive properties, and was thought to be a new scaffold material for its high similarity of natural bone both in composition and in hierarchical nanostructure in bone tissue engineering [20–25]. It has been demonstrated that nanostructured materials, compared with conventional materials, may promote greater amounts of specific protein interactions, thereby more efficiently stimulating new bone formation. It has also been indicated that when features or ingredients of scaffolds are nanoscale, a variety of interactions can be stimulated at the cellular level [26–29].

The aim of the present study was to investigate nHAC/CSH as a carrier material for vancomycin in the treatment of chronic osteomyelitis to repair bone defects and inhibit related infections simultaneously. An *in vivo* study of the efficacy of this drug-loaded bone cement was performed in an experimental model of chronic bone infection caused by MRSA.

2. Materials and Methods

2.1. Material Preparation and Physicochemical Properties Characterization. The powders of nHAC and CSH were prepared as previously described. In brief, nHAC were obtained by precipitation of Ca^{2+} and PO_4^{3-} on the collagen molecule from its precursors (CaCl_2 and NaH_2PO_4), followed by product freeze-drying. And the CSH were prepared from CSD (calcium sulphate dehydrate) by hydrothermal synthesis [30, 31]. In this study, the VCM/nHAC/CSH were prepared by mixing 5 wt% VCM·HCl, 5 wt% nHAC, and 90 wt% CSH uniformly. Control samples (nHAC/CSH) were also prepared

using the same process without VCM. The samples were mixed with deionized water at 0.5 ratio of liquid to solid (L/S) and stirred to form homogeneous paste within 20 s and then stored in 100% humidity at 37°C to set.

The composition of materials was characterized by X-ray diffraction (XRD, D/max-2500X) using monochromated $\text{CuK}\alpha$ radiation ($\lambda = 1.5405 \text{ \AA}$, 120 mA, 40 kV) in a continuous scan mode with a scanning speed of 8°/min, and the 2θ range was from 10° to 90°.

Composite samples were sputter-coated with gold film for scanning electron microscopy (SEM, Quanta 200 FEG, Netherlands) examinations at the voltage of 20 kV.

2.2. Cell Experiment. In order to evaluate the biocompatibility of cement, cell counting kit-8 (CCK-8) method was used to quantitatively evaluate the proliferation of murine osteoblastic MC3T3-E1 (a clonal osteogenic cell line derived from newborn mouse calvarias, which is often used in bone tissue engineering research). Cell growth and adhesion behaviors on the scaffolds surfaces were examined by SEM observation. MC3T3-E1 cells were cultured in Dulbecco's Modified Eagle Medium supplemented with 10% fetal bovine serum, 50 $\mu\text{g/mL}$ penicillin, and 50 $\mu\text{g/mL}$ streptomycin at 37°C in a humidified atmosphere of 5% CO_2 and 95% air incubator. Two types of composite cements (nHAC/CSH and VCM/nHAC/CSH) were cut into small cubes (with 5 mm in diameter and 2 mm in thickness) for 96-well plate, sterilized by ^{60}Co γ -irradiation at the dose of 16 kGy. The cells were seeded onto the sterilized cements at a density of 1×10^5 cells/mL, and 100 μL of such cell suspension was added to each well. For SEM examination (JSM-T300, JEOL, Tokyo, Japan), cells were collected after 24 h incubation and then fixed with 2.5% glutaraldehyde in PBS for 0.5 h. After dehydration with a series of graded ethanol (30, 50, 70, 80, 90, 95, and 100%), the samples were critical-point-dried and then coated with gold film for SEM examination. In order to evaluate cell proliferation, CCK-8 assay (Dojindo Molecular Technologies Inc.) was performed according to the manufacturer's protocol. Briefly, after incubating at 37°C and 5% CO_2 for indicated time (1, 3, and 5 days), the culture medium was replaced with 100 μL fresh medium containing 10 μL CCK-8 solution in each well for another 3 h incubation before measurement at 450 nm with a micro plate reader (Bio-Rad, Model 680). Four repeated measurements for each time point of each group ($n = 4$) were carried out for statistical analysis.

2.3. In Vivo Study. The animal experiments were carried on by the approval of the Ethics Committee of the General Hospital of People's Liberation Army. The *in vivo* study was conducted on New Zealand rabbits (3.5–4.0 kg). Bone infection was induced in the condylus lateralis femoris in 30 rabbits using the model of Norden et al. under general anaesthesia. The site of operation was shaved and cleaned with alcohol. The medullary cavity was exposed through a lateral approach and a small hole was made ($\Phi 7 \text{ mm} \times 9 \text{ mm}$). 0.2 mL 5% sodium morrhuate was directly delivered into the cavity followed by 0.2 mL bacterial suspension with

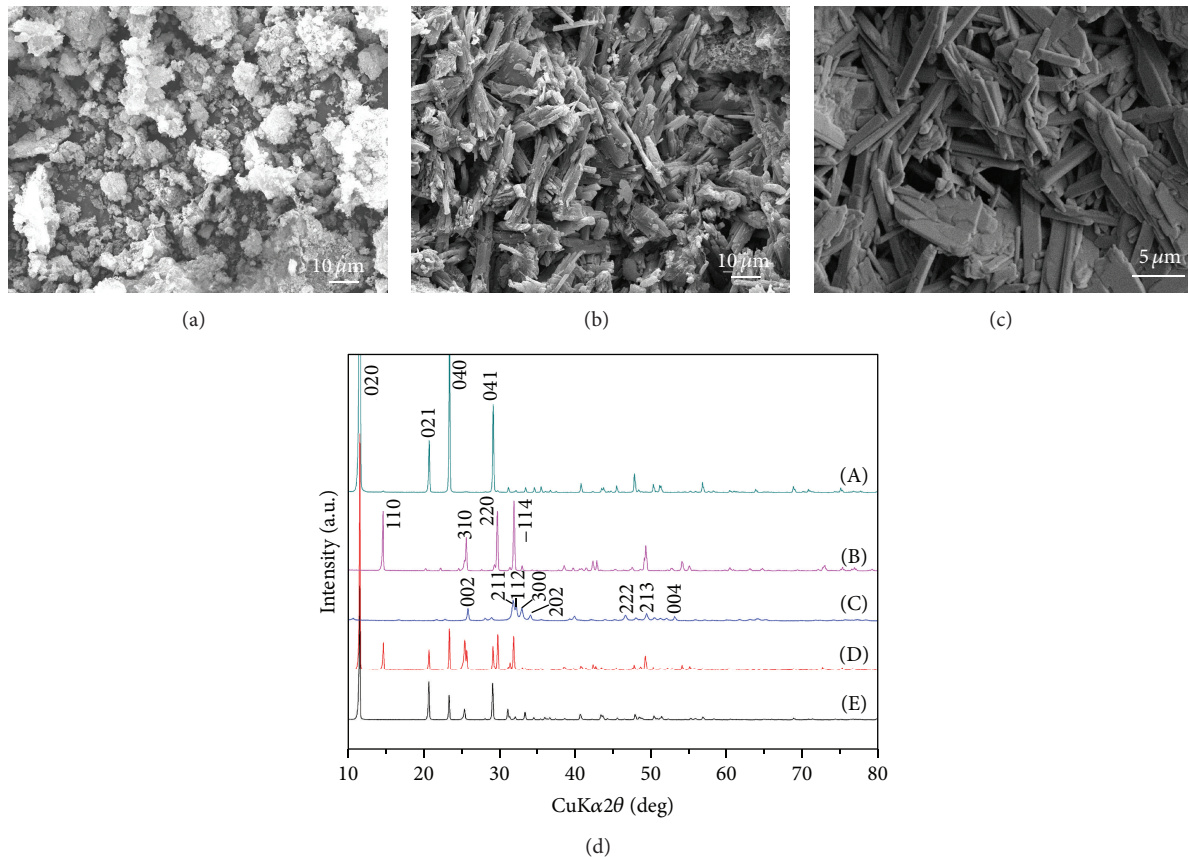


FIGURE 1: SEM micrographs of (a) nHAC, (b) CSH crystal, and (c) CSD crystal and XRD patterns of (d)(A) CSD, (d)(B) CSH, (d)(C) nHAC, (d)(D) compound of VCM/nHAC/CSH, and (d)(E) set cement of VCM/nHAC/CSH.

1×10^8 CFU/mL *S. aureus* (MRSA, ATCC 43300, Shanghai Harmony Biotechnology Co., Ltd.). The wound was closed by suturing. Three weeks after induction of infection, all rabbits were infected and treated by focal debridement. Control group were injected by nHAC/CSH loading without antibiotics, whereas animals of treatment group were injected by VCM/nHAC/CSH for 3 months.

After surgery, rabbit femoris in defect regions were extracted and fixed in 4% paraformaldehyde and then decalcified in EDTA and dehydrated in ethanol before they were embedded in paraffin. Sections were prepared and stained with hematoxylin and eosin and Masson's trichrome. Histomorphometry was carried out using a light microscope (BX51, Olympus) under 40x magnification. For the evaluation of fibrosis, picrosirius red staining was performed using 0.1% picrosirius red solution. Micro-computed tomography was used to observe the bone reconstitution.

2.4. Statistical Analysis. All the data were statistically analyzed using SPSS 13.0 software and expressed as the standard deviation of the mean. The *t*-test was performed and $p < 0.05$ was commonly accepted to be statistically significant.

3. Result and Discussion

3.1. Characterization of the Physicochemical Properties of VCM/nHAC/CSH Scaffold. The conversion of CSD phase to α -CSH phase by hydrothermal synthesis was confirmed by XRD analyses (Figures 1(d)(A) and 1(d)(B)) and revealed complete transformation of CSD with new diffraction peaks located at 14.75° , 25.58° , 29.76° , and 31.94° , which were correlated with the characteristic crystal planes of 110, 310, 220, and -114 for α -CSH phase.

Also the characteristic peaks of nHAC located at 25.91° , 31.82° , 32.20° , 32.93° , and 34.10° and correlated with crystal planes of 002, 211, 112, 300, and 202 (Figure 1(d)(C)) were shown. The broadening of the diffraction peaks of nHAC implied the small grain size and low crystallinity. nHAC powder was composed of some irregular particles as shown in Figure 1(b). The similarities to natural bone in the microstructure of nHAC have been verified via conventional and high-resolution transmission electron microscopy by Zhang et al. [32]. After the hydration reaction from VCM/nHAC/CSH powder to set cement, the XRD peaks of which were changed to 11.64° , 20.75° , 23.41° , and 29.14° , corresponding to crystal planes of 020, 021, 040, and 041. Such changes indicated that the CSH with rod-like structure

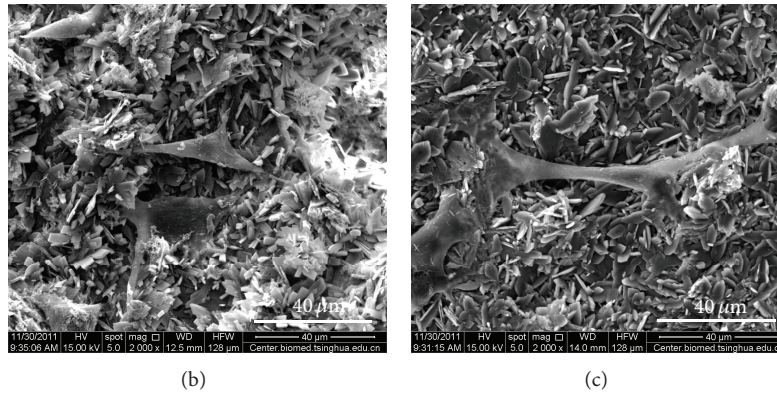
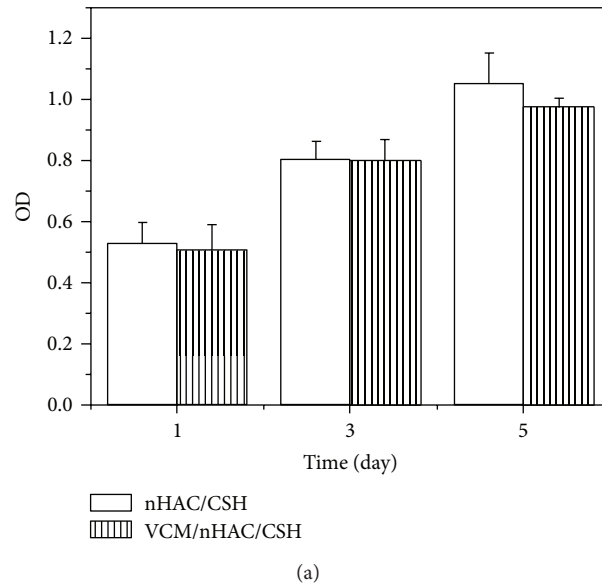


FIGURE 2: (a) Cells proliferation on the nHAC/CSH and VCM/nHAC/CSH scaffolds evaluated by CCK-8 assay and SEM micrographs of cells on (b) VCM/nHAC/CSH and (c) nHAC/CSH.

in the powder was transformed into CSD with sheet crystal structure in the set cement during the hydration reaction, as shown in Figures 1(b) and 1(c).

In our previous study, it was demonstrated that final setting time was about 15~20 min. The porosity of the scaffold was 38.8% and the compressive mechanical strength was about 4.8 MPa, which was more than the lower limit of natural cancellous bone (1 MPa) [31].

3.2. CCK-8 Assay. In order to evaluate the cell toxicity of VCM, CCK-8 method was used to measure the proliferation of MC3T3-E1 cells on the scaffold surfaces. Figure 2(a) shows the proliferation results of cells cultured for 1, 3, and 5 days, respectively. For all times, the OD values of VCM/nHAC/CSH were not significantly lower than that of the nHAC/CSH for each point in time. This is not surprising since the antibacterial property of VCM is also expected to have an adverse effect on the osteoblastic cell viability. However, it was also shown that the cell growth on both groups increased significantly from 1 day to 5 days ($p < 0.05$). Beyond that, cells performed well in attachment and

spreading on both of bone materials with multiple filopodia. These results indicated that the VCM/nHAC/CSH scaffold with 5 wt% VCM addition had satisfied *in vitro* biocompatibility.

3.3. In Vivo Study. In the previous study, the materials were shown to be *in vitro* antibacterial. The inhibition ratio of VCM/nHAC/CSH was more than 99.8% and the distinct inhibition zone of 18 mm was formed in *Staphylococcus aureus* bacterium incubation dish with VCM/nHAC/CSH disc in the center of agar matrix for 16 hours of incubation. On HE and Masson histological analysis at 12 weeks after implantation, single islands of new trabecular bone formed, and a number of active nonaligned osteocytes and osteoblasts at the periphery of bone trabecula were frequently observed in the VCM/nHAC/CSH group. No signs of necrosis and inflammation were found in the group of VCM/nHAC/CSH at this time. By contrast, all rabbits revealed evidence of chronic infections, and there were many bone necroses in the control group. Histological observation in this study demonstrated the effectiveness of treatment in an experimental

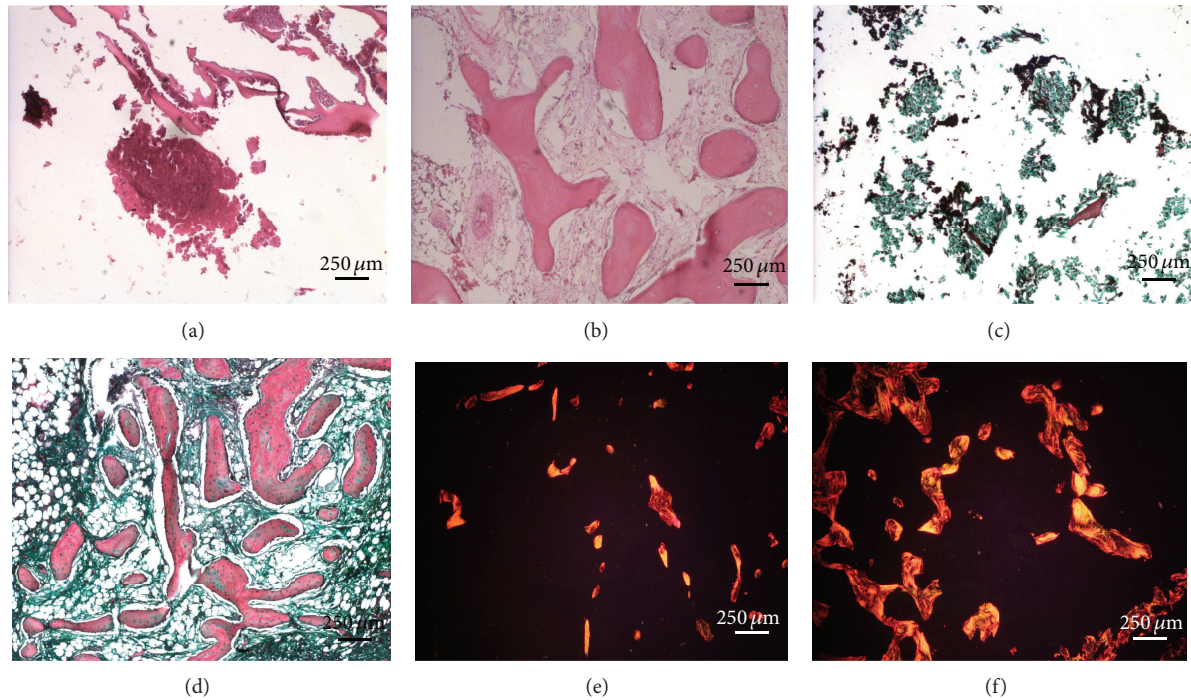


FIGURE 3: Histological cross sections (40x) after infection with MRSA (40x): (a) cross section (HE) and (c) cross section (Masson) of nHAC/CSH group after 12 weeks of implantation; (b) cross section (HE) and (d) cross section (Masson) of VCM/nHAC/CSH group after 12 weeks of treatment and picrosirius red stained cross section after 12 weeks of implantation; (e) nHAC/CSH group; (f) VCM/nHAC/CSH group.

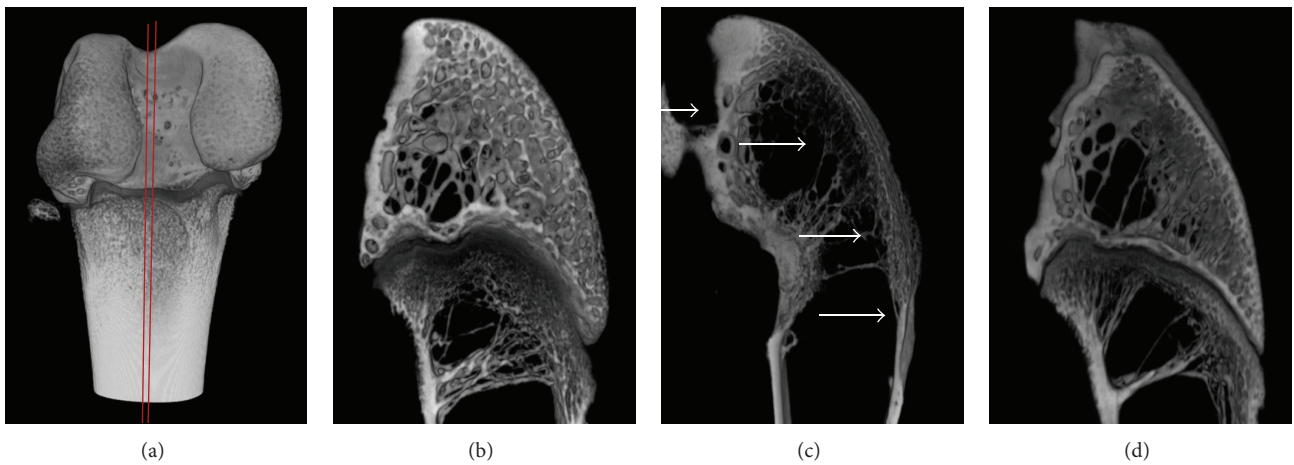


FIGURE 4: Micro-CT graphs taken 12 weeks after focal debridement. (a) Cross section position (red line), (b) normal bone, (c) nHAC/CSH group, and (d) VCM/nHAC/CSH group.

model of chronic bone infection caused by MRSA within 12 weeks.

Picrosirius red staining is one of the best techniques of collagen histochemistry. Sirius red enhances the birefringence in oriented collagens as it attaches to collagens in parallel; then we can see the red-orange colored light from sirius red stained collagens in polarized light microscopy. As the enhancement of birefringence is limited in fibrous tissues, this method can be used to identify fibrous collagen. In this study, the tissues were fixed in a solution of 10%

neutral buffered formalin, embedded in paraffin, sectioned at a thickness of 5 μm , and stained with picrosirius red. There were more fibrous tissues in the VCM/nHAC/CSH group than that in nHAC/CSH group in picrosirius red stained cross section after infection with MRSA following 12 weeks of treatment as shown in Figures 3(e) and 3(f).

The results also were confirmed by the micro-computed tomography graphs of implanted materials on the antibacterial bone defect as shown in Figure 4. After 12 weeks, the bone tissues were destroyed in different places of rabbit

femoris (pointed with the arrows in Figure 4(c)) because of infection without drug release in nHAC/CSH group. But, in the treatment group (Figure 4(d)), the bone reconstruction was better than control group (Figure 4(c)) and close to normal femoris bone (Figure 4(b)).

All results above suggested that the inflammation may actually inhibit the growth of bone tissue in nHAC/CSH group, and the treatment of inflammation along with bone repair was effective in VCM/nHAC/CSH group.

The best treatment of contaminated or infected bone defects, such as chronic osteomyelitis, is to control infection and repair bone defect at the same time. This requires an osteoinductive bone graft composite with ideal release antibiotic capabilities, mechanical properties, and other related properties. In this study, the nHAC/CSH was used as a carrier of vancomycin (VCM) for the treatment of osteomyelitis, and the VCM/nHAC/CSH composite has ideal self-setting, antibacterial, porous, degradable, good mechanical properties, and better osteogenic activity. So the materials can act not only as void filler facilitating tissue regeneration but also as carrier for inhibiting infection in the healing process.

The bioactivity of the scaffold was determined by the components such as CSH and nHAC, of which CSH as the main ingredient has been used in bone augmentation for many years in virtue of its self-setting ability *in situ* as well as filling the defect. One major drawback in the use of calcium sulphate is insufficient osteogenic activity. Calcium ions were released during dissolution of calcium sulfate. Its dissolution leads to acidic microenvironment responsible for local inflammatory processes at the site of implantation in human bone. Inflammatory tissue was found to disappear after 60 days in bone but to remain in soft tissue implantation sites of white New Zealand rabbits [33]. On the other hand, local increases in calcium ion concentration may affect osteoblast genesis and function, and they may act as a stimulus to osteoblast differentiation. Besides, in live tissue, HA and collagen are the major mineral and organic component of human bones. Recently, various hydroxyapatite (HA) or collagen based composites were developed as potential biomaterials for bone substitutes due to their compositional analogy to bone [34]. Some research uses modified HA as antimicrobial coatings or carrier [35]. In this paper, nHAC was added to calcium sulphate to enhance biocompatibility of calcium sulphate in a composite material, which was developed based on biomimetically synthetic mineralized collagen fibrils. The inorganic phase in the composite is carbonate-substituted HA with low crystallinity as well as nanometer size, and organic phase of type I collagen matrix has a characteristic quarter staggered arrangement of tropocollagen molecules assembled and aligned with an axial period of approximately 67 nm. The matrix serves as a template for orderly deposition of mineral platelets [28]. Studies have demonstrated that nanostructured materials with cell favorable surface properties may promote greater amounts of specific protein interactions to more efficiently stimulate new bone growth compared to conventional materials [29]. The composite has been proven to be with unique osteoinduction and osteoconduction and successfully applied in clinical treatment.

Since the 1980s, vancomycin has become the first choice for treating refractory hip infections because of its high efficacy against gentamicin-resistant bacteria, its rare bacterial resistance, and its low incidence of side effect [8]. In this study, vancomycin can be mixed with powdered nHAC/CSH at the site of bone defect and sustained release on the course of operation. However, loading is not limited to one specific antibiotic (e.g., tobramycin or gentamicin) but can be done according to antibiograms offering individual treatment options. Calcium sulphate's capillary porosity also can be used for impregnation of already hardened calcium sulphate pellets with various antibiotic solutions, which would be reported in our subsequent research.

In *in vivo* study, after three weeks of induction of infection and 12 weeks of treatment with VCM/nHAC/CSH, no evidence of infection or foreign body reaction was observed. The scaffold had almost been completely degraded and a lot of new trabecular bones had formed in the implant site. By contrast, all rabbits in the control groups of nHAC/CSH showed evidence of chronic infections.

4. Conclusion

In this study, we first used the VCM/nHAC/CSH bone substitute as a degradable local antibiotic delivery system for the treatment of chronic osteomyelitis. The implants were successful as vancomycin carriers in inhibiting infection in rabbits osteomyelitis mode during the course of this study. Moreover, the implants performed excellent biocompatibility. Our results suggested that the implants can be considered a new system for local vancomycin delivery and the effectiveness of VCM/nHAC/CSH bone substitute in the treatment of *S. aureus* induced chronic osteomyelitis and simultaneously stimulated bone regeneration.

Conflict of Interests

The authors declare that there is no conflict of interests regarding the publication of this paper.

Acknowledgments

This work is in part supported by the Natural Science Foundation for Young Scientists of Shanxi Province (no. 2014021039-6), the Qualified Personnel Foundation of Taiyuan University of Technology (QPFT) (no. tyut-rc201270a), the Youth Foundation of Taiyuan University of Technology (nos. 1205-04020102, 2013Z020, and 2014TD066), the National High-Tech Program (no. 2011AA030105), the Technical Services Project of Taiyuan University of Technology (no. 143230043-J), the National Science Foundation of China (nos. 50830102, 51303119, 21161003, and 20701010), MOST of China (no. 2011DFA31430), Grants of Science and Technology of Guangdong Province (no. 2010B031500005), and the Natural Science Foundation of Jiangsu Province (BK20130309).

References

- [1] X. M. Li, C. A. van Blitterswijk, Q. L. Feng, F. Z. Cui, and F. Watari, "The effect of calcium phosphate microstructure on bone-related cells in vitro," *Biomaterials*, vol. 29, no. 23, pp. 3306–3316, 2008.
- [2] X. M. Li, H. F. Liu, X. F. Niu et al., "Osteogenic differentiation of human adipose-derived stem cells induced by osteoinductive calcium phosphate ceramics," *Journal of Biomedical Materials Research Part B: Applied Biomaterials*, vol. 97, no. 1, pp. 10–19, 2011.
- [3] X. M. Li, Y. Huang, L. S. Zheng et al., "Effect of substrate stiffness on the functions of rat bone marrow and adipose tissue derived mesenchymal stem cells in vitro," *Journal of Biomedical Materials Research Part A*, vol. 102, no. 4, pp. 1092–1101, 2014.
- [4] C. L. Nelson, S. G. Hickmon, and B. H. Harrison, "Elution characteristics of gentamicin-PMMA beads after implantation in humans," *Orthopedics*, vol. 17, no. 5, pp. 415–416, 1994.
- [5] S. Deb, R. Doiron, L. DiSilvio, S. Punyani, and H. Singh, "PMMA bone cement containing a quaternary amine comonomer with potential antibacterial properties," *Journal of Biomedical Materials Research B: Applied Biomaterials*, vol. 85, no. 1, pp. 130–139, 2008.
- [6] D. Neut, O. S. Kluin, J. Thompson, H. C. van der Mei, and H. J. Busscher, "Gentamicin release from commercially-available gentamicin-loaded PMMA bone cements in a prosthesis-related interfacial gap model and their antibacterial efficacy," *BMC Musculoskeletal Disorders*, vol. 11, article 258, 2010.
- [7] H. L. Tan, W. T. Lin, and T. T. Tang, "The use of antimicrobial-impregnated PMMA to manage periprosthetic infections: controversial issues and the latest developments," *International Journal of Artificial Organs*, vol. 35, no. 10, pp. 832–839, 2012.
- [8] S. G. Yan, X. Z. Cai, W. Q. Yan, X. S. Dai, and H. B. Wu, "Continuous wave ultrasound enhances vancomycin release and antimicrobial efficacy of antibiotic-loaded acrylic bone cement in vitro and in vivo," *Journal of Biomedical Materials Research B: Applied Biomaterials*, vol. 82, no. 1, pp. 57–64, 2007.
- [9] Z. P. Xie, X. Liu, W. T. Jia, C. Q. Zhang, W. H. Huang, and J. Q. Wang, "Treatment of osteomyelitis and repair of bone defect by degradable bioactive borate glass releasing vancomycin," *Journal of Controlled Release*, vol. 139, no. 2, pp. 118–126, 2009.
- [10] M. Larsson, A. Bergstrand, L. Mesiah, C. Van Vooren, and A. Larsson, "Nanocomposites of polyacrylic acid nanogels and biodegradable polyhydroxybutyrate for bone regeneration and drug delivery," *Journal of Nanomaterials*, vol. 2014, Article ID 371307, 9 pages, 2014.
- [11] X. Lian, H. Liu, X. Wang, S. Xu, F. Cui, and X. Bai, "Antibacterial and biocompatible properties of vancomycin-loaded nano-hydroxyapatite/collagen/poly (lactic acid) bone substitute," *Progress in Natural Science: Materials International*, vol. 23, no. 6, pp. 549–556, 2013.
- [12] M.-P. Ginebra, C. Canal, M. Espanol, D. Pastorino, and E. B. Montufar, "Calcium phosphate cements as drug delivery materials," *Advanced Drug Delivery Reviews*, vol. 64, no. 12, pp. 1090–1110, 2012.
- [13] U. Joosten, A. Joist, G. Gosheger, U. Liljenqvist, B. Brandt, and C. Von Eiff, "Effectiveness of hydroxyapatite-vancomycin bone cement in the treatment of *Staphylococcus aureus* induced chronic osteomyelitis," *Biomaterials*, vol. 26, no. 25, pp. 5251–5258, 2005.
- [14] H. A. Doty, M. R. Leedy, H. S. Courtney, W. O. Haggard, and J. D. Bumgardner, "Composite chitosan and calcium sulfate scaffold for dual delivery of vancomycin and recombinant human bone morphogenetic protein-2," *Journal of Materials Science: Materials in Medicine*, vol. 25, no. 6, pp. 1449–1459, 2014.
- [15] M. V. Thomas and D. A. Puleo, "Calcium sulfate: properties and clinical applications," *Journal of Biomedical Materials Research Part B: Applied Biomaterials*, vol. 88, no. 2, pp. 597–610, 2009.
- [16] D. Stubbs, M. Deakin, P. Chapman-Sheath et al., "In vivo evaluation of resorbable bone graft substitutes in a rabbit tibial defect model," *Biomaterials*, vol. 25, no. 20, pp. 5037–5044, 2004.
- [17] G. Orsini, J. Ricci, A. Scarano et al., "Bone-defect healing with calcium-sulfate particles and cement: an experimental study in rabbit," *Journal of Biomedical Materials Research Part B: Applied Biomaterials*, vol. 68, no. 2, pp. 199–208, 2004.
- [18] Z. G. Huan and J. Chang, "Self-setting properties and in vitro bioactivity of calcium sulfate hemihydrate-tricalcium silicate composite bone cements," *Acta Biomaterialia*, vol. 3, no. 6, pp. 952–960, 2007.
- [19] P. Wang, E.-J. Lee, C.-S. Park et al., "Calcium sulfate hemihydrate powders with a controlled morphology for use as bone cement," *Journal of the American Ceramic Society*, vol. 91, no. 6, pp. 2039–2042, 2008.
- [20] C. Du, F. Z. Cui, X. D. Zhu, and K. De Groot, "Three-dimensional nano-HAp/collagen matrix loading with osteogenic cells in organ culture," *Journal of Biomedical Materials Research*, vol. 44, no. 4, pp. 407–415, 1999.
- [21] F.-Z. Cui, Y. Li, and J. Ge, "Self-assembly of mineralized collagen composites," *Materials Science and Engineering R: Reports*, vol. 57, no. 1–6, pp. 1–27, 2007.
- [22] C. Du, F. Z. Cui, W. Zhang, Q. L. Feng, X. D. Zhu, and K. de Groot, "Formation of calcium phosphate/collagen composites through mineralization of collagen matrix," *Journal of Biomedical Materials Research*, vol. 50, no. 4, pp. 518–527, 2000.
- [23] S. S. Liao, F. Z. Cui, W. Zhang, and Q. L. Feng, "Hierarchically biomimetic bone scaffold materials: nano-HA/collagen/PLA composite," *Journal of Biomedical Materials Research Part B: Applied Biomaterials*, vol. 69, no. 2, pp. 158–165, 2004.
- [24] S. S. Liao and F.-Z. Cui, "In vitro and in vivo degradation of mineralized collagen-based composite scaffold: nanohydroxyapatite/collagen/poly(L-lactide)," *Tissue Engineering*, vol. 10, no. 1–2, pp. 73–80, 2004.
- [25] Z. Chen, H. Liu, X. Liu, and F.-Z. Cui, "Injectable calcium sulfate/mineralized collagen-based bone repair materials with regulable self-setting properties," *Journal of Biomedical Materials Research Part A*, vol. 99, no. 4, pp. 554–563, 2011.
- [26] X. M. Li, H. F. Liu, X. F. Niu et al., "The use of carbon nanotubes to induce osteogenic differentiation of human adipose-derived MSCs in vitro and ectopic bone formation in vivo," *Biomaterials*, vol. 33, no. 19, pp. 4818–4827, 2012.
- [27] X. Li, H. Gao, M. Uo et al., "Maturation of osteoblast-like SaoS2 induced by carbon nanotubes," *Biomedical Materials*, vol. 4, no. 1, Article ID 015005, 2009.
- [28] C. Du, F. Z. Cui, Q. L. Feng, X. D. Zhu, and K. De Groot, "Tissue response to nano-hydroxyapatite/collagen composite implants in marrow cavity," *Journal of Biomedical Materials Research*, vol. 42, no. 4, pp. 540–548, 1998.
- [29] X. M. Li, L. Wang, Y. B. Fan, Q. L. Feng, F.-Z. Cui, and F. Watari, "Nanostructured scaffolds for bone tissue engineering," *Journal of Biomedical Materials Research Part A*, vol. 101, no. 8, pp. 2424–2435, 2013.

- [30] Z. Chen, H. Liu, X. Liu et al., "Improved workability of injectable calcium sulfate bone cement by regulation of self-setting properties," *Materials Science and Engineering C*, vol. 33, no. 3, pp. 1048–1053, 2013.
- [31] X. Lian, X. Wang, and F. Cui, "In vitro antibacterial properties of vancomycin-loaded nano-hydroxyapatite/collagen/ calcium sulfate hemihydrates (VCM/nHAC/CSH) bone substitute," *Materials Science Forum: Advances in Functional and Electronic Materials*, vol. 745-746, pp. 6–12, 2013.
- [32] W. Zhang, S. S. Liao, and F. Z. Cui, "Hierarchical self-assembly of nano-fibrils in mineralized collagen," *Chemistry of Materials*, vol. 15, no. 16, pp. 3221–3226, 2003.
- [33] M. A. Rauschmann, T. A. Wichelhaus, V. Stirnal et al., "Nano-crystalline hydroxyapatite and calcium sulphate as biodegradable composite carrier material for local delivery of antibiotics in bone infections," *Biomaterials*, vol. 26, no. 15, pp. 2677–2684, 2005.
- [34] X. M. Li, Q. L. Feng, X. H. Liu, W. Dong, and F. Z. Cui, "Collagen-based implants reinforced by chitin fibres in a goat shank bone defect model," *Biomaterials*, vol. 27, no. 9, pp. 1917–1923, 2006.
- [35] C. S. Ciobanu, C. L. Popa, and D. Predoi, "Sm:HAp nanopowders present antibacterial activity against *Enterococcus faecalis*," *Journal of Nanomaterials*, vol. 2014, Article ID 780686, 9 pages, 2014.

Review Article

The Effects of Surface Properties of Nanostructured Bone Repair Materials on Their Performances

Feng Zhao,¹ Jian Wang,¹ Hongjuan Guo,² Shaojun Liu,¹ and Wei He³

¹Department of Orthopedics, The First Hospital of Hebei Medical University, Shijiazhuang 050031, China

²Department of Outpatient Service Office, The First Hospital of Hebei Medical University, Shijiazhuang 050031, China

³Department of Hand Surgery, The Third Hospital of Hebei Medical University, Shijiazhuang 050051, China

Correspondence should be addressed to Wei He; love_v@126.com

Received 3 November 2014; Accepted 16 December 2014

Academic Editor: Shuming Zhang

Copyright © 2015 Feng Zhao et al. This is an open access article distributed under the Creative Commons Attribution License, which permits unrestricted use, distribution, and reproduction in any medium, provided the original work is properly cited.

Nanotechnology has been expected to be an extraordinarily promising method for bone repair. Meanwhile, the promise of nanobiomaterials for therapeutic applications has been widely reported, and a lot of studies have been made in terms of repairing bone using nanomaterials accompanied by rapid development of nanotechnology. Compared with conventional biomaterials, nanostructured implants have been shown to possess positive effects on cellular functions because of their unique surface properties, such as nanotopography, increased wettability, larger surface area, and microenvironment similar to extracellular matrix. Moreover, many positive cellular responses have been found to take place at the interface between nanostructured implants and host bone. In this paper, we will give a review about the effects of surface properties of nanostructured bone repair materials on their performances in terms of several aspects and a detailed interpretation or introduction on the specific cellular recognitions at the interface between nanostructured implants and host bone.

1. Introduction

With the increase in the elderly population, the need for orthopedic implants is growing at an increasing speed. Before, allografts and autografts are common methods to cure bone defects. However, great limitation exists in the above measure; for instance, as with autografts, autologous bone regeneration does not possess enough strength to support the whole body [1, 2]. At present, synthetic implants are most employed in bone repair, but some drawbacks, such as fatigue, fracture, lack of biocompatibility, restrict its implication greatly on a larger scale. It is the hope that these materials will repair bone quickly and effectively so that the patient can return to a normal healthy life style. However, it has been estimated that the service life of present implant materials used today as bone fixation ranges from 10 to 15 years [3, 4]. Such limited lifetime is absolutely not good news for more and more patients, especially young patients. Short service life will cause secondary damage to their body. It is necessary to create a novel bone implant, which could offer a framework for regenerating and healing the host bone and

blood vessel instead of replacing missing bone temporarily. In other words, an ideal implant should at least consist of two points as follows: interacting with the host tissue well and promoting differentiation of osteogenic cells (Figure 1).

As to the common implantation, once implanted into body under the condition of surrounding tissue, the common implantations are apt to get loosened under physiological loading conditions, thus leading to implant failure in the end. In the final analysis, the osseointegration between implant materials and bone tissue was not formed really was responsible for the loose phenomenon “into” was not formed really as a result of implantations’ loosening. Therefore, the success of both the orthopedic implant and the tissue engineered construct is highly dependent on the selected biomaterial. One of the key factors identified in the failure of both types of implants was insufficient tissue regeneration around the biomaterial immediately after implantation. It is known that the introduction of an implant into a living organism causes specific reactions in the biological environment. The biomolecules and cells together with the intrinsic properties

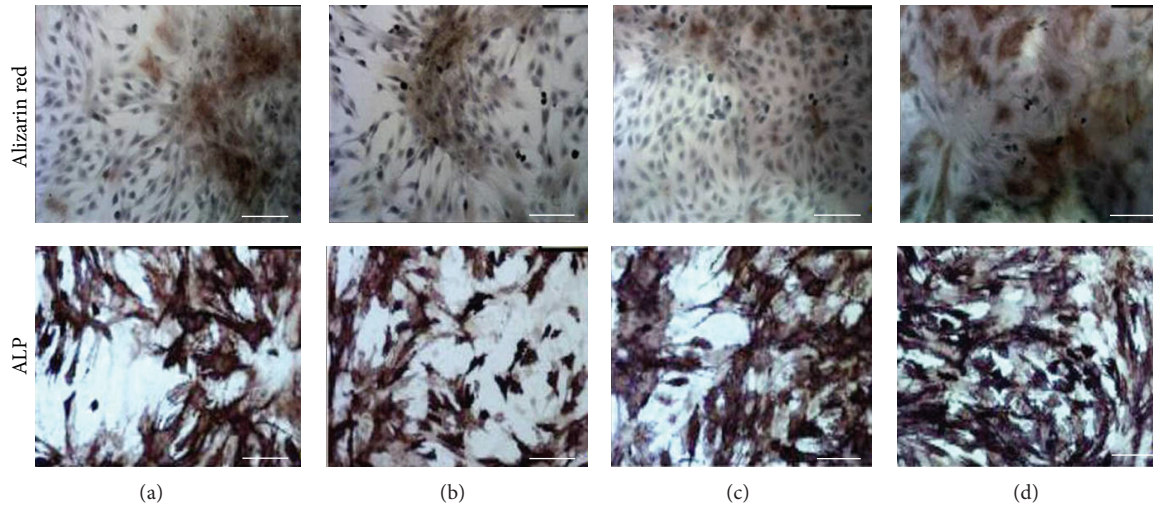


FIGURE 1: Histological and chemical characterization of hMSCs cultured on different films with varying surface roughness. ALP activity as a marker of early osteoblastic differentiation displayed activity in all films. The content of calcium could be stained by Alizarin Red. Compared with other films, the roughest film could significantly promote the differentiation of hMSCs in the direction of osteoblasts (size of surface roughness: (a) < (b) < (c) < (d), and scale bars stand for 200 μm). (Adapted with permission from [5]. Copyright 2011 Elsevier Ltd).

of the chosen biomaterials determine the biocompatibility and longevity of the implants. Since the interaction of those biomolecules and cells with the biomaterial surface is a vital element in the evaluation of the biomaterial, biomaterial scientists have reexamined the pertinent host-cell interactions in order to design materials that facilitate favorable interactions and enhance tissue regeneration. Ultimately, improved symbiosis should result in an accelerated healing time, increase in implant longevity, and a reduction in the necessity for revision surgery.

With the tremendous development of nanotechnology in material science and engineering, biomedical engineering becomes the most promising and challenging field involved in the application of nanostructured materials [6–17]. Nanotechnology represents the manner to manipulation atoms and molecules over the scale of nanometer and generates the materials with at least one dimension in nanoscale. In comparison to the bulk material, the nanomaterials possess many specific characteristics due to the “quantum mechanical effect” [18–20]. Moreover, research has shown that all living systems are governed by molecular behavior at nanometer scales. The molecular building blocks of life proteins, nucleic acids, lipids, and carbohydrates are examples of materials that possess unique properties determined by the size, folding, and patterns at the nanoscale. Also, the surface properties of nanostructured implant structure are similar to extracellular matrix (ECM) to a great extent. For all the above reasons, cells in our body are predisposed to interact with nanostructured surfaces [21]. Consequently, to perform a surface modification at nanolevel will offer a better matrix for osteoblasts to grow and to function in theory. For example, osteoblasts on nanosized Ti, Ti6Al4V powder-modified metal surfaces have improved adhesion and functions when compared to macrophase ones [22–24]. To further improve and optimize the properties of the existing

nanostructured implants for biomedical devices and adapt more desired nanostructured devices with desirable surface characteristics, modifications of nanostructured implants for biomedical application are essential [25–29]. In the paper, we will give a detailed interpretation on the nonspecific cellular recognition in the interface of nanostructured implant surfaces and defected bone; what is more, the effect of the surface property of nanostructured implant on bone repair, such as nanotopography, surface chemistry, and hydrophilic and hydrophobic properties, will be introduced in terms of several aspects. Overall, we believe, through the particular nanoscale modification on the surface of implants, nanostructured implant shows a bright future in the treatment of bone repair.

2. Nanostructured Implant Surfaces' Cellular Recognition

In terms of designing an ideal implant and controlling the nanostructured implants' surface, the mechanism of recognition between cells and nanostructured implant surfaces plays an extremely vital role. For purpose of having a good understanding of the interaction between the surface of nanostructured implant and bone under biological environment, more detailed research should be conducted. Additionally, the preparation method of implants with needed nanomorphology and other surface properties should also be studied correspondingly. Provided that we have a well knowledge of not only the mechanism of cellular recognition and nanostructured implant surfaces, but also preparation method of various desirable nanostructured implants, it will provide a possibility to regulate anticipated biological effects by means of controlling the surface nanostructure of implants. Every effort has been made to investigate how to design nanostructured implants to promote desirable responses from surrounding cells for better osseointegration.

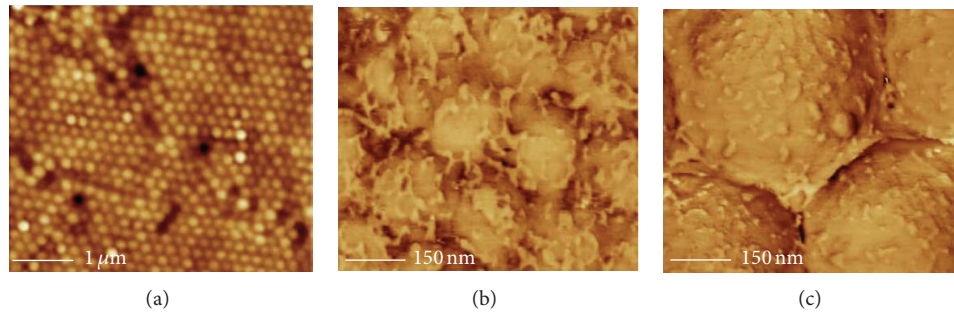


FIGURE 2: AFM images of fibronectin coated PLGA cast nanosphere surfaces. (a) PLGA with 200 nm surface features only. (b) Phase images of fibronectin adsorbed on PLGA with 200 nm surface features showed significant interconnectivity between fibronectins. (c) Phase images of fibronectin adsorbed on PLGA with 500 nm surface features showed no interconnectivity between proteins. (Adapted with permission from [34]. Copyright 2008 Elsevier Ltd).

It has been proved that proteins will be adsorbed from bodily fluids such as bone marrow, blood, and other tissues prior to cell adhesion (such as osteoblasts). Moreover, specific proteins (such as fibronectin and vitronectin) in biological fluids, such as blood plasma, mediate the adhesion, differentiation, and growth of desirable cells on an implant surface [30] (Figure 2). For this reason, many investigators are now paying close attention to manipulating initial protein adsorption events by altering selected properties of implant surfaces. In the study of introducing stainless steel hydroxyapatite ceramics into composites, Tulinski and Jurczyk hold the viewpoint that nanocrystalline nickel-free stainless steels and nickel-free stainless steel/hydroxyapatite nanocomposites could be promising bionanomaterials for use as hard tissue replacement implants; what is more, they considered that the surface roughness and the surface topography influenced the proliferation of cells [31]. Gagner et al. [32] made a relatively intensive study about the control of protein adsorption and subsequent biological outcomes by regulating the surface of nanoparticles. Chun and Webster considered that the incorporation of inorganic nanomaterials into the biological environment is necessary. Implant structures (such as orthopedic prosthetics) have been shown to benefit greatly from nanostructured surfaces that could promote osteoblasts integration and limit bacterial adhesion and inflammation, while matching the material properties of the surrounding bone system at the same time [33].

Peng et al. summarized the nanostructured materials currently used in musculoskeletal tissue engineering including natural polymers, synthetic polymers, and inorganic materials [35]. Moreover, nanostructured materials can be synthesized with controlled composition, size, geometry, and morphology. Most importantly, they deemed that, by means of modifying the surface of these materials, it could enhance biocompatibility, immune compatibility, and cell adhesion of nanostructured materials for different applications in musculoskeletal tissue scaffolds.

Exactly, changes in implant surface energy, surface chemical composition, and topographical features influence the type and concentration of adsorbed proteins [36]. Accordingly, the efficacy of bone regeneration is determined mainly by surface characteristics such as the chemical composition

and physical properties of the implant that controls initial protein adsorption, which could mediate cells adhesion. Together, this is this new direction aimed at intelligently designing implant surfaces to control protein interactions important for subsequent cell adhesion that may provide answers to those problems which have plagued current orthopedic implants. The core of all the issue is to alter the surface chemistries and nanotopographies of orthopedic implant in nanoscale.

3. The Factors of Surface Property of Nanostructured Implant

Through the above description, we could make sense that the nanotopography and surface properties of nanostructured implant determine the response of cells. Several factors, such as nanotopography, hydrophilic and hydrophobic properties, and surface chemistry, greatly affect the growth of bone on the implants; moreover, the above influence factors have been focused on the terms of enhanced orthopedic implant [37, 38].

3.1. Nanotopography. How to optimize cell recognition and response by modified nanotopography is the focus of discussion in orthopedic tissue engineering [39, 40], since nanotopography of implants has been considered to have great effect on both proliferation and differentiation of osteoblastic cells. The properties of substrate have a great effect on cells' response [41]. For the purpose of forming specific nanotopography on substrate, several means should be employed. For instance, Lee et al. successfully prepared titanium alloy with nanohydroxyapatite coatings on using an electrochemical deposition method [42] (Figure 3). A novel model system for studying the influence of nanoscale surface properties on the osseointegration in rat tibia was created by Ballo et al. [43]. They conducted the histological evaluation on the ground sections at 7 days and 28 days after implantation. In their study, the main distinction appeared in the process of formation of new bone in the marrow bone compartments after 28 days of implantation. In comparison with 120 nm and control surfaces, implant surfaces with 60 nm features took

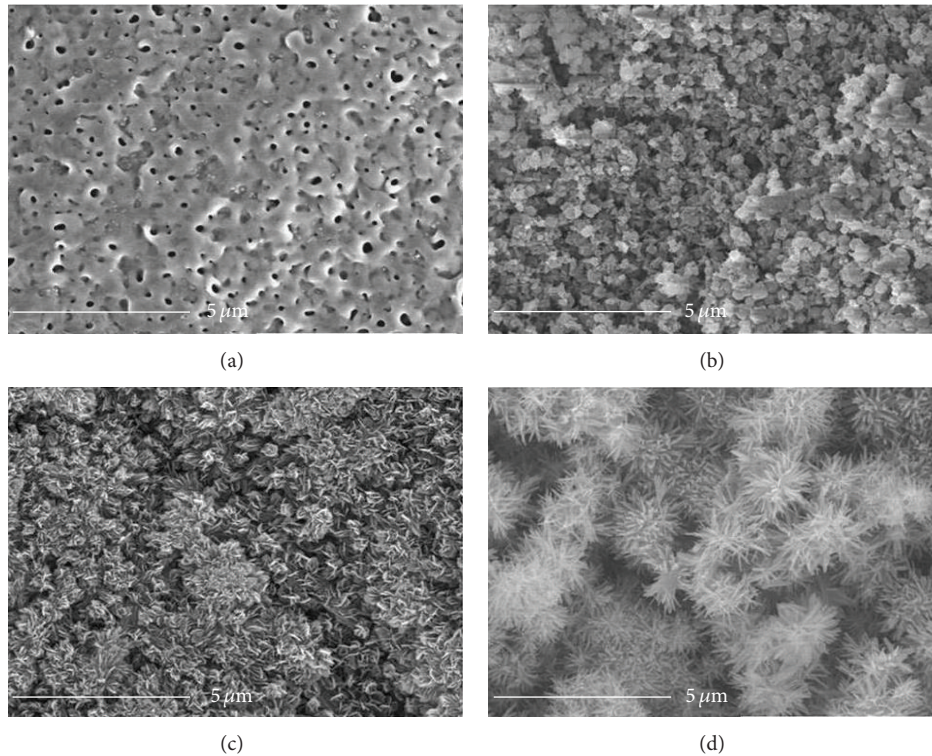


FIGURE 3: FE-SEM images of nanophase hydroxyapatite coatings deposition on anodized Ti with increases in deposition time in the electrolyte at 85°C: (a) initial anodized commercially pure titanium without hydroxyapatite coatings, (b) 5 min, (c) 30 min, and (d) 60 min deposition times for hydroxyapatite coatings layer. (Adapted with permission from [42]. Copyright 2013 Elsevier Ltd).

on obviously higher bone-implant contact. They considered that this phenomenon connected with the 60 nm protrusions, with higher density and curvature. In the end, Ballo et al. considered that the aforementioned model system could actually be applied for the systematic variation of surface nanofeatures density and chemistry, which provided the possibility for research of interactions between various nanoscale surfaces and bones.

Moreover, in order to prove that carbon nanofibers were suitable for bone prosthetic application, carbon nanofibers' cytocompatibility properties and cell adhesion were determined on different cells respectively by Price et al. [44]. For the purpose of determining the enhancement of osteoblasts adhesion in a selective way by nanophase carbon fibers, the cell adhesion assays were conducted on conventional and nanophase carbon fibers compacts by Price et al. By comparison, they concluded that enhanced select osteoblasts adhesion appeared on PLGA casts of nanophase carbon fibers. Most importantly, Price et al. demonstrated that carbon fibers with nanometer dimensions may be more appropriate materials to selectively increase osteoblasts adhesion, which is desperately needed for successful orthopedic/dental implant applications as a result of high degree of nanometer surface roughness. The influence of surface topography of ceramic abutments on the proliferation and attachment of human oral fibroblasts was studied by Mustafa et al. [45]. In accordance with their viewpoints, they considered that, compared to polished surfaces, obviously, more cells were

attached to the milled and sintered surfaces after 3 days of cell culture, which demonstrated higher proliferation capacity on those types of surfaces. What is more, with the increase of surface roughness ceramics, the ability to promote initial fibroblast adhesion decreased in comparison with smooth surfaces. Similar trends have been reported for polymers of the same surface chemistry, but only the degree of nanometer surface roughness has been altered [46]. Consequently, different surfaces with nanophase features possess distinct microstructure, thus influencing cells' event [47].

All in all, from the above studies, we could have an understanding that several cells concerned with bone formation are very sensitive to changes in surface roughness features in the nanometer compared with conventional surface; in other words, nanostructured implant could promote the event and response of specific cells obviously (Figure 4). Most importantly, it provides a possibility by means of adjusting surface nanotopography of nanostructured implant to alter cells adsorption and activity.

3.2. Hydrophilic and Hydrophobic Properties. It is widely reported that hydrophilic surface could boost cell adhesion and activity better [48–51]. Consequently, many polymers used for tissue engineering are hydrophobic in their native state and require surface modification or wetting procedures before cell seeding [52]. Wang et al. improved the endothelialization on 316L stainless steel by means of altering surface wettability via sol-gel method using tetraethoxysilane

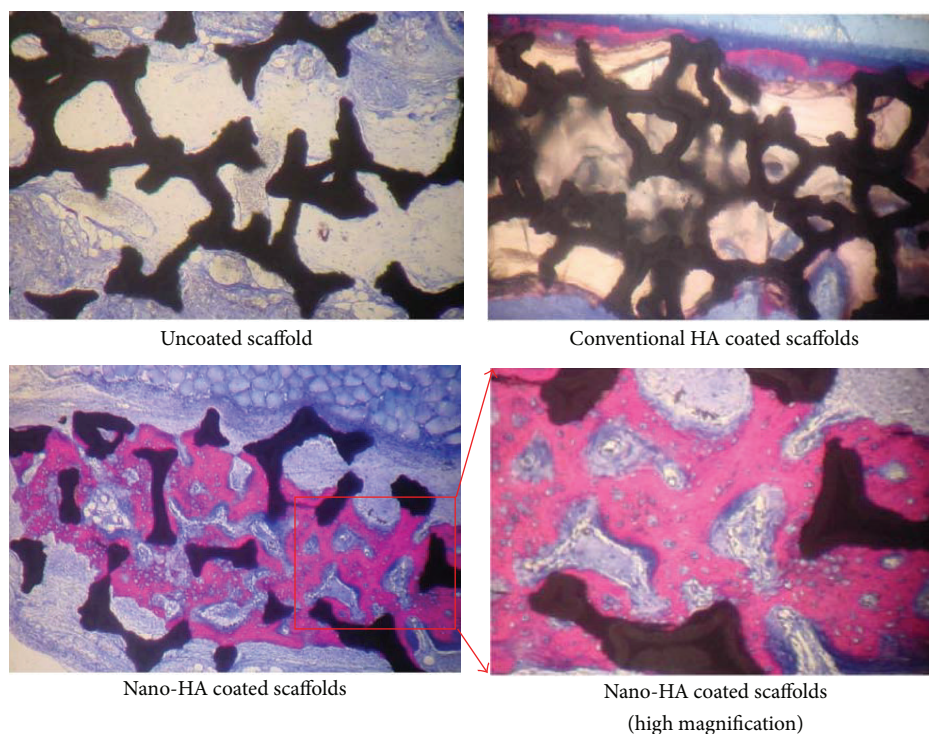


FIGURE 4: Histology of rat calvaria after 6 weeks of implantation of uncoated tantalum, conventional HA coated tantalum, and nanocrystalline HA coated tantalum. Greater amounts of new bone formation occur in the rat calvaria when implanting nanocrystalline HA coated tantalum than uncoated and conventional HA coated tantalum. Red area stands for new bone and blue stands for collagen. (Adapted with permission from [79]. Copyright 2006 Elsevier Ltd).

(TEOS) and methyltriethoxysilane (MTES, Aladdin) as silica precursors, nitric acid and acetic acid as catalysts, and absolute ethanol as solvent [53]. They successfully regulated the hydrophilicity and hydrophobicity of the final coatings by controlling TEOS/MTES molar ratios (100 : 0, 70 : 30, and 40 : 60) (Figure 5).

Moreover, Webster and colleagues demonstrated that aqueous contact angles were three times smaller when alumina grain size was decreased from 167 to 24 nm. They also reported that the adsorption of vitronectin, which stimulates osteoblasts adhesion, increased on nanophase ceramics with greater wettability. Moreover, when vitronectin adsorbed on nanophase ceramics, it was unfolded to a larger extent than on conventional ceramics, which exposed larger numbers of osteoblasts adhesive epitopes in the absorbed proteins [30]. Similar to ceramics, increased wettability of polymer composites has been achieved through the use of nanophase ceramics in order to increase bone cell function. Specifically, Kay et al. demonstrated that titania nanosized particles embedded in PLGA promoted osteoblast adhesion compared with conventional sized titania in PLGA [54]. On the other word, Macak et al. [55] thought that the signs of the antibodies reduce cell adsorption in the hydrophobic surfaces, while cell adsorption will be stimulated in the hydrophilic surfaces. However, Cai et al. [56] investigated the influence of titanium film micro- and nanoscale topography on protein adsorption and cell growth. However, by means of measuring the content of albumin and fibrinogen adsorption, they found

no statistically significant differences in protein adsorption for the films with different topographies. Moreover, no statistically significant influences of surface roughness on osteoblasts proliferation and cell viability were detected in their study. More effective data should be shared with regard to the wettability of nanostructured implant in enhancing the performance of orthopedic implants and we firmly believe that the nanostructured implant will cause desirable cells response and activity by means of modifying the hydrophilic and hydrophobic properties of implants.

3.3. Surface Chemistry. Besides the factors above, implant surface chemistry plays an important role in protein adsorption and subsequent cell adhesion and cell proliferation (Figure 6). Consequently, surface chemistry will also make a difference in the field of implants [57]. As we know, hydroxyapatite (HA) is used in the biomedical industry as the coating for titanium implants. HA is also used as the structural material for dental, maxillofacial, and orthopedic implants [58]. It has been proved that carbon nanotubes could be used to promote cells' division and proliferation [59–63]. Facca et al. [60] made a research on the osseointegration of nanodesigned composite coatings on titanium implants in vivo. They investigated study of plasma-sprayed carbon nanotubes (CNT) reinforced hydroxyapatite (HA) coating on titanium implants embedded in rodents' bone. No adverse effect or cytotoxicity of CNT addition on bone tissues and cells was observed. Normal bone growth was

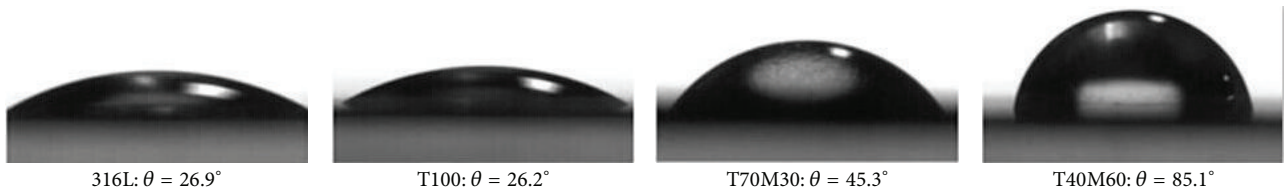


FIGURE 5: Contact angle photographs of a water droplet placed on 316L and other different sol-gel coatings. (Adapted with permission from [53]. Copyright 2012 Elsevier Ltd).

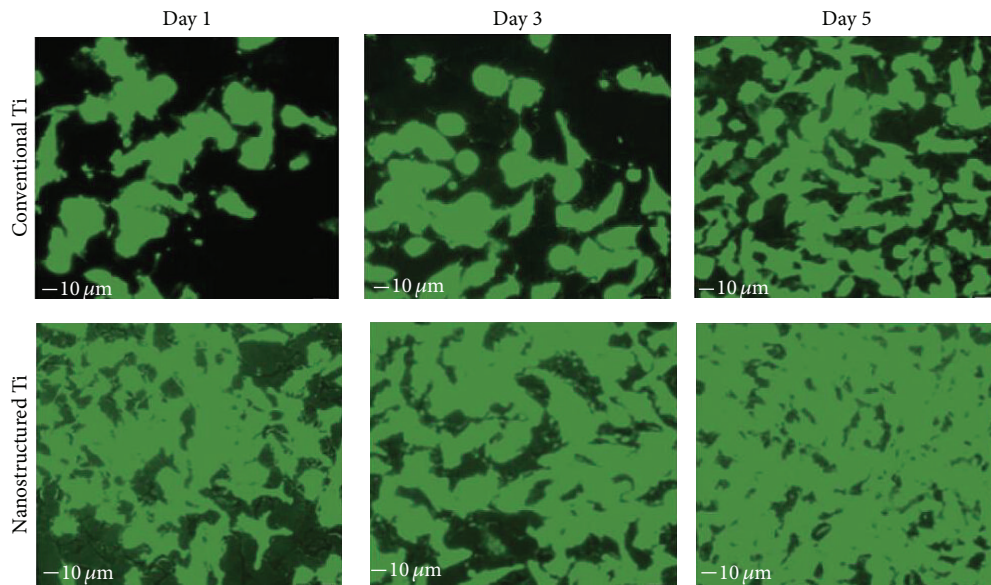


FIGURE 6: Fluorescent microscopy images of endothelial cell proliferation on nanostructured Ti compared to conventional Ti. (Adapted with permission from [34]. Copyright 2008 Elsevier Ltd).

observed around HA/CNT coated implants. CNT addition induces higher osseointegration as compared to HA. Facca et al. demonstrated that CNT addition resulted in the growth of new bone and improved osseointegration as observed from the adhesion of HA/CNT coating. Moreover, the elastic modulus of the newly grown bone was comparable with the distant bone, suggesting excellent mechanical integrity of the implant, which was consistent with previous studies [61, 62]. Finally, they considered that longer implantation is needed to further appreciate the quality of osseointegration and to evaluate safety of HA-CNT coating prior to clinical application and the study had a far-reaching significance in orthopedic applications, healing time, and osseointegration.

Besides, titanium oxide in nanoscale with different nanostructures could take on positive effects on growth rates, bone forming, and even acceleration of osteodifferentiation of MSCs [64–70]. Brammer et al. [71] discussed the effects of TiO₂ nanotube surfaces for bone regeneration. They considered that the unique 3D tube shaped nanostructure created by electrochemical anodization will have great effects on osteogenic cells and become a very promising method in orthopedic material surface designs. In addition to nanoceramic materials, another kind of commonly used materials in orthopedic implant is medical metals. As to

the method of modification of metals implants in nanoscale, various techniques have been employed in creating different topographies on the surface of implants ranging in micron scale [72–74]. Biological activity and events could be boosted in the interface of implants and bone to some extent due to the existence of micron scale surface features [75–78]. However, it is widely acknowledged that the interactions between implants and host tissue could be regulated and controlled by means of nanolevel signal transmission [79–81]. That is the reason why various strategies have been devised and implemented to nanoengineered surfaces that can directly influence biological functionalities [79, 82]. For example, Variola et al. [83] discussed the state-of-the-art nanotechnology-based approaches currently adopted to modify the surface of metals used for orthopedic and dental applications and also briefly considered their use in the cardiovascular field; moreover, they also debated the effects of nanoengineered surfaces on various in vitro molecular and cellular events and the potential influence of nanotopography on biomechanical events at interfaces. In a word, via the ability of nanostructured surfaces to activate stem cells and accelerate bone formation, bone reconstruction will be completed well without any tissue encapsulation [84–86]; moreover, this will translate into faster healing, improved

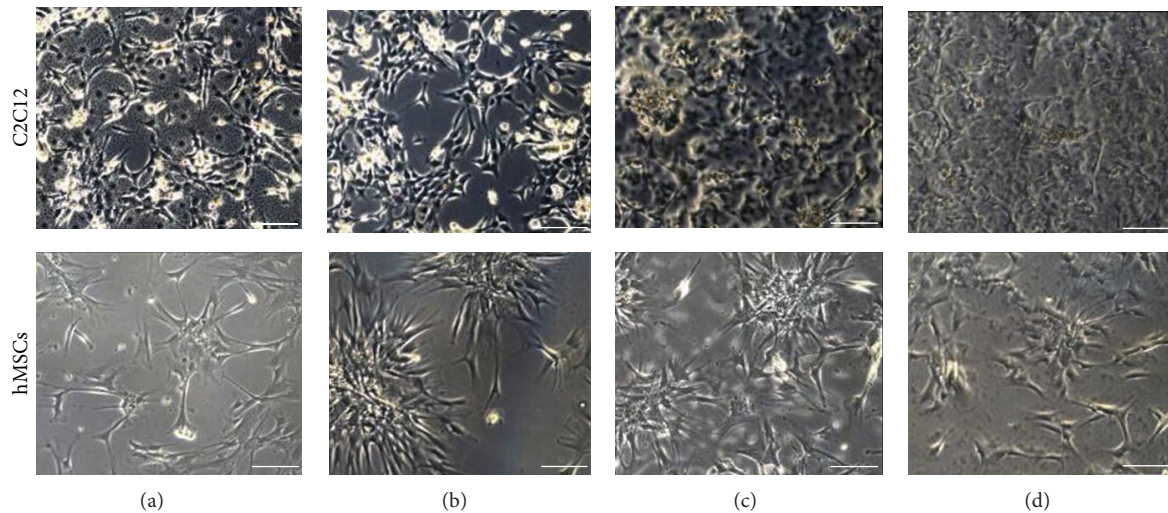


FIGURE 7: Image of C2C12 cells and hMSCs' proliferation on different films with varying surface roughness at day 3. Obviously, low surface roughness facilitated the proliferation for C2C12 cells, but the opposite case happened for hMSCs. (Size of surface roughness: (a) < (b) < (c) < (d), and scale bars stand for 200 μm). (Adapted with permission from [5]. Copyright 2011 Elsevier Ltd).

stability of dental and orthopedic prostheses, and critical aspects especially in aging patients with poor bone support.

3.4. Surface Charge. As to the concept of "surface properties," it involves so many aspects, and surface charge is vital factor to affect the cells' adhesion and activities. For example, the fact that electrostatic interaction (zeta potential) could have a great impact on different protein adsorption and cellular uptake of nanoparticles was demonstrated by Patil et al. [87]. Moreover, Cai et al. investigated the influence of titanium thin films' surface chemistry and surface electric charge properties on protein adsorption and cell proliferation. For purpose of producing surface with different surface charge, different functional groups, such as $-\text{NH}_2$ or $-\text{COOH}$, were functionalized on the surface of titanium film [88]. Finally, they concluded the lower the zeta-potential of functionalized titanium films, the lower the adsorption of fibrinogen [89]. Similarly, Chung et al. made a research on the influence of surface charge on high-performance cellular uptake and cytotoxicity of mesoporous silica nanoparticles in human mesenchymal stem cells. The tested surface was modified by especial chloride, and they determined the uptake of mesoporous silica nanoparticles using flow cytometry. In addition to human mesenchymal stem cells, 3T3-L1 cells were also employed for a contrast in terms of uptake behavior between different cells. In the end, they found that there was a distinct relationship between surface charge and cells' event. Additionally, as with the cells' response of MSNs charged positively, inhibition action was observed in 3T3-L1 cells but not in the case of human mesenchymal stem cells; moreover, a qualitative control could be made on the human mesenchymal stem with regard to their uptake behavior [89].

3.5. Surface Roughness. The effect of surface roughness on cells' behavior and activity has been investigated. Due to

contact with the host tissue directly, the surface roughness of the nanostructured implants has a great potential influence on cells' response. For instance, the effect of surface roughness and calcium phosphate coating on the bone response of titanium implants was investigated by Hayakawa et al. [90]. Titanium implants with different kinds of surface roughness were implanted into left and right tibial diaphysis and femoral condyles of the rabbits. In the end, they considered that, from the point of healing effect, a sputtered calcium phosphate coating on an implant performed best in terms of the bone response. Certainly, the conditions of implant surface and local implant site made a combined interaction on the final bone behavior. In addition, Hu et al. studied the effect of surface roughness on the myogenic and osteogenic differentiation of cells on silk-elastin biomaterials [5]. They regulated the surface roughness of materials by adjusting the ratio of tropoelastin and silk. Specifically, Hu et al. prepared several thick films with different surface roughness and then cultured human bone marrow stem cells on different films to observe the effect of surface roughness on the proliferation of C2C12 cells and hMSCs. They concluded that low surface roughness and high stiffness in the silk-tropoelastin materials promoted proliferation and myogenic differentiation of C2C12 cells. In contrast, high surface roughness with micro/nanoscale surface patterns was favored by hMSCs (Figure 7).

Moreover, the influence of surface roughness of the titanium alloy Ti6Al4V on human bone marrow cells' response and protein adsorption was studied by Deligianni et al. [91]. They deemed that cell attachment and proliferation were positively proportional to the roughness of Ti alloy; also, a larger amount of total protein and fibronectin existed on rough substratum, finally, precisely because of the distinction of adsorption in two proteins above on Ti alloy with different surface roughness, leading to the different condition in cell attachment. What is more, a rigorous study of osteoblasts and

fibroblasts' response to surface roughness was conducted by Kunzler et al. using the method of gradients of surface roughness [92]. For the purpose of forming roughness gradients, which included a wide range of roughness values, they created a specific modification process on the substratum. Calvarial osteoblasts and human gingival fibroblasts were experiments cells for studying the influence of surface roughness on cells' activity and event. Eventually, an obviously increased calvarial osteoblasts cell proliferation emerged with increasing surface roughness. However, human gingival fibroblasts took on contrary proliferation behavior, that is to say, proliferation decreasing with increasing roughness. Consequently, it fully illustrated that the response of cells to surface roughness is different depending on the cell type.

4. Conclusion and Prospective

In last several years, the development of approaches to repair bone defect has obtained great progress, one of most reasons of that is the appearance of novel nanomaterials with kinds of outstanding performance, and more excellent nanostructured implants are being on the way to be born. Despite the fact that nanostructured implants have great advantages in promoting cells' response and bone formation, a potential tremendous hidden danger still exists in using nanostructured implant. First of all, whether the nanoparticles are safe or dangerous is an issue being discussed constantly. Once put into our body, it cannot be guaranteed that implants containing nanoparticles are safe enough; even if they are safe themselves, due to long time of embedding in the surroundings of tissue, nanostructured implants will release certain nanophase particles that possibly do harm to our body. Moreover, the potential biohazards of nanosized wear particles at bone-prosthesis interface are also an important event necessary to be considered. However, the trend of nanostructured implant cannot be stopped, and the direction of future research is to get needed cell behavior by means of controlling the microstructure of implants. It has been shown that each of the above individual parameters can have a significant effect on the structure and function of adsorbed specific protein and biomolecule. Only if we have a good learning of relationship between surface properties and cells' response, can we create novel nanobiomaterials with needed structures. Clearly, more investigation on the toxicity of nanophase materials should be carried out, aiming to make accurate comparisons with conventionally sized particles in determining their potential toxicity. All in all, in spite of kinds of challenges ahead, sorts of fact proved that nanophase materials represent an important growing area of research that may improve bonding between an implant and surrounding bone. We firmly believe nanostructured implant with various surface properties will have an extremely bright future in improving orthopedic implant efficacy.

Conflict of Interests

The authors have no conflict of interests.

Authors' Contribution

Feng Zhao and Jian Wang contributed equally to this work.

References

- [1] M.-H. Cheng, E. M. Brey, A. Allori et al., "Ovine model for engineering bone segments," *Tissue Engineering*, vol. 11, no. 1-2, pp. 214–225, 2005.
- [2] M. J. Miller, "Osseous tissue engineering in oncologic surgery," *Seminars in Surgical Oncology*, vol. 19, no. 3, pp. 294–301, 2000.
- [3] E. Palin, H. Liu, and T. J. Webster, "Mimicking the nanofeatures of bone increases bone-forming cell adhesion and proliferation," *Nanotechnology*, vol. 16, no. 9, pp. 1828–1835, 2005.
- [4] P. Bills, L. Brown, X. Jiang, and L. Blunt, "A metrology solution for the orthopaedic industry," *Journal of Physics: Conference Series*, vol. 13, no. 1, pp. 316–319, 2005.
- [5] X. Hu, S.-H. Park, E. S. Gil, X.-X. Xia, A. S. Weiss, and D. L. Kaplan, "The influence of elasticity and surface roughness on myogenic and osteogenic-differentiation of cells on silk-elastin biomaterials," *Biomaterials*, vol. 32, no. 34, pp. 8979–8989, 2011.
- [6] X. Li, L. Wang, Y. Fan, Q. Feng, F.-Z. Cui, and F. Watari, "Nanostructured scaffolds for bone tissue engineering," *Journal of Biomedical Materials Research Part A*, vol. 101, no. 8, pp. 2424–2435, 2013.
- [7] C. Nelson, A. Magge, T. S. Bernard, Y. Khan, and C. T. Laurencin, "Nanostructured composites for bone repair," *Journal of Biomaterials and Tissue Engineering*, vol. 3, no. 4, pp. 426–439, 2013.
- [8] C. M. Niemeyer, "Nanoparticles, proteins, and nucleic acids: biotechnology meets materials science," *Angewandte Chemie—International Edition*, vol. 40, no. 22, pp. 4128–4158, 2001.
- [9] D. Cui and H. Gao, "Advance and prospect of bionanomaterials," *Biotechnology Progress*, vol. 19, no. 3, pp. 683–692, 2003.
- [10] X. Li, Y. Fan, and F. Watari, "Current investigations into carbon nanotubes for biomedical application," *Biomedical Materials*, vol. 5, no. 2, Article ID 022001, 2010.
- [11] G. M. Whitesides, "The 'right' size in nanobiotechnology," *Nature Biotechnology*, vol. 21, no. 10, pp. 1161–1165, 2003.
- [12] T. A. Desai, "Micro- and nanoscale structures for tissue engineering constructs," *Medical Engineering & Physics*, vol. 22, no. 9, pp. 595–606, 2001.
- [13] X. Li, X. Liu, J. Huang, Y. Fan, and F.-Z. Cui, "Biomedical investigation of CNT based coatings," *Surface and Coatings Technology*, vol. 206, no. 4, pp. 759–766, 2011.
- [14] L. A. Bauer, N. S. Birenbaum, and G. J. Meyer, "Biological applications of high aspect ratio nanoparticles," *Journal of Materials Chemistry*, vol. 14, no. 4, pp. 517–526, 2004.
- [15] L. Mazzola, "Commercializing nanotechnology," *Nature Biotechnology*, vol. 21, no. 10, pp. 1137–1143, 2003.
- [16] X. Li, H. Liu, X. Niu et al., "Osteogenic differentiation of human adipose-derived stem cells induced by osteoinductive calcium phosphate ceramics," *Journal of Biomedical Materials Research Part B: Applied Biomaterials*, vol. 97, no. 1, pp. 10–19, 2011.
- [17] K. L. Lee, G. A. Ngai, S. C. Varghese, L. Duan, and J. A. Cooper, "Nanostructures for ligament and tendon regeneration," *Journal of Biomaterials and Tissue Engineering*, vol. 3, no. 4, pp. 409–425, 2013.
- [18] J. Wang, "Nanomaterial-based amplified transduction of biomolecular interactions," *Small*, vol. 1, no. 11, pp. 1036–1043, 2005.

- [19] M. C. Powell and M. S. Kanarek, "Nanomaterial health effects—part 1: background and current knowledge," *Wisconsin Medical Journal*, vol. 105, no. 2, pp. 16–20, 2006.
- [20] J. M. Slocik and R. R. Naik, "Probing peptide-nanomaterial interactions," *Chemical Society Reviews*, vol. 39, no. 9, pp. 3454–3463, 2010.
- [21] F. S. Kaplan, W. C. Hayes, T. M. Keaveny et al., "Form and function of bone," in *Orthopaedic Basic Science*, pp. 127–184, American Academy of Orthopaedic Surgery, Rosemont, Ill, USA, 1994.
- [22] T. J. Webster, C. Ergun, R. H. Doremus, R. W. Siegel, and R. Bizios, "Enhanced functions of osteoblasts on nanophase ceramics," *Biomaterials*, vol. 21, no. 17, pp. 1803–1810, 2000.
- [23] T. J. Webster and J. U. Ejiogor, "Increased osteoblast adhesion on nanophase metals: Ti, Ti6Al4V, and CoCrMo," *Biomaterials*, vol. 25, no. 19, pp. 4731–4739, 2004.
- [24] T. J. Webster and T. A. Smith, "Increased osteoblast function on PLGA composites containing nanophase titania," *Journal of Biomedical Materials Research Part A*, vol. 74, no. 4, pp. 677–686, 2005.
- [25] S. M. Moghimi and J. Szebeni, "Stealth liposomes and long circulating nanoparticles: critical issues in pharmacokinetics, opsonization and protein-binding properties," *Progress in Lipid Research*, vol. 42, no. 6, pp. 463–478, 2003.
- [26] X. Li, Y. Yang, Y. Fan, Q. Feng, F.-Z. Cui, and F. Watari, "Bio-composites reinforced by fibers or tubes as scaffolds for tissue engineering or regenerative medicine," *Journal of Biomedical Materials Research Part A*, vol. 102, no. 5, pp. 1580–1594, 2014.
- [27] Q. A. Pankhurst, J. Connolly, S. K. Jones, and J. Dobson, "Applications of magnetic nanoparticles in biomedicine," *Journal of Physics D: Applied Physics*, vol. 36, no. 13, pp. R167–R181, 2003.
- [28] M. O. Oyewumi and R. J. Mumper, "Influence of formulation parameters on gadolinium entrapment and tumor cell uptake using folate-coated nanoparticles," *International Journal of Pharmaceutics*, vol. 251, no. 1–2, pp. 85–97, 2003.
- [29] S. M. Moghimi, A. C. Hunter, and J. C. Murray, "Long-circulating and target-specific nanoparticles: theory to practice," *Pharmacological Reviews*, vol. 53, no. 2, pp. 283–318, 2001.
- [30] K. C. Dee, D. A. Puleo, and R. Bizios, *An Introduction to Tissue-Biomaterial Interactions*, John Wiley & Sons, Hoboken, NJ, USA, 2002.
- [31] M. Tulinski and M. Jurczyk, "Nanostructured nickel-free austenitic stainless steel/hydroxyapatite composites," *Journal of Nanoscience and Nanotechnology*, vol. 12, no. 11, pp. 8779–8782, 2012.
- [32] J. E. Gagner, S. Shrivastava, X. Qian, J. S. Dordick, and R. W. Siegel, "Engineering nanomaterials for biomedical applications requires understanding the nano-bio interface: a perspective," *The Journal of Physical Chemistry Letters*, vol. 3, no. 21, pp. 3149–3158, 2012.
- [33] Y. W. Chun and T. J. Webster, "The role of nanomedicine in growing tissues," *Annals of Biomedical Engineering*, vol. 37, no. 10, pp. 2034–2047, 2009.
- [34] L. Zhang and T. J. Webster, "Nanotechnology and nanomaterials: promises for improved tissue regeneration," *Nano Today*, vol. 4, no. 1, pp. 66–80, 2009.
- [35] H. Peng, X. Liu, R. Wang, F. Jia, L. Dong, and Q. Wang, "Emerging nanostructured materials for musculoskeletal tissue engineering," *Journal of Materials Chemistry B*, vol. 2, no. 38, pp. 6435–6461, 2014.
- [36] S. B. Kennedy, N. R. Washburn, C. G. Simon Jr., and E. J. Amis, "Combinatorial screen of the effect of surface energy on fibronectin-mediated osteoblast adhesion, spreading and proliferation," *Biomaterials*, vol. 27, no. 20, pp. 3817–3824, 2006.
- [37] B. D. Boyan, C. H. Lohmann, D. D. Dean, V. L. Sylvia, D. L. Cochran, and Z. Schwartz, "Mechanisms involved in osteoblast response to implant surface morphology," *Annual Review of Materials Science*, vol. 31, pp. 357–371, 2001.
- [38] D. A. Puleo and A. Nanci, "Understanding and controlling the bone-implant interface," *Biomaterials*, vol. 20, no. 23–24, pp. 2311–2321, 1999.
- [39] K. Anselme and M. Bigerelle, "Statistical demonstration of the relative effect of surface chemistry and roughness on human osteoblast short-term adhesion," *Journal of Materials Science: Materials in Medicine*, vol. 17, no. 5, pp. 471–479, 2006.
- [40] A. M. Cortizo, "Effect of surface topography of collagen scaffolds on cytotoxicity and osteoblast differentiation," *Journal of Biomaterials and Tissue Engineering*, vol. 8, pp. 125–132, 2012.
- [41] X. Li, Y. Huang, L. Zheng et al., "Effect of substrate stiffness on the functions of rat bone marrow and adipose tissue derived mesenchymal stem cells in vitro," *Journal of Biomedical Materials Research Part A*, vol. 102, no. 4, pp. 1092–1101, 2014.
- [42] K. Lee, Y.-H. Jeong, Y.-M. Ko, H.-C. Choe, and W. A. Brantley, "Hydroxyapatite coating on micropore-formed titanium alloy utilizing electrochemical deposition," *Thin Solid Films*, vol. 549, pp. 154–158, 2013.
- [43] A. Ballo, H. Agheli, J. Lausmaa, P. Thomsen, and S. Petronis, "Nanostructured model implants for *in vivo* studies: influence of well-defined nanopore topography on *de novo* bone formation on titanium implants," *International Journal of Nanomedicine*, vol. 6, pp. 3415–3428, 2011.
- [44] R. L. Price, K. Ellison, K. M. Haberstroh, and T. J. Webster, "Nanometer surface roughness increases select osteoblast adhesion on carbon nanofiber compacts," *Journal of Biomedical Materials Research Part A*, vol. 70, no. 1, pp. 129–138, 2004.
- [45] K. Mustafa, A. Odén, A. Wennerberg, K. Hultén, and K. Arvidson, "The influence of surface topography of ceramic abutments on the attachment and proliferation of human oral fibroblasts," *Biomaterials*, vol. 26, no. 4, pp. 373–381, 2005.
- [46] R. J. Vance, D. C. Miller, A. Thapa, K. M. Haberstroh, and T. J. Webster, "Decreased fibroblast cell density on chemically degraded poly-lactic-co-glycolic acid, polyurethane, and polycaprolactone," *Biomaterials*, vol. 25, no. 11, pp. 2095–2103, 2004.
- [47] X. Li, C. A. van Blitterswijk, Q. Feng, F. Cui, and F. Watari, "The effect of calcium phosphate microstructure on bone-related cells *in vitro*," *Biomaterials*, vol. 29, no. 23, pp. 3306–3316, 2008.
- [48] K. Webb, V. Hlady, and P. A. Tresco, "Relationships among cell attachment, spreading, cytoskeletal organization, and migration rate for anchorage-dependent cells on model surfaces," *Journal of Biomedical Materials Research*, vol. 49, no. 3, pp. 362–368, 2000.
- [49] H. Liao, A. S. Andersson, D. Sutherland, S. Petronis, B. Kasemo, and P. Thomsen, "Response of rat osteoblast-like cells to microstructured model surfaces *in vitro*," *Biomaterials*, vol. 24, no. 4, pp. 649–654, 2003.
- [50] X. Li, Q. Feng, X. Liu, W. Dong, and F. Cui, "Collagen-based implants reinforced by chitin fibres in a goat shank bone defect model," *Biomaterials*, vol. 27, no. 9, pp. 1917–1923, 2006.
- [51] J. K. Koper and J. Jakubowicz, "Correlation of wettability with surface structure and morphology of the anodically oxidized titanium implants," *Journal of Biomaterials and Tissue Engineering*, vol. 4, no. 6, pp. 459–464, 2014.

- [52] X. Liu and P. X. Ma, "Polymeric scaffolds for bone tissue engineering," *Annals of Biomedical Engineering*, vol. 32, no. 3, pp. 477–486, 2004.
- [53] M. Wang, Y. Wang, Y. Chen, and H. Gu, "Improving endothelialization on 316L stainless steel through wettability controllable coating by sol-gel technology," *Applied Surface Science*, vol. 268, pp. 73–78, 2013.
- [54] S. Kay, A. Thapa, K. M. Haberstroh, and T. J. Webster, "Nanos-structured polymer/nanophase ceramic composites enhance osteoblast and chondrocyte adhesion," *Tissue Engineering*, vol. 8, no. 5, pp. 753–761, 2002.
- [55] J. M. Macak, H. Tsuchiya, A. Ghicov et al., "TiO₂ nanotubes: Self-organized electrochemical formation, properties and applications," *Current Opinion in Solid State and Materials Science*, vol. 11, no. 1-2, pp. 3–18, 2007.
- [56] K. Cai, J. Bossert, and K. D. Jandt, "Does the nanometre scale topography of titanium influence protein adsorption and cell proliferation?" *Colloids and Surfaces B: Biointerfaces*, vol. 49, no. 2, pp. 136–144, 2006.
- [57] A. Palmquist, H. Engqvist, J. Lausmaa, and P. Thomsen, "Commercially available dental implants: review of their surface characteristics," *Journal of Biomaterials and Tissue Engineering*, vol. 2, no. 2, pp. 112–124, 2012.
- [58] A. A. Campbell, "Bioceramics for implant coatings," *Materials Today*, vol. 6, no. 11, pp. 26–30, 2003.
- [59] X. Li, H. Gao, M. Uo et al., "Maturation of osteoblast-like SaoS2 induced by carbon nanotubes," *Biomedical Materials*, vol. 4, no. 1, Article ID 015005, 2009.
- [60] S. Facca, D. Lahiri, F. Fioretti et al., "In vivo osseointegration of nano-designed composite coatings on titanium implants," *ACS Nano*, vol. 5, no. 6, pp. 4790–4799, 2011.
- [61] K. Balani, R. Anderson, T. Laha et al., "Plasma-sprayed carbon nanotube reinforced hydroxyapatite coatings and their interaction with human osteoblasts in vitro," *Biomaterials*, vol. 28, no. 4, pp. 618–624, 2007.
- [62] D. Lahiri, A. P. Benaduce, F. Rouzaud et al., "Wear behavior and in vitro cytotoxicity of wear debris generated from hydroxyapatite-carbon nanotube composite coating," *Journal of Biomedical Materials Research Part A*, vol. 96, no. 1, pp. 1–12, 2011.
- [63] X. Li, H. Liu, X. Niu et al., "The use of carbon nanotubes to induce osteogenic differentiation of human adipose-derived MSCs in vitro and ectopic bone formation in vivo," *Biomaterials*, vol. 33, no. 19, pp. 4818–4827, 2012.
- [64] K. C. Popat, R. H. Daniels, R. S. Dubrow, V. Hardev, and T. A. Desai, "Nanostructured surfaces for bone biotemplating applications," *Journal of Orthopaedic Research*, vol. 24, no. 4, pp. 619–627, 2006.
- [65] K. C. Popat, L. Leoni, C. A. Grimes, and T. A. Desai, "Influence of engineered titania nanotubular surfaces on bone cells," *Biomaterials*, vol. 28, no. 21, pp. 3188–3197, 2007.
- [66] E. E. L. Swan, K. C. Popat, C. A. Grimes, and T. A. Desai, "Fabrication and evaluation of nanoporous alumina membranes for osteoblast culture," *Journal of Biomedical Materials Research Part A*, vol. 72, no. 3, pp. 288–295, 2005.
- [67] X. M. Li, W. Liu, L. W. Sun et al., "Effects of physicochemical properties of nanomaterials on their toxicity," *Journal of Biomedical Materials Research Part A*, 2015.
- [68] J. Park, S. Bauer, K. A. Schlegel, F. W. Neukam, K. D. von Mark, and P. Schmuki, "TiO₂ nanotube surfaces: 15 nm—an optimal length scale of surface topography for cell adhesion and differentiation," *Small*, vol. 5, no. 6, pp. 666–671, 2009.
- [69] J. Park, S. Bauer, K. von der Mark, and P. Schmuki, "Nanosize and vitality: TiO₂ nanotube diameter directs cell fate," *Nano Letters*, vol. 7, no. 6, pp. 1686–1691, 2007.
- [70] S. Oh, K. S. Brammer, Y. S. J. Li et al., "Stem cell fate dictated solely by altered nanotube dimension," *Proceedings of the National Academy of Sciences of the United States of America*, vol. 106, no. 7, pp. 2130–2135, 2009.
- [71] K. S. Brammer, C. J. Frandsen, and S. Jin, "TiO₂ nanotubes for bone regeneration," *Trends in Biotechnology*, vol. 30, no. 6, pp. 315–322, 2012.
- [72] S. Guizzardi, C. Galli, D. Martini et al., "Different titanium surface treatment influences human mandibular osteoblast response," *Journal of Periodontology*, vol. 75, no. 2, pp. 273–282, 2004.
- [73] K. Anselme and M. Biggerelle, "Topography effects of pure titanium substrates on human osteoblast long-term adhesion," *Acta Biomaterialia*, vol. 1, no. 2, pp. 211–222, 2005.
- [74] X. Li, X. Liu, W. Dong et al., "In vitro evaluation of porous poly(L-lactic acid) scaffold reinforced by chitin fibers," *Journal of Biomedical Materials Research—Part B Applied Biomaterials*, vol. 90, no. 2, pp. 503–509, 2009.
- [75] M.-J. Kim, M.-U. Choi, and C.-W. Kim, "Activation of phospholipase D1 by surface roughness of titanium in MG63 osteoblast-like cell," *Biomaterials*, vol. 27, no. 32, pp. 5502–5511, 2006.
- [76] J.-W. Park, I.-S. Jang, and J.-Y. Sun, "Bone response to endosseous titanium implants surface-modified by blasting and chemical treatment: a histomorphometric study in the rabbit femur," *Journal of Biomedical Materials Research Part B: Applied Biomaterials*, vol. 84, no. 2, pp. 400–407, 2008.
- [77] H. Dagaard, B. Elmengaard, J. E. Bechtold, and K. Soballe, "Bone growth enhancement in vivo on press-fit titanium alloy implants with acid etched microtexture," *Journal of Biomedical Materials Research—Part A*, vol. 87, no. 2, pp. 434–440, 2008.
- [78] R. Celletti, V. C. Marinho, T. Traini et al., "Bone contact around osseointegrated implants: a histologic study of acid-etched and machined surfaces," *Journal of Long-Term Effects of Medical Implants*, vol. 16, no. 2, pp. 131–143, 2006.
- [79] H. Liu and T. J. Webster, "Nanomedicine for implants: a review of studies and necessary experimental tools," *Biomaterials*, vol. 28, no. 2, pp. 354–369, 2007.
- [80] X. Li, H. Gao, M. Uo et al., "Effect of carbon nanotubes on cellular functions in vitro," *Journal of Biomedical Materials Research Part A*, vol. 91, no. 1, pp. 132–139, 2009.
- [81] G. Mendonça, D. B. S. Mendonça, F. J. L. Aragão, and L. F. Cooper, "Advancing dental implant surface technology: from micron-to nanotopography," *Biomaterials*, vol. 29, no. 28, pp. 3822–3835, 2008.
- [82] F. Variola, F. Vetrone, L. Richert et al., "Improving biocompatibility of implantable metals by nanoscale modification of surfaces: an overview of strategies, fabrication methods, and challenges," *Small*, vol. 5, no. 9, pp. 996–1006, 2009.
- [83] F. Variola, J. B. Brunski, G. Orsini, P. T. de Oliveira, R. Wazen, and A. Nanci, "Nanoscale surface modifications of medically relevant metals: State-of-the art and perspectives," *Nanoscale*, vol. 3, no. 2, pp. 335–353, 2011.
- [84] F. Variola, J.-H. Yi, L. Richert, J. D. Wuest, F. Rosei, and A. Nanci, "Tailoring the surface properties of Ti6Al4V by controlled chemical oxidation," *Biomaterials*, vol. 29, no. 10, pp. 1285–1298, 2008.
- [85] X. Liu, X. Li, Y. Fan et al., "Repairing goat tibia segmental bone defect using scaffold cultured with mesenchymal stem

- cells,” *Journal of Biomedical Materials Research Part B: Applied Biomaterials*, vol. 94, no. 1, pp. 44–52, 2010.
- [86] R. E. McMahon, L. Wang, R. Skoracki, and A. B. Mathur, “Development of nanomaterials for bone repair and regeneration,” *Journal of Biomedical Materials Research Part B Applied Biomaterials*, vol. 101, no. 2, pp. 387–397, 2013.
- [87] S. Patil, A. Sandberg, E. Heckert, W. Self, and S. Seal, “Protein adsorption and cellular uptake of cerium oxide nanoparticles as a function of zeta potential,” *Biomaterials*, vol. 28, no. 31, pp. 4600–4607, 2007.
- [88] K. Cai, M. Frant, J. Bossert, G. Hildebrand, K. Liefeth, and K. D. Jandt, “Surface functionalized titanium thin films: zeta-potential, protein adsorption and cell proliferation,” *Colloids and Surfaces B: Biointerfaces*, vol. 50, no. 1, pp. 1–8, 2006.
- [89] T.-H. Chung, S.-H. Wu, M. Yao et al., “The effect of surface charge on the uptake and biological function of mesoporous silica nanoparticles in 3T3-L1 cells and human mesenchymal stem cells,” *Biomaterials*, vol. 28, no. 19, pp. 2959–2966, 2007.
- [90] T. Hayakawa, M. Yoshinari, K. Nemoto, J. G. C. Wolke, and J. A. Jansen, “Effect of surface roughness and calcium phosphate coating on the implant/bone response,” *Clinical Oral Implants Research*, vol. 11, no. 4, pp. 296–304, 2000.
- [91] D. D. Deligianni, N. Katsala, S. Ladas, D. Sotiropoulou, J. Amedee, and Y. F. Missirlis, “Effect of surface roughness of the titanium alloy Ti-6Al-4V on human bone marrow cell response and on protein adsorption,” *Biomaterials*, vol. 22, no. 11, pp. 1241–1251, 2001.
- [92] T. P. Kunzler, T. Drobek, M. Schuler, and N. D. Spencer, “Systematic study of osteoblast and fibroblast response to roughness by means of surface-morphology gradients,” *Biomaterials*, vol. 28, no. 13, pp. 2175–2182, 2007.

Research Article

Effects of Carboxylated Multiwalled Carbon Nanotubes on the Function of Macrophages

Xia Dong, Lanxia Liu, Dunwan Zhu, Hailing Zhang, Yingxin Li, and Xigang Leng

Tianjin Key Laboratory of Biomedical Materials, Institute of Biomedical Engineering, Chinese Academy of Medical Sciences and Peking Union Medical College, Tianjin 300192, China

Correspondence should be addressed to Xigang Leng; lengxgyky@163.com

Received 14 October 2014; Accepted 25 December 2014

Academic Editor: Shuming Zhang

Copyright © 2015 Xia Dong et al. This is an open access article distributed under the Creative Commons Attribution License, which permits unrestricted use, distribution, and reproduction in any medium, provided the original work is properly cited.

Multiwalled carbon nanotubes (MWCNTs) have tremendous potential in many areas of research and applications. Modification of MWCNTs with carboxyl group is one of the widely used strategies to increase their water dispersibility. However, the effect of carboxylation of MWCNTs on their interaction with macrophages remains unclear. The current study compared the impact of pristine MWCNTs (p-MWCNTs) and carboxylic acid functionalized MWCNTs (MWCNTs-COOH) on RAW264.7 cells by looking at the cell viability, phagocytic activity, production of cytokines (IL-1 β , IL-10, IL-12, and TNF- α), and intracellular reactive oxygen species (ROS). It was revealed that exposure to either p-MWCNTs or MWCNTs-COOH induced decreased viability of murine macrophage RAW 264.7 cells and moderately elevated phagocytic activity of murine peritoneal macrophages, but no statistical significance was found between the two groups. Increased production of ROS in macrophages was induced after exposure to either p-MWCNTs or MWCNTs-COOH. However, no significantly elevated production of cytokines (IL-1 β , IL-10, IL-12, and TNF- α) was observed from RAW 264.7 cells after exposure to the CNTs. Those data suggested that modification with carboxyl group did not exert obvious impact on the interaction of MWCNTs with macrophages.

1. Introduction

Carbon nanotubes (CNTs), which are usually classified into single-walled carbon nanotubes (SWCNTs) and multiwalled carbon nanotubes (MWCNTs) [1], have won enormous popularity in nanotechnology for their unique properties and applications. The rapid development of nanotechnology has renewed potential applications within commercial, environmental, and medical sectors, including electronic devices, polymer composites, enzymatic films, scaffolds for tissue engineering, and nanoscale constructs for intracellular drug/gene delivery or tracking and detecting diseases [2–6]. The broad range of increasing applications for CNTs will almost certainly result in increased potential for both human and environmental exposures to these nanomaterials. Therefore, it is essential to ascertain the potential hazards of CNTs to humans and other biological systems. A number of in vivo and in vitro studies have been conducted to evaluate the biological impacts of CNTs. In vivo studies demonstrated

that intratracheally introduced CNTs induced granulomas in rat and mice lungs [7, 8]. Studies on the cytotoxicity of CNTs against a variety of cell lines revealed that CNTs induced elevated release of IL-8 in human epidermal keratinocytes [9], DNA damage in mouse embryonic stem cells [10], apoptosis of T lymphocyte [11], and reduced proliferation of rat aortic smooth muscle cells [12].

Generally, metal dissolution, size effect, and surface chemistry have been cited as major factors indicating cytotoxicity of CNTs. Several investigations were conducted on SWCNTs with varying metal content to evaluate their cytotoxicity [13, 14]. The size, shape, and length of CNTs were also found to significantly impact on the cytotoxicity [15]. Modification of CNTs with different chemical groups was used to enhance their solubility and biocompatibility; each was likely to result in different cytotoxicity [16, 17]. Covalent functionalization by oxidation with strong oxidants to generate carboxylic acid groups or carboxylated fractions on the surface of the CNT is one of the widely used strategies

to increase their water miscibility. Various molecules can be further coupled to the surface of carboxylated CNTs (CNTs-COOH) for the desired applications. However, the impact of carboxylation of CNTs on their cytotoxicity is far from being completely understood.

Macrophages are the key cells in mediating the inflammatory responses to foreign substances, especially particulate substances such as nanoparticles, through phagocytosis and secretion of proinflammatory cytokines [18, 19]. Therefore, the interaction of CNTs with macrophages may affect the cytotoxicity of CNTs and could thus be employed to evaluate their biocompatibility. Previous study conducted by Shvedova et al. demonstrated that SWCNTs induced recruitment and activation of macrophages in the lung of exposed animals [20]. Results from other study showed that SWCNTs or MWCNTs were cytotoxic and genotoxic on murine macrophages [21–24] and could cause incomplete phagocytosis or mechanically pierce through the plasma membrane and result in oxidative stress and cell death in human macrophage cells [22].

The current study was aimed at evaluating the impact of carboxylation on the cytotoxicity of CNTs by comparing the interactions of pristine MWCNTs (p-MWCNTs) and carboxylated MWCNTs (MWCNTs-COOH) with murine macrophage cell line RAW264.7 cells. It was revealed that exposure to either p-MWCNTs or MWCNTs-COOH induced decreased viability of murine macrophage RAW 264.7 cells and elevated phagocytic activity of murine peritoneal macrophages, but no statistical significance was found between the two groups. Increased production of ROS in macrophages was induced after exposure to either p-MWCNTs or MWCNTs-COOH. However, no significantly elevated production of cytokines (IL-1 β , IL-10, IL-12, and TNF- α) was observed from RAW 264.7 cells after exposure to the CNTs.

2. Materials and Methods

2.1. Materials. p-MWCNTs and MWCNTs-COOH were purchased from Chengdu Organic Chemicals Co. Ltd. (Sichuan, China). The MWCNTs were characterized with transmission electron microscope (TEM) (JEM-1010, JEOL, Japan), scanning electron microscope (SEM) (X-650, HITACHI, Japan), and X-ray photoelectron spectroscopy (XPS) (PHI-1600 ESCA, Perkin-Elmer, USA) in our previous study [25]. It was demonstrated that the two MWCNTs had a similar surface topography and size (average outside diameters of 10 to 20 nm and average length of 10 to 30 μ m). It also revealed the presence of carboxyl groups on the MWCNTs-COOH and the absence of any metal elements on the two kinds of MWCNTs. Murine macrophage cell line RAW264.7 was obtained from ATCC (Manassas, VA, USA). FBS was obtained from Hyclone (Logan, UT, USA). Lipopolysaccharide (LPS) and 2',7'-dichlorofluorescein (DCF) were purchased from Sigma-Aldrich (St. Louis, MO, USA). CellTiter-Glo Luminescent Cell Viability Assay Kits were purchased from Promega (Madison, WI, USA). Immunoassay Kits for murine cytokines (IL-1 β , IL-10, IL-12, and TNF- α) were

purchased from BioSource International, Inc. (Camarillo, California, USA).

2.2. Preparation of CNT Suspensions. The MWCNTs were dispersed in PBS to prepare stock suspensions (2 mg/mL) and sonicated (Ultra sonic processor KQ22000DE) at 25°C, 80 W for 20 min. The stock suspensions were then heat-sterilized. To prepare test concentrations, the solution was sonicated again and then serially diluted with serum-free DMEM medium.

2.3. Cell Viability Assay. RAW264.7 cells were grown in DMEM supplemented with 1% L-glutamine, 1% penicillin/streptomycin, and 10% heat inactivated FBS. The cells were seeded into a 96-well plate at a density of 5×10^4 cells/mL (100 μ L per well) and incubated for 24 hours at 37°C in a humidified 5% CO₂ incubator. The cells were then divided into 3 groups (6 wells/group) and treated with different concentrations (1, 10, 100, and 200 μ g/mL, resp.) of p-MWCNTs, MWCNTs-COOH, and fresh medium alone (negative control), respectively, leaving 8 wells without cells as blank control. After 12, 24, 48, and 72 hours of cocultivation, 100 μ L of CellTiter-Glo Reagent was added to each well and incubated at room temperature for 10 minutes to stabilize the luminescent signal. The luminescent intensity was measured in a microtiter plate reader (VARIOSKAN FLASH, Thermo, MA, USA). The viability of cell was calculated with the following formula: cell viability ratio (%) = $(A_{\text{test}} - A_{\text{blank}}) / (A_{\text{negative}} - A_{\text{blank}}) \times 100$.

2.4. ELISA for Cytokines. RAW264.7 cells were seeded in a 24-well plate at a density of 5×10^4 cells/mL (2 mL per well) and cocultivated with p-MWCNTs or MWCNTs-COOH at the concentrations of 1, 10, 100, and 200 μ g/mL, respectively. The cells treated with 1 μ g/mL LPS were used as the positive control, whereas the untreated cells were employed as the negative control. After 12, 24, 48, and 72 hours of cocultivation, aliquots of the cell supernatant were collected, centrifuged, and stored at -80°C for cytokine determination. The concentration of cytokines (IL-1 β , IL-10, IL-12, and TNF- α) in the cell supernatant was determined by enzyme-linked immunosorbent assay according to the manufacturer's instructions. Optical density was measured at 450 nm using a microtiter plate reader (VARIOSKAN FLASH, Thermo, MA, USA). Each ELISA test was performed in duplicate and the experiment was repeated three times. The amount of the cytokines in the cell supernatants was calculated by reference to the standard curve constructed with fixed concentrations of the human recombinant cytokines provided in the kits.

2.5. Detection of Phagocytic Activity of the Macrophages. A total of 24 mice (25 g, male) were randomly divided into 4 groups (six/group). Groups 1, 2, and 3 were peritoneally injected with 1 mL of p-MWCNTs (200 μ g/mL), MWCNTs-COOH (200 μ g/mL), and LPS (1 μ g/mL) solution, respectively, leaving group 4 untreated. 24 hours after inoculation, the murine peritoneal macrophages were harvested by centrifugation and suspended in 0.9% NaCl solution.

After that, 50 μL of the cell suspension containing 2×10^6 cells/mL was incubated with equal volume of freshly prepared suspension of 5% chicken red blood cells (CRBCs) at 37°C for 30 minutes. The phagocytosis of the CRBCs by macrophages was observed under a microscope (Leica, Germany) with a magnification of 1000 after staining with Wright-Giemsa. The phagocytic rate (PR) and phagocytic index (PI) were calculated with the following formulas: PR = (the number of macrophages containing CRBC/total number of the macrophages) \times 100%; PI = (total number of the phagocytosed CRBC/total number of macrophages).

2.6. ROS Detection. The formation of intracellular ROS was measured by monitoring the increase in the intensity of fluorescence generated by 2',7'-dichlorofluorescein (DCF). RAW264.7 cells were seeded in a 24-well plate at a density of 5×10^4 cells/mL (2 mL per well) and coincubated with p-MWCNTs or MWCNTs-COOH at the concentrations of 1, 10, 100, and 200 $\mu\text{g/mL}$, respectively, with the cells treated with 100 μM H_2O_2 as positive control and the untreated cells as negative control. After 12, 24, 48, and 72 hours of incubation, the cells were washed with PBS twice and subsequently incubated with 500 μL DCFH-DA diluted with serum-free medium (1:1000) for 30 minutes at 37°C in a humidified 5% CO_2 incubator. After that, the liquid was removed and the plate was washed with PBS three times to remove the unaffiliated fluorescent probes. 500 μL of serum-free medium was added and incubated for 30 minutes at 37°C, followed by measuring the fluorescent intensity in a microtiter plate reader (VARIOSKAN FLASH, Thermo, USA) with exciting wavelength of 485 nm and emitting wavelength of 535 nm.

2.7. Statistical Analysis. Data were presented as the mean of six individual observations with standard deviation. The statistical analysis was performed using the ANOVA (a one-way analysis of variance), followed by Bonferroni *t*-test for comparison with the control group. Statistical significance was determined at $P < 0.05$.

3. Results and Discussion

Knowledge about the biological impact of functionalized CNTs and the underlying mechanisms is crucial for designing CNTs with improved biocompatibility. Increasing efforts have been focused on studying the interaction between functionalized CNTs and cells, but the results remained conflicting. There were several reports showing that oxidation of CNTs was associated with decreased cytotoxicity and improved biocompatibility, while other studies reported that functionalized CNTs were more cytotoxic. Bellucci et al. compared the toxicity of pristine and oxidized MWCNTs on human T cells and observed that oxidized CNTs were more toxic than pristine CNTs [26]. Jos et al. showed that toxic effects in Caco cells were induced from 100 $\mu\text{g/mL}$ SWCNTs-COOH, but the cytotoxic effect of pristine CNTs at the same concentration was not observed in their study [27]. Liu et al. recently demonstrated that CNTs-COOH induced autophagic cell death in A549 cells through the

AKT-TSC2-mTOR pathway and caused acute lung injury *in vivo*, whereas polyaminobenzene sulfonic acid-CNT (PABS-CNT) and polyethylene Glycol-CNT (PEG-CNT) did not [28]. The effects of carboxylic acid functionalized CNTs on macrophages are of great interest due to the pivotal role macrophages play in the interaction between the body and foreign particulate substances including CNTs. Albeit there have been several studies reporting the interaction between pristine CNTs and macrophages, little information has been accumulated regarding the impact of carboxylic acid functionalized CNT on macrophages. The primary goal of the present study was to investigate the interaction between MWCNTs-COOH and macrophages.

The divergent findings about the biological effects of functionalized CNTs may attribute to a variety of factors including the sizes and shapes of CNTs, metal impurities, and adsorption of the FBS onto the surface of the CNTs, which can seriously influence the toxicological evaluation of CNT. Therefore, it is pivotally important to characterize the CNTs before toxicity assessment. Both p-MWCNT and MWCNT-COOH employed in the current study were characterized with TEM, SEM, and XPS in our previous investigation [25], which demonstrated the existence of carboxyl group on the surface of MWCNT-COOH, the similarity of MWCNT-COOH with p-MWCNT in morphology and size, and absence of any detectable metal residues on both CNTs. Since CNT might adsorb the FBS proteins in the culture medium and thus lead to decreased cell viability [29], the stock suspension of both CNTs used in the present study was prepared with PBS in an attempt to avoid the adsorption of the FBS proteins in the culture medium onto the surface of the CNTs before incubation with cells.

While MTT assay has been widely used in the assessment of cell viability, it may result in unreliable results when employed for toxicological evaluation of CNT due to the fact that CNT can interact with formed MTT-formazan crystals and thus interfere with the evaluation of the toxicity of CNTs, leading to quite different results as compared with that utilizing water soluble tetrazolium salts (WST-1) [30]. It was also reported that CNT can interact with a number of other dyes, including WST-1, Neutral Red, and Alamar BlueTM [31], most likely through physical sorption. This can lead to false reading of the toxicity and make these assays inappropriate for quantitative evaluation of the toxicity of CNT. Therefore, we chose to evaluate the cytotoxicity of the CNTs by CellTiter-Glo Luminescent Cell Viability Assay, which determines the number of active cells based on the luciferase reaction generating a stable "glow-type" luminescent signal, which is not influenced by CNT. As shown in Figure 1, both p-MWCNT and MWCNT-COOH induced decreased viability of RAW264 cells in a dose-dependent manner; however, there is no significant difference between the two groups. The CNT at 1 $\mu\text{g/mL}$ was not found to cause any obvious cytotoxicity within 72 hours of exposure. 24 hours of exposure to 10 $\mu\text{g/mL}$ CNTs led to significantly decreased cell viability ($61.46 \pm 3.65\%$ for MWCNT-COOH and $60.37 \pm 4.41\%$ for p-MWCNT), and even sharper decrease in cell viability was observed after exposure to 100 and 200 $\mu\text{g/mL}$ of p-MWCNT or MWCNT-COOH. However, the

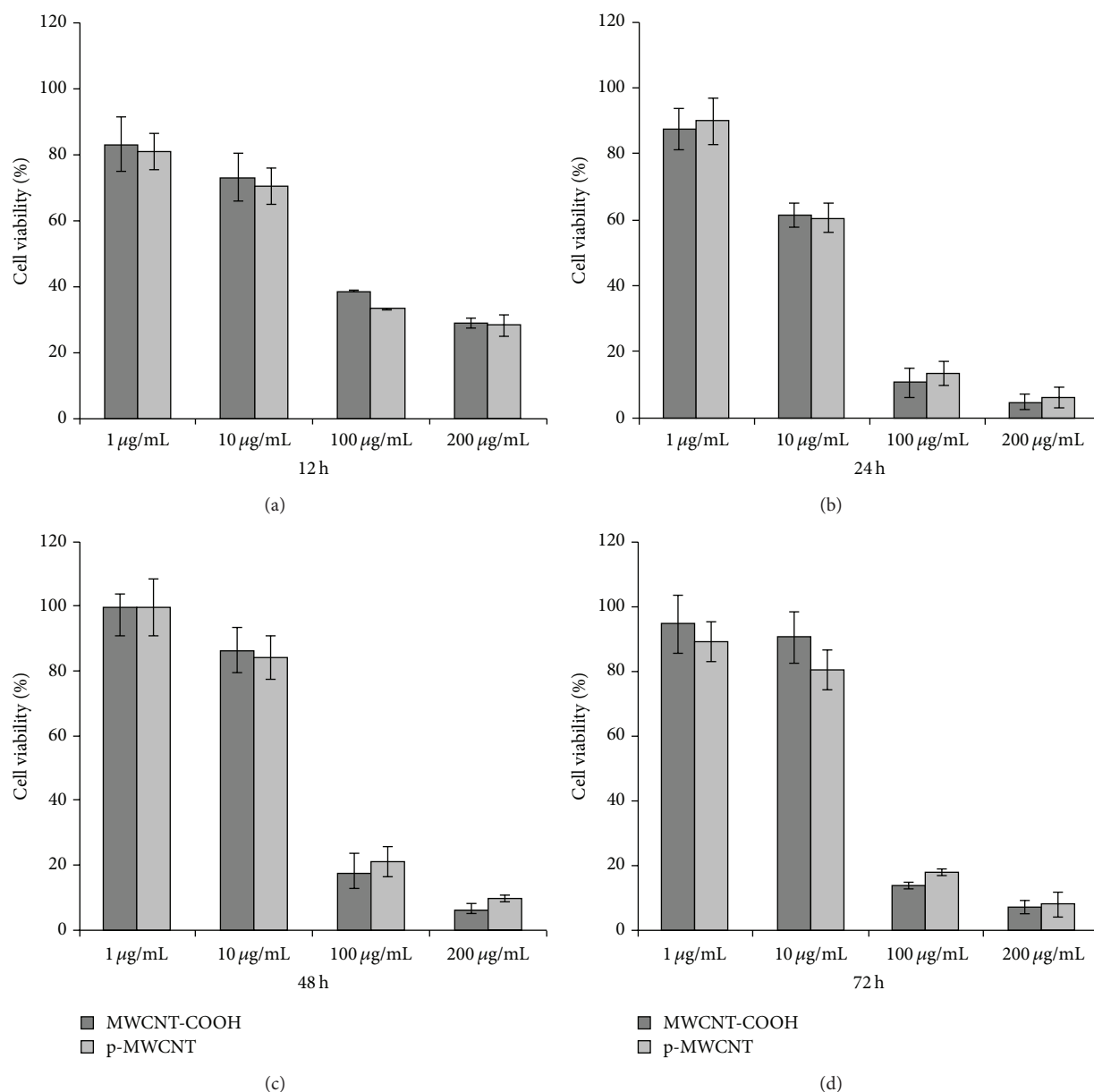


FIGURE 1: The effect of p-MWCNTs and MWCNTs-COOH on the cell viability.

cell viability bounced back after 48 hours of exposure ($86.35 \pm 7.01\%$ in MWCNT-COOH group and $84.01 \pm 6.82\%$ in p-MWCNT group). This observation was different from our previous report that MWCNT-COOH was less toxic against normal liver cell line LO2 cells, providing further evidence of the cell type dependence of CNT cytotoxicity [25]. It is also worth noting that the cytotoxicity reached to the highest level after 24 hours of incubation, and after that, cell viability gradually recovered, which indicated that RAW264.7 cells had a self-adaptation and self-renewal process after 24 hours of exposure to p-MWCNT or MWCNT-COOH.

Since macrophages are important cells for mediating the inflammatory responses to foreign particulate substances through phagocytosis and secretion of proinflammatory cytokines, it is also vitally important to learn the

impact of MWCNTs-COOH on the cytokine production by macrophages and their phagocytic activity. Four different cytokines were selected in the current study, which included IL-1 β , IL-10, IL-12, and TNF- α . Three of them, including IL-1 β , IL-12, and TNF- α , are proinflammatory cytokines which upregulate the inflammatory response [32], whereas IL-10 is an anti-inflammatory cytokine which downregulates the release of cytokines [33, 34]. It was shown from Figure 2 that neither p-MWCNTs nor MWCNTs-COOH induced any significant changes in the production of the 4 cytokines by RAW264.7 cells at the concentrations ranging from 1 to 200 µg/mL for up to 72 hours of coincubation. However, LPS, a strong inflammation-stimulating agent that is able to induce release of inflammatory cytokines by macrophages, induced significantly elevated release of the four cytokines,

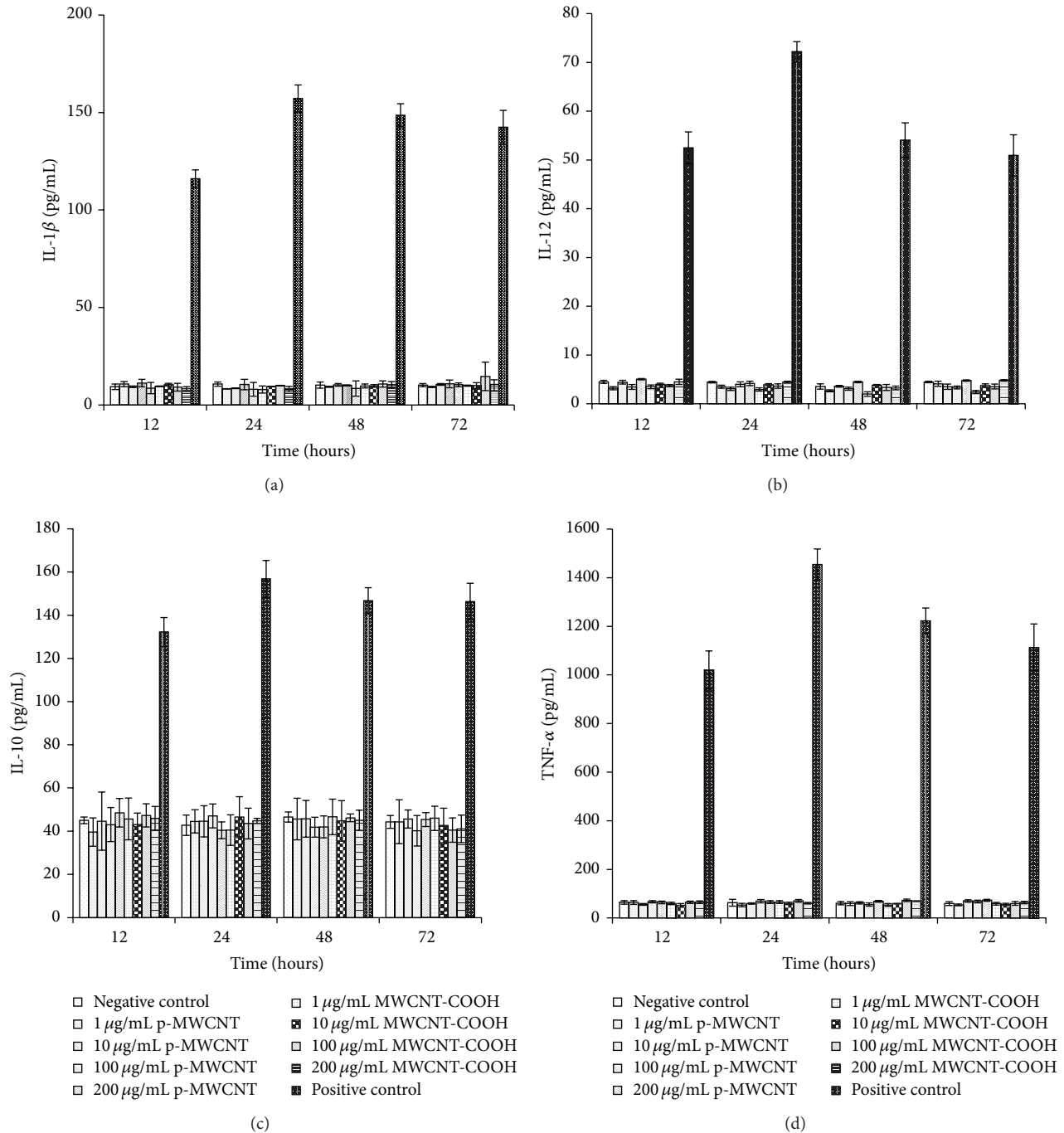


FIGURE 2: The impact of p-MWCNTs and MWCNTs-COOH on the production of cytokines in RAW264.7 cells. (a) IL-1 β , (b) IL-12, (c) IL-10, and (d) TNF- α .

confirming the reactivity of the RAW264.7 cells to the inflammatory stimuli. To learn if the CNTs would affect the phagocytic activity of the macrophages, p-MWCNTs or MWCNTs-COOH at a concentration of 200 μ g/mL were injected into the peritoneal cavity of mice and the murine peritoneal macrophages were harvested 24 hours later to assess the phagocytic activity. As demonstrated in Table 1, PR was $25.13 \pm 6.79\%$, $26.67 \pm 5.46\%$, $48.38 \pm 3.74\%$,

and $17.17 \pm 4.35\%$ for the p-MWCNTs exposure group, MWCNTs-COOH exposure group, LPS exposure group, and negative control, respectively, whereas PI was 0.804 ± 0.068 , 0.795 ± 0.113 , 1.929 ± 0.203 , and 0.542 ± 0.069 for the p-MWCNTs exposure group, MWCNTs-COOH exposure group, LPS exposure group, and negative control, respectively. These results indicated that both p-MWCNTs and MWCNTs-COOH induced moderately elevated phagocytic

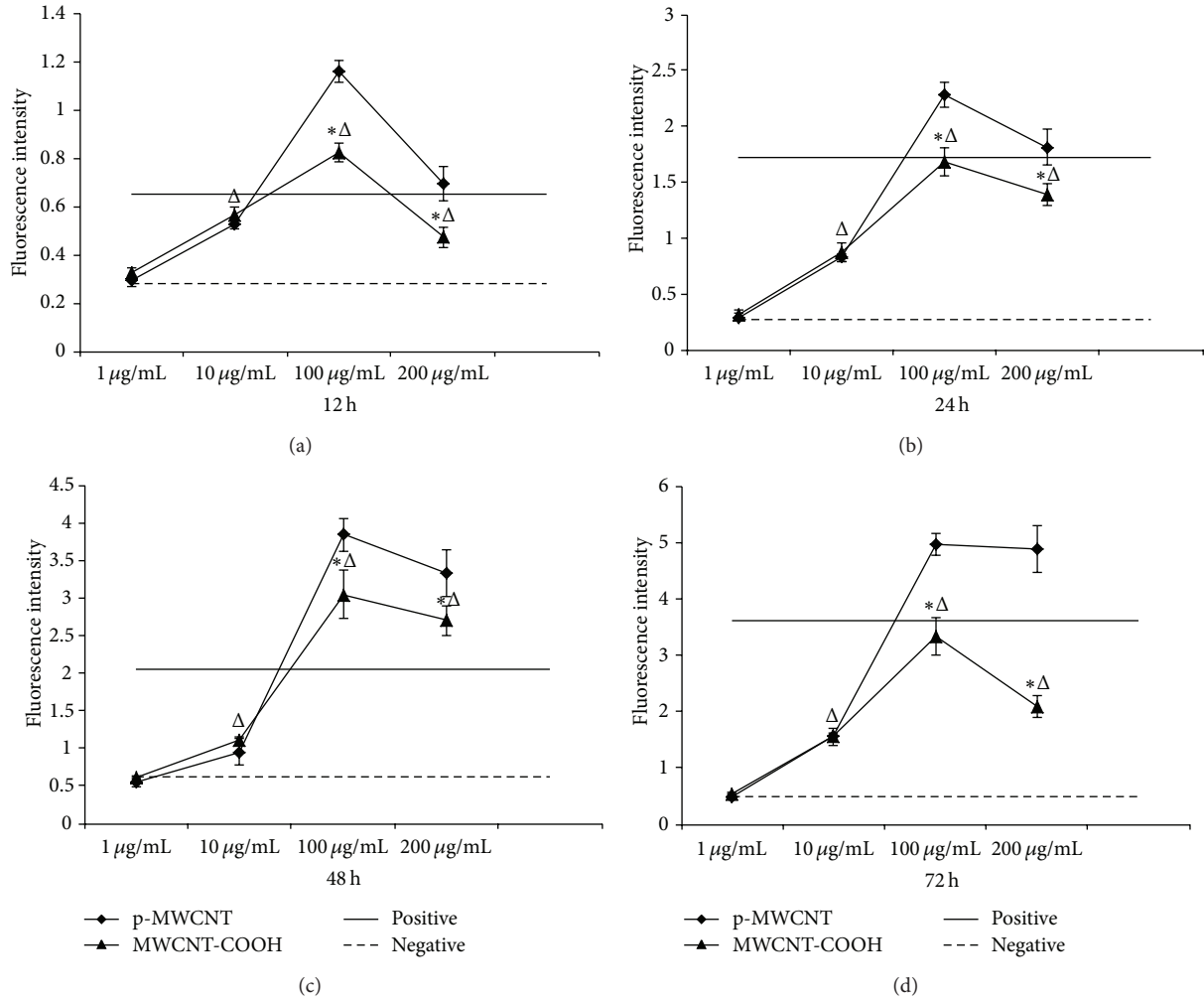


FIGURE 3: Production of ROS induced by exposure to the CNTs. $^{\Delta}P < 0.05$ as compared with negative control. $*P < 0.05$ as compared with p-MWCNT group.

TABLE 1: Phagocytic activity of the macrophages in contact with the carbon nanotubes.

	Phagocytic rate (%)	Phagocytic index
Negative control	17.17 ± 4.35	0.542 ± 0.069
p-MWCNTs	$25.13 \pm 6.79^*$	$0.804 \pm 0.068^*$
MWCNTs-COOH	$26.67 \pm 5.46^*$	$0.795 \pm 0.113^*$
LPS	$48.38 \pm 3.74^*$	$1.929 \pm 0.203^*$

* $P < 0.05$ as compared with negative control.

activity of the murine peritoneal macrophages, but no statistical significance was observed between the two CNT exposure groups.

Several different mechanisms might be involved in the nanotoxicity, in which the induction of oxidative stress by free radical formation plays a critical role [35]. Reactive oxygen species (ROS) generated during the response of cells to nanomaterials including CNT [13, 14, 36], when in excess, might cause damage to cells through oxidation of biological macromolecules including lipids, proteins, and DNA [37]. To verify

whether exposure to the MWCNTs might induce production of ROS in RAW264.7 cells, intracellular ROS accumulation was determined using 2',7'-dichlorofluorescein diacetate (DCFH-DA), a nonfluorescent compound that accumulates in cells upon deacetylation and then reacts with ROS to form fluorescent dichlorofluorescein (DCF). Figure 3 showed that ROS production increased significantly in the cells treated with p-MWCNT or MWCNT-COOH as compared with the untreated cells at each time point and concentration except 1 µg/mL and ROS production was even higher in the cells treated with 100 or 200 µg/mL of p-MWCNT than that in the cells treated with the same amount of MWCNT-COOH at each time point. No significant difference was observed between p-MWCNT and MWCNT-COOH group at the concentrations of 1 and 10 µg/mL. Our previous study [25] demonstrated that p-MWCNTs induced higher ROS production in LO2 cells and higher degree of cytotoxicity as compared with MWCNT-COOH, indicating the positive correlation of ROS production with cytotoxicity. In the present study, it was revealed that p-MWCNT and MWCNT-COOH

induced similar degree of cytotoxicity against RAW264.7 cells even though the intracellular ROS production generated by p-MWCNT was significantly higher than that by MWCNT-COOH at higher concentrations. One possible explanation for this divergent finding might be that macrophages, as a kind of phagocytes, are more resistant to the ROS induced cell damage as compared to other types of cells including LO2 cells.

4. Conclusion

The present study compared the impact of p-MWCNT and MWCNT-COOH on RAW264.7 cells. It revealed that MWCNTs-COOH demonstrated a similar effect on RAW264.7 cells as compared with p-MWCNTs in terms of cytotoxicity, phagocytic activity, and cytokine production, although p-MWCNTs at higher concentration induced higher ROS production in the cells as compared with MWCNTs-COOH. Those data suggested that modification with carboxyl group did not exert obvious impact on the interaction of MWCNTs with macrophages.

Conflict of Interests

The authors declare that there is no conflict of interests regarding the publication of this paper.

Acknowledgments

This research was jointly supported by the National Natural Science Foundation of China (Grant nos. 81271693 and 31200674), Natural Science Foundation of Tianjin (Grant no. 11JCZDJC20300), PUMC Youth Fund, and Fundamental Research Funds for the Central Universities (Grant no. 3332013060).

References

- [1] P. M. Ajayan, "Nanotubes from carbon," *Chemical Reviews*, vol. 99, no. 7, pp. 1787–1800, 1999.
- [2] M. F. L. de Volder, S. H. Tawfik, R. H. Baughman, and A. J. Hart, "Carbon nanotubes: present and future commercial applications," *Science*, vol. 339, no. 6119, pp. 535–539, 2013.
- [3] S. Y. Madani, N. Naderi, O. Dissanayake, A. Tan, and A. M. Seifalian, "A new era of cancer treatment: carbon nanotubes as drug delivery tools," *International Journal of Nanomedicine*, vol. 6, pp. 2963–2979, 2011.
- [4] D. Kato and O. Niwa, "Carbon-based electrode materials for DNA electroanalysis," *Analytical Sciences*, vol. 29, no. 4, pp. 385–392, 2013.
- [5] J. Li, Y. Xue, B. Han et al., "Application of X-ray phase contrast imaging technique in detection of pulmonary lesions induced by multi-walled carbon nanotubes in rats," *Journal of Nanoscience and Nanotechnology*, vol. 8, no. 7, pp. 3357–3362, 2008.
- [6] V. Neves, E. Heister, S. Costa et al., "Design of double-walled carbon nanotubes for biomedical applications," *Nanotechnology*, vol. 23, no. 36, Article ID 365102, 2012.
- [7] J. Muller, F. Huaux, N. Moreau et al., "Respiratory toxicity of multi-wall carbon nanotubes," *Toxicology and Applied Pharmacology*, vol. 207, no. 3, pp. 221–231, 2005.
- [8] C. W. Lam, J. T. James, R. McCluskey, and R. L. Hunter, "Pulmonary toxicity of single-wall carbon nanotubes in mice 7 and 90 days after intratracheal instillation," *Toxicological Sciences*, vol. 77, no. 1, pp. 126–134, 2004.
- [9] N. A. Monteiro-Riviere, R. J. Nemanich, A. O. Inman, Y. Y. Wang, and J. E. Riviere, "Multi-walled carbon nanotube interactions with human epidermal keratinocytes," *Toxicology Letters*, vol. 155, no. 3, pp. 377–384, 2005.
- [10] M. Bottini, S. Bruckner, K. Nika et al., "Multi-walled carbon nanotubes induce T lymphocyte apoptosis," *Toxicology Letters*, vol. 160, no. 2, pp. 121–126, 2006.
- [11] L. Zhu, D. W. Chang, L. Dai, and Y. Hong, "DNA damage induced by multiwalled carbon nanotubes in mouse embryonic stem cells," *Nano Letters*, vol. 7, no. 12, pp. 3592–3597, 2007.
- [12] P. M. V. Raja, J. Connolly, G. P. Ganesan et al., "Impact of carbon nanotube exposure, dosage and aggregation on smooth muscle cells," *Toxicology Letters*, vol. 169, no. 1, pp. 51–63, 2007.
- [13] A. A. Shvedova, V. Castranova, E. R. Kisin et al., "Exposure to carbon nanotube material: assessment of nanotube cytotoxicity using human keratinocyte cells," *Journal of Toxicology and Environmental Health. Part A*, vol. 66, no. 20, pp. 1909–1926, 2003.
- [14] V. E. Kagan, Y. Y. Tyurina, V. A. Tyurin et al., "Direct and indirect effects of single walled carbon nanotubes on RAW 264.7 macrophages: role of iron," *Toxicology Letters*, vol. 165, no. 1, pp. 88–100, 2006.
- [15] A. Magrez, S. Kasas, V. Salicio et al., "Cellular toxicity of carbon-based nanomaterials," *Nano Letters*, vol. 6, no. 6, pp. 1121–1125, 2006.
- [16] S. Vardharajula, S. Z. Ali, P. M. Tiwari et al., "Functionalized carbon nanotubes: biomedical applications," *International Journal of Nanomedicine*, vol. 7, pp. 5361–5374, 2012.
- [17] E. Fröhlich, C. Meindl, A. Höfler, G. Leitinger, and E. Roblegg, "Combination of small size and carboxyl functionalisation causes cytotoxicity of short carbon nanotubes," *Nanotoxicology*, vol. 7, no. 7, pp. 1211–1224, 2013.
- [18] Y. Ohtsuka, M. Munakata, H. Ukita et al., "Increased susceptibility to silicosis and TNF- α production in C57BL/6J mice," *The American Journal of Respiratory and Critical Care Medicine*, vol. 152, no. 6, pp. 2144–2149, 1995.
- [19] B. T. Mossman and A. Churg, "Mechanisms in the pathogenesis of asbestosis and silicosis," *American Journal of Respiratory and Critical Care Medicine*, vol. 157, no. 5, part 1, pp. 1666–1680, 1998.
- [20] A. A. Shvedova, E. R. Kisin, R. Mercer et al., "Unusual inflammatory and fibrogenic pulmonary responses to single-walled carbon nanotubes in mice," *American Journal of Physiology—Lung Cellular and Molecular Physiology*, vol. 289, no. 5, pp. L698–L708, 2005.
- [21] S. Hirano, S. Kanno, and A. Furuyama, "Multi-walled carbon nanotubes injure the plasma membrane of macrophages," *Toxicology and Applied Pharmacology*, vol. 232, no. 2, pp. 244–251, 2008.
- [22] C. Cheng, K. H. Müller, K. K. K. Koziol et al., "Toxicity and imaging of multi-walled carbon nanotubes in human macrophage cells," *Biomaterials*, vol. 30, no. 25, pp. 4152–4160, 2009.
- [23] M. L. di Giorgio, S. di Bucchianico, A. M. Ragnelli, P. Aimola, S. Santucci, and A. Poma, "Effects of single and multi walled

- carbon nanotubes on macrophages: cyto and genotoxicity and electron microscopy," *Mutation Research/Genetic Toxicology and Environmental Mutagenesis*, vol. 722, no. 1, pp. 20–31, 2011.
- [24] B. Chen, Y. Liu, W. M. Song, Y. Hayashi, X. C. Ding, and W. H. Li, "In vitro evaluation of cytotoxicity and oxidative stress induced by multiwalled carbon nanotubes in murine RAW 264.7 macrophages and human A549 lung cells," *Biomedical and Environmental Sciences*, vol. 24, no. 6, pp. 593–601, 2011.
- [25] Z.-B. Liu, B. Zhou, H.-Y. Wang et al., "Effect of functionalized multi-walled carbon nanotubes on L02 cells," *Zhongguo Yi Xue Ke Xue Yuan Xue Bao*, vol. 32, no. 4, pp. 449–455, 2010.
- [26] S. Bellucci, A. Bergamaschi, M. Bottini, A. Magrini, and T. Mustelin, "Biomedical platforms based on composite nanomaterials and cellular toxicity," *Journal of Physics: Conference Series*, vol. 61, pp. 95–98, 2007.
- [27] A. Jos, S. Pichardo, M. Puerto, E. Sánchez, A. Grilo, and A. M. Cameán, "Cytotoxicity of carboxylic acid functionalized single wall carbon nanotubes on the human intestinal cell line Caco-2," *Toxicology in Vitro*, vol. 23, no. 8, pp. 1491–1496, 2009.
- [28] H.-L. Liu, Y.-L. Zhang, N. Yang et al., "A functionalized single-walled carbon nanotube-induced autophagic cell death in human lung cells through Akt-TSC2-mTOR signaling," *Cell Death and Disease*, vol. 2, article e159, 2011.
- [29] A. Casey, M. Davoren, E. Herzog, F. M. Lyng, H. J. Byrne, and G. Chambers, "Probing the interaction of single walled carbon nanotubes within cell culture medium as a precursor to toxicity testing," *Carbon*, vol. 45, no. 1, pp. 34–40, 2007.
- [30] J. M. Wörle-Knirsch, K. Pulskamp, and H. F. Krug, "Oops they did it again! Carbon nanotubes hoax scientists in viability assays," *Nano Letters*, vol. 6, no. 6, pp. 1261–1268, 2006.
- [31] A. Casey, E. H. Herzog, M. Davoren, F. M. Lyng, H. J. Byrne, and G. Chambers, "Spectroscopic analysis confirms the interactions between single walled carbon nanotubes and various dyes commonly used to assess cytotoxicity," *Carbon*, vol. 45, no. 7, pp. 1425–1432, 2007.
- [32] E. J. R. Anderson, M. A. McGrath, T. Thalhamer, and I. B. McInnes, "Interleukin-12 to interleukin 'infinity': the rationale for future therapeutic cytokine targeting," *Springer Seminars in Immunopathology*, vol. 27, no. 4, pp. 425–442, 2006.
- [33] J.-L. Mege, S. Meghari, A. Honstetter, C. Capo, and D. Raoult, "The two faces of interleukin 10 in human infectious diseases," *The Lancet Infectious Diseases*, vol. 6, no. 9, pp. 557–569, 2006.
- [34] A. Taylor, J. Verhagen, K. Blaser, M. Akdis, and C. A. Akdis, "Mechanisms of immune suppression by interleukin-10 and transforming growth factor- β : the role of T regulatory cells," *Immunology*, vol. 117, no. 4, pp. 433–442, 2006.
- [35] S. Lanone and J. Boczkowski, "Biomedical applications and potential health risks of nanomaterials: molecular mechanisms," *Current Molecular Medicine*, vol. 6, no. 6, pp. 651–663, 2006.
- [36] K. Pulskamp, S. Diabaté, and H. F. Krug, "Carbon nanotubes show no sign of acute toxicity but induce intracellular reactive oxygen species in dependence on contaminants," *Toxicology Letters*, vol. 168, no. 1, pp. 58–74, 2007.
- [37] K. Kitagawa, M. Matsumoto, T. Oda et al., "Free radical generation during brief period of cerebral ischemia may trigger delayed neuronal death," *Neuroscience*, vol. 35, no. 3, pp. 551–558, 1990.

Research Article

Synthesis of Luminescent Ag Nanoclusters with Antibacterial Activity

Ying-Fan Liu,^{1,2} Lei Wang,¹ Chun-Po Bu,³ Guo-Qing Wang,¹ Yan-Hui Zhang,¹ Shao-Ming Fang,^{1,2} and Wan-Zhen Shi³

¹ Henan Provincial Key Laboratory of Surface and Interface Science, Zhengzhou University of Light Industry, No. 166, Science Avenue, Zhengzhou 450001, China

² Henan Collaborative Innovation Center of Environmental Pollution Control and Ecological Restoration, Zhengzhou University of Light Industry, No. 166, Science Avenue, Zhengzhou 450001, China

³ College of Chemical and Environmental Engineering, Shandong University of Science and Technology, Qingdao, Shandong 266510, China

Correspondence should be addressed to Ying-Fan Liu; yfliu@zzuli.edu.cn and Shao-Ming Fang; mingfang@zzuli.edu.cn

Received 5 August 2014; Accepted 14 October 2014

Academic Editor: Xiaoming Li

Copyright © 2015 Ying-Fan Liu et al. This is an open access article distributed under the Creative Commons Attribution License, which permits unrestricted use, distribution, and reproduction in any medium, provided the original work is properly cited.

This paper focuses on the synthesis of novel Ag nanoclusters (NCs) using DHLA as capping reagents in aqueous solution by a photoreduction method. Luminescence studies indicated that the DHLA-Ag NCs exhibited strong blue emission with maximum peak at 480 nm. The maximum emission of the NCs can be greatly improved with irradiating time by around 15-fold from 3 h to 67 h. By means of mycelium growth rate, the results showed that the Ag NCs with smaller sizes had a good antimicrobial effect.

1. Introduction

Luminescent nanomaterials are currently attracting enthusiastic interest due to their applications in biomedical field such as cell imaging or photodynamic therapy [1–3], solar cells [4], lasers [5], lighting, and display technologies [6]. For bioimaging applications, luminescent semiconductor nanocrystals (quantum dots) have several advantages over the conventional organic fluorophores [7–10]. One issue with the use of small molecule fluorophores is a lack of photostability under prolonged excitation. Quantum dots also have excellent photostability, but there are potential cytotoxicity issues due to containing highly toxic metals such as cadmium [11, 12]. Therefore, there always is a challenge to explore alternate luminescent materials.

Silver nanodots are a new class of fluorophores with photophysical properties approaching those of semiconductor quantum dots. Silver nanodots also were named as silver nanoclusters, silver clusters, or silver quantum dots, consisting of several to roughly hundred atoms, possess sizes comparable to the Fermi wavelength of electrons, and

exhibit molecule-like properties, including discrete electronic transitions and strong fluorescence. Extensive efforts have been devoted to the facile preparation of highly fluorescent, water-soluble metallic nanoclusters [13–16]. Zhang et al. utilized photoreduction to synthesize Ag clusters. A mixture of silver ions and poly(N-isopropylacrylamide-acrylic acid-2-hydroxy acrylate) microgel was irradiated with 365 nm light. As the irradiation continued, the solution became light pink, then purple, and dark red in the end [17]. Similar approach was reported with multiarm polymer [18]. Instead of UV light, visible light was applied to photoactivate a mixture of silver ions and poly(methacrylic acid) (PMAA) [19]. An increase in the silver/methacrylic acid (Ag/MAA) molar ratio resulted in red shifts of the absorption peaks and the corresponding emission peaks. A typical example is Ag clusters which exhibited a photoluminescence emission peak at 610 nm with excitation peaks at 400 nm and 450 nm. Such stabilization might be ascribed to the strong interaction between carboxylic acid and silver ions. DNA or RNA exhibit strong affinity for silver ions; therefore, DNA or RNA molecules have been widely utilized to template

the formation of Ag nanoparticles [20–24]. Thiol is one of the common chelating groups for synthesizing silver clusters. However, weakly luminescent Ag species were reported using ether 2,3-dimercaptosuccinic acid and mercaptosuccinic acid [25, 26] ordihydrolipoic acid (DHHLA) [27–29]. In these data, the nanoparticles were usually synthesized by sodium borohydride reduction reaction. There is an urgent need to design luminescent materials with high PL QY, good stability, and low cytotoxicity. DHHLA as the capping reagents has been used to synthesize the CdTe, HgTe, and Ag₂S QDs due to the fact that the bidentate DHHLA can simultaneously attach to two surface sites on the QDs resulting in more stable interaction of stabilizer reagents and NCs [30–32]. Recently, Zhang et al. reported a stepwise method to prepare stable green-emitting Ag NCs. For their method, parent Ag NPs were firstly prepared using a chemical reduction method in the presence of gelatin; then, dihydrolipoic acid (DHHLA) was chosen as the etching ligand [33].

Here, we present a new strong UV photochemical reduction synthesis of water-soluble luminescent Ag NCs using DHHLA as the capping reagents to stabilize the Ag NCs in the solution. In the present work, we found that luminescence of DHHLA-capped Ag NCs could be greatly improved by around 15-fold from 3 to 67 h. Also, by means of mycelium growth rate [34], antibacterial ability of the Ag NCs was tested.

2. Experimental Section

2.1. Chemicals. Lipoic acid (TA, 99%) and NaBH₄ (96%) were obtained from Sigma, Inc. AgNO₃ was obtained from Shanghai Chemical Reagents Company. High purity deionized water (>18.3 MΩ/cm) was produced by Millipore A10 Milli-Q.

2.2. Preparation of Dihydrolipoic Acid (DHHLA). DHHLA was prepared by treating TA with NaBH₄ using a method described in a previous report [27]. TA (5.225 g, 25 mmol) was dissolved in deionized water (200 mL) and then NaBH₄ (1.91 g, 50 mmol) was slowly added to the stirred solution as a reductant. The solution was stirred at room temperature for 2 h and then heated to 100°C until no more gas (H₂) was generated. The final concentration of the DHHLA aqueous solution was 0.125 M.

2.3. Synthesis of Ag Nanoclusters. Water-soluble fluorescent Ag nanoclusters were prepared as follows: a solution of AgNO₃ in water (85 mg, 0.5 mmol) was added to the DHHLA solution (0.125 M, 200 mL) under room-temperature conditions with stirring. Silver was reduced to the zero-valent state by strong UV irradiation at $\lambda = 365$ nm (UV intensity of 400 W). Aliquots of the reaction solution were removed at regular intervals for UV absorption and luminescence experiments. Samples were precipitated by acetone and dried in a vacuum oven for XPS characterization. Finally, the DHHLA-Ag precipitate was dried and collected as a brown yellow powder. TEM sample was prepared by dropping the aqueous Ag nanoclusters solution onto carbon-coated copper grids and the excessive solvent was evaporated.

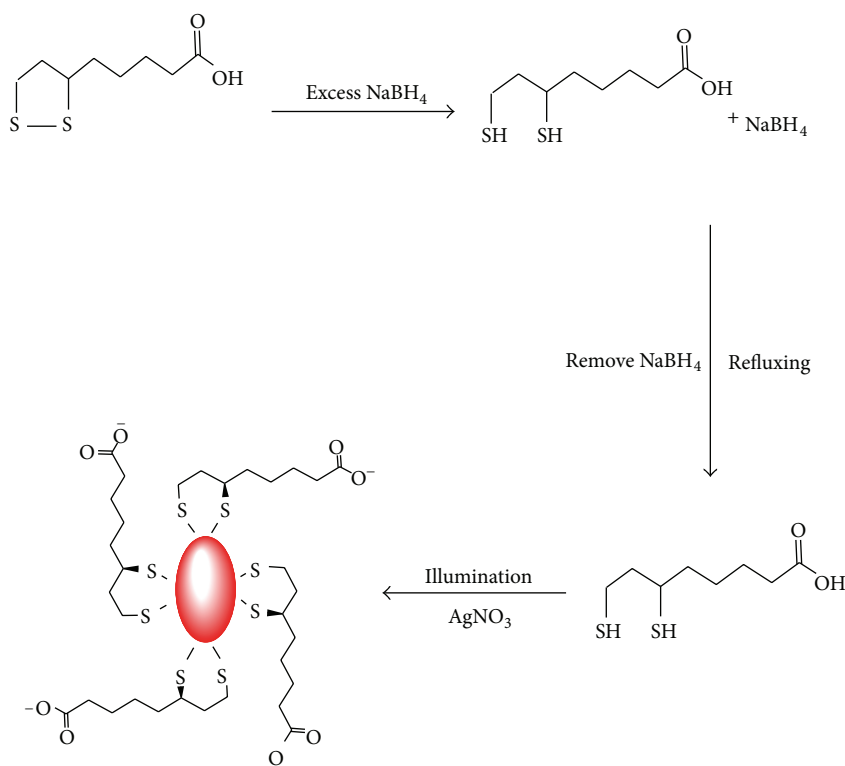
2.4. Assay for Antimicrobial Activity of Ag NCs against Wheat Phytoalexin. The antimicrobial activity of Ag-DHHLA complex, Ag (200 nm), and Ag (2 nm) NCs was investigated against wheat phytoalexin. The concentration of Ag-DHHLA complex, Ag (200 nm), and Ag (2 nm) NCs was the same as 62.5 μ M. As a positive control of growth, microorganisms containing only water were used. Bacteria colony with a disk shape and diameter of 40 mm was reverse placed on the center of the agar plates, added into antimicrobial reagents, respectively, and then cultured in the incubator at 20°C. The antibacterial inhibition rate of the Ag NCs was calculated from the diameter of bacterial colony when its growth diameter was 2/3 of the diameter of diffusion disk. The inhibition rate = $(D_1 - D_2)/(D_1 - 0.4)$, D_1 being the diameter of control bacteria colony and D_2 being the diameter of test bacteria colony.

2.5. Characterization. UV-vis absorption and luminescence spectra were measured at room temperature with a Shimadzu UV-3100 spectrophotometer and a Hitachi 7000 fluorescence spectrometer, respectively. Luminescence spectra were taken at the excitation wavelength $\lambda_{\text{ex}} = 390$ nm. Time-resolved luminescence measurements were carried out on a Fluorolog-3 spectrofluorometer with 390 nm LED lamp. Ludox was applied for PL lifetime measurement in order to eliminate the influence of light scattering (i.e., excitation and emission). Powder XRD measurements were taken on a Philips X'Pert PRO X-ray diffractometer. Transmission electron microscopy (TEM) was performed on a Philips FEI Tecnai G2 F20 S-Twin.

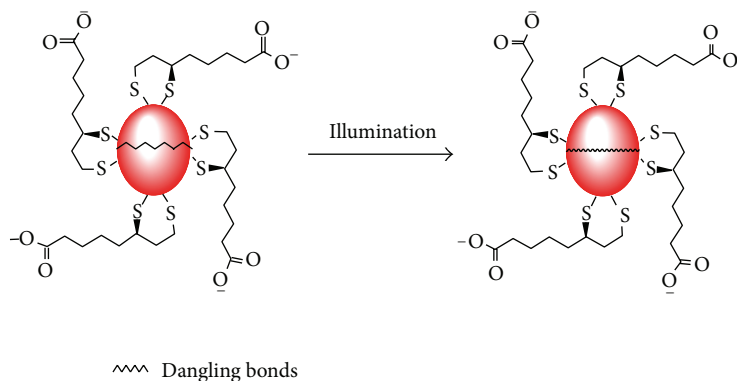
3. Results and Discussion

3.1. The Synthesis and Optical Properties of Ag NCs. Our previous research shows that luminescent pen-stabilized Ag NCs can be prepared by photoreduction method [35], but the luminescence intensity of the system is gradually decreased after irradiating for several ten min. In this study, we selected DHHLA molecules as capping reagents to synthesize Ag NCs in the aqueous phase. Scheme 1 gives the synthetic route of DHHLA and Ag NCs.

To produce Ag NCs, a freshly prepared aqueous solution of 2 mM silver nitrate was added to the solution of DHHLA in a molar ratio $[\text{Ag}^+]/[\text{DHHLA}]$ of 50 : 1. The system was mixed and subjected to strong UV irradiation at $\lambda = 365$ nm (UV intensity of 400 W) for various time intervals. The system was mixed for half an hour. Subsequently, photoreduction was carried out under UV irradiation at $\lambda = 365$ nm for various time intervals. During a total irradiation time of 67 h, the color of the solution gradually changed from colorless to yellow. Figure 1(a) shows absorption spectra of the solution of DHHLA with Ag⁺ ions after UV irradiation for different periods of time. When the irradiation time was increased from 3 to 67 h, the absorption band-edge slightly red shifted and the intensity of the absorbance was gradually increased, which indicated that size of the Ag NCs became correspondingly bigger and the concentration of Ag NCs was gradually increased upon prolonged UV irradiation. We noticed that, after an irradiation time of 3 h, the reaction mixture of



SCHEME 1: Synthesis of DHLA and Ag NCs.



SCHEME 2: Illustration of the change of surface dangling bonds on the Ag NCs.

the DHLA and Ag^+ ions became luminescence (Figure 1(b)). Irradiation between 3 and 67 h led to an emission peak centered at about 480 nm and spanning the wavelength range 408–630 nm. For irradiating times of 3, 12, 25, 33, 42, 63, and 67 h, Ag NCs are obtained with maximum blue luminescent emission at 470, 472, 476, 477, 479, 482, and 485 nm, respectively. A strong increase in intensity was observed with increasing irradiating time, eventually resulting in a 15-fold increase compared to the original emission. When irradiated for 67 h, the intensity reaches a plateau. By further irradiation, the system started to precipitate. The lifetime of the Ag NCs was also measured. Figure S1 (see Supplementary Material available online at <http://dx.doi.org/10.1155/2015/792095>)

shows the time-resolved luminescence decay curves of the Ag NCs, which can be satisfactorily fitted into triexponential function. The decay lifetime of the NCs with blue emission is $\tau_1 = 3.65$ ns (52%), $\tau_2 = 0.56$ ns (31%), and $\tau_3 = 12.9$ ns (17%) and has a 9.4 ns average excited state lifetime. The blue emitter $\text{Ex}_{350}/\text{Em}_{440}$ usually exhibits a very short lifetime (0.01 ns) [36, 37], whereas 9.4 ns ($\text{Ex}_{390}/\text{Em}_{480}$) is the longest reported lifetime of such thiol-stabilized Ag NCs.

As shown in Figure 1(b), the intensity is simply enhanced as illumination is prolonged. The fact that illumination can result in increase of the luminescence of Ag nanocrystals has little been reported. Scheme 2 gives illustration of the change of surface dangling bonds on the Ag NCs. Due

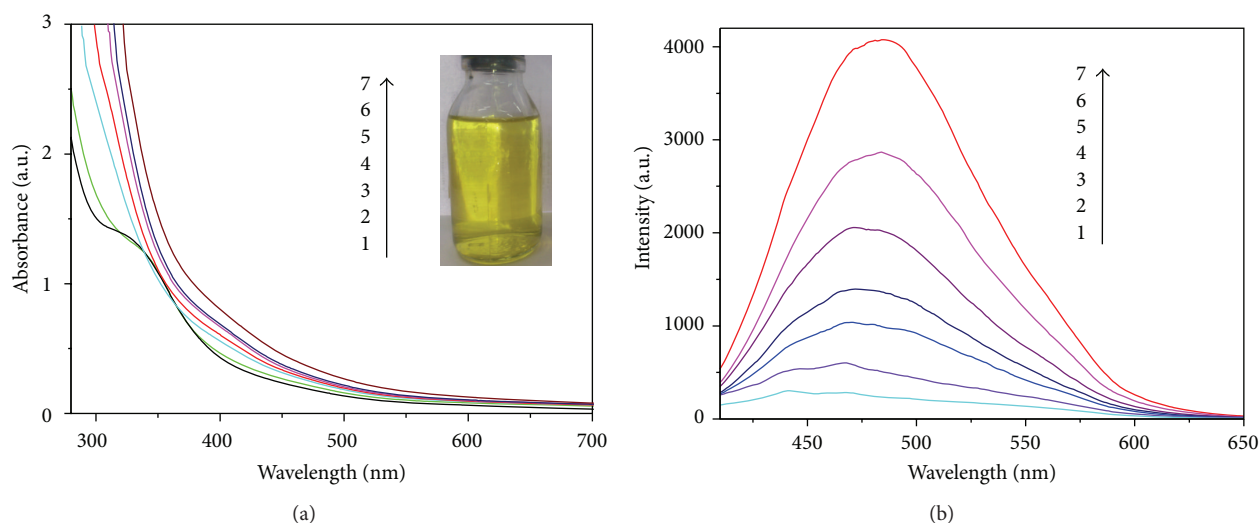


FIGURE 1: UV-vis (a) and luminescence spectra (b) of the Ag NCs after different periods of UV irradiation: (1) 3, (2) 12, (3) 25, (4) 33, (5) 42, (6) 63, and (8) 67 h. The inset shows the images of Ag NCs illuminated under room natural light. The excitation wavelength was set as 390 nm.

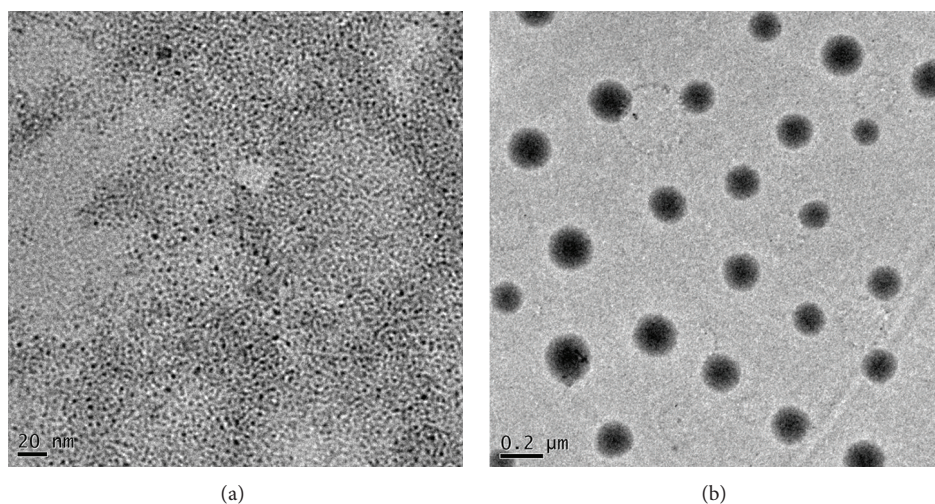


FIGURE 2: Typical TEM images of DHLA-capped Ag NCs obtained after irradiating for 12 h (a) and 63 h (b).

to the large surface/volume ratio, nanoclusters have lots of surface dangling bonds which become reactive upon illumination. Therefore, illumination-assisting enhancement effects were probably explained by the rearrangement of NC surface atoms and thus the decrease of dangling bonds.

It was interesting that the photoluminescence (480 nm) of DHLA-stabilized Ag NCs could also be obtained at the excitation wavelength $\lambda_{\text{ex}} = 780$ nm, which seemed to be “upconversion” phenomenon and agreed with the relevant document [38]. However, when a long pass filter, for example, 520 nm, in the excitation part of fluorimeter was put, the photoluminescence of the NCs could not be observed. Therefore, the “upconversion” is actually due to 390 nm light that passes through fluorimeter (half of 780 nm).

3.2. TEM, XRD, XPS, and EDX Characterization. Typical TEM images for Ag NCs are shown in Figure 2. These

images show that the Ag NCs possess a good dispersed crystalline structure and have the average diameters of about 2 nm after irradiating for 12 h. Further irradiating for 63 h, larger sized NCs formed and the average diameter of the NCs is about 200 nm. Although the diameter of the NCs increased 100-fold, the NCs still possess a good dispersed crystalline structure and the luminescence of these NCs is greatly improved.

Powder X-ray diffractions (XRD) were carried out on the as-formed product. The XRD of the Ag NCs powder sample (Figure 3) exhibits a broad and intense (121) peak of silver at $2\theta = \sim 35^\circ$, which agreed with previous result [35]. X-ray photoelectron spectroscopy was measured for the surface analysis of the washed DHLA-capped Ag NCs. A full survey scan and Ag and S photoelectron spectra of the Ag NCs are displayed in Figure 4. Besides the Ag levels, these spectra are dominated by the Cls and Ols signals stemming from

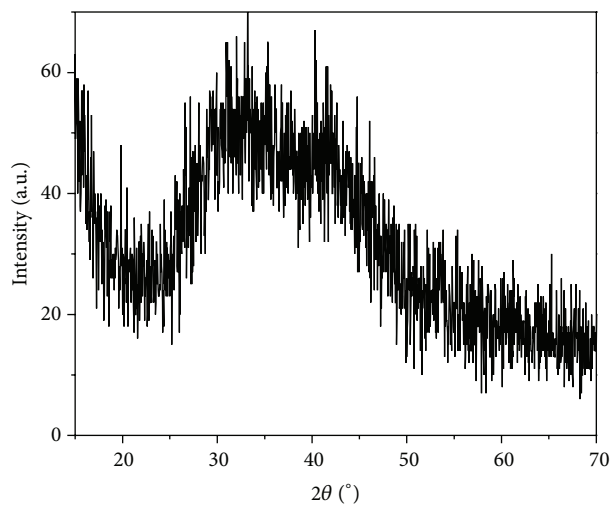


FIGURE 3: XRD pattern of Ag NCs.

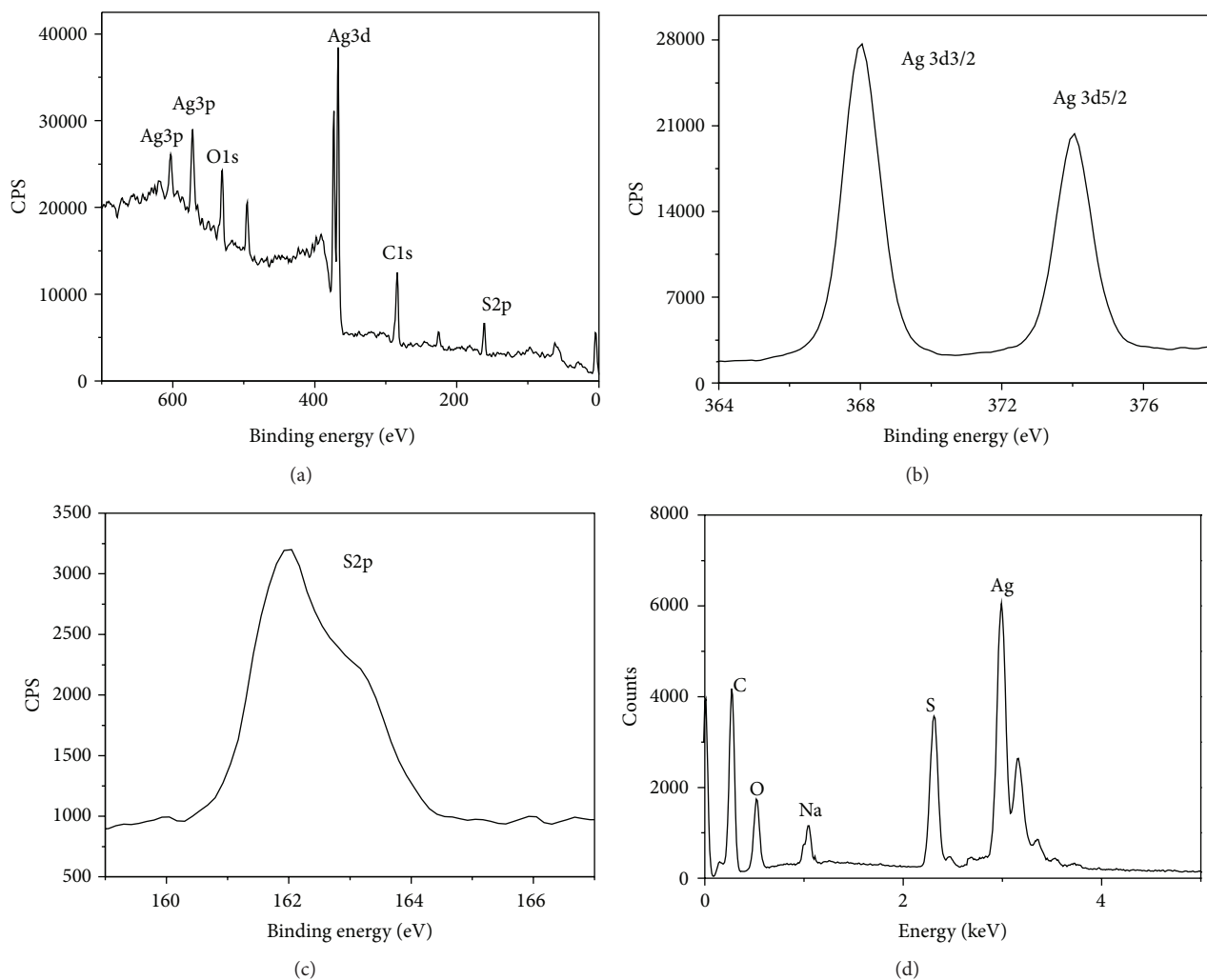


FIGURE 4: The XPS spectra of (a) the whole survey, (b) Ag 3d, and (c) S 2p of the as-prepared Ag NCs. (d) Typical EDX spectra of DHLA-capped Ag NCs.

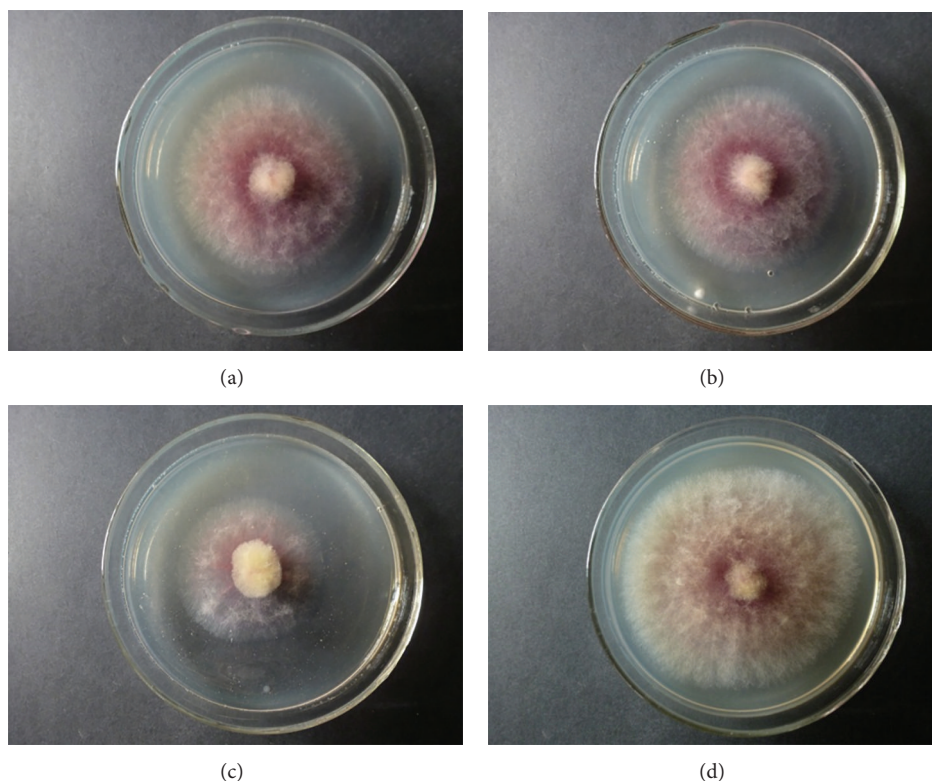


FIGURE 5: Antibacterial ability of Ag NCs. Photographs were taken after incubation for 5d at 20°C. (a), (b), and (c) represent Ag-DHLA complex, 2 nm Ag NCs, and 200 nm Ag NCs, respectively; (d) represents water (control). The inhibition rates of (a), (b), and (c) against wheat phytoalexin were 15.47%, 25.46%, and 49.64%, respectively. The concentration of Ag-DHLA complex was 62.5 μ M.

the capping agent. XPS spectra in Figure 4 show that there exist Ag3d and S2p. The two peaks in Figure 4(b) of 368 eV and 374 eV can be assigned to the binding energy of Ag 3d_{5/2} and Ag 3d_{3/2}, respectively, which is characteristic of Ag product [39]. The peak at 161.9 eV belongs to S2p_{1/2} in a stabilizer DHLA. X-ray photoelectron spectroscopy (XPS) provides evidence for the formation of Ag NCs.

Further, we carried out energy dispersive X-ray spectroscopy (EDX) measurements for DHLA-capped Ag NCs. The EDX spectrum shows the existence of Ag and S in the Ag samples (Figure 4(d)). The silver sulfur and peak peaks are at 2.99 keV and 2.3 keV, respectively, the latter mainly from the stabilizer DHLA.

3.3. Assay for Antimicrobial Activity of Ag NCs. Recently silver nanoparticles became a fresh member of antimicrobial Ag family due to their higher specific surface area and high fraction of surface atoms compared to bulk Ag [40, 41]. By means of mycelium growth rate, the results showed that, at the same conditions, the inhibition rates of Ag⁺, Ag (200 nm), and Ag (2 nm) against wheat phytoalexin were 15.47%, 25.46%, and 49.64%, respectively (Figure 5). Therefore, the Ag NCs with smaller sizes had a good antimicrobial effect, which might be caused by their larger surface area and higher surface energy. Ag NCs break permeability of outer membrane, inhibit respiration and growth of cells, and destroy the structure of membrane, resulting in cell decomposition and death eventually.

4. Summary

In summary, to the best of our knowledge, this is the first report of a synthesis of DHLA-capped Ag NCs by photoreduction method. The prepared DHLA-stabilized Ag NCs exhibited strong PL emission with maximum peak at 480 nm. Because luminescence of these NCs can be greatly improved, they may be found in vast applications, not only in chemistry and biology such as biolabeling and imaging but also in forensic science. The test of antimicrobial activity showed that the Ag NCs with smaller sizes had a good antimicrobial effect.

Conflict of Interests

The authors declare that there is no conflict of interests regarding the publication of this paper.

Acknowledgments

This work was financially supported by the Natural Science Foundation of China (nos. 21171150 and 21271159) and Henan Province Science and Technology Programs (no. 112102210002).

References

- [1] X. Michalet, F. F. Pinaud, L. A. Bentolila et al., "Quantum dots for live cells, in vivo imaging, and diagnostics," *Science*, vol. 307, no. 5709, pp. 538–544, 2005.

- [2] X. M. Li, L. Wang, Y. B. Fan, Q. L. Feng, F. Z. Cui, and F. Watari, "Nanostructured scaffolds for bone tissue engineering," *Journal of Biomedical Materials Research Part A*, vol. 101, pp. 2424–2435, 2013.
- [3] X. Li, H. Liu, X. Niu et al., "The use of carbon nanotubes to induce osteogenic differentiation of human adipose-derived MSCs *in vitro* and ectopic bone formation *in vivo*," *Biomaterials*, vol. 33, no. 19, pp. 4818–4827, 2012.
- [4] H. Q. Wang, M. Batentschuk, A. Osvet, L. Pinna, and C. J. Brabec, "Rare-earth ion doped up-conversion materials for photovoltaic applications," *Advanced Materials*, vol. 23, no. 22–23, pp. 2675–2680, 2011.
- [5] T. Danger, J. Koetke, R. Brede, E. Heumann, G. Huber, and B. H. T. Chai, "Spectroscopy and green upconversion laser emission of Er^{3+} -doped crystals at room temperature," *Journal of Applied Physics*, vol. 76, no. 3, pp. 1413–1422, 1994.
- [6] A. Rapaport, J. Milliez, M. Bass, A. Cassanho, and H. Jenssen, "Review of the properties of up-conversion phosphors for new emissive displays," *Journal of Display Technology*, vol. 2, no. 1, pp. 68–78, 2006.
- [7] F. Wang and X. G. Liu, "Recent advances in the chemistry of lanthanide-doped upconversion nanocrystals," *Chemical Society Reviews*, vol. 38, no. 4, pp. 976–989, 2009.
- [8] W.-H. Zhang, C.-X. Sui, X. Wang, G.-J. Yin, Y.-F. Liu, and D. Zhang, "Characterization of Cr(V) -induced genotoxicity using CdTe nanocrystals as fluorescent probes," *Analyst*, 2014.
- [9] C.-X. Sui, Y.-F. Liu, W.-H. Zhang, P.-A. Li, and D. Zhang, " CdTe - CdSe nanocrystals capped with dimethylaminoethanethiol as ultrasensitive fluorescent probes for chromium(VI)," *Microchimica Acta*, vol. 181, no. 3–4, pp. 347–353, 2014.
- [10] Y.-F. Liu, L. Wang, W.-Z. Shi, Y.-H. Zhang, and S.-M. Fang, "Synthesis and characterization of chiral Ag_2S and Ag_2S - Zn nanocrystals," *RSC Advances*, vol. 4, no. 95, pp. 53142–53148, 2014.
- [11] Z. Deng, Y. Zhang, J. Yue, F. Tang, and Q. Wei, "Green and orange CdTe quantum dots as effective pH-sensitive fluorescent probes for dual simultaneous and independent detection of viruses," *Journal of Physical Chemistry B*, vol. 111, no. 41, pp. 12024–12031, 2007.
- [12] N. Lewinski, V. Colvin, and R. Drezek, "Cytotoxicity of nanoparticles," *Small*, vol. 4, no. 1, pp. 26–49, 2008.
- [13] G. Maduraiveeran and R. Ramaraj, "Potential sensing platform of silver nanoparticles embedded in functionalized silicate shell for nitroaromatic compounds," *Analytical Chemistry*, vol. 81, no. 18, pp. 7552–7560, 2009.
- [14] H. Xu and K. S. Suslick, "Water-soluble fluorescent silver nanoclusters," *Advanced Materials*, vol. 22, no. 10, pp. 1078–1082, 2010.
- [15] L. Shang, S. Dong, and G. U. Nienhaus, "Ultra-small fluorescent metal nanoclusters: synthesis and biological applications," *Nano Today*, vol. 6, no. 4, pp. 401–418, 2011.
- [16] T. Zhou, M. Rong, Z. Cai, C. Yang, and X. Chen, "Sonochemical synthesis of highly fluorescent glutathione-stabilized Ag nanoclusters and S_2 -sensing," *Nanoscale*, vol. 4, no. 14, pp. 4103–4106, 2012.
- [17] J. Zhang, S. Xu, and E. Kumacheva, "Photogeneration of fluorescent silver nanoclusters in polymer microgels," *Advanced Materials*, vol. 17, no. 19, pp. 2336–2340, 2005.
- [18] Z. Shen, H. W. Duan, and H. Frey, "Water-soluble fluorescent Ag nanoclusters obtained from multiarm star poly(acrylic acid) as "molecular hydrogel" templates," *Advanced Materials*, vol. 19, no. 3, pp. 349–352, 2007.
- [19] I. Díez, M. Pusa, S. Kulmala et al., "Color tunability and electrochemiluminescence of silver nanoclusters," *Angewandte Chemie*, vol. 48, no. 12, pp. 2122–2125, 2009.
- [20] J. T. Petty, J. Zheng, N. V. Hud, and R. M. Dickson, "DNA-templated Ag nanocluster formation," *Journal of the American Chemical Society*, vol. 126, no. 16, pp. 5207–5212, 2004.
- [21] L. Berti and G. A. Burley, "Nucleic acid and nucleotide-mediated synthesis of inorganic nanoparticles," *Nature Nanotechnology*, vol. 3, no. 2, pp. 81–87, 2008.
- [22] C. M. Ritchie, K. R. Johnsen, J. R. Kiser, Y. Antoku, R. M. Dickson, and J. T. Petty, "Ag nanocluster formation using a cytosine oligonucleotide template," *Journal of Physical Chemistry C*, vol. 111, no. 1, pp. 175–181, 2007.
- [23] P. R. O'Neill, L. R. Velazquez, D. G. Dunn, E. G. Gwinn, and D. K. Fygenson, "Hairpins with poly-C loops stabilize four types of fluorescent Ag_n : DNA," *The Journal of Physical Chemistry C*, vol. 113, no. 11, pp. 4229–4233, 2009.
- [24] Y. Wei, R. Liu, Z. Sun et al., "Luminescent silver nanoclusters anchored by oligonucleotides detect human telomerase ribonucleic acid template," *Analyst*, vol. 138, no. 5, pp. 1338–1341, 2013.
- [25] Z. Wu, E. Lanni, W. Chen, M. E. Bier, D. Ly, and R. Jin, "High yield, large scale synthesis of thiolate-protected Ag_7 clusters," *Journal of the American Chemical Society*, vol. 131, no. 46, pp. 16672–16674, 2009.
- [26] T. U. B. Rao, B. Nataraju, and T. Pradeep, " Ag_9 quantum cluster through a solid-state route," *Journal of the American Chemical Society*, vol. 132, no. 46, pp. 16304–16307, 2010.
- [27] P. T. K. Chin, M. van der Linden, E. J. van Harten et al., "Enhanced luminescence of Ag nanoclusters via surface modification," *Nanotechnology*, vol. 24, no. 7, Article ID 075703, 2013.
- [28] L. Shang, R. M. Dörlich, V. Trouillet, M. Bruns, and G. U. Nienhaus, "Ultrasmall fluorescent silver nanoclusters: protein adsorption and its effects on cellular responses," *Nano Research*, vol. 5, no. 8, pp. 531–542, 2012.
- [29] B. Adhikari and A. Banerjee, "Facile synthesis of water-soluble fluorescent silver nanoclusters and Hg^{II} sensing," *Chemistry of Materials*, vol. 22, no. 15, pp. 4364–4371, 2010.
- [30] Y.-F. Liu, B. Xie, Z.-G. Yin, S.-M. Fang, and J.-B. Zhao, "Synthesis of highly stable CdTe/CdS quantum dots with biocompatibility," *European Journal of Inorganic Chemistry*, vol. 2010, no. 10, pp. 1501–1506, 2010.
- [31] W. H. Zhang, J. Yang, and J. S. Yu, "Synthesis of stable near-infrared emitting HgTe/CdS core/shell nanocrystals using dihydrolipoic acid as stabilizer," *Journal of Materials Chemistry*, vol. 22, no. 13, pp. 6383–6388, 2012.
- [32] Y. Zhang, Y. Zhang, G. Hong et al., "Biodistribution, pharmacokinetics and toxicology of Ag_2S near-infrared quantum dots in mice," *Biomaterials*, vol. 34, no. 14, pp. 3639–3646, 2013.
- [33] C. Zhang, X. Sun, J. Li, and Y.-N. Liu, "Synthesis of Ag nanoclusters by a pH-dependent etching method in aqueous solution," *Nanoscale*, vol. 5, no. 14, pp. 6261–6264, 2013.
- [34] I. Sondi and B. Salopek-Sondi, "Silver nanoparticles as antimicrobial agent: a case study on *E. coli* as a model for Gram-negative bacteria," *Journal of Colloid and Interface Science*, vol. 275, no. 1, pp. 177–182, 2004.
- [35] Y.-F. Liu, G.-Q. Wang, J.-B. Zhao, L. Jiang, S.-M. Fang, and Y.-A. Sun, "Synthesis of chiral silver nanoclusters capped with small molecules," *Colloids and Surfaces A*, vol. 426, pp. 12–17, 2013.
- [36] T. U. B. Rao and T. Pradeep, "Luminescent Ag_7 and Ag_8 clusters by interfacial synthesis," *Angewandte Chemie*, vol. 49, no. 23, pp. 3925–3929, 2010.

- [37] G. de Cremer, E. Coutiño-Gonzalez, M. B. J. Roeffaers et al., "Characterization of fluorescence in heat-treated silver-exchanged zeolites," *Journal of the American Chemical Society*, vol. 131, no. 8, pp. 3049–3056, 2009.
- [38] Q. Cui, Y. Shao, K. Ma, S. Xu, F. Wu, and G. Liu, "Upconversion emission of fluorescent silver nanoclusters and in situ selective DNA biosensing," *Analyst*, vol. 137, no. 10, pp. 2362–2366, 2012.
- [39] S. Pan, X. Liu, and X. Wang, "Preparation of Ag₂S-Graphene nanocomposite from a single source precursor and its surface-enhanced Raman scattering and photoluminescent activity," *Materials Characterization*, vol. 62, no. 11, pp. 1094–1101, 2011.
- [40] X. M. Wang, W. R. Gao, S. P. Xu, and W. Q. Xu, "Luminescent fibers: *in situ* synthesis of silver nanoclusters on silk via ultraviolet light-induced reduction and their antibacterial activity," *Chemical Engineering Journal*, vol. 210, pp. 585–589, 2012.
- [41] T. Xu, L. Wu, Y. Yu, W. Li, and J. Zhi, "Synthesis and characterization of diamond-silver composite with anti-bacterial property," *Materials Letters*, vol. 114, pp. 92–95, 2014.

Research Article

Targeted *In Vivo* Imaging of Mouse Hindlimb Ischemia Using Fluorescent Gelatin Nanoparticles

Ju Zhang,¹ Gang Wang,¹ Duo Mao,¹ Aitian Han,¹ Nannan Xiao,¹ Xin Qi,²
Dan Ding,¹ and Deling Kong¹

¹State Key Laboratory of Medicinal Chemical Biology, Key Laboratory of Bioactive Materials, Ministry of Education, College of Life Sciences, and Collaborative Innovation Center of Chemical Science and Engineering (Tianjin), Nankai University, Tianjin 300071, China

²Tianjin Union Medicine Center (Nankai University Affiliated Hospital), Clinical and Translation Medicine Lab, Tianjin 300121, China

Correspondence should be addressed to Xin Qi; qixinx2011@126.com and Dan Ding; dingd@nankai.edu.cn

Received 16 October 2014; Accepted 17 December 2014

Academic Editor: Shuming Zhang

Copyright © 2015 Ju Zhang et al. This is an open access article distributed under the Creative Commons Attribution License, which permits unrestricted use, distribution, and reproduction in any medium, provided the original work is properly cited.

Critical limb ischemia is one of the most advanced forms of peripheral artery disease, which seriously threat the human health and even cause amputation. In this study, we developed a fluorescent gelatin nanoparticle (FGNP) by covalent conjugation of the nanoparticles with two fluorogens, Cy7 and rhodamine B. The FGPNs have a volume average hydrodynamic diameter of about 168 nm, which also show low cytotoxicity against NIH/3T3 normal cells. The *in vivo* ischemia bioimaging studies in live mice and in ischemic limb slices demonstrate that the FGPNs can be preferentially accumulated to the ischemic site, which can thus serve as a safe and effective probe for targeted visualization of ischemia in the limb.

1. Introduction

The research on biocompatible nanomaterials for diagnosis and treatment of diseases has attracted increasing interest, as these nanomaterials exhibit the merits of improved water solubility of hydrophobic therapeutic/imaging agents, targeted delivery of the agents in a cell- or tissue-specific manner, and codelivery of both treatment and imaging agents for simultaneous theranostics [1–3]. Ischemic disease refers to the restriction in blood supply to tissues/organs, which would result in the damage to or dysfunction of tissues and may lead to tissue death. Ischemic disease would occur in a variety of tissues including heart (myocardial infarction), bowel (ischemic colitis and mesenteric ischemia), brain (stroke), skin (cyanosis), and limb (critical limb ischemia). Among them, critical limb ischemia is one of the most advanced forms of peripheral artery disease, which seriously threat the human health and even cause amputation [4, 5]. In the past decades, however, considerable efforts have been made on the nanotechnology systems aimed at therapeutics and diagnostics of cancer. There have been very few works

focused on the treatment and imaging of ischemic limb disease using biocompatible nanomaterials [6]. As a consequence, the unique advantages of nanotechnology motivate us to explore biocompatible nanomaterials to address some issues in the field of ischemic limb disease.

Biocompatible and biodegradable polymeric nanoparticles have been extensively investigated in recent years for both therapeutic and diagnostic purposes of cancers, which hold great promise as reliable, effective, and safe systems for *in vivo* applications and further clinical translation [7]. Many types of polymeric nanomaterials such as self-assembling synthetic polymers, polysaccharide, and protein nanoparticles have shown their uniqueness in various biomedical utilities [8, 9]. Among these colloidal systems, protein-based nanomaterials have received great attention as they have the advantages of less immunogenicity, nontoxicity, facile preparation, and long-term storage stability. Besides, protein-based nanomaterials are also allowed for flexible surface functionalization by virtue of the large number of pendant functional groups in the protein structure [10, 11]. As a naturally occurring protein, gelatin that is obtained by hydrolytic degradation

of collagen has a long history of safe applications in the areas of medicine, cosmetics, and food [12–14]. Due to the aforementioned reasons, gelatin was selected in the present study as the starting material to fabricate biocompatible fluorescent nanoparticles.

In this contribution, we report the preparation of fluorescent gelatin nanoparticles (FGNPs), which can target visualization of the ischemia in the mouse hind limb. The gelatin nanoparticles were synthesized via a two-desolvation method [13, 14], which were subsequently covalently conjugated with two fluorogens, Cy7 and rhodamine B, in order to trace the gelatin nanoparticles in both noninvasive manner and single-cell resolution. The imaging studies in a mouse ischemic hind limb model reveal that FGNPs can be preferentially accumulated into the ischemic muscles from blood circulation. This study thus offers fundamental guidelines to use biocompatible nanomaterials for the treatment and diagnosis of ischemic diseases, which will inspire more exciting research in this emerging field.

2. Materials and Methods

2.1. Materials. Gelatin type A from porcine skin (175 Bloom Sigma-Aldrich, Steinheim, Germany) and rhodamine B isothiocyanate were purchased from Sigma Aldrich. Cy7 NHS ester was obtained from Lumiprobe Co., Ltd. All the other starting materials were obtained from Alfa. Commercially available reagents were used without further purification, unless noted otherwise.

2.2. Characterization. UV-vis spectra were recorded on a Shimadzu UV-1700 spectrometer. Emission spectra were recorded on a Perkin-Elmer LS 55 spectrofluorometer. The nanoparticle size was measured with Zetasizer Nano ZS (Nano-ZS, MALVERN). The morphology of the nanoparticles was studied by scanning electron microscopy (SEM, JSM-6700F, JEOL, Japan) at an accelerating voltage of 10 kV. The sample was fixed on a stub with a double-sided sticky tape and then coated with a platinum layer using an autofine coater (JEOL, Tokyo, Japan) for 60 s in vacuum at a current intensity of 10 mA. The morphology of NPs was also investigated by transmission electron microscopy (TEM, JEM-2010F, JEOL, Japan).

2.3. Preparation of FGNPs. 1 g of gelatin powder was dissolved in 20 mL of deionized water under magnetic stirring at 40°C. Subsequently, a large amount of acetone was added to achieve the desolvation and rapid sedimentation of the gelatin. After discarding the supernatant, the gelatin colloid was redissolved in 20 mL of deionized water. The pH value of the solution was adjusted to 2.7 using a 1 M HCl solution. The gelatin nanoparticles were formed by controlled precipitation of the aqueous gelatin solution with acetone under continuous stirring. After that, 7.5 μ L of 50% glutaraldehyde was added to cross-link the gelatin nanoparticles, which was allowed to be stirred overnight. The gelatin nanoparticle suspension was purified by ultrafiltration (molecule weight cutoff 12 kDa) to remove the acetone and extra cross-linker. The stock solution of gelatin nanoparticles was prepared at

the concentration of 5 mg/mL. To prepare FGNPs, Cy7 NHS ester was dissolved in DMSO at 1 mg/mL. The suspension of gelatin nanoparticles was adjusted to pH around 8.0 by 0.2 N of sodium hydroxide solution. Subsequently, 100 μ L of the dye solution was added to 2 mL of the gelatin nanoparticle stock solution, which was agitated gently for 12 h. The Cy7-labeled gelatin nanoparticles were purified by ultrafiltration (molecule weight cutoff 12 kDa) to remove unconjugated Cy7. The rhodamine B isothiocyanate was also labeled to the gelatin nanoparticles under the same procedure.

2.4. Cell Viability Assay. Cytotoxicity of the FGNPs was evaluated with mouse NIH/3T3 cells using a cell counting kit-8 (CCK-8) viability assay. In this experiment, the cells were divided into two groups, the control group and the sample group. In detail, the cells were seeded with a density of 5×10^3 cells/well in 96-well microtiter plates and preincubated for 24 h under 5% CO₂ in the cell incubator at 37°C using DMEM cell culture media (Hyclone). The cells in sample group were then treated with a series of concentrations of FGNPs. After 24 h incubation, 10 μ L of CCK-8 (Dojindo, Japan) solution that was predissolved in cell culture medium was added to each well. After incubation for 40 min, the absorbance of each well was measured by a microplate reader (Thermo Scientific Varioskan Flash) at the wavelength of 450 nm. The proliferation rates of NIH/3T3 cells after incubation with FGNPs were presented as the ratio of absorbance of cells in sample group to that of cells in control group. There were six parallel samples in each group.

2.5. Bioimaging in a Mouse Ischemic Hind Limb Model. All animal studies were conducted under a protocol approved by Nankai University. ICR mice (20–30 g, 8–10 weeks old) were purchased from Vital River Laboratory Animal Technology Co., Ltd. (Beijing, China). The mice were anesthetized by intraperitoneal injection of 4% chloral hydrate solution at a dosage of 8 μ L per gram body weight. Unilateral hind limb ischemia in the left leg was induced in male ICR mice by ligation and excision of the right femoral artery distal to the inguinal ligament. The ischemic limb-bearing mice were then injected with 200 μ L of FGNPs via the tail vein. The mice were then anesthetized and placed on an animal plate heated to 37°C. The time-dependent biodistribution of the FGNPs in ischemic limb-bearing mice was imaged using a Maestro EX *in vivo* fluorescence imaging system (CRi, Inc.). The light with a central wavelength at 735 nm was selected as the excitation source. *In vivo* spectral imaging from 780 nm to 950 nm (10 nm step) was carried out with an exposure time of 150 ms for each image frame. The autofluorescence was removed using spectral unmixing software. Scans were carried out at 4 h and 24 h after injection, respectively. In addition, at 4 h and 24 h after injection, respectively, the ischemic limb-bearing mice intravenously injected with FGNPs were sacrificed and the tissues including spleen, liver, lung, kidney, and ischemic and nonischemic limbs were isolated and imaged using the Maestro system. The average fluorescence intensity of each harvested tissue ($n = 3$ mice per group) was calculated for a semiquantitative biodistribution study using the Maestro software.

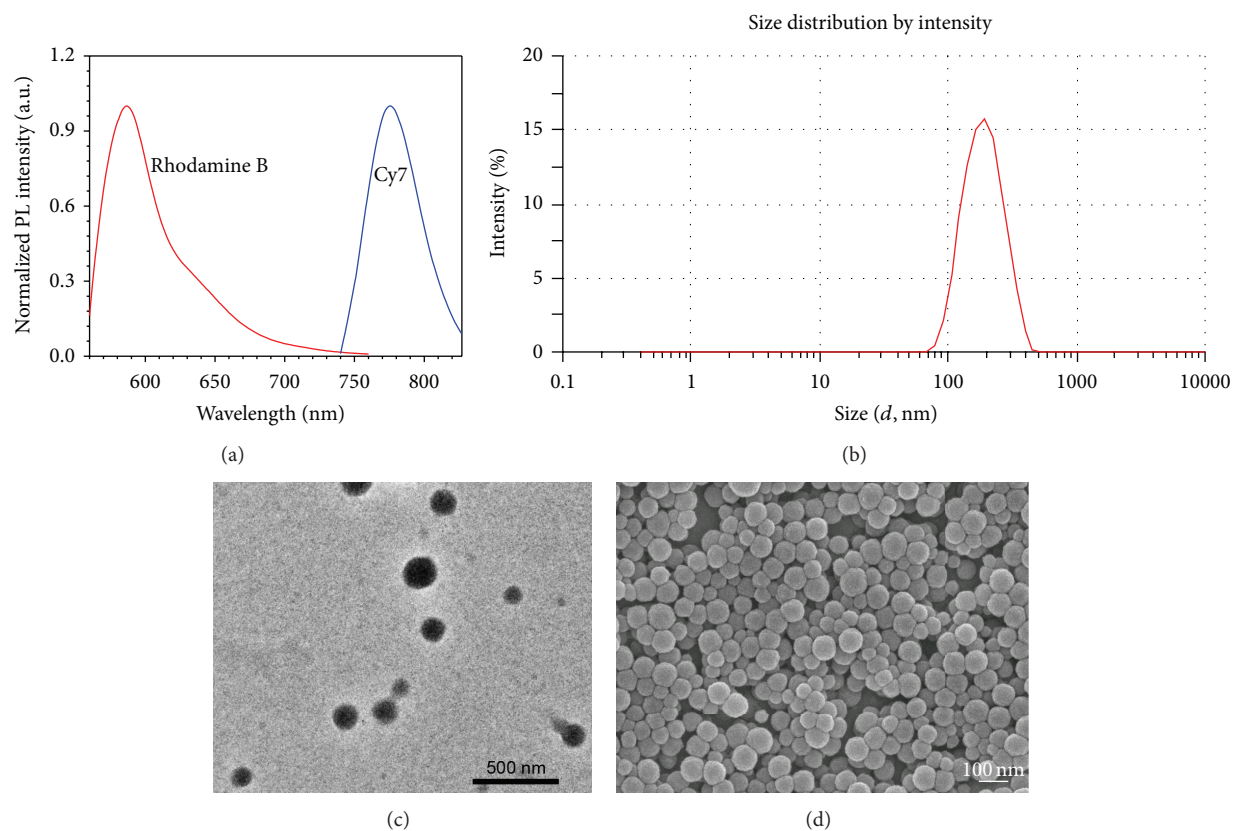


FIGURE 1: (a) Photoluminescence spectra of FG NPs in water upon excitation at 543 nm (for rhodamine B) and 735 nm (for Cy7), respectively. (b) Size distribution of FG NPs measured by DLS. (c) TEM and (d) SEM images of FG NPs.

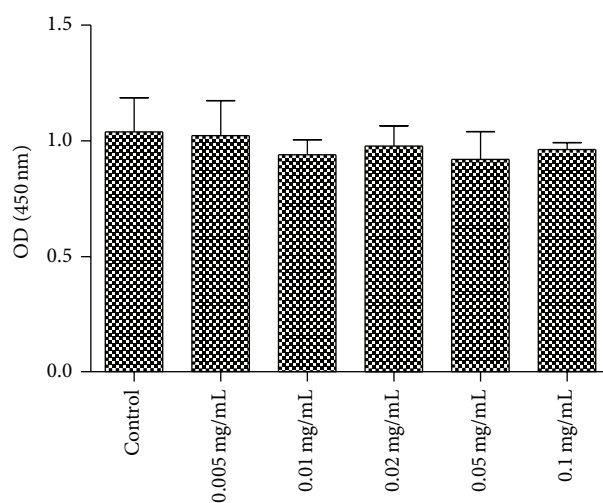


FIGURE 2: Proliferation rates of NIH/3T3 cells after incubation with FG NPs at various concentrations for 24 h by CCK-8 assay.

2.6. Immunostaining Study. To investigate the distribution of FG NPs in relation to blood vessels, the ischemic limb slices were obtained from the ischemic limb-bearing mice treated with FG NPs for 24 h. The ischemic limbs

were fixed in 4% paraformaldehyde for 2 h, incubated in 20% sucrose/PBS overnight, and embedded in Optimal Cutting Temperature (OCT) compound (Tissue-Tek). Sections (6 μ m) were immunostained with monoclonal

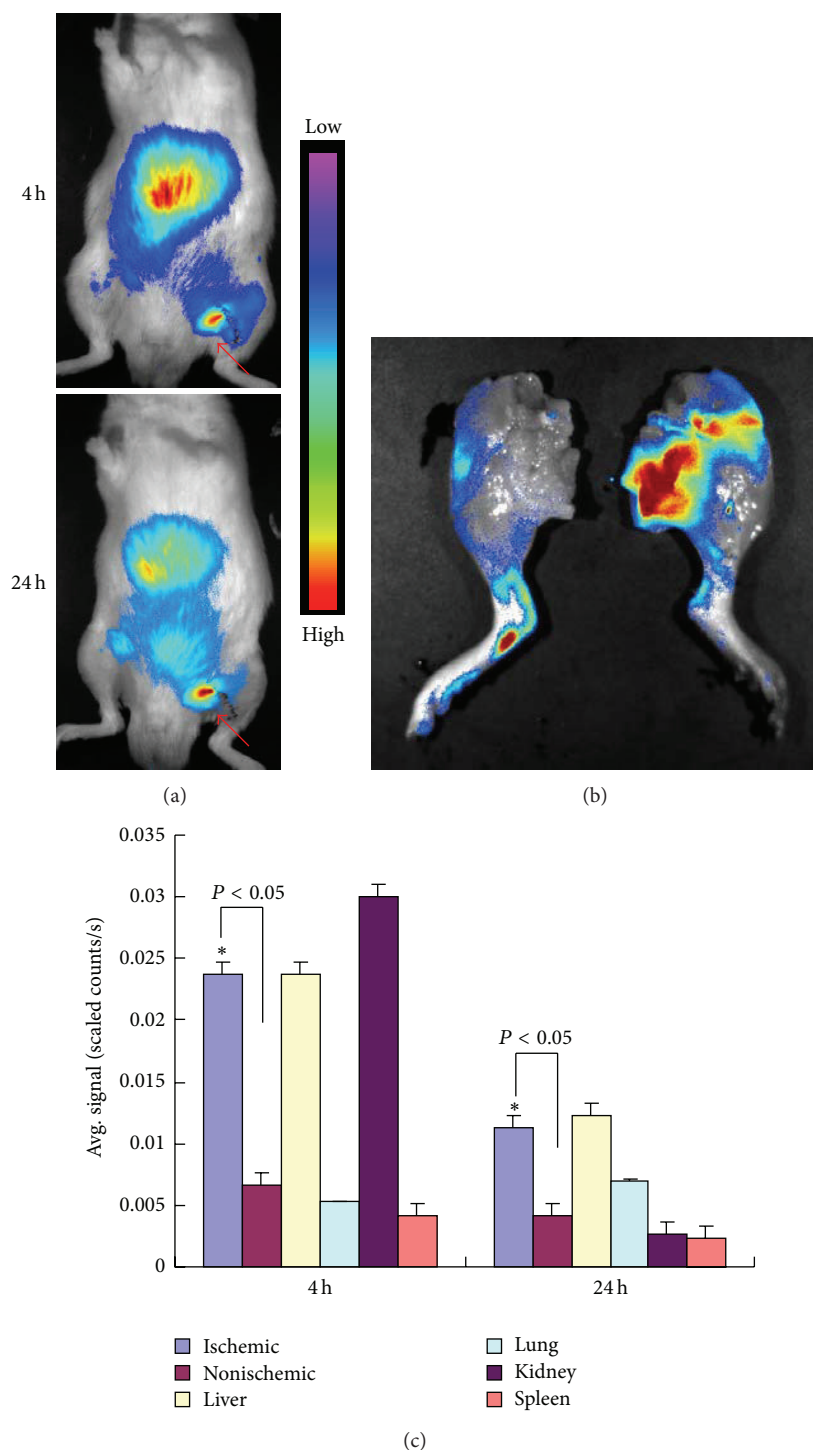


FIGURE 3: (a) *In vivo* noninvasive fluorescence imaging of ischemic limb-bearing mice after intravenous injection of FG-NPs for 4 h and 24 h, respectively. The red arrows indicate the ischemic site. (b) *Ex vivo* fluorescence imaging of ischemic and nonischemic limbs from mice treated with FG-NPs for 24 h. (c) Semiquantitative biodistribution analysis of FG-NPs in the indicated tissues at 4 h and 24 h after injection, respectively. Data are presented as mean \pm standard deviation ($n = 3$). * represents statistical significance ($P < 0.05$).

antibody against platelet/endothelial cell adhesion molecule 1 (PECAM-1; PharMingen). Alexa Fluor 488-conjugated anti-rat antibody was used as secondary antibody (Molecular Probes). The FG-NPs were excited at 543 nm and the blood vessels were imaged upon excitation at 488 nm.

2.7. Histology Observation. The tissues including liver, spleen, and kidney from the ischemic limb-bearing mice that received FG-NPs were selected for histology observation on the 7th day after injection ($n = 3$ mice per group). The organs were dissected and fixed in 10% neutral buffered

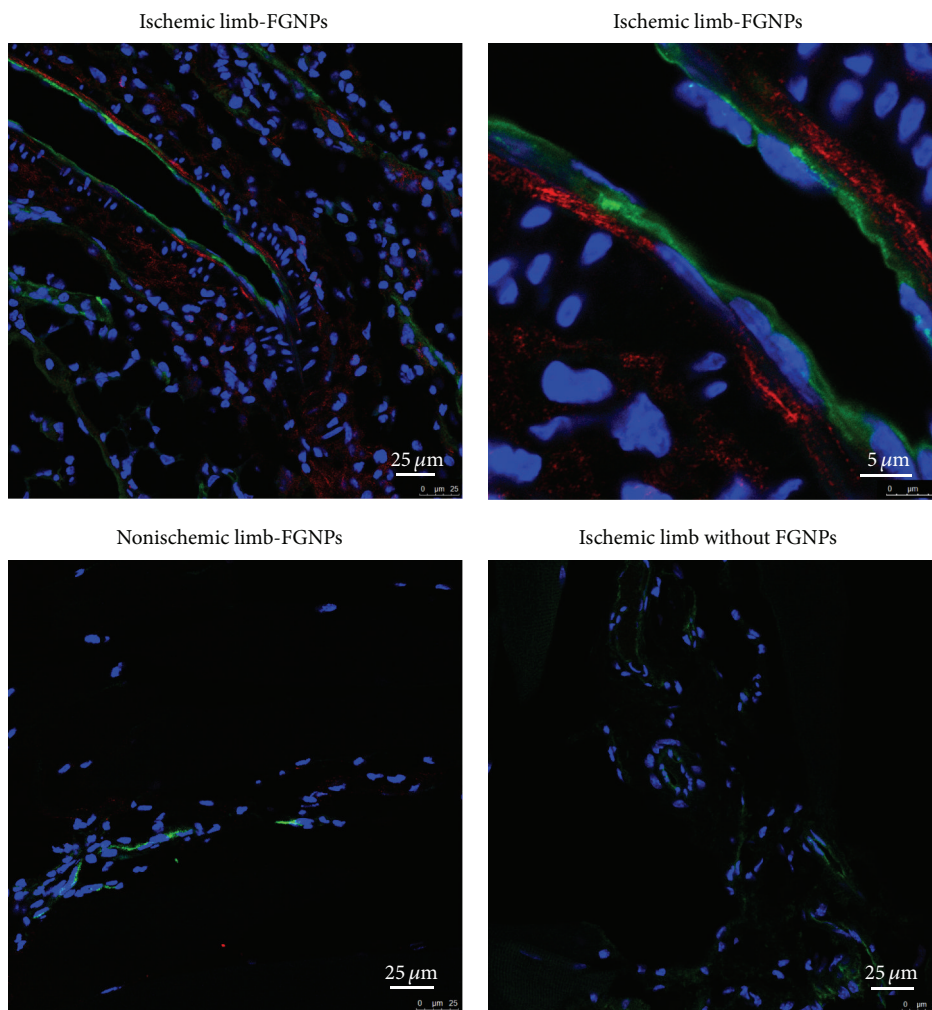


FIGURE 4: Confocal fluorescence images of ischemic and nonischemic limb slices from mice after intravenous injection with FG-NPs for 24 h. The blood vessels were immunostained against platelet/endothelial cell adhesion molecule 1 (PECAM-1). The cell nuclei were stained with 4',6-diamidino-2-phenylindole (DAPI).

formalin. Thereafter, the tissues were processed routinely into paraffin, sectioned at a thickness of $4\ \mu\text{m}$, and stained with hematoxylin and eosin (H&E). The slices obtained were examined by optical microscopy.

2.8. Statistical Analysis. Quantitative data were expressed as mean \pm standard deviation. Statistical comparisons were made by ANOVA analysis and Student's *t*-test. *P* value < 0.05 was considered statistically significant.

3. Results and Discussion

3.1. Preparation and Characterization of FG-NPs. Gelatin nanoparticles were prepared by the two-desolvation method through addition of acetone into gelatin aqueous solution, followed by nanoparticle cross-linking with glutaraldehyde. To track the gelatin nanoparticles *in vivo*, a near-infrared fluorescent dye, Cy7, was labeled to gelatin nanoparticles, allowing for noninvasive live animal imaging. Moreover,

to visualize nanoparticles in tissue slices with single-cell resolution, rhodamine B was also conjugated to the nanoparticles, affording Cy7 and rhodamine B dual-labeled gelatin nanoparticles (FG-NPs). The emission spectra of FG-NPs in water upon excitation at 543 nm and 735 nm, respectively, are shown in Figure 1(a). The FG-NPs have emission peaks centered at 587 nm and 776 nm, respectively, at each excitation wavelength, which demonstrates that the FG-NPs are labeled with both fluorogens. The dynamic light scattering (DLS) result suggests that the FG-NPs have a volume average hydrodynamic diameter of around 168 nm (Figure 1(b)). The zeta potential of the FG-NPs is measured to be $-1.6\ \text{mV}$. Transmission electron microscopy (TEM) and scanning electron microscopy (SEM) images of FG-NPs are shown in Figures 1(c) and 1(d), which indicate that the FG-NPs are spherical in shape with an average size of about 134 nm. This is smaller as compared to that determined by DLS owing to the shrinkage of nanoparticles in the dry state [15]. Furthermore, the cell proliferation rates of NIH/3T3 normal cells after incubation

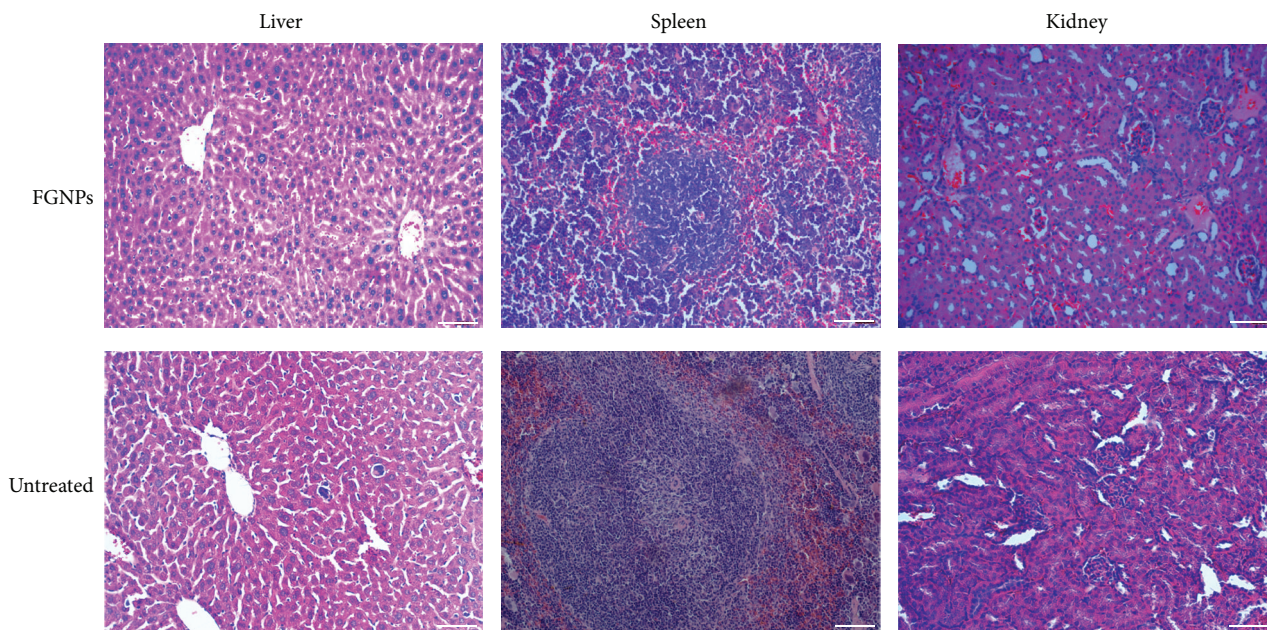


FIGURE 5: Typical images taken from H&E-stained liver, spleen, and kidney slices from mice treated with and without FG NPs. The scale bar is 100 μm .

with FG NPs at different concentrations for 24 h were quantitatively determined by the CCK-8 assay, as shown in Figure 2. The result indicates that the FG NPs are nontoxic against NIH/3T3 cells, suggesting that the FG NPs are biocompatible and promising for further *in vivo* applications.

3.2. Targeted Visualizing of Ischemia in the Mouse Limb.

The application of FG NPs in imaging ischemic limb in live mice was also studied by the noninvasive live animal fluorescence imaging technique. In this experiment, a hind limb ischemia mouse model was established and employed. After intravenous injection with the FG NPs, the ischemic limb-bearing mice were imaged with a Maestro EX *in vivo* fluorescence imaging system. The light with a central wavelength at 735 nm was selected as the excitation source to excite Cy7 in the FG NPs. Through spectral unmixing utilizing the Maestro software, the mouse autofluorescence was removed. Figure 3(a) shows the *in vivo* distribution of FG NPs in the ischemic limb-bearing mice 4 h and 24 h after injection, respectively. As shown in Figure 3(a), the red arrows indicate the ischemic site and intense fluorescence signals are observed in the ischemic site of the mouse hind limb at both 4 h and 24 h after administration. The sharp fluorescence intensity contrast between ischemic and nonischemic limbs reveals that the FG NPs can serve as an effective probe for ischemic site visualization in a highly sensitive manner. The ability of the FG NPs to clearly illustrate the ischemic site should be ascribed from the enhanced permeability and retention (EPR) effect, known as “passive” targeting [16], thanks to the nanoscale size of the FG NPs. At 24 h after injection, the mice were sacrificed and the ischemic as well as nonischemic limbs were excised for *ex vivo*

fluorescence imaging. As illustrated in Figure 3(b), the image demonstrates the prominent passive targeting capability of the FG NPs to the ischemic site.

Moreover, the main organs of the FG NP-administrated mice including liver, lung, kidney, and spleen were also excised and the average fluorescence signal of each harvested tissue at 4 h and 24 h after injection, respectively, was measured for a semiquantitative biodistribution analysis. As shown in Figure 3(c), besides the preferential accumulation in the ischemic limb, the FG NPs are mainly distributed in the liver and kidney tissues at 4 h after injection. With the time elapses, the fluorescence signals in both liver and kidney significantly decrease, indicating that the FG NPs can be excreted from the body by the corresponding pathways [17]. Furthermore, the difference in fluorescence intensity between ischemic and nonischemic limbs is statistically significant at both time points.

The ischemic and nonischemic limbs from mice after intravenous injection of FG NPs for 24 h were excised and sliced for immunostaining against platelet/endothelial cell adhesion molecule 1 (PECAM-1) in order to visualize the blood vessels in the limbs. As exhibited in Figure 4, it is obvious that the red fluorescence of FG NPs (from rhodamine B upon excitation at 543 nm) is localized near the blood vessels (green fluorescence). On the other hand, almost no detectable fluorescence signal from FG NPs can be observed near or close to the vasculature. These results reveal that the FG NPs can be accumulated into the ischemic site via the blood vessels in the ischemic muscle, confirming the prominent passive targeting ability of the FG NPs. As control, there is nearly no detectable red fluorescence in the slice of ischemic limb from mice without FG NP administration.

In addition, the main organs including liver, spleen, and kidney from mice injected with FG-NPs were performed on for histological analyses. Figure 5 shows the optical images from hematoxylin and eosin- (H&E-) stained slices in these tissues, which indicate that the FG-NPs would not cause any significant lesion to the normal organs compared with those from untreated mice, as verified by 3 independent pathologists. This result reveals that the FG-NPs hold great potential to be a safe and effective nanoprobe for visualization of ischemia in the limb.

4. Conclusions

We report the synthesis and characterization of a fluorescent gelatin nanoparticle, which possesses a mean size of around 168 nm measured by DLS, low cytotoxicity, and ability to visualize ischemic limb in both noninvasive manner and single-cell resolution. We have demonstrated that the FG-NPs can serve as a safe and efficient probe for imaging ischemic limb. This study will open up a new avenue for development of biocompatible nanomaterials in the therapeutics and diagnostics of ischemic diseases.

Conflict of Interests

The authors declare that there is no conflict of interests regarding the publication of this paper.

Authors' Contribution

Ju Zhang and Gang Wang contributed equally to this work.

Acknowledgments

This work was supported by grants from the National Basic Research Program of China (2011CB964903), NSFC (81220108015 and 81301311), and the Program for Changjiang Scholars and Innovative Research Team in University (IRT13023).

References

- [1] X. Gao, Y. Cui, R. M. Levenson, L. W. K. Chung, and S. Nie, "In vivo cancer targeting and imaging with semiconductor quantum dots," *Nature Biotechnology*, vol. 22, no. 8, pp. 969–976, 2004.
- [2] D. Ding, Z. Zhu, R. Li et al., "Nanospheres-incorporated implantable hydrogel as a trans-tissue drug delivery system," *ACS Nano*, vol. 5, no. 4, pp. 2520–2534, 2011.
- [3] L. Lian, F. Tang, J. Yang, C. Liu, and Y. Li, "Therapeutic angiogenesis of PLGA-heparin nanoparticle in mouse ischemic limb," *Journal of Nanomaterials*, vol. 2012, Article ID 193704, 6 pages, 2012.
- [4] H. N. Yang, J. S. Park, D. G. Woo, S. Y. Jeon, and K.-H. Park, "Transfection of VEGF₁₆₅ genes into endothelial progenitor cells and in vivo imaging using quantum dots in an ischemia hind limb model," *Biomaterials*, vol. 33, no. 33, pp. 8670–8684, 2012.
- [5] Y. Li, W. Liu, F. Liu et al., "Primed 3D injectable microniches enabling low-dosage cell therapy for critical limb ischemia," *Proceedings of the National Academy of Sciences*, vol. 111, no. 37, pp. 13511–13516, 2014.
- [6] J. Kim, L. Cao, D. Shvartsman, E. A. Silva, and D. J. Mooney, "Targeted delivery of nanoparticles to ischemic muscle for imaging and therapeutic angiogenesis," *Nano Letters*, vol. 11, no. 2, pp. 694–700, 2011.
- [7] Z. Ge and S. Liu, "Functional block copolymer assemblies responsive to tumor and intracellular microenvironments for site-specific drug delivery and enhanced imaging performance," *Chemical Society Reviews*, vol. 42, no. 17, pp. 7289–7325, 2013.
- [8] J.-H. Kim, Y.-S. Kim, K. Park et al., "Self-assembled glycol chitosan nanoparticles for the sustained and prolonged delivery of antiangiogenic small peptide drugs in cancer therapy," *Biomaterials*, vol. 29, no. 12, pp. 1920–1930, 2008.
- [9] D. Ding, Z. Zhu, Q. Liu et al., "Cisplatin-loaded gelatin-poly(acrylic acid) nanoparticles: synthesis, antitumor efficiency in vivo and penetration in tumors," *European Journal of Pharmacology and Biopharmaceutics*, vol. 79, no. 1, pp. 142–149, 2011.
- [10] M. G. Anhorn, S. Wagner, J. Kreuter, K. Langer, and H. von Briesen, "Specific targeting of HER2 overexpressing breast cancer cells with doxorubicin-loaded trastuzumab-modified human serum albumin nanoparticles," *Bioconjugate Chemistry*, vol. 19, no. 12, pp. 2321–2331, 2008.
- [11] H. Wang, J. Liu, A. Han et al., "Self-assembly-induced far-red/near-infrared fluorescence light-up for detecting and visualizing specific protein-peptide interactions," *ACS Nano*, vol. 8, no. 2, pp. 1475–1484, 2014.
- [12] C. L. Tseng, W. Y. Su, K. C. Yen, K. C. Yang, and F. H. Lin, "The use of biotinylated-EGF-modified gelatin nanoparticle carrier to enhance cisplatin accumulation in cancerous lungs via inhalation," *Biomaterials*, vol. 30, no. 20, pp. 3476–3485, 2009.
- [13] C. Wong, T. Stylianopoulos, J. Cui et al., "Multistage nanoparticle delivery system for deep penetration into tumor tissue," *Proceedings of the National Academy of Sciences of the United States of America*, vol. 108, no. 6, pp. 2426–2431, 2011.
- [14] G. Kaul and M. Amiji, "Long-circulating poly(ethylene glycol)-modified gelatin nanoparticles for intracellular delivery," *Pharmaceutical Research*, vol. 19, no. 7, pp. 1061–1067, 2002.
- [15] D. Ding, C. C. Goh, G. Feng et al., "Ultrabright organic dots with aggregation-induced emission characteristics for real-time two-photon intravital vasculature imaging," *Advanced Materials*, vol. 25, no. 42, pp. 6083–6088, 2013.
- [16] M. Morille, T. Montier, P. Legras et al., "Long-circulating DNA lipid nanocapsules as new vector for passive tumor targeting," *Biomaterials*, vol. 31, no. 2, pp. 321–329, 2010.
- [17] Z. Liu, C. Davis, W. Cai, L. He, X. Chen, and H. Dai, "Circulation and long-term fate of functionalized, biocompatible single-walled carbon nanotubes in mice probed by Raman spectroscopy," *Proceedings of the National Academy of Sciences of the United States of America*, vol. 105, no. 5, pp. 1410–1415, 2008.

Research Article

Clinical Use of the Nanohydroxyapatite/Polyamide Mesh Cage in Anterior Cervical Corpectomy and Fusion Surgery

Hui Xu,^{1,2} Xiaofeng Ren,¹ Dawei Wang,¹ Yongfei Zhao,² Yan Wang,²
Geng Cui,² Songhua Xiao,² and Xuesong Zhang²

¹Department of Orthopedics, Liaocheng People's Hospital, 67 Dongchang West Road, Liaocheng, Shandong Province 252004, China

²Department of Orthopedics, Chinese People's Liberation Army General Hospital, Beijing 100853, China

Correspondence should be addressed to Yongfei Zhao; lakezyf@hotmail.com and Xuesong Zhang; zhangxuesong301@sina.com

Received 13 October 2014; Accepted 26 December 2014

Academic Editor: Shuming Zhang

Copyright © 2015 Hui Xu et al. This is an open access article distributed under the Creative Commons Attribution License, which permits unrestricted use, distribution, and reproduction in any medium, provided the original work is properly cited.

Purpose. This study was to report the clinical use of biomimetic nanohydroxyapatite/polyamide 66 (n-HA/PA 66) mesh cages in anterior cervical corpectomy and fusion (ACCF) surgery. **Method.** 95 patients who underwent single level anterior cervical corpectomy and fusion for cervical spondylosis myelopathy (CSM) in our hospital were reviewed and divided into 2 groups according to using nanohydroxyapatite/polyamide mesh cage and titanium mesh cage (TMC). Demographic data of patients and surgical, clinical, and radiological data before operation and at last follow-up were collected and compared. **Result.** The operation time, surgical blood loss, complications, and Japanese Orthopaedic Association scores (JOA scores) of two groups were similar. At the last follow-up both the two groups obtained 100% solid bone fusion, but the TMC group had higher rate of severe cage subsidence than the n-HA/PA 66 group (27% versus 2%). **Conclusion.** Nanohydroxyapatite/polyamide 66 mesh cage is safe and effective in ACCF and can be a substitution to titanium mesh cage.

1. Introduction

Nanohydroxyapatite/polyamide 66 (n-HA/PA 66) is a bio-composite made by nanotechnology using hydroxyapatite and polyamide [1]. Nanotechnology is popular in biomaterial field and is widely accepted by researchers [2–4]. Hydroxyapatite (HA) and natural bone mineral have similar composition and structure, so HA was considered as an ideal bone repair material due to its osteoconductivity. However the brittleness of HA decide that it only can be used in no load-bearing bone repair. When the HA was used as a strut it easily broke [5, 6]. Because chemical structure and active groups of polyamide (PA) are similar to collagen protein, it has good biocompatibility. PA also has excellent mechanical properties because of the strong hydrogen bonds in PA macromolecules [7, 8]. N-HA/PA 66 composite combined the advances of the two materials. So it was considered as an ideal material in bone defect repair and reconstruction.

N-HA/PA 66 composite was developed by thermal-press molding technique [9]. The porosity of the materials is 36% to 57% and average diameter of the pores is 280 μm to 500 μm . Good interface is provided by the irregular pores between n-HA/PA 66 and host bone; thus new bone tissue can grow in the pores. The porous n-HA/PA 66 composite is credited to have biological safety and to be effective [10, 11]. Devices made by this material have been used for bone repair and reconstruction successfully in recent years [12–14].

N-HA/PA 66 composite cages for anterior cervical discectomy and fusion (ACDF) or anterior cervical corpectomy and fusion (ACCF) were reported by several researchers and show good clinical results [15–17]. They concluded that the n-HA/PA 66 composite cages were even better than the titanium mesh cages which are widely used in the world currently. However a new material needs more studies to verify the efficacy and safety before it is widely accepted and used, so we reviewed the patients who received the operation

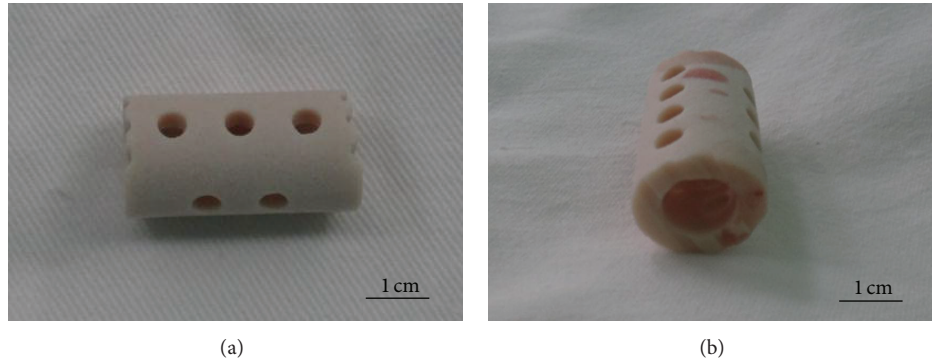


FIGURE 1: Lateral and axial view of the n-HA/PA 66 mesh cage.

of ACCF with nanohydroxyapatite/polyamide mesh cage and compared the outcomes to titanium mesh cage.

2. Patients and Methods

2.1. Patients. From January 2009 to June 2011, patients who underwent ACCF for cervical spondylosis myelopathy (CSM) in our hospital were reviewed. The patients' age, sex, height, photographs, radiographs, and clinical records were prospectively collected in our department database. The inclusion criteria were (1) patients with myelopathy, (2) the follow-up being at least 2 years, and (3) single-level ACCF surgery. The exclusion criteria were (1) cervical spondylosis radiculopathy or fracture, (2) cervical deformities or neoplasia, and (3) patients with multilevel corpectomy. 95 patients were included in this study with the age range 45–73 years. The patients were divided into two groups by using n-HA/PA 66 composite cages or titanium mesh cages (TMC).

2.2. N-HA/PA 66 Composite Cage. N-HA/PA 66 mesh cage (Figure 1) (National Nano Technology Co. Sichuan, China) was made of n-HA/PA 66 composite and it has a series of length and diameter size for individual's variation. This product was approved by Chinese FDA in 2005. Figure 2 is the TEM micrographs of n-HA/PA 66.

2.3. Surgical Technique. After general anesthesia, the neck of patients was padded in extension position. The Smith-Robinson method was used to perform anterior exposure [18]. Then the target cervical excision was confirmed by mobile digital imaging system, and cervical corpectomy and decompression were performed. The vertebral bone fragments were collected and used as graft material. The endplate of the upper and lower vertebrae was prepared with curette. Then TMC or n-HA/PA 66 mesh cages were selected with appropriate lengths, filled with local autologous bone, and implanted into corpectomy space (Figure 3). The anterior cervical plate was fixed to upper and lower cervical vertebrae with screws for further stabilization. After surgery, a soft cervical collar was used for six weeks.

2.4. Outcomes Assessment. Blood loss, operation time, complications of surgery, and hospital stay were recorded and

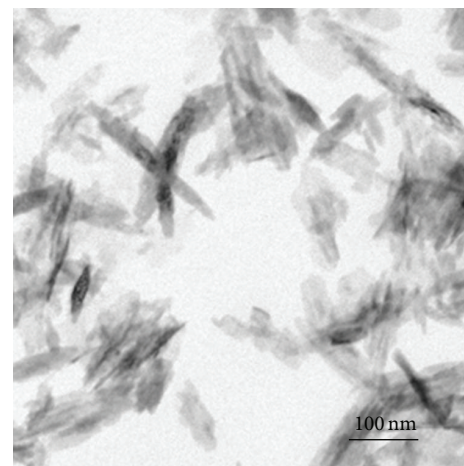


FIGURE 2: TEM micrographs of n-HA/PA 66.

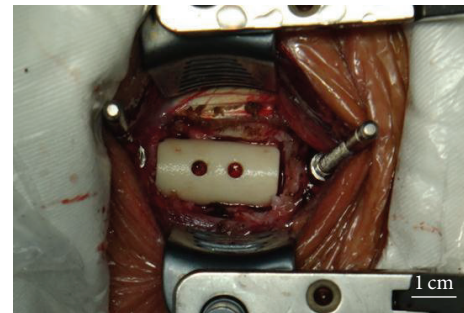


FIGURE 3: Implanting the cage after corpectomy.

compared between two groups. The Japanese Orthopedic Association (JOA) CSM scale was used to assess clinical result of each patient before surgery and at last follow-up.

The patients had radiological follow-up immediately, at one, three, and six months and then annually after surgery. The cervical spine radiographs were performed at each follow-up examination. Lateral plain radiographs were used to evaluate fusion status and cage subsidence. When trabecular bone grew across the interfaces, fusion was considered. If there was lucency between implants and

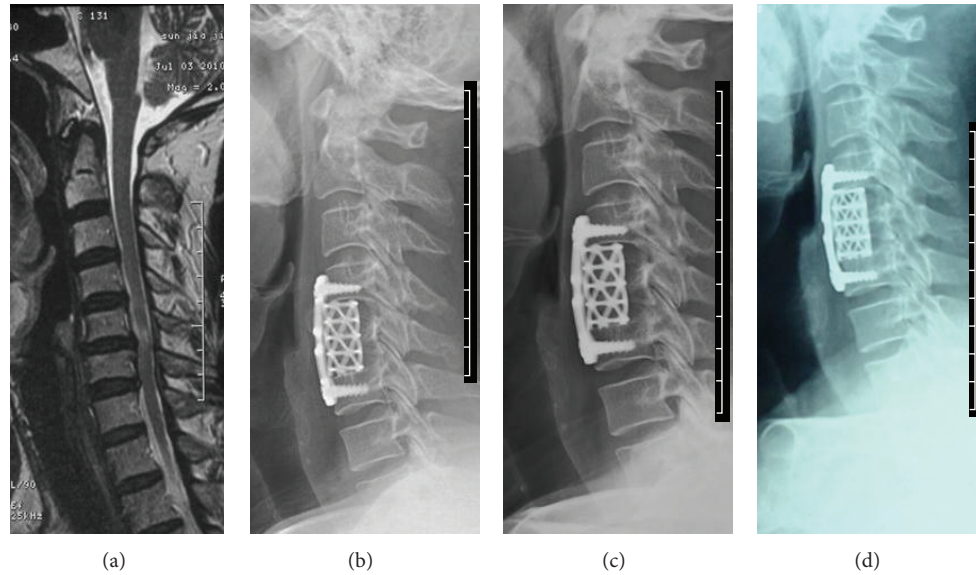


FIGURE 4: A 60-year-old man underwent anterior cervical corpectomy and fusion with a titanium mesh cage for CSM. (a) The compression located in the C5 level on the cervical MRI. (b) Lateral radiograph immediately after surgery. (c) 3 months after surgery the endplates were clear. (d) Two years after surgery the endplates were undefined and mild subsidence was observed.

vertebral endplates, nonunion would be considered. The change of fusion segments' height was defined as subsidence. When cage subsidence was bigger than three millimeters it was considered as severe subsidence. Five independent spine surgeons measured these radiographic parameters and the average value was calculated for final analysis.

2.5. Statistical Analysis. In this study all statistical analyses were performed using SPSS 17.0 statistic software (SPSS, Chicago, Illinois, USA). Student's *t*-test was used to compare mean data, and Pearson's Chi-squared test was performed for categorical data. $P < 0.05$ was considered as statistical significance.

3. Results

The anterior fusion was performed using TMC mesh cage in 59 patients (Figure 4) and n-HA/PA 66 mesh cage in 36 patients (Figures 5 and 6). The demographics of cases are shown in Table 1. There was no statistical difference between these two groups (all $P > 0.05$).

3.1. Surgical and Clinical Outcome. The operations were successfully performed in all patients. One patient of TMC group was reoperated 3 months after primary surgery because of screw loosening and plate displacement. No major procedure-related complications were found. There were no postoperative hematoma or wound infection in two groups. Some patients had dysphagia postoperatively, but they all were covered within 1 month. Duration of hospitalization, operation time, and blood loss were not statistically different between groups. The last follow-up JOA scores of both groups improved significantly compared to preoperative JOA scores.

TABLE 1: Demographic data of patients.

	n-HA/PA 66 (<i>n</i> = 36)	TMC (<i>n</i> = 59)	<i>P</i>
M/F	19 : 17	28 : 31	0.61
Age (years)	56.4 ± 12.8	58.6 ± 14.3	0.45
Smoker/nonsmoker	7 : 29	11 : 48	0.92
Follow-up (months)	30.6 ± 10.8	32.1 ± 12.8	0.56
Pathogenic level			
C4	3	4	
C5	10	19	
C6	15	25	
C7	8	11	

Sex, age, smoker, and follow-up were not statistically different between two groups.

However, there was no statistical difference between groups (Table 2).

3.2. Radiographic Result. There was no case of cage breakage in the two groups at the last follow-up. However, there were 3 cases of screw loosening in TMC group. At the last follow-up, the fusion rate was 100% in two groups. 1 and 16 severe cage subsidence instances were observed in n-HA/PA 66 group and TMC group respectively, which have statistical difference (Table 3).

4. Discussion

Anterior cervical corpectomy and fusion (ACCF) is used when the anterior compression surpasses the disc level such

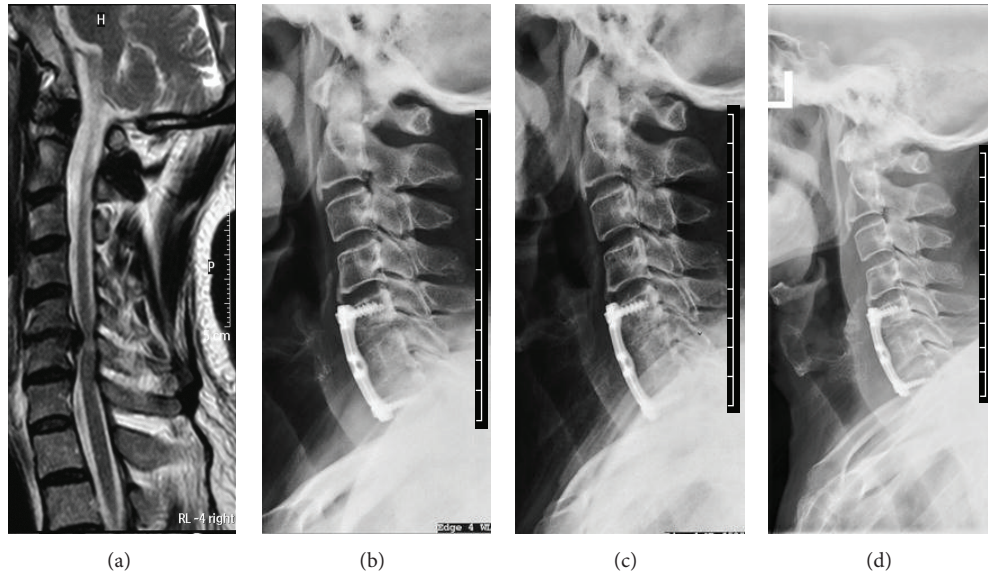


FIGURE 5: A 67-year-old man underwent cervical corpectomy and fusion with an n-HA/PA 66 mesh cage for CSM. (a) The compression located in the C6 level on the preoperative cervical MRI. (b) Lateral radiograph immediately after surgery. (c) 3 months after surgery. (d) Two years after surgery. The fusion status cannot be identified on the lateral radiograph, but cervical alignment, plate, and screws were not changed during follow-up.

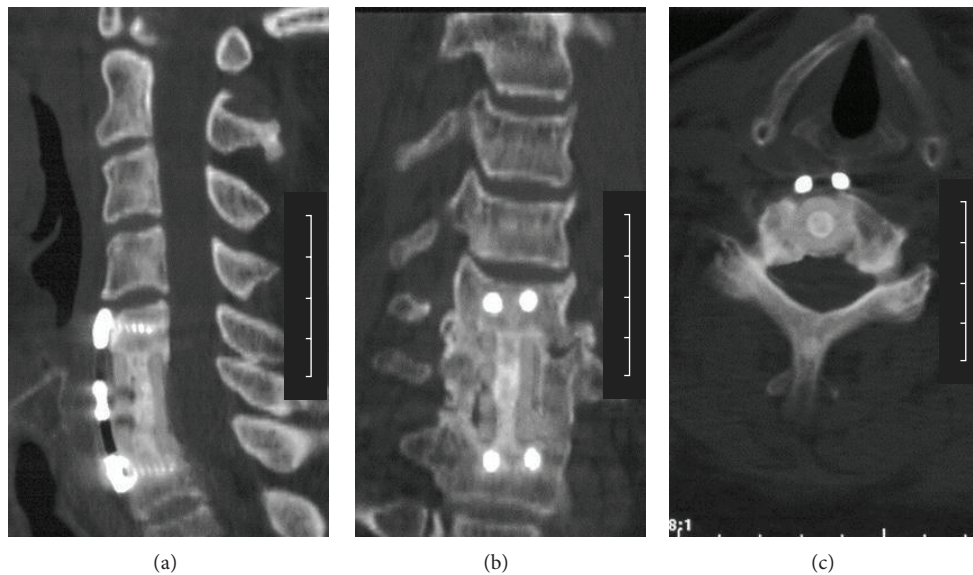


FIGURE 6: The same patient of Figure 5. One year after surgery solid fusion was seen on multiplane CT scan.

as ossification of the posterior longitudinal ligament (OPLL). Currently structural autografts, allografts, and cages are used as support structure implant in ACCF. However the donor site morbidity and the risk of disease transmission with allograft are concerns of many surgeons. Furthermore, there is much autologous local bone which can be used in the cage [19]. So cage devices become the best choice for cervical reconstruction. The cage filled with local bone can provide support, osteoinduction, and osteoconduction and has a high rate of osseous fusion.

Titanium mesh cage is widely used in anterior cervical corpectomy and fusion currently. And the clinical outcomes were favorable [20, 21]. However the high rate of cage subsidence has been observed in the past researches. Chen et al. found that TMC subsidence (more than one millimeter) occurred in 79.7% of patients and severe subsidence (more than three millimeters) in 19% of cases. They also concluded that severe TMC subsidence was correlated with bad clinical outcomes [22]. More recently, polymethylmethacrylate (PMMA), polyetheretherketone (PEEK), and carbon fiber

TABLE 2: Surgical and clinical outcomes.

	n-HA/PA66 (n = 36)	TMC (n = 59)	P
Hospitalization (day)	5.1 ± 1.6	4.9 ± 1.8	0.59
Operation time (mins)	120 ± 24	114 ± 32	0.33
Blood loss (mL)	124 ± 56	116 ± 54	0.49
Dysphagia	4	7	0.91
JOA scale preop	8.2 ± 1.4	8.5 ± 1.8	0.40
Last follow-up	14.1 ± 1.6*	13.4 ± 1.9*	0.07

* Compared to JOA scale preop $P < 0.05$.

TABLE 3: Radiographic result.

	n-HA/PA66 (n = 36)	TMC (n = 59)	P
Cage breakage	0	0	1
Screw loosening	0	3	0.28
Solid fusion	36	59	1
Reoperation	0	1	1
Cage subsidence*	1	16	0.006

* Cage subsidence was statistically different between two groups.

reinforced polymer (CFRP) cages have been developed for ACCF. But they are not widely used currently. At present, many nanomaterials have been used for bone regeneration because of their satisfactory osteogenic activity [23, 24]. A new n-HA/PA 66/glass fibre composite was developed by Qiao et al. and is still in experiment stage [25, 26].

The clinical results of n-HA/PA 66 cage have been gradually reported in recent years. Zhao et al. reported a 94.3% fusion rate and a 2.9% cage subsidence rate in their 35 patients [15]. Yang et al. found a fusion rate of 97% in 35 patients who underwent ACCF with an n-HA/PA 66 mesh cage fusion. They also compared the outcomes between the n-HA/PA 66 mesh cage and the TMC [17]. In their single-level cervical corpectomy series, solid bony fusion was found in 84% of patients in the TMC group at one year and in 94% four years after surgery. Solid fusion was found in 94% of patients in the n-HA/PA 66 mesh group at one year and in 97% four years after surgery. The rate of severe cage subsidence was 22% in TMC group and 6% in n-HA/PA 66 group. They also reported that the postoperative VAS and JOA points in TMC group were poorer than the ones in n-HA/PA 66 group. In our series, we found that the clinical results were similar between two groups. The operation time, surgical blood loss, complications, and JOA score of two groups were similar. At the last follow-up both the two groups obtained 100% solid fusion. But the TMC group had higher rate of severe cage subsidence than the n-HA/PA 66 group (27% versus 2%). We think the reason is that n-HA/PA 66 material has superior elasticity, good interface, and big contact surface which lead to sooner fusion. Severe cage subsidence can lead to screws loosening and plate displacement. One patient of TMC group underwent reoperation because of the symptoms caused by plate displacement in our cases.

There were several disadvantages in this research. First, this study was a retrospective research and further prospective study is necessary. Second, the method of estimating fusion rate was not accurate. The fusion in this study may be considered as “clinical fusion.” Flexion and extension X-ray films, CT scan, and even MRI should be used to judge the fusion status in future researches.

In conclusion, the n-HA/PA 66 mesh cage had safety and efficiency in ACCF. It was successfully used in ACCF and had good outcomes that can be a substitution to traditional TMC cage.

Conflict of Interests

The authors have no conflict of interests.

Authors' Contribution

Xuesong Zhang and Yongfei Zhao contributed equally to this paper.

References

- [1] M. Huang, J. Feng, J. Wang, X. Zhang, Y. Li, and Y. Yan, “Synthesis and characterization of nano-HA/PA66 composites,” *Journal of Materials Science: Materials in Medicine*, vol. 14, no. 7, pp. 655–660, 2003.
- [2] X. H. Liu, X. M. Li, Y. B. Fan et al., “Repairing goat tibia segmental bone defect using scaffold cultured with mesenchymal stem cells,” *Journal of Biomedical Materials Research Part B: Applied Biomaterials*, vol. 94B, no. 1, pp. 44–52, 2010.
- [3] X. M. Li, Y. Huang, L. S. Zheng et al., “Effect of substrate stiffness on the functions of rat bone marrow and adipose tissue derived mesenchymal stem cells in vitro,” *Journal of Biomedical Materials Research Part A*, vol. 102, no. 4, pp. 1092–1101, 2014.
- [4] X. Li, L. Wang, Y. Fan, Q. Feng, F. Z. Cui, and F. Watari, “Nanostructured scaffolds for bone tissue engineering,” *Journal of Biomedical Materials Research—Part A*, vol. 101, no. 8, pp. 2424–2435, 2013.
- [5] H. H. K. Xu and C. G. Simon Jr., “Fast setting calcium phosphate-chitosan scaffold: mechanical properties and biocompatibility,” *Biomaterials*, vol. 26, no. 12, pp. 1337–1348, 2005.
- [6] S. S. Kim, M. Sun Park, O. Jeon, C. Yong Choi, and B. S. Kim, “Poly(lactide-co-glycolide)/hydroxyapatite composite scaffolds for bone tissue engineering,” *Biomaterials*, vol. 27, no. 8, pp. 1399–1409, 2006.
- [7] S. I. Lee and B. C. Chun, “Mechanical properties and fracture morphologies of poly(phenylene sulfide)/nylon66 blends—effect of nylon66 content and testing temperature,” *Journal of Materials Science*, vol. 35, pp. 1187–1193, 2000.
- [8] Y. W. Wang, Q. Wu, J. Chen, and G. Q. Chen, “Evaluation of three-dimensional scaffolds made of blends of hydroxyapatite and poly(3-hydroxybutyrate-co-3-hydroxyhexanoate) for bone reconstruction,” *Biomaterials*, vol. 26, no. 8, pp. 899–904, 2005.
- [9] H. Li, Y. Li, Y. Yan, J. Li, A. Yang, and H. Xiang, “Fabrication of porous n-HA/PA66 composite for bone repair,” *Key Engineering Materials*, vol. 330–332, pp. 321–324, 2007.

- [10] H. Wang, Y. Li, Y. Zuo, J. Li, S. Ma, and L. Cheng, "Biocompatibility and osteogenesis of biomimetic nano-hydroxyapatite/polyamide composite scaffolds for bone tissue engineering," *Biomaterials*, vol. 28, no. 22, pp. 3338–3348, 2007.
- [11] Y. Xiong, C. Ren, B. Zhang et al., "Analyzing the behavior of a porous nano-hydroxyapatite/polyamide 66 (n-HA/PA66) composite for healing of bone defects," *International Journal of Nanomedicine*, vol. 9, no. 1, pp. 485–494, 2014.
- [12] X. Yang, Y. Song, L. Liu, H. Liu, J. Zeng, and F. Pei, "Anterior reconstruction with nano-hydroxyapatite/polyamide-66 cage after thoracic and lumbar corpectomy," *Orthopedics*, vol. 35, no. 1, pp. e66–e73, 2012.
- [13] X. Yang, Y. Song, Q. Kong, Q. Gong, F. Pei, and C. Tu, "Short-term effectiveness of nano-hydroxyapatite/polyamide-66 intervertebral cage for lumbar interbody fusion in patients with lower lumbar degenerative diseases," *Zhongguo Xiu Fu Chong Jian Wai Ke Za Zhi*, vol. 26, no. 12, pp. 1425–1429, 2012.
- [14] Y. Liu, S. Liu, and X. Su, "Core decompression and implantation of bone marrow mononuclear cells with porous hydroxylapatite composite filler for the treatment of osteonecrosis of the femoral head," *Archives of Orthopaedic and Trauma Surgery*, vol. 133, no. 1, pp. 125–133, 2013.
- [15] Z. Zhao, D. Jiang, Y. Ou, K. Tang, X. Luo, and Z. Quan, "A hollow cylindrical nano-hydroxyapatite/polyamide composite strut for cervical reconstruction after cervical corpectomy," *Journal of Clinical Neuroscience*, vol. 19, no. 4, pp. 536–540, 2012.
- [16] X. Yang, L. Liu, Y. Song, Q. Kong, J. Zeng, and C. Tu, "Outcome of single level anterior cervical discectomy and fusion using nano-hydroxyapatite/polyamide-66 cage," *Indian Journal of Orthopaedics*, vol. 48, no. 2, pp. 152–157, 2014.
- [17] X. Yang, Q. Chen, L. Liu et al., "Comparison of anterior cervical fusion by titanium mesh cage versus nano-hydroxyapatite/polyamide cage following single-level corpectomy," *International Orthopaedics*, vol. 37, no. 12, pp. 2421–2427, 2013.
- [18] Y. Fengbin, W. Xinwei, Y. Haisong, C. Yu, L. Xiaowei, and C. Deyu, "Dysphagia after anterior cervical discectomy and fusion: a prospective study comparing two anterior surgical approaches," *European Spine Journal*, vol. 22, no. 5, pp. 1147–1151, 2013.
- [19] A. M. T. Chau, L. L. Xu, J. H.-Y. Wong, and R. J. Mobbs, "Current status of bone graft options for anterior interbody fusion of the cervical and lumbar spine," *Neurosurgical Review*, vol. 37, no. 1, pp. 23–37, 2014.
- [20] K. R. Eck, K. H. Bridwell, F. F. Ungacta, M. A. Lapp, L. G. Lenke, and K. Daniel Riew, "Analysis of titanium mesh cages in adults with minimum two-year follow-up," *Spine*, vol. 25, no. 18, pp. 2407–2415, 2000.
- [21] A. E. Castellvi, A. Castellvi, and D. H. Clabeaux, "Corpectomy with titanium cage reconstruction in the cervical spine," *Journal of Clinical Neuroscience*, vol. 19, no. 4, pp. 517–521, 2012.
- [22] Y. Chen, D. Chen, Y. Guo et al., "Subsidence of titanium mesh cage: a study based on 300 cases," *Journal of Spinal Disorders and Techniques*, vol. 21, no. 7, pp. 489–492, 2008.
- [23] X. M. Li, H. F. Liu, X. F. Niu et al., "Osteogenic differentiation of human adipose-derived stem cells induced by osteoinductive calcium phosphate ceramics," *Journal of Biomedical Materials Research—Part B Applied Biomaterials*, vol. 97, no. 1, pp. 10–19, 2011.
- [24] X. M. Li, H. F. Liu, X. F. Niu et al., "The use of carbon nanotubes to induce osteogenic differentiation of human adipose-derived MSCs in vitro and ectopic bone formation in vivo," *Biomaterials*, vol. 33, no. 19, pp. 4818–4827, 2012.
- [25] B. Qiao, J. Li, Q. Zhu et al., "Bone plate composed of a ternary nano-hydroxyapatite/polyamide 66/glass fiber composite: biomechanical properties and biocompatibility," *International Journal of Nanomedicine*, vol. 9, no. 1, pp. 1423–1432, 2014.
- [26] B. Su, X. Peng, D. Jiang et al., "In vitro and in vivo evaluations of nano-hydroxyapatite/polyamide 66/glass fibre (n-HA/PA66/GF) as a novel bioactive bone screw," *PLoS ONE*, vol. 8, no. 7, Article ID e68342, 2013.

Research Article

The Preparation and *In Vitro* Evaluations of a Nanoscaled Injectable Bone Repair Material

Xinhui Liu,¹ Chao Zhu,¹ Yijiong Li,² Yueling Yan,² Chuanyong Hou,¹ Hua Wang,¹ Yelin Yang,¹ Guoping Guan,¹ and Qingling Feng³

¹Orthopaedics, The Affiliated Jiangning Hospital of Nanjing Medical University, Nanjing 211100, China

²Orthopaedics, The First Hospital of Hebei Medical University, Shijiazhuang 050031, China

³Department of Materials Science and Engineering, Tsinghua University, Beijing 100084, China

Correspondence should be addressed to Xinhui Liu; professorlxh2008@163.com

Received 19 September 2014; Revised 6 January 2015; Accepted 7 January 2015

Academic Editor: Shuming Zhang

Copyright © 2015 Xinhui Liu et al. This is an open access article distributed under the Creative Commons Attribution License, which permits unrestricted use, distribution, and reproduction in any medium, provided the original work is properly cited.

There are usually two forms of bone repair materials, block and granular, for common clinical use. This paper describes a novel injectable material, nano-HA/collagen/alginate (nHAC/Alg) composite biomaterial, including its preparation and evaluations *in vitro*. Based on the idea of bionics and the study of collagen/calcium phosphate salt composite materials, the injectable bone repair material was developed. Then, human bone marrow stem cells (hBMSCs) were cultured on the nHAC/Alg material. The cell attachment, proliferation, and differentiation were evaluated with inverted microscope, scanning electron microscope, laser scanning confocal microscope, 3-(4,5-dimethyl-2-thiazolyl)-2,5-diphenyl-2-H-tetrazolium bromide (MTT) analysis, and alkaline phosphatase (ALP) test. The results showed that nHAC/Alg not only had no negative effect on cellular functions but also promotes cell proliferation and differentiation into osteogenic cells, which suggests that the nanoscaled injectable bone repair material has good clinical application prospects for bone repair.

1. Introduction

Bone substitute is a common tool used in orthopaedics and dentistry to bridge bone deficiencies that may be due to trauma, disease, or surgery [1]. Nowadays, the design and the fabrication of injectable systems are becoming more and more important in minimally invasive surgical procedures and are given a special attention [2–8]. In particular the injectable bone substitutes (IBSs) that contained cements, pastes, putties, and gels have gained extreme interests in the field of bone regeneration. Compared to solid and preset scaffolds, IBSs are using a syringe through a very small incision, which could reduce patient malaise and shorten the time of surgical and recovery procedure. Meanwhile, IBSs could be a good filler of irregularly shaped bone defects and an intimate contact between the injected material and the bone surface [9]. In 2006, Liu and his team developed a novel injectable bone substitute material which consists of chitosan, citric acid, and glucose solution as the liquid phase

and tricalcium phosphate powder as the solid phase [10]. In 2009, a paper presented an improved sol-gel technique, which includes a premineralization step of atelocollagen providing a suspension of microfibrils in which the synthesis of the inorganic component was conducted at low temperature for the preparation of hydroxyapatite-atelocollagen composites suitable as precursor, for osseous regeneration [11]. In 2011, Ghanaati and coworkers described an injectable bone substitute being composed of beta-tricalcium phosphate granules, methylcellulose, and hyaluronic acid [12]. In 2012, Hu and his team composited a kind of compound of calcium sulfate hemihydrate (CSH) and nano-HA/collagen (nHAC) as an injectable and self-setting scaffold in bone graft substitute [13]. In 2013, D'Este and his members showed a well-established trend for bone substitutes, called combination of hydrogels and calcium phosphate particles [14], while Lian and his members developed a kind of mineralized collagen based composite nano-hydroxyapatite/collagen/poly called VCM/nHAC/PLA which showed good biocompatibilities

in vitro and *in vivo* [15]. In 2014, Chen and his team developed the nHAC/CSH composite as an injectable bone repair material with controllable injectability and self-setting properties prepared by introducing CSH into nHAC [16]. Meanwhile, Zheng et al. developed nanohydroxyapatite (nano-HA) reinforced collagen-alginate hydrogel (nHCA) that was prepared by the *in situ* synthesis of nano-HA in collagen gel followed by the addition of alginate and Ca^{2+} . The addition of alginate and nano-HA contributes to the increase in both mechanical and biological properties. This study may provide a valuable reference for the design of an appropriate composite scaffold for osteochondral tissue engineering [17].

By biomimetic strategy, many researchers have focused on the nHAC composites, which has shown a great promise in clinical applications because of their similar structural analogy to natural bone [18, 19]. The nHAC based scaffolds have now been successfully applied in the field of clinical applications, especially for the hard tissue repair [20].

In this study, we described a novel injectable material, composed of nHAC and alginate Alg. Then, human bone marrow stem cells (hBMSCs) were cultured on the nHAC/Alg material. The cell attachment, proliferation, and differentiation were evaluated and discussed.

2. Materials and Methods

2.1. Instruments and Equipment. In this study, centrifuge (produced by Heraeus company in Germany), inverted microscope (produced by Chongguang company in Chongqing), immunofluorescence microscope (produced by Lycra company in Germany), multiple tags immune analysis system (1420, WALLAC BLCTOR), CO_2 incubators (produced by Shellab company in Germany), Philips 525 M scanning electron microscope (produced by Philips company in Germany), and laser scanning confocal microscope (produced by Lycra company in Germany) were used to finish a series of testing experiments.

2.2. Reagent and Materials. The materials used in this study included 50 mL plastic bottle and 6, 24, 96-well culture plate (produced by Nunc company in Denmark), lymphocyte separation medium (percoll, 1.073 g/mL, produced by Huamei company in Shanghai), medium DMEM, heparin, L-ascorbic acid, dexamethasone Dex and sodium glycerol-phosphate (produced by Gibco company in America), trypsin (produced by Sigma company in America), FBS (fetal bovine serum, produced by Sijiqing company in Hangzhou), Rhodamine (produced by molecular probe company in USA), Leica Microsystems Heidelberg (produced by GmbH company in Germany), acid soluble type I collagen gel (solid content: 1%, produced by Beijing Beihua Fine Chemicals Co.), trisodium phosphate and calcium sulfate (produced by Beijing Yihua Fine Chemicals Co.), alginate (produced by China National Biotec Group chemical reagent co.), and calcium carbonate (produced by Beijing Modern Oriental Fine Chemicals Co.).

2.3. Preparation of nHAC/Alg. Firstly, sodium alginate and sodium phosphate ($\text{Na}_3\text{PO}_4 \cdot \text{H}_2\text{O}$) were mixed in deionized water and stirred for more than 20 minutes to obtain complete dissolution of the pale yellow aqueous solution of alginic acid. Then, calcium sulfate and deionized water according to the set ratio were mixed in a beaker and then stirred until no significant magnetic particles existed, followed by being put for more than 24 hours to remove the static electricity. Thirdly, nHAC powders were dissolved into deionized water and stirred completely until the material like bone paste was gotten, which were then mixed with the prepared alginic acid and stirred completely to get a kind of uniform mixture A, which were then mixed with calcium sulfate pulp to get uniform mixture B that was kept quietly for some time until the crosslinking took place completely inside material B. Many previous studies have shown that the alginate hydrogel is satisfactory carrier to prepare injectable biomaterials. [13, 21–25] At last, the materials will have exposure in the Co60 irradiation (2.5 Mrad) for disinfection and sterilization for further use.

2.4. The Separation of hBMSCs. Firstly, normal iliac bone marrow was extracted from healthy donors. Then, the bone marrow was centrifugated using three-gradient centrifugation with lymphocyte separation medium. The part above the white ring was taken over and put into DMEM medium which contains 10% fetal bovine serum medium and glutamine. Then the cell solution was put in T-50 culture bottle with cell amount of $3 \times 10^5/\text{mL}$, which was then incubated at 37°C and 5% CO_2 . The first replacement of medium was done at 48 hours. Afterwards, the medium was changed every other day. When the cells attached to and grew into confluence on the bottom of bottle, 0.5% trypsin was used to digest the attached cells down.

2.5. The Qualitative Observation of the Osteogenic Differentiation of the hBMCSs. On the basis of the original medium, dexamethasone $10^{-8}/\text{mol}$, β -glycerin sodium phosphate 10 mmol/L, and ascorbic acid 50 $\mu\text{g}/\text{mL}$ were added as osteogenesis conditioned medium that was replaced every other day. After 3 weeks, the hBMSCs were observed under microscope.

2.6. The Culture of the hBMSCs on the nHAC/Alg Materials. The third generation of hBMSCs (2×10^4 cells/ cm^2) was cultured on the nHAC/Alg material, incubated for four hours at 37°C and 5% CO_2 . Then, the culture medium was added when the cells attached well to the materials. The culture medium was changed every 3 days. Culture plates washed by NaOH were used as blank control.

2.7. Inverted Microscope Observation. The cell growth situation on the culture plates, the cell induced situation, and the cell growth situation cultured on the material were observed, respectively, under the inverted microscope daily.

2.8. Scanning Electron Microscope Observation

2.8.1. The nHAC/Alg Materials. The nHAC/Alg materials were cut into 1-2 mm thick discs and fixed with 2% glutaraldehyde, followed by critical-point drying and gold-plating. Then, the material surface was observed with Philips 525 M scanning electron microscope.

2.8.2. The nHAC/Alg Materials Cultured with the Cells. The nHAC/Alg materials were cut into 1-2 mm thick discs. Then the cells were cultured on the materials for 3 and 7 days according to 2.6. And then, the samples were fixed with 2% glutaraldehyde, followed by critical-point drying and gold-plating. Then, the material surface cultured with the cells was observed with Philips 525 M scanning electron microscope.

2.9. Laser Scan Confocal Microscope (LSCM) Observation. The nHAC/Alg was cut into 1-2 mm thick discs, immersed in 1% Rhodamine solution for 5 minutes, immersed in distilled water for 30 minutes, dried, and disinfected by Co60 irradiation. The hBMSCs were dyed by DAPI (60 μm per unit) for half an hour, then washed for 3 times, and vaccinated on the materials which had been dyed by Rhodamine. The growth of cells which had been cultured for 2 days and 4 days on the material would be observed under the laser confocal microscope.

2.10. Determination of Cellular Activity with MTT. nHAC/Alg was cut into 1-2 mm thick discs and then fixed on 24-well culture plate for prewetting. Twelve wells were each set by a piece of material and another twelve wells were set as blank controls without material. The hBMSCs were cultured with 5×10^4 /sample, incubated for four hours. Then 2 mL culture medium was added into each well. On the second, fourth, and sixth day, four wells would be selected to add 20 μL MTT (5 mg/mL), incubated for four hours and then stopped. The supernatant of each well was abandoned. Every well had an addition of 150 μL DMSO and was oscillated for 10 min to make crystal dissolve completely. Finally, the plate was read with a BIO-TEK automate microplate reader at 540 nm.

2.11. Determination of Alkaline Phosphatase Activity. nHAC/Alg was cut into 1-2 mm thick discs and then fixed on 24-well culture plate for prewetting. Twelve wells were each set by a piece of material and another twelve wells were set as blank controls without material. The hBMSCs (1×10^5 /mL) were cultured on these samples and incubated for four hours. Then 2 mL culture medium containing heparin, ascorbic acid, dexamethasone, and glycerin sodium phosphate was added into each well. At 2, 4, and 6 days, the plate was read with a BIO-TEK automate microplate reader at 405 nm.

2.12. Statistical Methods. The data obtained will be analyzed with SPSS10.0 statistical software for statistical analysis. $P < 0.05$ indicated that there was a statistical difference.

3. Result

3.1. Inverted Microscope Observation

3.1.1. Observation of hBMSCs. After 24 hours of inoculation, there were still some floating blood cells with a large number of breed in bone marrow cell suspension which experienced three-step centrifugal (Figure 1(a)). A few hBMSCs whose cell appearance was fiber samples could be observed with the replacement of solution. After 48 hours' inoculation and first replacement of solution with removing the vast floating adherent cells, a small amount of hBMSCs had full stretch into long spindle cells (Figure 1(b)). After 72 hours' inoculation, hBMSCs cells began division and proliferation with a significant increase of volume (Figure 1(c)). After 7 days' inoculation with a further proliferation, a clear demarcation appeared between the nuclei pulp, nucleus located in the central, and single nucleolus in the majority. The shining cell body and strong refraction showed the cells with long spindle in good condition. These cells were close to each other to form early colony formation (Figure 1(d)). After 14 days, cells proliferated in colony growth and became mutual connection (Figure 1(e)). These monolayer cells represented with 0.25% trypsin digestion.

3.1.2. Observation of hBMSCs' Osteogenesis Induction. The morphology of the hBMSCs changed to short, square and fusiform shape after osteogenic induction (Figure 2). This result suggested that the hBMSCs can be induced into osteogenic cells.

3.1.3. Observation of the Proliferation of the hBMSCs on the Material. Because the material is opaque, the cells on the material surface were difficult to be observed under inverted microscope. The growth of the cells on the material could be observed through the pore when the material had been cut into 1 mm piece. On the first day, the cells adhered to the pore and the surroundings (Figure 3(a)). As the time went on, the cells on the material gradually attached to and proliferated well on the wall of the pore (Figure 3(b)).

3.2. Scanning Electron Microscope Observation. nHAC/Alg is a kind of porous framework material with random polygonal holes, 5–15 μm thick flat hole wall, and 100–300 μm aperture. The holes of the horizontal and vertical formed the connected structure (Figure 4(a)). On the third day of culture, the cells with extended pseudopodia adhered to the nHAC/Alg's surface and pores. A lot of visible microvilli on the cell surface showed the cells in a good condition (Figure 4(b)). On the 7th day, with the increase of cell number, there have been granular calcium crystals deposited on the cell surface. Cells are interconnected and the cell morphology preserved (Figure 4(c)).

3.3. LSCM Observation. The nHAC/Alg material that was dyed by Rhodamine appeared green and the hBMSCs that were dyed by DAPI appeared blue. The materials cultured with the cells, respectively, for 2 and 4 days were cut

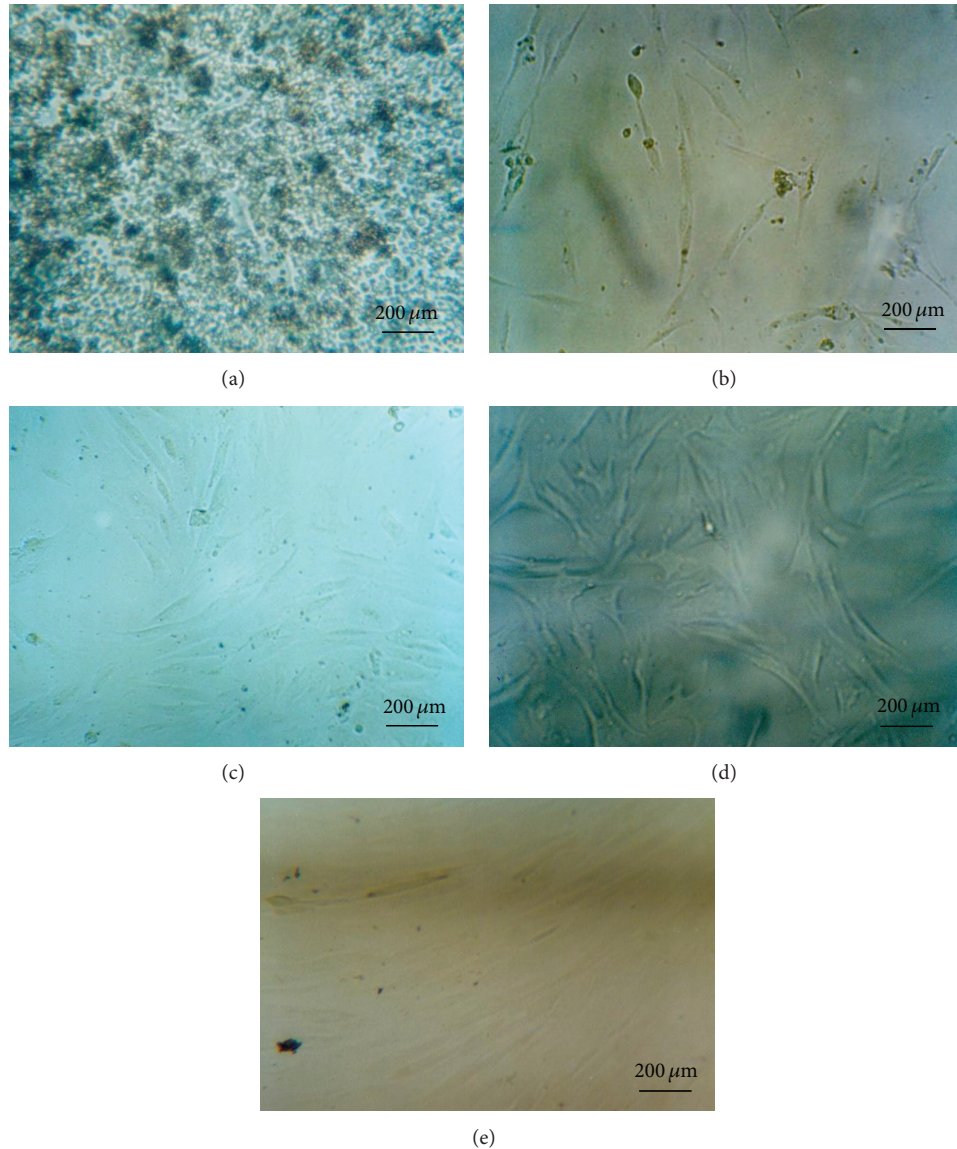


FIGURE 1: The cell morphology after the culture of (a) 24 hours; (b) 48 hours; (c) 72 hours; (d) 7 days; and (e) 14 days.

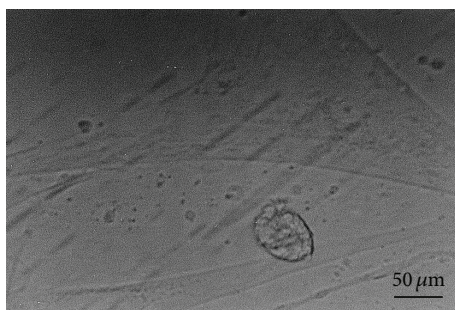


FIGURE 2: The cell morphology after osteogenic induction.

into thin pieces along the longitudinal direction to see the distribution of the cells inside the material. At day 2, dyed-blue hBMSCs attached better not only to the surface

but also inside the pores of the dyed-green nHAC/Alg (longitudinal distance 19.5 μm) (Figure 5(a)). At day 4, the blue area has become larger because the cells attached to the materials have proliferated significantly (longitudinal distance 22.7 μm) (Figure 5(b)).

3.4. Determination of Cell Activity Determined by MTT Method. Figure 6 shows the 490 nm wavelength light absorption value of materials cultured for 2, 4, and 6 days. It was shown that there was no significant difference between the value of the cells cultured on the materials and that of control ($P < 0.05$) at each time point.

3.5. Determination of Alkaline Phosphatase Activity. Alkaline phosphatase activities of the cells cultured on nHAC/Alg materials and control at culture time of 2, 4, and 6 days

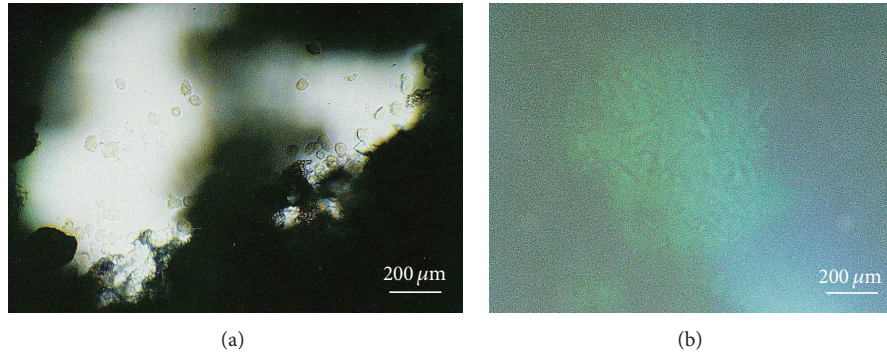


FIGURE 3: The situation of the cell attachment and proliferation on the wall of pores of the nHAC/Alg materials after the culture of (a) 1 day and (b) 4 days.

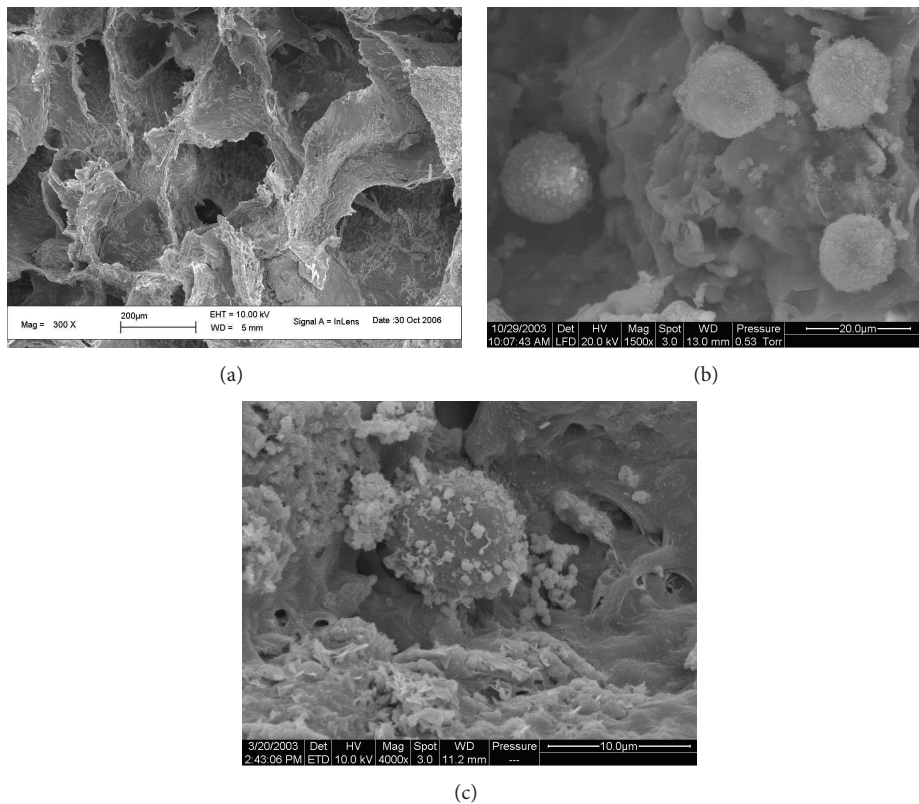


FIGURE 4: Scanning electron microscopes of (a) the nHAC/Alg surface; (b) the nHAC/Alg surface cultured with the hBMSCs cells on the third day; and (c) the nHAC/Alg surface cultured with the hBMSCs cells on the 7th day.

were shown in Figure 7. The values of the control did not change significantly ($P > 0.05$) during the test period. At each time point, the value of the cells cultured on the materials was significantly higher than that of control. During the test period, the value of the cells cultured on the materials significantly increased ($P < 0.05$).

4. Discussion

How to evaluate the biocompatibility of nHAC/Alg is the key point to judge whether it is suitable to be bone substitute.

The composite of nHAC/Alg and hBMSCs observed under inverted phase contrast microscope showed that the cell growth on the material had no abnormalities. But that is just one aspect of the biocompatibility. Whether the cultured cells had normal physiological function is the most important criterion to evaluate the biocompatibility of biomaterials.

The principle of LSCM was installing a laser scanning device on the fluorescence microscope imaging, using the computer for image processing and ultraviolet or visible fluorescence probe to get the fluorescence image of cells or tissue's internal fine structures. LSCM can not only reveal

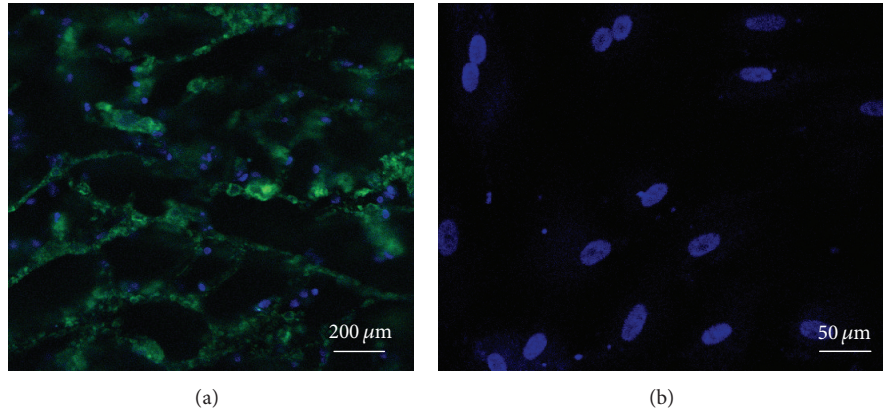


FIGURE 5: LSCM of the nHAC/Alg cultured with the hBMSCs cells at day 2 and (b) the nHAC/Alg cultured with the hBMSCs cells at day 4.

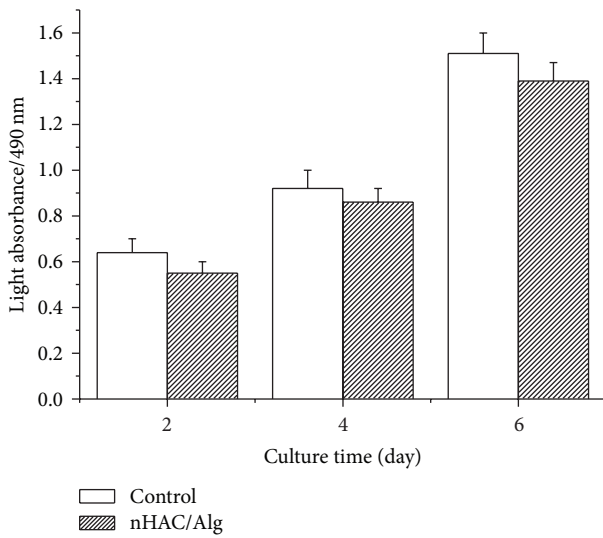


FIGURE 6: The results of MTT at discrete time of 2, 4, and 6 days.

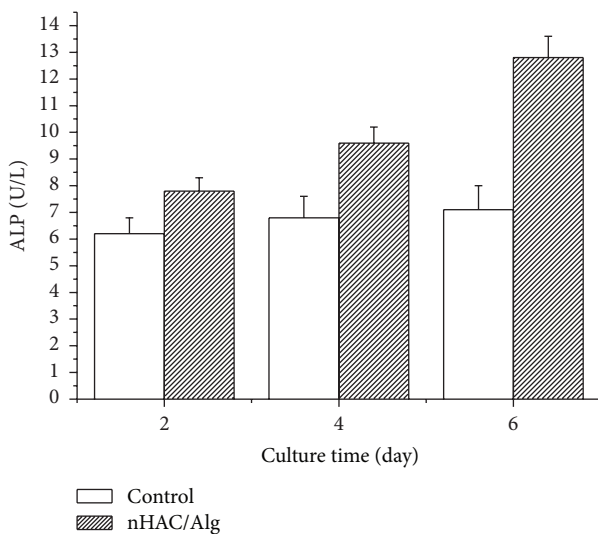


FIGURE 7: Alkaline phosphatase activity of the cells cultured on nHAC/Alg materials and control at discrete time of 2, 4, and 6 days.

the cell's internal structure and provide the cell length, width, thickness, fault area, and cell volume, but also give a three-dimensional concept. Without damaging cells, LSCM can observe and measure living cells and even living tissue. So, the sample can still be used in other studies [26, 27]. The shape of the living cells on materials can be directly observed by LSCM, which can collect images through the mark on the material or fluorescence substance of the cells [28]. The cells and material carrier were, respectively, labeled by fluorescent dye of different colors and then were complex cultured. It was shown in this study that dyed-blue hBMSCs attached better not only to the surface but also inside the pores of the nHAC/Alg. It was also shown by SEM that the cells adhered to the nHAC/Alg's surface and walls of pores with extended pseudopodia.

Recently, MTT was usually used to test the toxic effects of materials on cells. The principle is that succinic dehydrogenase of living cells mitochondria can make exogenous tetrazolium salts reduction into difficult soluble violet crystal which deposited in cells while dead cells cannot. Dimethyl sulfoxide can dissolve the crystal and indirectly reflect the number of living cells through the determination of light absorption value [29]. The experiment results showed that there was no significant difference between the light absorption value of the cells cultured on the nHAC/Alg materials and that of control ($P < 0.05$) at each time point, which suggested that the materials could support the cell proliferation well.

ALP is an early marker of osteoblast differentiation and is one of the symbols of mature osteoblast differentiation [30]. Many experimenters used ALP to evaluate the situation of varieties of biological experiments and the level of the osteogenic differentiation of cells [31, 32]. The results of this study showed that, at each time point, the value of the cells cultured on the materials was significantly higher than that of control. During the test period, the value of the cells cultured on the materials significantly increased ($P < 0.05$), which suggested the nHAC/Alg materials could promote the differentiation of the hBMSCs into osteogenic cells.

Our findings could make connection with the work of Han et al. [33] who reported the preparation of the calcium

silicate/alginate (CS/Alg) composites and the evaluations of its behavior as bioactive injectable hydrogels.

Above all, the hBMSCs attached better not only to the surface but also inside the pores of the nHAC/Alg material. The material could support the cell proliferation well. Most importantly, the nHAC/Alg materials could promote the differentiation of the hBMSCs into osteogenic cells, which suggested that this nanoscaled injectable material should be a satisfactory candidate as bone repair material.

5. Conclusion

In this study, we have prepared a kind of novel nanoscaled injectable bone repair materials (nHAC/Alg). The nHAC/Alg not only had no negative effect on cellular functions but also promotes cell proliferation and differentiation into osteogenic cells, which suggests that the nanoscaled injectable bone repair material has good clinical application prospects for bone repair.

Conflict of Interests

The authors have no conflict of interests.

Acknowledgment

The authors acknowledge the financial support from the Natural Science Foundation of Jiangsu Province of China (no. BK20141436).

References

- [1] M. Navarro, S. Del Valle, S. Martínez et al., "New macroporous calcium phosphate glass ceramic for guided bone regeneration," *Biomaterials*, vol. 25, no. 18, pp. 4233–4241, 2004.
- [2] J. F. Mano, R. A. Sousa, L. F. Boesel, N. M. Neves, and R. L. Reis, "Bioinert, biodegradable and injectable polymeric matrix composites for hard tissue replacement: state of the art and recent developments," *Composites Science and Technology*, vol. 64, no. 6, pp. 789–817, 2004.
- [3] N. T. Khanarian, J. Jiang, L. Q. Wan, V. C. Mow, and H. H. Lu, "A hydrogel-mineral composite scaffold for osteochondral interface tissue engineering," *Tissue Engineering Part A*, vol. 18, no. 5-6, pp. 533–545, 2012.
- [4] J. S. Temenoff and A. G. Mikos, "Injectable biodegradable materials for orthopedic tissue engineering," *Biomaterials*, vol. 21, no. 23, pp. 2405–2412, 2000.
- [5] M.-P. Ginebra, C. Canal, M. Espanol, D. Pastorino, and E. B. Montufar, "Calcium phosphate cements as drug delivery materials," *Advanced Drug Delivery Reviews*, vol. 64, no. 12, pp. 1090–1110, 2012.
- [6] X. M. Li, X. H. Liu, W. Dong et al., "In vitro evaluation of porous poly(L-lactic acid) scaffold reinforced by chitin fibers," *Journal of Biomedical Materials Research—Part B Applied Biomaterials*, vol. 90, no. 2, pp. 503–509, 2009.
- [7] H. H. K. Xu, M. D. Weir, E. F. Burguera, and A. M. Fraser, "Injectable and macroporous calcium phosphate cement scaffold," *Biomaterials*, vol. 27, no. 24, pp. 4279–4287, 2006.
- [8] M. D'Este, M. Alini, and D. Eglin, "Single step synthesis and characterization of thermoresponsive hyaluronan hydrogels," *Carbohydrate Polymers*, vol. 90, no. 3, pp. 1378–1385, 2012.
- [9] J. D. Kretlow, L. Klouda, and A. G. Mikos, "Injectable matrices and scaffolds for drug delivery in tissue engineering," *Advanced Drug Delivery Reviews*, vol. 59, no. 4-5, pp. 263–273, 2007.
- [10] H. Liu, H. Li, W. Cheng, Y. Yang, M. Zhu, and C. Zhou, "Novel injectable calcium phosphate/chitosan composites for bone substitute materials," *Acta Biomaterialia*, vol. 2, no. 5, pp. 557–565, 2006.
- [11] I. M. Pelin, S. S. Maier, G. C. Chitanu, and V. Bulacovschi, "Preparation and characterization of a hydroxyapatite-collagen composite as component for injectable bone substitute," *Materials Science and Engineering C*, vol. 29, no. 7, pp. 2188–2194, 2009.
- [12] S. Ghanaati, M. Barbeck, U. Hilbig et al., "An injectable bone substitute composed of beta-tricalcium phosphate granules, methylcellulose and hyaluronic acid inhibits connective tissue influx into its implantation bed in vivo," *Acta Biomaterialia*, vol. 7, no. 11, pp. 4018–4028, 2011.
- [13] N.-M. Hu, Z. Chen, X. Liu et al., "Mechanical properties and *in vitro* bioactivity of injectable and self-setting calcium sulfate/nano-HA/collagen bone graft substitute," *Journal of the Mechanical Behavior of Biomedical Materials*, vol. 12, pp. 119–128, 2012.
- [14] M. D'Este and D. Eglin, "Hydrogels in calcium phosphate moldable and injectable bone substitutes: sticky excipients or advanced 3-D carriers?" *Acta Biomaterialia*, vol. 9, no. 3, pp. 5421–5430, 2013.
- [15] X. Lian, H. Liu, X. Wang, S. Xu, F. Cui, and X. Bai, "Antibacterial and biocompatible properties of vancomycin-loaded nano-hydroxyapatite/collagen/poly (lactic acid) bone substitute," *Progress in Natural Science: Materials International*, vol. 23, pp. 549–556, 2013.
- [16] Z. G. Chen, L. Z. Kang, Q. Y. Meng et al., "Degradability of injectable calcium sulfate/mineralized collagen-based bone repair material and its effect on bone tissue regeneration," *Journal of Biomedical Materials Research*, vol. 45, pp. 94–102, 2014.
- [17] L. Zheng, X. F. Jiang, X. N. Chen, H. S. Fan, and X. D. Zhang, "Evaluation of novel *in situ* synthesized nano-hydroxyapatite/collagen/alginate hydrogels for osteochondral tissue engineering," *Biomedical Materials*, vol. 9, no. 6, Article ID 065004, 2014.
- [18] J. Aizenberg, J. C. Weaver, M. S. Thanawala, V. C. Sundar, D. E. Morse, and P. Fratzl, "Skeleton of *Euplectella* sp.: structural hierarchy from the nanoscale to the macroscale," *Science*, vol. 309, no. 5732, pp. 275–278, 2005.
- [19] X. M. Li, Y. Yang, Y. B. Fan, Q. L. Feng, F.-Z. Cui, and F. Watari, "Biocomposites reinforced by fibers or tubes as scaffolds for tissue engineering or regenerative medicine," *Journal of Biomedical Materials Research Part A*, vol. 102, no. 5, pp. 1580–1594, 2014.
- [20] C. Du, F. Z. Cui, W. Zhang, Q. L. Feng, X. D. Zhu, and K. de Groot, "Formation of calcium phosphate/collagen composites through mineralization of collagen matrix," *Journal of Biomedical Materials Research*, vol. 50, no. 4, pp. 518–527, 2000.
- [21] X. Liu, D. Yu, J. Xu et al., "The experimental study on promoting the ilizarov distraction osteogenesis by the injection of liquid Alg/nHAC biocomposites," *International Journal of Polymer Science*, vol. 2014, Article ID 238247, 9 pages, 2014.

- [22] C. Peng, Z.-A. Zhu, G.-L. Li et al., "Enhancement of bone healing in rabbit ulnar critical bone defect by injectable nano-hydroxyapatite/ collagen/(calcium sulfate hemihydrate) mixed with autogenous bone marrow," *Journal of Biomaterials and Tissue Engineering*, vol. 3, no. 5, pp. 534–541, 2013.
- [23] Z. Huang, Q. L. Feng, B. Yu, and S. J. Li, "Biomimetic properties of an injectable chitosan/nano-hydroxyapatite/ collagen composite," *Materials Science and Engineering C*, vol. 31, no. 3, pp. 683–687, 2011.
- [24] Z. Huang, J. Tian, B. Yu, Y. Xu, and Q. Feng, "A bone-like nano-hydroxyapatite/collagen loaded injectable scaffold," *Biomedical Materials*, vol. 4, no. 5, Article ID 055005, 2009.
- [25] S.-L. Gan and Q.-L. Feng, "Preparation and characterization of a new injectable bone substitute-carrageenan/nano-hydroxyapatite/collagen," *Acta Academiae Medicinae Sinicae*, vol. 28, no. 5, pp. 710–713, 2006.
- [26] J. J. Kazama, F. Gejyo, S. Ejiri et al., "Application of confocal laser scanning microscopy to the observation of bone biopsy specimens," *Bone*, vol. 14, no. 6, pp. 885–889, 1993.
- [27] X. Li, Y. Huang, L. Zheng et al., "Effect of substrate stiffness on the functions of rat bone marrow and adipose tissue derived mesenchymal stem cells in vitro," *Journal of Biomedical Materials Research—Part A*, vol. 102, no. 4, pp. 1092–1101, 2014.
- [28] C. Maggiano, T. Dupras, M. Schultz, and J. Biggerstaff, "Spectral and photobleaching analysis using confocal laser scanning microscopy: a comparison of modern and archaeological bone fluorescence," *Molecular and Cellular Probes*, vol. 20, no. 3–4, pp. 154–162, 2006.
- [29] R. Scherließ, "The MTT assay as tool to evaluate and compare excipient toxicity in vitro on respiratory epithelial cells," *International Journal of Pharmaceutics*, vol. 411, no. 1–2, pp. 98–105, 2011.
- [30] X. M. Li, H. F. Liu, X. F. Niu et al., "The use of carbon nanotubes to induce osteogenic differentiation of human adipose-derived MSCs in vitro and ectopic bone formation in vivo," *Biomaterials*, vol. 33, no. 19, pp. 4818–4827, 2012.
- [31] J. Liu, H. K. Nam, C. Campbell, K. C. S. Gasque, J. L. Millán, and N. E. Hatch, "Tissue-nonspecific alkaline phosphatase deficiency causes abnormal craniofacial bone development in the *Alpl*^{−/−} mouse model of infantile hypophosphatasia," *Bone*, vol. 67, pp. 81–94, 2014.
- [32] X. M. Li, H. F. Liu, X. F. Niu et al., "Osteogenic differentiation of human adipose-derived stem cells induced by osteoinductive calcium phosphate ceramics," *Journal of Biomedical Materials Research, Part B—Applied Biomaterials*, vol. 97, no. 1, pp. 10–19, 2011.
- [33] Y. Han, Q. Zeng, H. Li, and J. Chang, "The calcium silicate/alginate composite: preparation and evaluation of its behavior as bioactive injectable hydrogels," *Acta Biomaterialia*, vol. 9, no. 11, pp. 9107–9117, 2013.

Research Article

Investigations into the Biocompatibility of Nanohydroxyapatite Coated Magnetic Nanoparticles under Magnetic Situation

Qing Li,^{1,2} Gang Zhou,¹ Tong Wang,² Yongzhao Hou,¹ Xuliang Deng,³ and Yan Wei³

¹Key Laboratory for Biomechanics and Mechanobiology of Ministry of Education, School of Biological Science and Medical Engineering, Beihang University, Beijing 100191, China

²2nd Dental Center, Peking University School and Hospital of Stomatology, Beijing 100081, China

³Department of Geriatric Dentistry, Peking University School and Hospital of Stomatology, Beijing 100081, China

Correspondence should be addressed to Yan Wei; kqweiyan@126.com

Received 13 November 2014; Revised 30 December 2014; Accepted 30 December 2014

Academic Editor: Shuming Zhang

Copyright © 2015 Qing Li et al. This is an open access article distributed under the Creative Commons Attribution License, which permits unrestricted use, distribution, and reproduction in any medium, provided the original work is properly cited.

Regenerative medicine consisting of cells and materials offers a new approach for repairing and regenerating the organs and tissues. More and more researches focused on the magnetic nanobiomaterials due to its superior advantages to traditional materials. However, the toxicity of nanosized magnetic particles cannot be ignored, especially under the magnetic situation. This study aims to study the biocompatibility of nanohydroxyapatite (n-HA-) coated magnetic nanoparticles under the magnetic situation. n-HA-coated magnetic nanoparticles were fabricated through an ultrasound-assisted coprecipitation method. Subsequently, these materials were analyzed by transmission electron microscope (TEM) and X-ray diffraction (XRD) and then were cultured with mesenchyme stem cells derived from human bone marrow (hMSC-BM). In vitro experiment proved the satisfactory biocompatibility of n-HA-coated magnetic nanoparticles. These important factors (ALP, OCN, and OPN) influence the osteogenic differentiation of hMSC-BM. It was found that the hMSC-BM with combination of n-HA/Fe₃O₄ and magnetic stimulation presented higher degree of osteoblast-related markers than that in each alone. This research demonstrated that a novel nanohydroxyapatite coated magnetic nanoparticle is safe under the magnetic situation. Therefore, these n-HA-coated magnetic nanoparticles are promising biomagnetic materials for future applications.

1. Introduction

In recent years, nanosized magnetic biomaterials have shown their bright future in the regenerative medicine [1–4]. It is well known that magnetic nanoparticles [5–7] are endowed with extensive biological effects. By virtue of their ability to interact with living cells, they can stimulate the growth and elongation of cells under the influence of external magnetic fields [8]. Specifically, the development of magnetic nanoparticles for the application in biomedical field contains both magnetic hyperthermia and medical imaging. At present, drug or gene delivery is experiencing a tremendous development [4]. As the research revealed, magnetic nanoparticles could significantly facilitate the proliferation and differentiation of MSCs (mesenchymal stem cells, MSCs) [9, 10]. The magnetic CaPO₄/Fe₃O₄ composite could promote new bone formation

after being implanted into the subcutaneous of rats [11]. Magnet can also affect the flow of Ca²⁺ in cell plasma, which will directly or indirectly cause the reconstruction of microfilaments, micropipes, and surficial glycosyl and consequently impact the cell morphology and cell membrane rebuilding [12–16]. With these unique biological effects, magnetic materials were considered to possess great potentials in regenerative medicine.

Nonetheless, attributing to the physicochemical characteristics of the nanomaterial like its small shape, size, and unrecognized surface reaction, this novel material also draws far-reaching attention on its biosafety [17, 18]. It is observed that the direct biomedical application of the nanomaterials like Fe₃O₄ is likely to cause cellular toxicity [19, 20]. Therefore, nontoxicity is perhaps the most basic requirement for magnetic materials to be applied in biomedical field. For this

purpose, synthesized Fe_3O_4 is generally coated with proper ligands or moieties before use so as to weaken the cellular toxicity while enhancing the biocompatibility [21, 22].

Featured with prominent bioactivity and biocompatibility, nanohydroxyapatite (n-HA) becomes a perfect candidate and thus is extensively applied in the field of tissue regeneration [23–27]. Contrasted with traditional micromaterials, n-HA can arouse a higher level of biological plasticity with its superior advantage of a high surface-to-volume ratio [28]. Thus, n-HA was added to coat magnetic nanoparticles to overcome its cytotoxic effect in the former study [29].

Electromagnetic biology mainly explores the impacts of electric and magnetic fields on the living organs. From the researches on this subject in the past dozens of years, it has been convincingly proved that through perceiving the direction of the geomagnetic field, various species like sea turtles, birds, and butterflies can navigate for a long distance, while mammalian species are able to line up on the earth [30, 31]. Besides the impacts of the geomagnetic field on species behavior, the electromagnetic biology also explores the underlying negative impacts of diverse environmental electromagnetic fields (EMFs). The EMFs from mobile phones and power lines are representative ones daily. There are also static magnetic fields (SMF) from magnetic levitation and magnetic resonance imaging system [32]. Particularly, more and more researches have demonstrated that SMF treatments will trigger genotoxicity, apoptosis, and cellular differentiation in different types of cells [33]. Nonetheless, none of former researches has appropriately studied the impacts of magnetic nanoparticles integrated with SMF exposure on cytotoxicity. For electromagnetic biology, it makes sense to measure the cellular toxicity of magnetic nanoparticles under magnetic environment, for magnetic nanoparticles like Fe_3O_4 will be magnetized under SMF and may impose unrecognized negative impacts on living organs.

In terms of biomedical application, this novel nanostructure demands strict assessment on its biological security under the magnetic situation. Therefore, this research aimed to characterize the biocompatibility of a novel magnetic hydroxyapatite composite under the magnetic environment. Firstly, the properties of the developed n-HA-coated magnetic nanoparticles were characterized by XRD and TEM. Then, we created a novel magnetic force bioreactor which exposed a magnetic force during the cell culture. Besides, the in vitro bioactivity and biocompatibility of magnetic composite nanoparticles were investigated with the hMSC-BM cells under this magnetic environment.

2. Materials and Methods

The chemical reagents applied in this research were all in analytical grade.

2.1. Synthesis of n-HA. Through a precipitation approach, n-HA slurry was synthesized [34]. In brief, trisodium phosphate ($\text{Na}_3\text{PO}_4 \cdot 12\text{H}_2\text{O}$) (Beijing Chemical Reagents, 0.31 mol/L) solution was dropwise added to the calcium nitrate ($\text{Ca}(\text{NO}_3)_2 \cdot 4\text{H}_2\text{O}$, Beijing Chemical Reagents, 95 wt%

pure, 0.55 mol/L) according to a Ca/P molar ratio of 5:3. During the reaction, the solution was kept stirring vigorously and the pH was regulated to 14 via adding a certain ammonia solution ($\text{NH}_4 \cdot \text{OH}$, Beijing Chemical Reagents) at 25°C. Through titration and aging for one day (24 hours), the precipitates could be collected via centrifuging the suspension and washing them in the distilled water. Eventually, the HA powder could be acquired when the solution dried.

2.2. Synthesis of n-HA-Coated Magnetic Nanoparticles. $\text{FeCl}_3 \cdot 6\text{H}_2\text{O}$ (0.55 mol/L), $\text{FeCl}_2 \cdot 4\text{H}_2\text{O}$ (0.25 mol/L), and $\text{Ca}(\text{NO}_3)_2 \cdot 4\text{H}_2\text{O}$ (0.55 mol/L) were jointly dissolved in water so as to prepare the solution [A]. Besides, $\text{Na}_3\text{PO}_4 \cdot 12\text{H}_2\text{O}$ (0.3 mol/L) and $\text{NH}_3 \cdot \text{H}_2\text{O}$ (1.55 mol/L) were also dissolved in water to prepare solution [B]. Subsequently, the solution [B] was dropwise added to the solution [A] with ultrasound-assisted stirring. After ultrasound-assisted dispersion at 25°C for 5 hours, the solution was left still for aging for 24 hours at room temperature. Afterwards, the precipitates could be screened from mother liquor through centrifugation, washed in the distilled water, and then centrifuged several times. Eventually, the n-HA-coated magnetic nanoparticles powder could be collected after drying.

2.3. Characterization of Materials. The crystal structure of the synthesized materials was characterized by the X-ray diffractometry (XRD, X'Pert pro-MPD PANalytical B.V.) with Cu/K α radiation ($\lambda = 0.15405 \text{ nm}$) (40 kV, 40 mA). The powder morphology could be analyzed by transmission electron microscopy (TEM) which was implemented by a JEOL JEM 1200EX (120 kV). The magnetic performance was characterized by a Vibrating Sample Magnetometer 7307 at room temperature (25°C).

2.4. Cell Cultures with Magnetic Nanoparticles. Primary cultures of human mesenchymal stem cells-bone marrow (hMSC-BM, Sciencell, USA) were cultured as monolayers in Alpha Minimum Essential Medium (α -MEM, GIBCO), supplemented with 10% (v/v) fetal bovine serum (FBS; Sigma), 1% (v/v) L-glutamine (Invitrogen Corp., Carlsbad, CA, USA), and a 1% (v/v) antibiotic and antimycotic formulation containing penicillin G sodium and streptomycin sulfate (Invitrogen Corp., Carlsbad, CA, USA). In addition, the medium was renewed every other day, while the cultures were kept at 37°C within a humid atmosphere with 5% CO_2 . When the confluence reached 90%, the cells were passaged (P1). After passaging three times (P3), the cells were exposed to proliferation and differentiation assays.

Fe magnetic nanoparticles were added into culture medium at 138 $\mu\text{g/mL}$ during cell cultures. n-HA-coated magnetic nanoparticles were added into culture medium at 138 $\mu\text{g/mL}$ during cell cultures. The cells cultured with Fe and n-HA were seeded in plates with culture medium and exposed to a magnetic force bioreactor (Figure 1) every one hour at every other day of cyclic loading intervals for a 14-day period. The magnetic flux density of the central field is about 0.2 T.

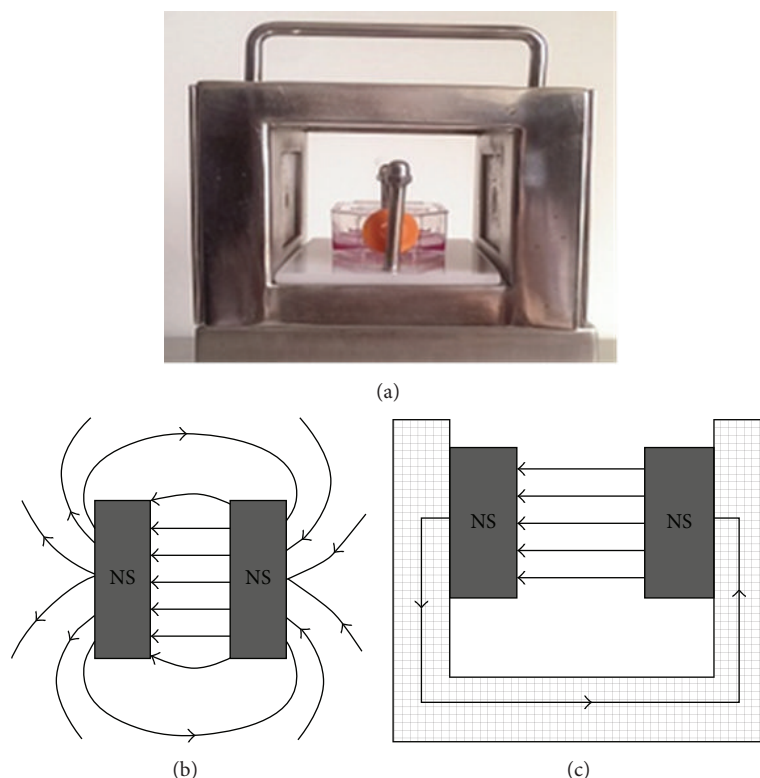


FIGURE 1: The magnetic force bioreactor and the diagram of the magnetic principle ((a) the picture of magnetic force bioreactor shows the cell culture is located in the central field; (b) the distribution of magnetic induction line when two different polarity magnets face each other; (c) the distribution of magnetic induction line when two different polarity magnets face each other with a steel case device.).

2.5. Cell Viability. The cell viability was determined by CCK-8 kit (Beyotime, China). In brief, 10 μL of the kit reagent was added into the cells, then processed as the above-mentioned steps in 96-well plates, and cultured for 2 hours. In this way, the cell viability could be evaluated via the ELISA plate reader at 450 nm. The cells were exposed to proliferation assays using CCK8 kits at 1d, 3d, 5d, 7d, and 14d.

2.6. SEM Observation. All cell suspensions (5 mL) were plated at the density of 1×10^6 cells mL^{-1} in plates with sterile specimens of materials for the cell attachment assays. SEM micrographs were carried out at one day following the original cell coculturing with the materials. In brief, the cocultured structures could be harvested, then washed with PBS, and lastly fixed with 4% glutaraldehyde. After 3 rinses with water, these samples could be dehydrated via a series of graded alcohol solutions and dried overnight. The specimens were observed by SEM at an acceleration voltage of 30 kV (QUANTA 250 FEG, USA).

2.7. Immunofluorescence Assay. For the immunofluorescence observation of cytoskeleton of hMSC-BM, the cells were gently bathed with 0.01 M PBS 3 times before being fixed with 4% glutaraldehyde PBS solution for 20 min at 4°C . Afterwards, cells were rinsed with PBS and incubated with 0.5% Triton X-100 for 5 minutes to increase cell membrane's penetrability. The cells were subsequently blocked with 1% BSA solution for

1 hour at room temperature. After removing BSA solution, the cells were incubated with rhodamine phalloidin (Cat. PHDR1) in a dark place at room temperature for half an hour. Then the samples were rinsed twice for 30 s with PBS and incubated in Hoechst 33258 (10 $\mu\text{g}/\text{mL}$) in a dark place at room temperature for 5 min to show the cell nucleus. Again, the samples were washed 3 times for 3 min with PBS. Finally, these samples were mounted with 95% glycerin PBS solution. Images were taken under a confocal microscope (Olympus IX71, Fluoview, Japan) with an excitation filter at 535 nm and an emission filter at 585 nm for rhodamine and an excitation filter at 550 nm and an emission filter at 460 nm for Hoechst 33258, respectively.

2.8. ALP Activity Analysis. The activity ALP derived from the cells could be decided through a dynamic colorimetric assay. hMSC-BM were cultured separately in 24-well plates containing osteogenic medium; at each time-point, the cultures were rinsed with cellular culture media and separated with 0.3 M Tris Triton buffer (10 mM Tris, pH 7.5, 0.1% Triton X-100). The samples then were solicited for 5 min at 25 W on a piece of ice. Subsequently, they were centrifuged at 2000 rpm for 10 min and diluted ten times with the same buffer. A moiety of every supernatant was poured into p-nitrophenyl phosphate solution (Randox) at room temperature in a 96-well plate and the absorbancy of the colored product of p-nitrophenol was surveyed at 405 nm per min for 5 minutes using the ELISA

TABLE 1: Chain reaction primers used for detection in this study.

Primers sequence	Target gene	Product size (bp)
CAGGCGCTACCTGTATCAATG GTGGTCAGCCAACTCGTCA	OCN	112
GTGCATACAAGGCCATCC GTGGGTTTCAGCACTCTGG	OPN	116
TGCGCAGAAAACAAGATGAG CACCTTCACCGTTCCAGTTT	ACTIN	114

plate reader. The slope of the absorbancy to time plot was utilized to measure the ALP activity. The calibration curve of p-nitrophenol at room temperature was adopted to decide the enzymatic activity in units of nmol substrate transformed into product every minute.

2.9. Western Blotting Analysis. HMSC-BM cells were lysed in a RIPA buffer with supplementation of protease inhibitors (SinoGene Scientific, Beijing, China) and phosphatase inhibitors (SinoGene Scientific, Beijing China). Protein concentration was determined by the Bradford method. 30 μ g protein lysate was mixed with 2x loading buffer at 1:1 and heated for 10 min at 95°C before being loaded for gel electrophoresis.

The proteins and protein marker (SM1881, Thermo Fermentas) could be separated through SDS-PAGE (4% stacking gel and 12% separating gel) at 120 V for 2 h. Proteins were then transferred into the PVDF membranes via a Bio-Rad mini transfer system. The membranes were blocked in a rapid blocking buffer for 5 min and then probed with primary antibodies against OCN and OPN at a dilution of 1:1000 for 2 h. After rinsing three times with PBS for 10 minutes per rinse, HRP-conjugated anti-mouse and anti-rabbit antibodies (Micro Analysis Inc.) were applied to the membranes at a dilution of 1:2000 for 1 h. Chemiluminescent signals were developed with an ECL Kit (ECL, Engreen) and exposed to X-ray films in a dark room. Then the membranes were stripped by a stripping buffer (SinoGene Scientific) and reprobed with β -actin (M20010, Abmart). The level of actin was measured as an internal control.

2.10. RT-PCR Analysis. Total RNA was separated from samples with a SG TriEx HiPure RNA Extraction Kit (SinoGene Scientific, China). RNA concentration was measured at 260 nm and its purity was assessed with Biophotometer (Eppendorf, Germany) at a ratio of 260:280 nm. RNA samples were processed with DNaseI (EN0523, Fermentas) to clear away the contaminated genomic DNA and analyzed on 1.5% agarose gels. Reverse transcription was performed through a Thermo First cDNA Synthesis Kit (SinoGene Scientific China) with random hexamer primers. The average amount of RNA used in the reverse transcription reaction was 1 μ g and its purity was around 2.0 (260:280 nm ratio).

qPCR per tube contained 10 μ L of 2x SG Green qPCR Mix (with ROX), (SinoGene Scientific, China), 250 nM of each primer (list of primers as Table 1), PCR grade water, and 1 μ L

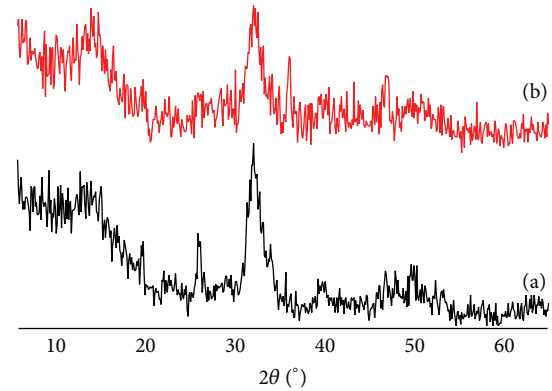


FIGURE 2: XRD patterns of nanoparticles ((a) n-HA; (b) n-HA-coated magnetic nanoparticles).

of cDNA template (diluted in a 1:2 or 1:10 ratio). All samples were assayed in duplicate with each run. The PCR cycling program consisted of 10 min at 95°C, followed by 40 cycles of 15 s at 95°C and 60 s at 58°C. An additional step was used (95°C for 15 s, 58°C or 55°C for 30 s, and 95°C for 15 s) for dissociation curve analysis.

2.11. Statistical Analysis. The data are defined as the mean \pm S.E.M. In terms of statistical comparison, this research adopted the *t*-test or one-way ANOVA as well as Tukey's test. **P* < 0.05, ***P* < 0.01, and ****P* < 0.001 were deemed to be of statistical significance.

3. Results

3.1. XRD Measurement. X-ray diffraction of the synthesized materials would generate characteristic peaks (see Figure 2). These were broad diffraction peaks, which indicated a weak crystal construct, a representative of nonstoichiometric HA (referred from JCPDS 09-0432). With the Jade 9.0 software, the average particle size of synthesized HA could be measured as 28.47 ± 0.4 nm in the n-HA-coated magnetic nanoparticles system, and the characteristic peaks of Fe_3O_4 also appeared in Figure 2(b). The diffraction peaks at 36.51° , 47.09° , 57.08° , and 62.96° corresponding to the planes of (311), (400), (333), and (440) clearly proved the pattern of the spinal structures on ferrite. This result conforms to former publications of similar phenomena. Nevertheless, the samples presented such variations in crystalline structure. In this regard, HA, with a space group of P63/m, $a = b = 0.935\sim 0.947$ nm and $c = 0.677\sim 0.692$ nm, is in the hexagonal system. According to Rietveld analysis, there was a rise of the axis from 0.9407 to 0.9429 and a rise of *c* axis from 0.6878 to 0.6881 due to the Ca replacement with ion species at a smaller radius. Contrasted with the HA group, *a*, *b*, and *c* axes all grew within the n-HA-coated magnetic nanoparticles. With coating n-HA, the nanocomposite's cell structure rose to 0.5282 nm^3 . These variations correspondingly reflect the distortion of HA. The distortion might be explained as follows: the magnetic iron oxide particles substituted -OH, which is parallel to the *c* axis, and subsequently they enter the HA crystal lattice, which

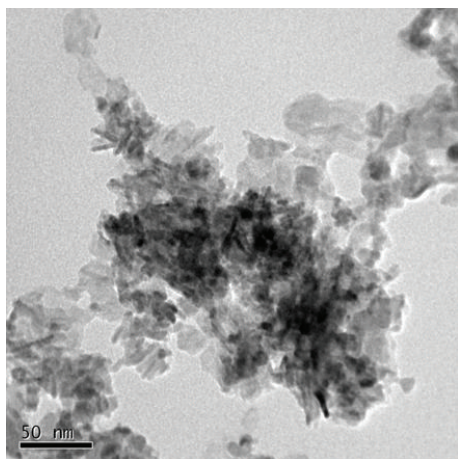


FIGURE 3: TEM of n-HA-coated magnetic nanoparticles.

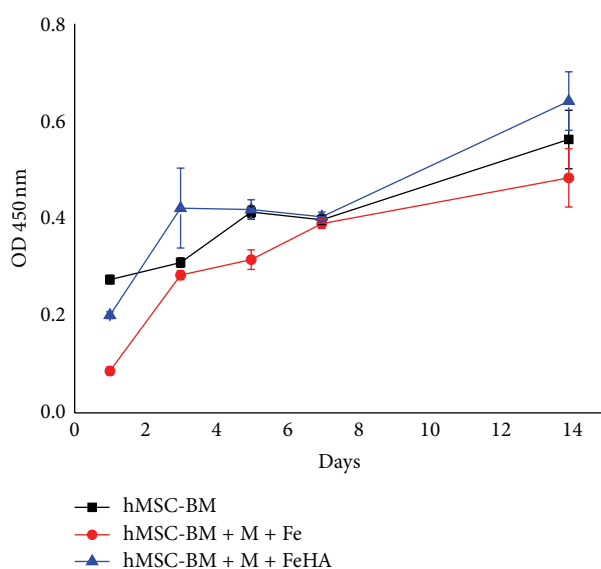


FIGURE 4: In vitro cell proliferation of nanoparticles materials.

leads to such variations on the crystal surface of HA (210) and (212). Coordinating with PO_4^{3-} of HA, the Fe ion in Fe_3O_4 serves as a bridge to PO_4^{3-} groups, becoming another reason for the variations in the HA unit cells.

3.2. TEM Observation. By investigating the morphology of n-HA-coated magnetic nanoparticles through TEM analysis, it was observed that a low concentration of dark spots (2–4 nm in size) corresponded to the inclusions of iron-rich phases (Figure 3). The Fe_3O_4 -HA composite was found to be quite heterogeneous in size, with 1–5 nm wide but reaching 15–40 nm long (Figure 3).

3.3. CCK8 Analysis. A CCK-8 assay was used to evaluate the cytotoxicity of the magnetic nanoparticles, and the OD values could indicate the cellular viability and multiplication on diverse materials. As seen in Figure 4, the OD values for the

n-HA-coated magnetic nanoparticles increased with culture duration, which indicated that this particular scaffold had no detrimental effect on the viability and proliferation of hMSC-BM cells. In addition, this trend suggested that the n-HA-coated magnetic nanoparticles had a better biocompatibility than the Fe magnetic nanoparticles.

3.4. SEM Observation. The morphologies of n-HA-coated magnetic nanoparticles under magnetic stimulation were investigated by SEM. The results proved that n-HA-coated magnetic nanoparticles were noncytotoxic and could support hMSC-BM attachment, spreading, and proliferation. The inductivity of these nanobiomaterials reveals an important role of cell growth (Figure 5). Due to their high surface-to-volume ratio, the nanobiomaterials could arouse a higher level of biological plasticity. Besides, the morphology and nanoscale structure in the surface of n-HA-coated magnetic nanoparticle also accelerated the rate of hMSC-BM proliferation.

3.5. Immunofluorescence Assay. Consisting of a great variety of particular proteins, the cell skeleton itself is an extremely dynamical system, which plays multiple roles in human diseases. To study the growth behaviors of hMSC-BM cells in three unlike materials, this research visualized the cells by the double staining technique in both cell skeleton and nucleus. In addition, fluorescence microscopy was employed to watch reorganization of cell skeleton after 7-day incubation (Figure 6). Cells processed with HA presented the stretched and linear arrays of actin microfilaments (Figure 6(c)). Moreover, cells also displayed the characteristics of osteoblast cells like the clear and big nucleus and spindle or polygonal appearance. Therefore, cell skeleton was clearly visible, and actin fibers were in bundles, each arranged in parallel and consistent with the long axis of the cell. However, there were limited cells on the Fe_3O_4 group, cell skeleton was fuzzy, and some actin fibrin concentrated together (Figure 6(b)). Compared with the control (Figure 6(a)), the Fe_3O_4 -HA composite (Figure 6(c)) presented excellent cytoskeletal reorganization. HA enhanced biocompatibility of Fe_3O_4 by coupling strategy which processed a composite build-up. Based on this analysis, it could be concluded that Fe_3O_4 -HA composites were noncytotoxic to hMSC-BM cells and equipped with great biocompatibility.

3.6. ALP Analysis. The gradual and progressive increase of ALP activity during the process of osteogenic differentiation could be found in both Fe and nHA groups, which suggested the successful osteogenic differentiation (Figure 7). Presented in the osteoblast membrane and participated in the synthesis and mineralisation of the bone matrix, the enzyme ALP is one of the most widely used markers of in vitro osteogenic differentiation [35, 36]. Its expression may increase up to 27 times during the process of osteogenic differentiation [37–40] under the magnetic situation.

3.7. Western Blot and PCR Analysis. In order to further confirm the differentiation of hMSC-BM cells, the expression of OCN and OPN was analyzed on the 3rd day and the

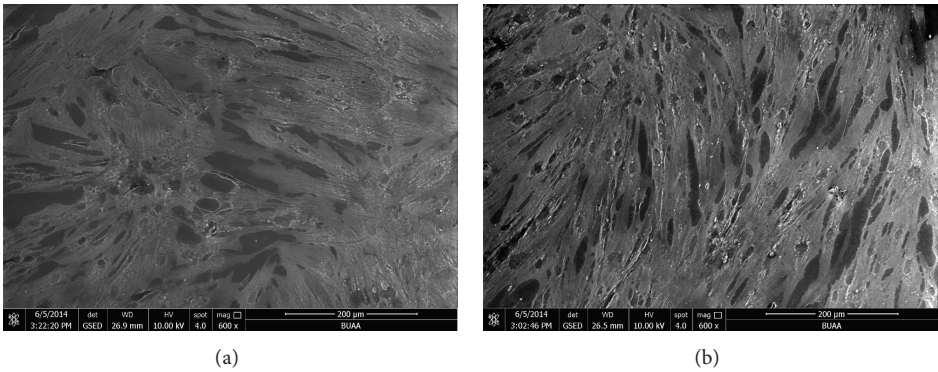


FIGURE 5: SEM of cell growth ((a) control without materials; (b) cocultured with $\text{Fe}_3\text{O}_4\text{-HA}$).

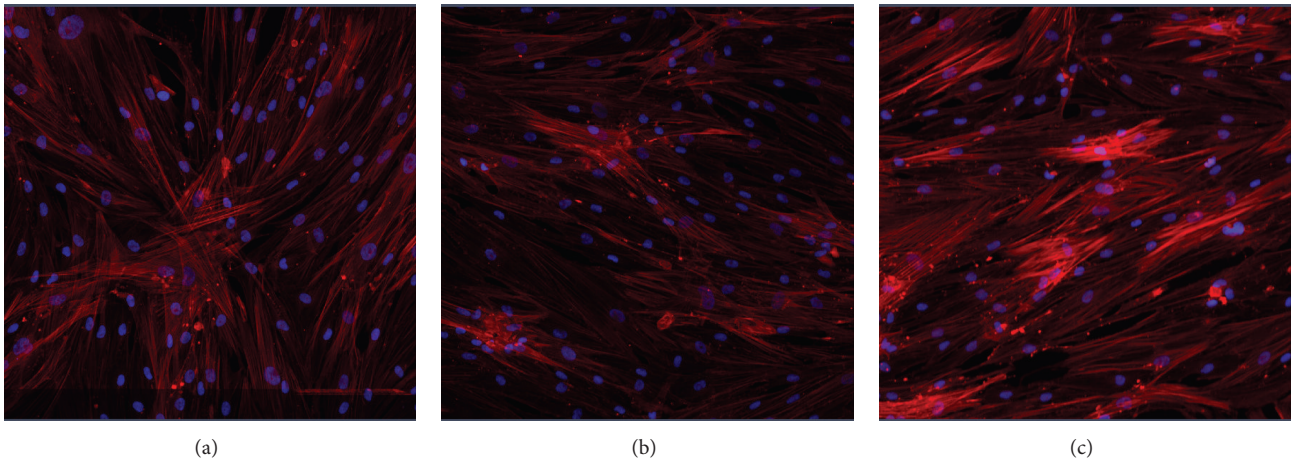


FIGURE 6: Fluorescence images for the organization of cell skeleton in hMSC-BM cells cocultured with different materials ((a) control without materials; (b) Fe_3O_4 ; (c) $\text{Fe}_3\text{O}_4\text{-HA}$) after seven days. Cells were stained as F-actin (red) and nucleus (blue). Scale bar 50 μm .

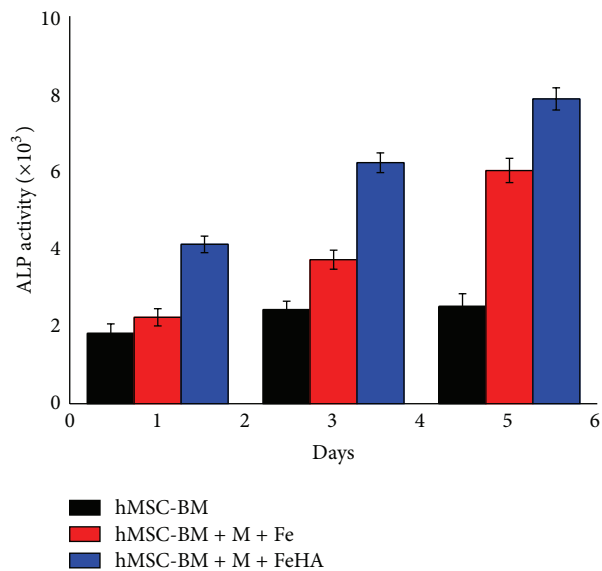


FIGURE 7: In vitro ALP activity of cell cocultured with nanoparticles.

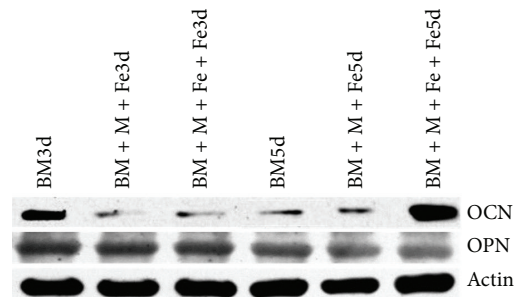


FIGURE 8: The Western blot results of osteoblast-related genes OCN and OPN expressions of hMSC-BM. On the 5th day, the expression levels of OCN and OPN increased contrast with the CON group.

5th day after culturing on the induced medium by Western blot (Figure 8). On the 3rd day, the expression levels of OCN and OPN decreased in contrast with the CON group, while on the 5th day, the expressions of OCN and OPN

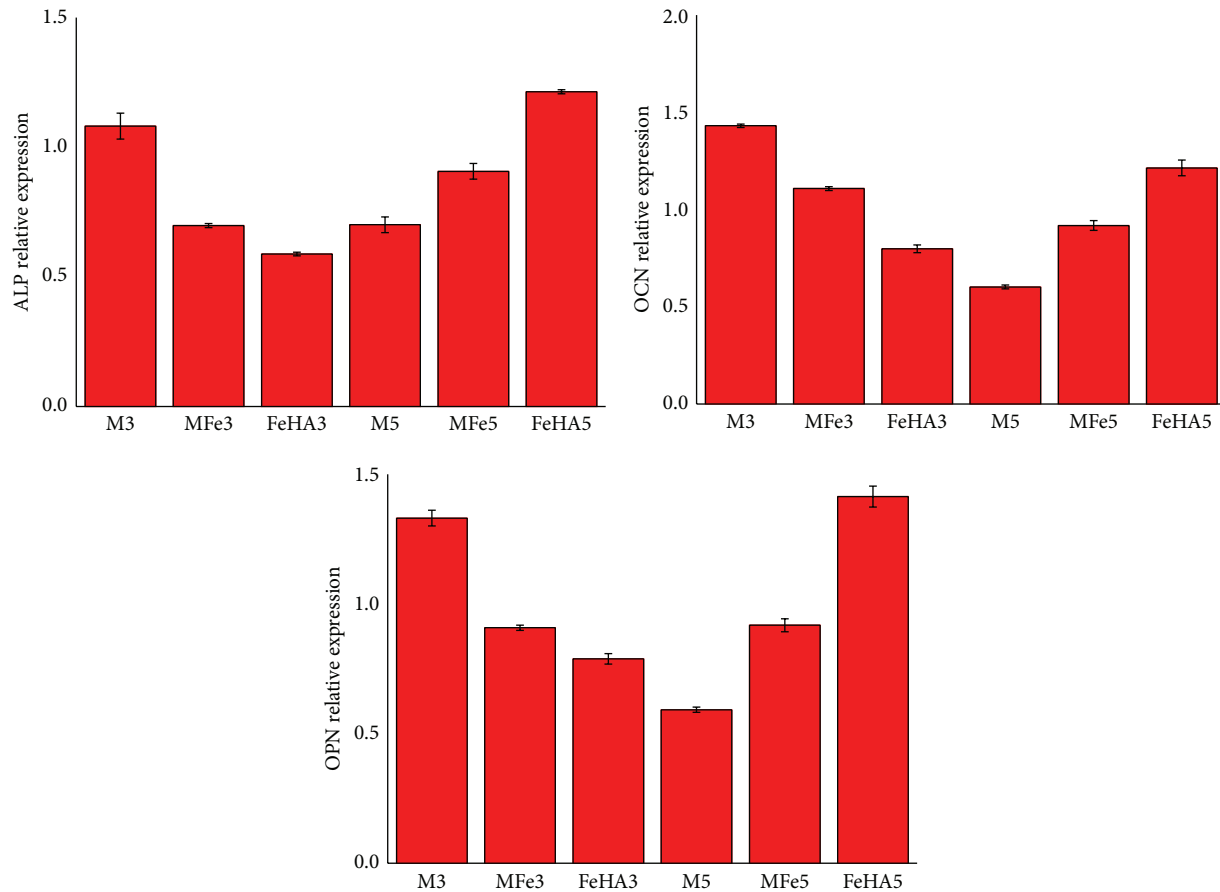


FIGURE 9: Impacts of different materials on osteoblast-related genes ALP, OCN, and OPN expressions of hMSC-BM. The results were expressed in the form of mean \pm SD values. In contrast with the CON group, on the 5th day of treatment, the expression levels of genes ALP, OCN, and OPN increased ($P < 0.05$).

increased in Fe and nHA group compared with the CON group. Inductions of osteoblast specific genes ALP, OCN, and OPN were examined by RT-PCR. Compared with the control group, the expression levels of genes OCN, OPN, and ALP increased in the treatment of the 5th day ($P < 0.05$) under the magnetic situation. The results of qPCR were consistent with the WB analysis, which showed that the expressions of ALP, OCN, and OPN increased in contrast with the CON group on the 5th day. The fold-change of gene expression data is shown in Figure 9.

4. Discussion

Recently, the nanoscale magnetic material has become a hotspot in the biomaterials field. Biocompatibility [24] is particularly significant in the magnetic nanoparticles. Moreover, it shall not arouse any unfavorable systemic or local influences on the beneficiary or recipient of the treatment. Instead, it is desired that the most proper beneficial cellular or tissue reaction under that particular condition can be generated and the related beneficial clinical performance of that treatment can be optimized. In this regard, the Fe-based particles occupy a great share in the magnetic

nanoparticles. However, Fe revealed some toxicity in its clinical application. Some study thus attempted to improve the Fe-based magnetic particles. For example, Latham and Williams explored to synthesize Fe_3O_4 improved by polymer so as to reduce the cell toxicity and enhance biocompatibility [22]. In this research, the second-phase theory was applied to form the n-HA-coated magnetic nanoparticles, because n-HA could increase the osteoinductivity of Fe_3O_4 . As the results of the SEM survey and immunofluorescence assay indicated, the Fe_3O_4 -HA composites could vigorously support the hMSC-BM attachment, proliferation, and spreading. In other words, Fe_3O_4 -HA magnetic particles exerted no cytotoxicity to hMSC-BM cells and owned perfect biocompatibility. In addition, HA, the second phase, improved the inductivity of those nanobiomaterials. It is known to all that the inductivity plays a vital role in cellular growth. In this regard, efficient approaches of artificial control in scale and shape for Fe_3O_4 and surface modification of Fe_3O_4 are usually adopted to lower the toxicity in Fe_3O_4 . However, some scientists proved that, through artificial coating and modification, Fe_3O_4 would lose its original characteristics, which are thus unparallel to the original ones in a basic sense. In specific, the second-phase modifying approaches include

the chemical modification and surface coat. By modifying the Fe_3O_4 , the inherent toxicity in Fe_3O_4 can be lowered. Therefore, it can significantly enhance the biocompatibility of Fe_3O_4 . In order to safely apply Fe_3O_4 in biomedicine, the new magnetic nanoparticles shall be equipped with high biocompatibility but low toxicity. From these data of results, the synthesized Fe_3O_4 -HA magnetic particles showed perfect biocompatibility and no cytotoxicity.

Besides, magnet can influence the flow of ions within the cells, especially the flow of Ca^{2+} . It can directly or indirectly cause the reconstruction of microfilaments, surficial glycosyl, and micropipes and finally influence the cellular morphology and cellular membrane growth. Nonetheless, the majority of researches aimed to characterize the biocompatibility of magnetic nanoparticles without considering the magnetic condition. Recently, an increasing number of scientists have discovered that magnetic condition can facilitate the bone regeneration. Therefore, the biocompatibility of the Fe_3O_4 -HA magnetic particle will be studied in the magnetic situation. With the biocompatible nanosized magnetic particles as a remote force mechanism without invading the sterile bioreactor environment, this paper specifically demonstrated the theoretical base, design, and preliminary results of a mechanically conditioning system for cellular culture. The magnetic force bioreactor was created for the magnetic condition. From Figure 1, it can be found that the cell disc can be located in the middle of the magnetic force bioreactor. The distribution of magnetic induction line can form between the different polarity magnets facing each other. The cells cultured with Fe and n-HA were seeded in plates with culture medium and exposed to a magnetic force bioreactor every one hour at every other day of cyclic loading intervals for a 14-day period. The magnetic flux density of the central field is up to 0.2 T. The mechanical condition of cellular structure in bioreactors is a vital element determining the characteristics of the generated tissue. It is the magnetic force bioreactor that produces the magnetic stress. Therefore, the mechanical condition under a bioreactor situation can be controlled. This new bioreactor is designed to solve problems with the ex vivo development of mechanically stable, functional, and connective tissues. The present bioreactors are relatively limited, because the biochemical reactions need to be initiated within cells which grow upon the biodegradable scaffold in the bioreactor through applying the mechanical force into the cellular membranes. The bioreactor with magnetic force is designed to utilize the force directly into the cellular membranes through coupling the biocompatible nanosized magnetic particles into the receptor sites and membrane surfaces. Aiming at deforming the cellular membranes and activating the mechanosensitive transmembrane Ca^{2+} channels, the forces on the sequence of some piconewtons are demanded. The deformation in the membranes as well as the activation in those ion channels will make the biochemical reaction cascades become necessary for the growth of functional tissues. Hence, mechanically weak scaffold materials can be utilized if these small forces are directly applied into the membranes. This is because the applied forces are generated remotely through connecting these particles into external

fields. During this process, the system can be closed so as to prevent infection. Besides, forces applied to the nanosized magnetic particles may be spatially different in 3 dimensions by changing the distance of different areas of the nanosized particles to the field source or through varying the properties of magnetic particles in various regions of the nanosized particles. The bioreactor can be further applied in human tissue in the future.

According to the analysis in this paper, it mainly finds that the nanoscale n-HA-coated magnetic (Fe_3O_4 -HA) particles prefer osteoblast from hMSC-BM, because of the Fe_3O_4 . n-HA increased the osteoinductivity of Fe_3O_4 . Moreover, it is indicated that n-HA modifies the microenvironment of cellular culture which exerts great influences on the differentiation of hMSC-BM. Specifically, n-HA gathers protein, shapes neomatrix, and greatly improves osteogenesis. The expression of ALP can rise up to 27 times in the magnetic condition compared with control. Based on the Western blot and PCR analysis, it can be easily observed that the expression level of genes OCN, ALP, and OPN was enhanced on the treatment of the 5th day ($P < 0.05$) in the magnetic condition. This indicates that the magnetic condition can greatly affect the cellular growth and cellular differentiation. For this project, an understanding of the magnetic forces may affect the interaction of the particles with the cell. In addition, the nanosize of n-HA-coated magnetic particles also plays a vital part in the fate of the stem cells. Particles of diameter less than 50 nm will act as the superparamagnets, which means they will become the paramagnetic materials with high susceptibility, while particles with diameter above 50 nm will serve as permanent magnetic dipoles. As the diameter of nanoscale n-HA-coated magnetic (Fe_3O_4 -HA) particles was around 15–40 nm, they belong to the superparamagnets. Attributing to their physicochemical characteristics, both nanomaterials and microparticles [41–43] have shown some cell toxicity and biostability. On the other hand, the cellular death was significantly correlated with its particle load. The particles were avoiding the phagocytic passage and a few even entered the nuclei through nuclear pores. It means that the number of nanoparticles must be normalized and controlled with target stem cell. Even if the engineered biomaterials are seeded with the stem cell, they will be regarded as the differentiation of cells in some situations. The appropriately designed size of nanomaterials is a potential and promising way for the clinical repair of tissues. Therefore, the n-HA-coated magnetic (Fe_3O_4 -HA) particles were concluded with better biocompatibility, which provided some useful information for its clinical applications.

5. Conclusions

To summarize, the n-HA-coated magnetic nanoparticles (n-HA/ Fe_3O_4) were prepared through precipitation approach. n-HA-coated magnetic nanoparticles increased cell viability and promoted hMSC-BM growth under magnetic situation. n-HA/ Fe_3O_4 increase up the process of osteogenic differentiation under the magnetic situation. Therefore, it will be a promising approach for bone engineering in future.

Conflict of Interests

The authors declare no possible conflict of interests.

Authors' Contribution

Qing Li and Gang Zhou contributed equally to this paper.

Acknowledgments

This study was supported by funds from National Natural Science Foundation of China (NSFC) Research Grant (nos. 81171000, 31100666, 11120101001, 61227902, 11172031, 10925208, and 51302005), the National High Technology Research and Development Program of China (2012AA022501), Science Foundation of Beijing Research Grant (no. Z121100005212009), the Key International S&T Cooperation Project (no. 2011DFA32190), National Basic Research Program of China (973 program, 2011CB710901 and 2012CB933900), National Key Technology R&D Program (nos. 2012BAI18B06, 2012BAI18B05, and 2012BAI07B01), the 111 Project of China (no. B13003), International Joint Research Center of Aerospace Biotechnology and Medical Engineering, Ministry of Science and Technology of China, Doctoral Scientific Fund Project of the Ministry of Education of China (no. 20130001120112), and the Fundamental Research Funds for the Central Universities of China. Additionally, the authors also acknowledge the support of the Peking University-Tsinghua University Joint Center for Life Sciences.

References

- [1] I. V. Vasylenko, S. V. Kolotilov, I. E. Kotenko et al., "Magnetic properties of nanosized γ -Fe₂O₃ and α -(Fe_{2/3}Cr_{1/3})₂O₃, prepared by thermal decomposition of heterometallic single-molecular precursor," *Journal of Magnetism and Magnetic Materials*, vol. 324, no. 4, pp. 595–601, 2012.
- [2] X. Li, Y. Yang, Y. Fan, Q. Feng, F.-Z. Cui, and F. Watari, "Bio-composites reinforced by fibers or tubes as scaffolds for tissue engineering or regenerative medicine," *Journal of Biomedical Materials Research—Part A*, vol. 102, no. 5, pp. 1580–1594, 2014.
- [3] X. Li, C. A. van Blitterswijk, Q. Feng, F. Cui, and F. Watari, "The effect of calcium phosphate microstructure on bone-related cells in vitro," *Biomaterials*, vol. 29, no. 23, pp. 3306–3316, 2008.
- [4] Q. Wu, X. L. Zhang, B. Wu, and W. Huang, "Effects of microwave sintering on the properties of porous hydroxyapatite scaffolds," *Ceramics International*, vol. 39, no. 3, pp. 2389–2395, 2013.
- [5] G. A. O. Jinhao, G. U. Hongwei, and X. U. Bing, "Multifunctional magnetic nanoparticles: design, synthesis, and biomedical applications," *Accounts of Chemical Research*, vol. 42, no. 8, pp. 1097–1107, 2009.
- [6] G. Unsoy, R. Khodadust, S. Yalcin, P. Mutlu, and U. Gunduz, "Synthesis of Doxorubicin loaded magnetic chitosan nanoparticles for pH responsive targeted drug delivery," *European Journal of Pharmaceutical Sciences*, vol. 62, pp. 243–250, 2014.
- [7] S. Venkateswarlu, B. N. Kumar, C. H. Prasad, P. Venkateswarlu, and N. V. V. Jyothi, "Bio-inspired green synthesis of Fe₃O₄ spherical magnetic nanoparticles using *Syzygium cumini* seed extract," *Physica B: Condensed Matter*, vol. 449, pp. 67–71, 2014.
- [8] C. Wilhelm and F. Gazeau, "Universal cell labelling with anionic magnetic nanoparticles," *Biomaterials*, vol. 29, no. 22, pp. 3161–3174, 2008.
- [9] A. Ito, E. Hibino, H. Honda et al., "A new methodology of mesenchymal stem cell expansion using magnetic nanoparticles," *Biochemical Engineering Journal*, vol. 20, no. 2-3, pp. 119–125, 2004.
- [10] K. Shimizu, A. Ito, T. Yoshida, Y. Yamada, M. Ueda, and H. Honda, "Bone tissue engineering with human mesenchymal stem cell sheets constructed using magnetite nanoparticles and magnetic force," *Journal of Biomedical Materials Research Part B: Applied Biomaterials*, vol. 82, no. 2, pp. 471–480, 2007.
- [11] G. Zhou, A. Ruhan, H. Ge et al., "Research on a novel poly (vinyl alcohol)/lysine/vanillin wound dressing: Biocompatibility, bioactivity and antimicrobial activity," *Burns*, vol. 40, no. 8, pp. 1668–1678, 2014.
- [12] V. N. Binhi, Y. D. Alipov, and I. Y. Belyaev, "Effect of static magnetic field on *E. coli* cells and individual rotations of ion-protein complexes," *Bioelectromagnetics*, vol. 22, no. 2, pp. 79–86, 2001.
- [13] A. Chionna, B. Tenuzzo, E. Panzarini, M. B. Dwikat, L. Abbro, and L. Dini, "Time dependent modifications of Hep G2 cells during exposure to static magnetic fields," *Bioelectromagnetics*, vol. 26, no. 4, pp. 275–286, 2005.
- [14] A. D. Rosen, "Membrane response to static magnetic fields: effect of exposure duration," *Biochimica et Biophysica Acta*, vol. 1148, no. 2, pp. 317–320, 1993.
- [15] S. H. Hamada, R. Witkus, and R. Griffith Jr., "Cell surface changes during electromagnetic field exposure," *Experimental Cell Biology*, vol. 57, no. 1, pp. 1–10, 1989.
- [16] A. Chionna, M. Dwikat, E. Panzarini et al., "Cell shape and plasma membrane alterations after static magnetic fields exposure," *European Journal of Histochemistry*, vol. 47, no. 4, pp. 299–308, 2003.
- [17] A. Nel, T. Xia, L. Mädler, and N. Li, "Toxic potential of materials at the nanolevel," *Science*, vol. 311, no. 5761, pp. 622–627, 2006.
- [18] T. Xia, N. Li, and A. E. Nel, "Potential health impact of nanoparticles," *Annual Review of Public Health*, vol. 30, pp. 137–150, 2009.
- [19] V. I. Shubayev, T. R. Pisanic II, and S. Jin, "Magnetic nanoparticles for theragnostics," *Advanced Drug Delivery Reviews*, vol. 61, no. 6, pp. 467–477, 2009.
- [20] V. Lorusso, L. Pascolo, C. Ferneti, P. L. Anelli, F. Uggeri, and C. Tiribelli, "Magnetic resonance contrast agents: from the bench to the patient," *Current Pharmaceutical Design*, vol. 11, no. 31, pp. 4079–4098, 2005.
- [21] H. Rui, R. J. Xing, Z. C. Xu, Y. L. Hou, S. Goo, and S. H. Sun, "Synthesis, functionalization, and biomedical applications of multifunctional magnetic nanoparticles," *Advanced Materials*, vol. 22, no. 25, pp. 2729–2742, 2010.
- [22] A. H. Latham and M. E. Williams, "Controlling transport and chemical functionality of magnetic nanoparticles," *Accounts of Chemical Research*, vol. 41, no. 3, pp. 411–420, 2008.
- [23] A. Tsetsekou, D. Brasinika, V. Vaou, and E. Chatzitheodoridis, "On the synthesis of tailored biomimetic hydroxyapatite nanoplates through a bioinspired approach in the presence of collagen or chitosan and l-arginine," *Materials Science and Engineering C: Materials for Biological Applications*, vol. 43, pp. 555–565, 2014.
- [24] X. Li, Y. Huang, L. Zheng et al., "Effect of substrate stiffness on the functions of rat bone marrow and adipose tissue

- derived mesenchymal stem cells in vitro," *Journal of Biomedical Materials Research Part A*, vol. 102, no. 4, pp. 1092–1101, 2014.
- [25] A. M. Sofronia, R. Baies, E. M. Anghel, C. A. Marinescu, and S. Tanasescu, "Thermal and structural characterization of synthetic and natural nanocrystalline hydroxyapatite," *Materials Science and Engineering C: Materials for Biological Applications*, vol. 43, pp. 153–163, 2014.
- [26] X. Li, Q. Feng, X. Liu, W. Dong, and F. Cui, "Collagen-based implants reinforced by chitin fibres in a goat shank bone defect model," *Biomaterials*, vol. 27, no. 9, pp. 1917–1923, 2006.
- [27] F. Mohandes, M. Salavati-Niasari, Z. Fereshteh, and M. Fathi, "Novel preparation of hydroxyapatite nanoparticles and nanorods with the aid of complexing agents," *Ceramics International*, vol. 40, no. 8, pp. 12227–12233, 2014.
- [28] R. Drevet, H. Benhayoune, and J. Michel, "Structural characterization of electrodeposited strontium substituted calcium phosphate coatings," *Journal of Biomaterials and Tissue Engineering*, vol. 1, no. 1, pp. 68–75, 2011.
- [29] M. Bricha, Y. Belmamouni, E. M. Essassi, J. M. F. Ferreira, and K. E. Mabrouk, "Hydrothermal synthesis and appraisal of mg-doped hydroxyapatite nanopowders," *Journal of Biomaterials and Tissue Engineering*, vol. 3, no. 5, pp. 570–580, 2013.
- [30] S. Johnsen and K. J. Lohmann, "The physics and neurobiology of magnetoreception," *Nature Reviews Neuroscience*, vol. 6, no. 9, pp. 703–712, 2005.
- [31] R. Wiltschko and W. Wiltschko, "Magnetoreception," *BioEssays*, vol. 28, no. 2, pp. 157–168, 2006.
- [32] M. Feychting, A. Ahlbom, and L. Kheifets, "EMF and health," *Annual Review of Public Health*, vol. 26, pp. 165–189, 2005.
- [33] L. Dini and L. Abbro, "Bioeffects of moderate-intensity static magnetic fields on cell cultures," *Micron*, vol. 36, no. 3, pp. 195–217, 2005.
- [34] G. Zhou, W. Song, Y. Hou, Q. Li, X. Deng, and Y. Fan, "Ultrasound-assisted fabrication of a biocompatible magnetic hydroxyapatite," *Journal of Biomedical Materials Research Part A*, vol. 102, no. 10, pp. 3704–3712, 2014.
- [35] X. Li, H. Gao, M. Uo et al., "Effect of carbon nanotubes on cellular functions in vitro," *Journal of Biomedical Materials Research Part A*, vol. 91, no. 1, pp. 132–139, 2009.
- [36] X. Li, H. Liu, X. Niu et al., "Osteogenic differentiation of human adipose-derived stem cells induced by osteoinductive calcium phosphate ceramics," *Journal of Biomedical Materials Research, Part B Applied Biomaterials*, vol. 97, no. 1, pp. 10–19, 2011.
- [37] A. A. Eid, K. A. Hussein, L. N. Niu et al., "Effects of tricalcium silicate cements on osteogenic differentiation of human bone marrow-derived mesenchymal stem cells in vitro," *Acta Biomaterialia*, vol. 10, no. 7, pp. 3327–3334, 2014.
- [38] S. Chen, D. A. Ryan, M. A. Dwyer, and J. R. Cashman, "Synergistic effect of Wnt modulatory small molecules and an osteoinductive ceramic on C2C12 cell osteogenic differentiation," *Bone*, vol. 67, pp. 109–121, 2014.
- [39] M. Kassem, B. M. Abdallah, and H. Saeed, "Osteoblastic cells: differentiation and transdifferentiation," *Archives of Biochemistry and Biophysics*, vol. 473, no. 2, pp. 183–187, 2008.
- [40] C. Wu, Y. Zhou, C. Lin, J. Chang, and Y. Xiao, "Strontium-containing mesoporous bioactive glass scaffolds with improved osteogenic/cementogenic differentiation of periodontal ligament cells for periodontal tissue engineering," *Acta Biomaterialia*, vol. 8, no. 10, pp. 3805–3815, 2012.
- [41] A. M. Mebert, D. E. Camporotondi, M. L. Foglia et al., "Controlling the interaction between cells and silica nanoparticles," *Journal of Biomaterials and Tissue Engineering*, vol. 3, no. 1, pp. 108–121, 2013.
- [42] X. Li, Y. Fan, and F. Watari, "Current investigations into carbon nanotubes for biomedical application," *Biomedical Materials*, vol. 5, no. 2, Article ID 022001, 2010.
- [43] H. T. Jin, S. Y. Liu, F. F. Guo, and B. B. Zhang, "Polymer-coated superparamagnetic iron oxide nanoparticles: synthesis, characterization and toxicity evaluation for MRI in mice," *Journal of Biomaterials and Tissue Engineering*, vol. 4, no. 6, pp. 443–449, 2014.

Review Article

The Transport and Deposition of Nanoparticles in Respiratory System by Inhalation

Huiting Qiao,^{1,2} Wenyong Liu,¹ Hongyu Gu,¹ Daifa Wang,¹ and Yu Wang¹

¹Key Laboratory for Biomechanics and Mechanobiology of Ministry of Education, School of Biological Science and Medical Engineering, Beihang University, Beijing 100191, China

²School of Biomedical Engineering, Science and Health Systems, Drexel University, Philadelphia, PA 19104, USA

Correspondence should be addressed to Yu Wang; wangyu@buaa.edu.cn

Received 18 September 2014; Accepted 25 December 2014

Academic Editor: Shuming Zhang

Copyright © 2015 Huiting Qiao et al. This is an open access article distributed under the Creative Commons Attribution License, which permits unrestricted use, distribution, and reproduction in any medium, provided the original work is properly cited.

The inhaled nanoparticles have attracted more and more attention, since they are more easily to enter the deep part of respiratory system. Some nanoparticles were reported to cause pulmonary inflammation. The toxicity of nanoparticles depends not only on its chemical component but also on the quantity and position of the deposition. The deposition of nanoparticles is not uniform and is influenced by airflow transport. The high deposition mainly occurs at the carinal ridges and the inside walls around the carinal ridges. Many factors could affect the transport and deposition of nanoparticles, such as particle size, flow rate, structure of airway, pulmonary function, and age. In this review, we discussed the methods and technique involved in particle transport and deposition studies. The features of particles deposition could be observed in clinic experiments and animal experiments. The mechanism of transport could be studied by numerical simulation. Numerical model and experiment study supplement each other. Some techniques such as medical imaging may support the study of nanoparticles transport and deposition. The knowledge of particles transport and deposition may be helpful both to defend the toxicity of inhaled particles and to direct inhaled drug delivery.

1. Introduction

More and more attention has been paid to air pollution. The high concentration of fine particle matter (PM 2.5) during the 2013 severe haze of north China has caused public worries [1, 2]. The most worries are due to the adverse effect of air pollution on health [3]. It is believed that the most airborne particles were derived from fossil, biomass, and solid fuels combustion [4–6]. The traffic exhausts have been verified as the source of particle matter [7, 8]. The particles emitted by engines have a high proportion of nanoparticles, though most of them are in accumulation mode [9]. Epidemiological studies have confirmed that air pollution makes adverse health effect, especially the pollutant in nanoscale [10, 11]. Thus, nowadays most attention paid to airborne pollutants lies in nanoparticles and ultrafine particles.

Though some studies did not differentiate ultrafine particles from nanoparticles [12], the different definitions have also been reported. The particles in nanoscales (<100 nm) in

one dimension could be generally called nanoparticles, while ultrafine particles are limited to 100 nm in all dimensions [13]. For the purposes of this review, we do not differentiate nanoparticles from ultrafine particles: they are both particles in nanoscales.

People have great expectation for nanotechnology and have been trying to apply nanomaterial in many fields [14, 15]. Thus airborne nanoparticles are unavoidable. For the reason of small size, nanoparticles may enter the deep part of human respiratory system with breathing. Pulmonary inflammation has been reported after inhalation exposure to nanoparticles [16, 17], so the toxicity of nanoparticles in air should be considered [18].

Respiratory system is an important pathway for substance to enter human body besides alimentary canal. Air enters the trachea through nasal and oral cavities, passing by the tracheobronchial tree, and arrives at the alveoli, so does some airborne nanoparticles. The transport and deposition of particles have great relations with the complicated airway.

The structures of respiratory system have been described by Weibel as a bifurcating tubes' model with 23-generation bifurcations, and the airways are named as G0–G23 [19, 20]. The airways from G0 to G16 belong to conducting zone, and the airways from G17 to G23 have the function of gas exchange. The upper airway, which begins from the nose and mouth to the trachea (G0), functions not only as the passage-way but also as a filter to protect the lower airway; however some small-scale pollutants could still enter the respiratory system and may cause disease [21–23].

Although many researches have confirmed that the toxicity of airborne particles changes along with their compositions [24], the quantity of transport and the position of deposition also have great relations with the toxicity of nanoparticles. This review aims at the toxicity of nanoparticles by inhalation with great emphasis on the transport and deposition of nanoparticles in respiratory system. The research methods for toxicity of airborne nanoparticles were compared. The potential application of a medical imaging technique was also mentioned.

2. The Toxicity of Nanoparticles by Inhalation

Airborne particles especially nanoparticles have been recognized as a potential risk for health. Since airborne nanoparticles enter human body by inhalation, respiratory system has higher risk exposed to nanoparticles [25]. In the view of epidemiology, the increased morbidity and mortality may have relations with particles in air [23, 26]; for example, fine particulate pollution is confirmed to be associated with all-cause, lung cancer and cardiopulmonary mortality [27]. For their small scale, nanoparticles can enter lower airway, reach alveoli, and can even pass the alveolar epithelium to intrapleural space [28]. Pulmonary inflammation could be caused when exposed to some nanoparticles [17].

Nanoparticles harm respiratory system mainly by the injury of epithelium [29], and the most important mechanism is the oxidative stress induced by nanoparticles [30, 31]. The adverse effects happen not only in respiratory system but also in extrapulmonary organs. Once nanoparticles reach pulmonary alveoli, some of them may pass through the alveolar epithelium and capillary endothelial cell and then enter the cardiovascular system and other internal organs [32]. In the long term exposure experiment using sensitive mouse model, inhaled nickel hydroxide could increase mitochondrial DNA damage in the aorta and exacerbate the progression of atherosclerosis as well as the inflammation in lung [30]. The pathological changes in liver have also been reported when inhalation exposed to ferric oxide and zinc oxide nanoparticles [33].

The toxicity of airborne nanoparticles depends on the chemical component of the nanomaterial. To confirm the toxicity of individual nanoparticles, the effect on health of nanoparticles has been studied, respectively. Some nanoparticles may cause pulmonary inflammation, while some nanoparticles may not. A great deal of metallic oxide and hydroxide may cause pulmonary inflammation. Nanoparticles of zinc oxide [34, 35], aluminum oxide [36], copper oxide [37, 38], cobalt oxide [37], iron oxide [39], cadmium oxide [40], and

nickel hydroxide [30, 41] have been reported to induce pulmonary inflammation and adverse effects, while no significant inflammation nor adverse effects have been observed when exposed to some nanomaterials, such as carbon nanoparticles [41], graphite nano platelets [42], carbon black [42], and silica [43].

The toxicity of nanoparticles depends not only on the chemical component, but also on dose, size, and other factors [13, 17]. For the nanoparticles of the same component, size and concentration are also crucial [44–46]. More obvious infection signs have been found in animal experiment after instillation of smaller size polystyrene particles [45]. The toxicity of some nanoparticles may also depend on concentration. Inflammatory processes appeared when the exposure concentration reached 0.5 mg/m^3 for multiwall carbon nanotubes and 10 mg/m^3 for graphene [42]. Significant inflammation could be observed when titanium dioxide was inhaled in high dose, compared with no significant pulmonary inflammation when it was inhaled in low and medium dose [47].

The toxicity of particles also depends on the position where the particles arrive and deposit [48]. Respiratory system has complicated bifurcate tree-structure airways which can be divided into conduction zone and respiratory zone. In conduction airway the particle matters may stick to the mucus and be removed with the help of cilia, as well as the phagocytosis of macrophage [49]. In alveoli, the important region for gas exchange, there is only macrophage protecting the body from infection [50]. When particles accumulate in alveoli, the pulmonary inflammation will be induced [17]. Thus the understanding of how nanoparticles transport and deposit is as important as the cytotoxic study.

3. The Means to Study Transport and Deposition of Nanoparticles

As the toxicity of nanoparticles has attracted great attention, the study of nanoparticles deposition is developing step by step. Many different methods have been used in particles deposition study, as shown in Figure 1. The study of particles transport and deposition could be classified as clinical or animal experiment studies and computer simulation studies. Each kind of study method is irreplaceable. They supplement each other. At first the relations between inhaled particle pollution and health were detected by epidemiological studies. At the same time clinical or animal experiment studies were conducted to understand the particles' deposition in respiratory system. Then mathematical models, including CFD model, were established to find more details of particles' transport and deposition.

The experiment studies include in vivo experiments and in vitro experiments. The respiratory tract deposition of particles could be determined from in vivo experiments during spontaneous breathing of volunteers, patients, and experimental animals [51–53]. For the reason of ethics, there are many limitations of in vivo experiments in volunteers and patients. For volunteers and patients, the total deposition fractions were derived by comparing the difference between

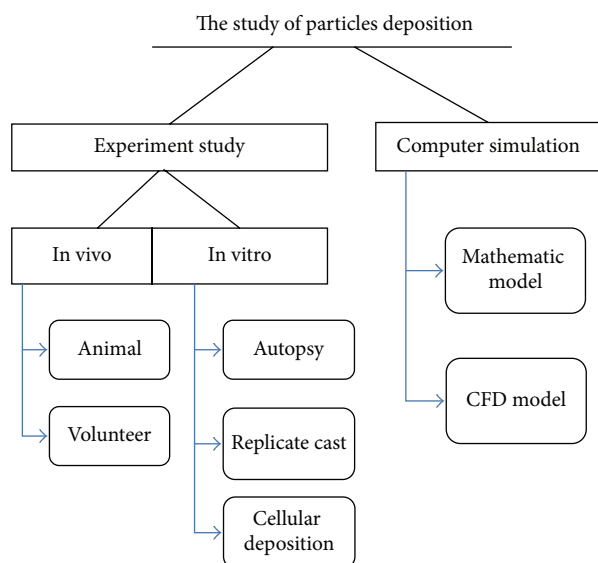


FIGURE 1: The classification of the method to study particles deposition.

inhaled and exhaled particle concentrations. In animal experiments, the accumulated particles were recovered and assessed from the excised tissue after sacrifice [54]. The lung tissue could be excised to proceed with pathological examination [55]. The response of the physiological system, such as the inflammation caused by inhaled particles [56], could be also observed during *in vivo* experiments. For patients and volunteers, induced sputum after inhalation could be obtained to analyze inflammation and immune function [52]. The *in vivo* experiment is good to observe the actual physiological response, but it is not enough to investigate the mechanism of transport, deposition, and toxicity of nanoparticles.

In the study of autopsy, the retained particles in human lung parenchyma could be examined [57], while, to understand how these particles were retained, some designed *in vitro* experiments proceeded. In the end of last century, many particle deposition experiments had been conducted with replicate human airway cast [15, 58, 59]. Gurman et al. and Cohen et al. used a replicate cast of human upper tracheobronchial tree to examine the deposition of particles [60, 61]. Some small airways were hard to build cast, so most of the casts were trimmed to airways with diameter >3 mm. In the study of Cohen et al., the replicate airway cast included 10-generation airway and retained 141 airways [58]. Most of the casts were made of silicone rubber [62] and just used to simulate the transport phenomenon of particles in tube; the deposition in cell was studied by cell exposure experiment [63]. The cell exposure experiment could be used to study the mechanism the toxicity of nanoparticles without cross-species correlation and ethical concerns, while the results of *in vitro* cell exposure experiment were different from those of *in vivo* experiment [64] because the cell culture system could not represent the multicellular organism.

To describe the transport and deposition of nanoparticles quantitatively, some mathematical models have been established based on the results of experiments [65]. Martin and

Finlay used a simple algebraic formulation to predict the total respiratory tract deposition fraction with an empirical fit to experiment data [66]. A two-compartment model has been established to describe the deposition and clearance of particles in surfactant layer of the alveolar surface and in the cell plasma of alveolar macrophages [67]. A semiempirical model has been used to study the particle deposition difference between a single breath and multiple breathing cycles [68]. This kind of mathematic model explained the result of experiment with lumped parameters, instead of providing detailed transport and deposition of local region.

It is difficult to observe and to accurately measure the local deposition of ultrafine particles in real-time experiment. Computational fluid dynamics (CFD) simulation could provide the detailed flow mechanics in airway and predict the deposition of nanoparticles [69]. In CFD studies, the structure of human airway is the basis for analyzing particle transport and deposition. The geometric model of airway was divided into tiny meshes; thus the deposition feature could be compared in very small local regions. The number of meshes and the time of simulation increase with the complexity of airway. Thus most of the CFD simulation just focused on some part of the airway. For example, Zhang and Kleinstreuer studied ultrafine particles deposition and heat transport with an oral airway model and G0–G3 airway model [70], and they studied inertial and gravitational deposition of microparticles in medium-size bronchial generations G6–G9 [71]. They also attempted to study the deposition in the entire tracheobronchial airway. Five levels of triple-bifurcation unit constituted a 16-generation model [72]. The simulation study was conducted for each triple-bifurcation unit. The respiratory zone of airway was not considered in existing CFD deposition studies because of the complexity of structure. Although the CFD technique has been utilized to study in many fields including the transport of particles in airway, the reliability of the simulation should be validated by data from experimental studies.

4. Factors Influence the Transport and Deposition of Particles in Respiratory System

The transport of particles with air flow in curved tubes of respiratory system can be described by fluid mechanics. In the study of gas-solid-two-phase flow, Stokes number is used to describe the behavior of particles in the flow, and Reynolds number is used to distinguish flow patterns. For low inspiratory flow rate, the transport of particles in airways can be described as laminar flow with secondary flow, while turbulence appears with the increase of flow rate [73]. Low Reynolds number $K-\omega$ model for turbulence can be used to study the transport and deposition of nanoparticles [74, 75]. Though the flow rate is oscillatory in spontaneous breathing, the flow fields seemed similar to those in steady state inhalation in case of the equivalent Reynolds number [76]. In most cases, the deposition fraction increases with the increase of Stokes number [77]. The deposition could also be influenced

by many factors, such as size of the particles, inhalation waveform, and also the structure of respiratory airway [12, 73, 78].

For the complicated airway structure, the deposition of particles is not uniform in the total respiratory system. Some parameters were introduced to describe the total and regional deposition. The deposition fraction (DF) is the mostly used not only for deposition in total respiratory system, but also for that in regional part, which is defined as the ratio of number of particles depositing to the number of particles entering the system. The deposition efficiency (DE) is derived as the ratio of particles depositing within a region to the particles entering that region. The deposition enhancement factor (DEF) is defined as the ratio of the number of particles depositing per unit area in local region to the average number of particles depositing per unit area in the whole bifurcation [79], which could indicate the deposition “hot spots” [12]. In the studies of Gurman et al., the replicate casts of human upper tracheobronchial model were used to examine the deposition of microparticles in 0–5 airway generations [60]. The DE of microparticles in each airway generation was different, especially between trachea and bronchi. The position-dependent deposition fraction feature also appears for nanoparticles. In the human tracheobronchial cast deposition experiments, Cohen showed the different DE of nanoparticles from airway generation 0 to generation 7 [58]. The DE in trachea (generation 0) was greater than that in main bronchi (generation 1), while the DF increased from the second generation airway to the sixth generation airway. In numerical study, the difference of deposition was also observed in great detail. The deposition fraction of different parts has been studied such as nasal cavity, nasopharynx, larynx, and trachea [80]. The deposition fraction in head airway is much higher than that in larynx and trachea. The local region with high DEF, meaning the hot spot of deposition, mainly occurs at the carinal ridges and the inside walls around the carinal ridges [12].

Size of particles plays an important role in particles transport and deposition in respiratory system. The transport of microparticles mainly depends on inertial impaction and sedimentation [71], while that of nanoparticles mostly relies on diffusion [74]. The particles in small scale are easier to enter the lung. From the analyses of particle content of autopsy lungs, it was found that the sizes of the particles and aggregates in autopsy lung were obviously smaller than the average sizes in air, which were mostly in nanoscale [25]. The places where particles deposit have great relation with particle size. For microparticles, the deposition in head airway is much greater than that in tracheobronchial and alveolar region. Only when the diameter of particle is less than $10\ \mu\text{m}$, the deposition in alveoli became obvious, and the ratio of the deposition in alveoli to that in total respiratory system increases remarkably for particles with diameter from $10\ \mu\text{m}$ to $0.5\ \mu\text{m}$ [81]. For nanoparticles, the total deposition and head airway deposition will increase with the decrease of nanoparticles diameter (from 100 nm to 1 nm) [82, 83]. In alveolar region and tracheobronchial region, the deposition fractions of nanoparticles increase firstly and then decrease along with the decrease of nanoparticle's diameter, while the deposition variations in these two regions are not synchronous [84].

The influence of flow rate on particles deposition has been studied by experiments and numerical simulation. In deposition experiments for microparticles and nanoparticles, it was found that the DE in high flow rate was less than that in low flow rate [58, 60]. The same results have been received from computer simulation that the flow rate may influence the deposition of particles [85]. While in some other measurement experiments, the influence of flow rate is not obvious [83], which may be because of the differences in the applied methodologies and the difference of airway model [84]. Besides the flow rate, the influence of inhale waveform has also been studied. The flow rate, cyclicity, and velocity inlet profile influence particle deposition to a certain extent [77, 78], while these influences seemed minor compared with the influence of particle size [12]. Some reports about flow influences were not coincident, which may be because of the difference of the airway models. It has been reported for microparticles, in bronchi, that the DE is greater under cyclic flow than under constant flow, but the DE in the entire tracheobronchial tree showed no observed difference under these two different means of flow [60].

The transport and deposition of nanoparticles in respiratory system also vary with age, lung function [51, 86, 87]. In volunteer respiratory tract deposition experiments, it was found that the deposition probability of nanoparticles had relations with the lung function and severity of the disease [51, 88]. In simulation study, there was a higher particle deposition rate for child than that for adults [75, 86]. The deposition variation is due to the difference of airway geometry and breath parameters. The deposition during exercise is obviously higher than that in rest, because of the different breath pattern [89]. The geometry model is also an important factor to study particles deposition. When considering the laryngeal model, the DF of microparticles in tracheobronchial airway increased, while that of nanoparticles in tracheobronchial decreased [90].

5. Other Techniques Involved in Particle Transport and Deposition Study

Some other techniques were also involved in the study of particles transport and deposition, such as medical imaging. Medical images can not only provide detailed anatomy structure of airway but also be used to observe the deposition in vivo. In some early studies, the airway casts were made from a cadaver [91]. With the development of medical imaging, the geometrical morphology of airway can be picked up from medical images. CT, MRI, and some other imaging techniques have been used in particles' transport and deposition study. Grgic et al. built a realistic extrathoracic model with simple geometric shape based on CT scan and MRI scan [92]. Then many realistic airway geometric models were constructed by CT scan and MRI scan [75, 80, 93], which make it possible to realize individual airway deposition CFD analysis. Together with the development of 3D printing technique [94], detailed individual airway solid model for in vitro experiment will be achievable.

Some molecular imaging techniques, which have been used to detect nanomedicine distribution, can also be used

in the deposition study of nanoparticles in respiratory system [95]. Fluorescent imaging has been used to detect the distribution of aerosols in each lung lobe [96]. The γ -camera has been used to scan bronchial airway after radiolabeled particles were inhaled [52]. SPECT and PET have been used to measure the deposition and postdeposition kinetics of some aerosol in the lung [97, 98]. Although the developed imaging technique such as PET can provide three-dimension kinetics of the tracers' distribution, up to now the poor spatial resolution is still the limitation to observing the transport process in detail.

Besides the knowledge on defense against the toxicity of nanoparticles, the transport and deposition of nanoparticles also have another potential application. Medicine in nanoscale could be inhaled through the tracheobronchial airways down into the alveolar region [32, 99]. The transport and deposition study of nanoparticles may also provide useful information for aerosol drug delivering system. With the assistance of medical imaging, the personalized risk assessment and individual drug delivery scheme could be achieved in future.

6. Conclusions

More and more nanoproducts appear together with the concern about the toxicity of nanoparticles by inhalation. Not only in occupational conditions but also in resident conditions, airborne nanoparticles have been detected, which bring the risk of toxicity by inhalation. Though strict exposure limits have been established to protect human body from the toxicity of airborne nanoparticles [100], knowledge on the transport and deposition of nanoparticles is also significant.

In this review, the methods for the particles deposition studies have been classified and listed. The advantages and disadvantages of each method have been mentioned. The nonuniform deposition feature of nanoparticles has been described, and the effect of factors of their transport and deposition has been discussed. The flow rate, respiratory pattern, and even individual airway structure may influence the particles deposition. The combination of medical imaging and other techniques may promote the study of the particle deposition.

Conflict of Interests

The authors declare that there is no conflict of interests regarding the publication of this paper.

Acknowledgments

This work was supported by National Nature Science Foundation of China (Grants nos. 81101123, 61108084, 61201313, 61190123, and 11272039), National Key Technology R&D Program (2012BAI14B04), Beijing Higher Education Young Elite Teacher Project, and the Fundamental Research Funds for the Central Universities of China.

References

- [1] L. T. Wang, Z. Wei, J. Yang et al., "The 2013 severe haze over southern Hebei, China: model evaluation, source apportionment, and policy implications," *Atmospheric Chemistry and Physics*, vol. 14, no. 6, pp. 3151–3173, 2014.
- [2] Y. Wang, L. Yao, L. Wang et al., "Mechanism for the formation of the January 2013 heavy haze pollution episode over central and eastern China," *Science China Earth Sciences*, vol. 57, no. 1, pp. 14–25, 2014.
- [3] Z. Cheng, J. Jiang, O. Fajardo, S. Wang, and J. Hao, "Characteristics and health impacts of particulate matter pollution in China (2001–2011)," *Atmospheric Environment*, vol. 65, pp. 186–194, 2013.
- [4] W. Li, C. Wang, H. Wang et al., "Distribution of atmospheric particulate matter (PM) in rural field, rural village and urban areas of northern China," *Environmental Pollution*, vol. 185, pp. 134–140, 2014.
- [5] Y. Sun, G. Zhuang, Y. Wang et al., "The air-borne particulate pollution in Beijing—concentration, composition, distribution and sources," *Atmospheric Environment*, vol. 38, no. 35, pp. 5991–6004, 2004.
- [6] Y. Cheng, G. Engling, K.-B. He et al., "The characteristics of Beijing aerosol during two distinct episodes: impacts of biomass burning and fireworks," *Environmental Pollution*, vol. 185, pp. 149–157, 2014.
- [7] D. B. Kittelson, W. F. Watts, and J. P. Johnson, "Nanoparticle emissions on Minnesota highways," *Atmospheric Environment*, vol. 38, no. 1, pp. 9–19, 2004.
- [8] D. B. Kittelson, W. F. Watts, and J. P. Johnson, "On-road and laboratory evaluation of combustion aerosols—part I: summary of diesel engine results," *Journal of Aerosol Science*, vol. 37, no. 8, pp. 913–930, 2006.
- [9] D. B. Kittelson, "Engines and nanoparticles: a review," *Journal of Aerosol Science*, vol. 29, no. 5–6, pp. 575–588, 1998.
- [10] D. Tang, T. Y. Li, J. C. Chow et al., "Air pollution effects on fetal and child development: a cohort comparison in China," *Environmental Pollution*, vol. 185, pp. 90–96, 2014.
- [11] G. Oberdörster, J. N. Finkelstein, C. Johnston et al., "Acute pulmonary effects of ultrafine particles in rats and mice," *Research Report*, no. 96, pp. 5–75, 2000.
- [12] Z. Zhang and C. Kleinstreuer, "Airflow structures and nanoparticle deposition in a human upper airway model," *Journal of Computational Physics*, vol. 198, no. 1, pp. 178–210, 2004.
- [13] V. Stone, H. Johnston, and M. J. D. Clift, "Air pollution, ultrafine and nanoparticle toxicology: cellular and molecular interactions," *IEEE Transactions on Nanobioscience*, vol. 6, no. 4, pp. 331–340, 2007.
- [14] Z. Abidin, M. A. Alim, R. Saidur et al., "Solar energy harvesting with the application of nanotechnology," *Renewable and Sustainable Energy Reviews*, vol. 26, pp. 837–852, 2013.
- [15] R. Lehner, X. Wang, S. Marsch, and P. Hunziker, "Intelligent nanomaterials for medicine: carrier platforms and targeting strategies in the context of clinical application," *Nanomedicine: Nanotechnology, Biology, and Medicine*, vol. 9, no. 6, pp. 742–757, 2013.
- [16] I. Gosens, J. A. Post, L. J. J. de la Fonteyne et al., "Impact of agglomeration state of nano- and submicron sized gold particles on pulmonary inflammation," *Particle and Fibre Toxicology*, vol. 7, article 37, 2010.

- [17] H. M. Braakhuis, M. V. D. Z. Park, I. Gosens, W. H. de Jong, and F. R. Cassee, "Physicochemical characteristics of nanomaterials that affect pulmonary inflammation," *Particle and Fibre Toxicology*, vol. 11, no. 1, article 18, 2014.
- [18] G. Oberdörster, E. Oberdörster, and J. Oberdörster, "Nanotoxicology: an emerging discipline evolving from studies of ultrafine particles," *Environmental Health Perspectives*, vol. 113, no. 7, pp. 823–839, 2005.
- [19] E. R. Weibel, B. Sapoval, and M. Filoche, "Design of peripheral airways for efficient gas exchange," *Respiratory Physiology & Neurobiology*, vol. 148, no. 1–2, pp. 3–21, 2005.
- [20] E. R. Weibel, *Morphometry of the Human Lung*, Springer, New York, NY, USA, 1963.
- [21] K. R. Smith, J. M. Samet, I. Romieu, and N. Bruce, "Indoor air pollution in developing countries and acute lower respiratory infections in children," *Thorax*, vol. 55, no. 6, pp. 518–532, 2000.
- [22] M. A. Reyna-Carranza, A. P. Moreno-Flores, and R. Lopez-Avitia, "Acute respiratory infections and its Spearman correlation with meteorological and air pollutants data from Mexicali, BC, Mexico," in *Proceedings of the Pan American Health Care Exchange (PAHCE '10)*, p. 17, Lima, Peru, March 2010.
- [23] M. Lippmann, K. Ito, A. Nadas, and R. T. Burnett, "Association of particulate matter components with daily mortality and morbidity in urban populations," *Research Report*, no. 95, pp. 5–82, 2000.
- [24] B. Brunekreef and S. T. Holgate, "Air pollution and health," *The Lancet*, vol. 360, no. 9341, pp. 1233–1242, 2002.
- [25] M. Brauer, C. Avila-Casado, T. I. Fortoul, S. Vedal, B. Stevens, and A. Churg, "Air pollution and retained particles in the lung," *Environmental Health Perspectives*, vol. 109, no. 10, pp. 1039–1043, 2001.
- [26] A. Ibaldo-Mulli, H. E. Wichmann, W. Kreyling, and A. Peters, "Epidemiological evidence on health effects of ultrafine particles," *Journal of Aerosol Medicine: Deposition, Clearance, and Effects in the Lung*, vol. 15, no. 2, pp. 189–201, 2002.
- [27] C. A. Pope III, R. T. Burnett, M. J. Thun et al., "Lung cancer, cardiopulmonary mortality, and long-term exposure to fine particulate air pollution," *Journal of the American Medical Association*, vol. 287, no. 9, pp. 1132–1141, 2002.
- [28] R. R. Mercer, A. F. Hubbs, J. F. Scabilloni et al., "Distribution and persistence of pleural penetrations by multi-walled carbon nanotubes," *Particle and Fibre Toxicology*, vol. 7, article 28, 2010.
- [29] N. R. Yacobi, H. C. Phuleria, L. Demaio et al., "Nanoparticle effects on rat alveolar epithelial cell monolayer barrier properties," *Toxicology in Vitro*, vol. 21, no. 8, pp. 1373–1381, 2007.
- [30] G. S. Kang, P. A. Gillespie, A. Gunnison, A. L. Moreira, K.-M. Tchou-Wong, and L.-C. Chen, "Long-term inhalation exposure to nickel nanoparticles exacerbated atherosclerosis in a susceptible mouse model," *Environmental Health Perspectives*, vol. 119, no. 2, pp. 176–181, 2011.
- [31] W. Lin, Y. Xu, C.-C. Huang et al., "Toxicity of nano- and micro-sized ZnO particles in human lung epithelial cells," *Journal of Nanoparticle Research*, vol. 11, no. 1, pp. 25–39, 2009.
- [32] S. Sultana, R. Ali, S. Talegaonkar, F. J. Ahmad, G. Mittal, and A. Bhatnagar, "In vivo lung deposition and sub-acute inhalation toxicity studies of nano-sized alendronate sodium as an antidote for inhaled toxic substances in Sprague Dawley rats," *Environmental Toxicology and Pharmacology*, vol. 36, no. 2, pp. 636–647, 2013.
- [33] L. Wang, L. Wang, W. Ding, and F. Zhang, "Acute toxicity of ferric oxide and zinc oxide nanoparticles in rats," *Journal of Nanoscience and Nanotechnology*, vol. 10, no. 12, pp. 8617–8624, 2010.
- [34] M. Ho, K.-Y. Wu, H.-M. Chein, L.-C. Chen, and T.-J. Cheng, "Pulmonary toxicity of inhaled nanoscale and fine zinc oxide particles: mass and surface area as an exposure metric," *Inhalation Toxicology*, vol. 23, no. 14, pp. 947–956, 2011.
- [35] W.-S. Cho, R. Duffin, S. E. M. Howie et al., "Progressive severe lung injury by zinc oxide nanoparticles; the role of Zn²⁺ dissolution inside lysosomes," *Particle and Fibre Toxicology*, vol. 8, article 27, 2011.
- [36] P. V. Rajsekhar, G. Selvam, A. Goparaju, P. B. Murthy, and P. N. Reddy, "Pulmonary responses of manufactured ultrafine aluminum oxide particles upon repeated exposure by inhalation in rats," *Indian Journal of Forensic Medicine and Toxicology*, vol. 7, no. 1, pp. 147–153, 2013.
- [37] W.-S. Cho, R. Duffin, F. Thielbeer et al., "Zeta potential and solubility to toxic ions as mechanisms of lung inflammation caused by metal/metal oxide nanoparticles," *Toxicological Sciences*, vol. 126, no. 2, pp. 469–477, 2012.
- [38] W.-S. Cho, R. Duffin, C. A. Poland et al., "Metal oxide nanoparticles induce unique inflammatory footprints in the lung: important implications for nanoparticle testing," *Environmental Health Perspectives*, vol. 118, no. 12, pp. 1699–1706, 2010.
- [39] A. Srinivas, P. J. Rao, G. Selvam, A. Goparaju, B. P. Murthy, and N. P. Reddy, "Oxidative stress and inflammatory responses of rat following acute inhalation exposure to iron oxide nanoparticles," *Human & Experimental Toxicology*, vol. 31, no. 11, pp. 1113–1131, 2012.
- [40] J. L. Blum, L. K. Rosenblum, G. Grunig, M. B. Beasley, J. Q. Xiong, and J. T. Zelikoff, "Short-term inhalation of cadmium oxide nanoparticles alters pulmonary dynamics associated with lung injury, inflammation, and repair in a mouse model," *Inhalation Toxicology*, vol. 26, no. 1, pp. 48–58, 2014.
- [41] G. S. Kang, P. A. Gillespie, A. Gunnison, H. Rengifo, J. Koberstein, and L.-C. Chen, "Comparative pulmonary toxicity of inhaled nickel nanoparticles; Role of deposited dose and solubility," *Inhalation Toxicology*, vol. 23, no. 2, pp. 95–103, 2011.
- [42] L. Ma-Hock, V. Strauss, S. Treumann et al., "Comparative inhalation toxicity of multi-wall carbon nanotubes, graphene, graphite nanoplatelets and low surface carbon black," *Particle and Fibre Toxicology*, vol. 10, no. 1, article 23, 2013.
- [43] C. M. Sayes, K. L. Reed, K. P. Glover et al., "Changing the dose metric for inhalation toxicity studies: short-term study in rats with engineered aerosolized amorphous silica nanoparticles," *Inhalation Toxicology*, vol. 22, no. 4, pp. 348–354, 2010.
- [44] M. Lundqvist, J. Stigler, G. Elia, I. Lynch, T. Cedervall, and K. A. Dawson, "Nanoparticle size and surface properties determine the protein corona with possible implications for biological impacts," *Proceedings of the National Academy of Sciences of the United States of America*, vol. 105, no. 38, pp. 14265–14270, 2008.
- [45] D. M. Brown, M. R. Wilson, W. MacNee, V. Stone, and K. Donaldson, "Size-dependent proinflammatory effects of ultrafine polystyrene particles: a role for surface area and oxidative stress in the enhanced activity of ultrafines," *Toxicology and Applied Pharmacology*, vol. 175, no. 3, pp. 191–199, 2001.
- [46] T. Stoeger, C. Reinhard, S. Takenaka et al., "Instillation of six different ultrafine carbon particles indicates a surface area threshold dose for acute lung inflammation in mice," *Environmental Health Perspectives*, vol. 114, no. 3, pp. 328–333, 2006.
- [47] W. McKinney, M. Jackson, T. M. Sager et al., "Pulmonary and cardiovascular responses of rats to inhalation of a commercial

- antimicrobial spray containing titanium dioxide nanoparticles,” *Inhalation Toxicology*, vol. 24, no. 7, pp. 447–457, 2012.
- [48] P. Gehr and J. Heyder, *Particle-Lung Interactions*, Taylor & Francis, London, UK, 2000.
- [49] M. Geiser, “Update on macrophage clearance of inhaled micro- and nanoparticles,” *Journal of Aerosol Medicine and Pulmonary Drug Delivery*, vol. 23, no. 4, pp. 207–217, 2010.
- [50] A. Vander, J. Sherman, and D. Luciano, *Human Physiology: The Mechanisms of Body Function*, McGraw-Hill, New York, NY, USA, 8th edition, 2001.
- [51] J. Löndahl, E. Swietlicki, J. Rissler et al., “Experimental determination of the respiratory tract deposition of diesel combustion particles in patients with chronic obstructive pulmonary disease,” *Particle and Fibre Toxicology*, vol. 9, article 30, 2012.
- [52] N. E. Alexis, J. C. Lay, K. Zeman et al., “Biological material on inhaled coarse fraction particulate matter activates airway phagocytes in vivo in healthy volunteers,” *Journal of Allergy and Clinical Immunology*, vol. 117, no. 6, pp. 1396–1403, 2006.
- [53] L. Geraets, A. G. Oomen, J. D. Schroeter, V. A. Coleman, and F. R. Cassee, “Tissue distribution of inhaled micro- and nano-sized cerium oxide particles in rats: results from a 28-day exposure study,” *Toxicological Sciences*, vol. 127, no. 2, pp. 463–473, 2012.
- [54] J. H. Vincent, A. M. Johnston, A. D. Jones, R. E. Bolton, and J. Addison, “Kinetics of deposition and clearance of inhaled mineral dusts during chronic exposure,” *British Journal of Industrial Medicine*, vol. 42, no. 10, pp. 707–715, 1985.
- [55] G. Oberdorster, J. Ferin, and B. E. Lehnert, “Correlation between particle size, in vivo particle persistence, and lung injury,” *Environmental Health Perspectives*, vol. 102, no. 5, pp. 173–179, 1994.
- [56] K. Ogino, R. Zhang, H. Takahashi et al., “Allergic airway inflammation by nasal inoculation of particulate matter (PM_{2.5}) in NC/Nga mice,” *PLoS ONE*, vol. 9, no. 3, Article ID e92710, 2014.
- [57] A. Churg and M. Brauer, “Human lung parenchyma retains PM_{2.5},” *American Journal of Respiratory and Critical Care Medicine*, vol. 155, no. 6, pp. 2109–2111, 1997.
- [58] B. S. Cohen, R. G. Sussman, and M. Lippmann, “Ultrafine particle deposition in a human tracheobronchial cast,” *Aerosol Science and Technology*, vol. 12, no. 4, pp. 1082–1091, 1990.
- [59] D. L. Swift, N. Montassier, P. K. Hopke, K. Karpen-Hayes, Y.-S. Cheng, and J. C. Strong, “Inspiratory deposition of ultrafine particles in human nasal replicate cast,” *Journal of Aerosol Science*, vol. 23, no. 1, pp. 65–72, 1992.
- [60] J. L. Gurman, M. Lippmann, and R. B. Schlesinger, “Particle deposition in replicate casts of the human upper tracheobronchial tree under constant and cyclic inspiratory flow. I. Experimental,” *Aerosol Science and Technology*, vol. 3, no. 3, pp. 245–252, 1984.
- [61] B. S. Cohen and B. Asgharian, “Deposition of ultrafine particles in the upper airways: an empirical analysis,” *Journal of Aerosol Science*, vol. 21, no. 6, pp. 789–797, 1990.
- [62] Y.-S. Cheng, Y. Zhou, and B. T. Chen, “Particle deposition in a cast of human oral airways,” *Aerosol Science and Technology*, vol. 31, no. 4, pp. 286–300, 1999.
- [63] E. Fröhlich and S. Salar-Behzadi, “Toxicological assessment of inhaled nanoparticles: role of in vivo, ex vivo, in vitro, and in Silico Studies,” *International Journal of Molecular Sciences*, vol. 15, no. 3, pp. 4795–4822, 2014.
- [64] C. M. Sayes, K. L. Reed, and D. B. Warheit, “Assessing toxicology of fine and nanoparticles: comparing in vitro measurements to in vivo pulmonary toxicity profiles,” *Toxicological Sciences*, vol. 97, no. 1, pp. 163–180, 2007.
- [65] S. S. Park and A. S. Wexler, “Particle deposition in the pulmonary region of the human lung: a semi-empirical model of single breath transport and deposition,” *Journal of Aerosol Science*, vol. 38, no. 2, pp. 228–245, 2007.
- [66] A. R. Martin and W. H. Finlay, “A general, algebraic equation for predicting total respiratory tract deposition of micrometer-sized aerosol particles in humans,” *Journal of Aerosol Science*, vol. 38, no. 2, pp. 246–253, 2007.
- [67] W. Koch and W. Stöber, “A simple pulmonary retention model accounting for dissolution and macrophage-mediated removal of deposited polydisperse particles,” *Inhalation Toxicology*, vol. 13, no. 2, pp. 129–148, 2001.
- [68] S. S. Park and A. S. Wexler, “Size-dependent deposition of particles in the human lung at steady-state breathing,” *Journal of Aerosol Science*, vol. 39, no. 3, pp. 266–276, 2008.
- [69] C. Kleinstreuer, Z. Zhang, and Z. Li, “Modeling airflow and particle transport/deposition in pulmonary airways,” *Respiratory Physiology and Neurobiology*, vol. 163, no. 1–3, pp. 128–138, 2008.
- [70] Z. Zhang and C. Kleinstreuer, “Species heat and mass transfer in a human upper airway model,” *International Journal of Heat and Mass Transfer*, vol. 46, no. 25, pp. 4755–4768, 2003.
- [71] C. Kleinstreuer, Z. Zhang, and C. S. Kim, “Combined inertial and gravitational deposition of microparticles in small model airways of a human respiratory system,” *Journal of Aerosol Science*, vol. 38, no. 10, pp. 1047–1061, 2007.
- [72] Z. Zhang, C. Kleinstreuer, and C. S. Kim, “Comparison of analytical and CFD models with regard to micron particle deposition in a human 16-generation tracheobronchial airway model,” *Journal of Aerosol Science*, vol. 40, no. 1, pp. 16–28, 2009.
- [73] C. Kleinstreuer and Z. Zhang, “Laminar-to-turbulent fluid-particle flows in a human airway model,” *International Journal of Multiphase Flow*, vol. 29, no. 2, pp. 271–289, 2003.
- [74] Z. Zhang, C. Kleinstreuer, J. F. Donohue, and C. S. Kim, “Comparison of micro- and nano-size particle depositions in a human upper airway model,” *Journal of Aerosol Science*, vol. 36, no. 2, pp. 211–233, 2005.
- [75] J. Xi, X. Si, J. W. Kim, and A. Berlinski, “Simulation of airflow and aerosol deposition in the nasal cavity of a 5-year-old child,” *Journal of Aerosol Science*, vol. 42, no. 3, pp. 156–173, 2011.
- [76] Z. Li, C. Kleinstreuer, and Z. Zhang, “Simulation of airflow fields and microparticle deposition in realistic human lung airway models. Part I: airflow patterns,” *European Journal of Mechanics, B/Fluids*, vol. 26, no. 5, pp. 632–649, 2007.
- [77] Z. Li, C. Kleinstreuer, and Z. Zhang, “Simulation of airflow fields and microparticle deposition in realistic human lung airway models. Part II: particle transport and deposition,” *European Journal of Mechanics, B/Fluids*, vol. 26, no. 5, pp. 650–668, 2007.
- [78] Z. Li, C. Kleinstreuer, and Z. Zhang, “Particle deposition in the human tracheobronchial airways due to transient inspiratory flow patterns,” *Journal of Aerosol Science*, vol. 38, no. 6, pp. 625–644, 2007.
- [79] I. Balásházy, T. Heistracher, and W. Hofmann, “Deposition enhancement factors for inhaled radon decay products in bronchial airway bifurcations,” *Journal of Aerosol Science*, vol. 28, supplement 1, pp. S597–S598, 1997.
- [80] P. Farhadi Ghalati, E. Keshavarzian, O. Abouali, A. Faramarzi, J. Tu, and A. Shakibafard, “Numerical analysis of micro- and nano-particle deposition in a realistic human upper airway,” *Computers in Biology and Medicine*, vol. 42, no. 1, pp. 39–49, 2012.

- [81] T. C. Carvalho, J. I. Peters, and R. O. Williams III, "Influence of particle size on regional lung deposition—what evidence is there?" *International Journal of Pharmaceutics*, vol. 406, no. 1-2, pp. 1–10, 2011.
- [82] P. W. Longest and L. T. Holbrook, "In silico models of aerosol delivery to the respiratory tract—development and applications," *Advanced Drug Delivery Reviews*, vol. 64, no. 4, pp. 296–311, 2012.
- [83] K.-H. Cheng, Y.-S. Cheng, H.-C. Yeh, and D. L. Swift, "An experimental method for measuring aerosol deposition efficiency in the human oral airway," *American Industrial Hygiene Association Journal*, vol. 58, no. 3, pp. 207–213, 1997.
- [84] J. Löndahl, W. Möller, J. H. Pagels, W. G. Kreyling, E. Swietlicki, and O. Schmid, "Measurement techniques for respiratory tract deposition of airborne nanoparticles: a critical review," *Journal of Aerosol Medicine and Pulmonary Drug Delivery*, vol. 27, no. 4, pp. 229–254, 2014.
- [85] W. Li, J. Q. Xiong, and B. S. Cohen, "The deposition of unattached radon progeny in a tracheobronchial cast as measured with iodine vector," *Aerosol Science and Technology*, vol. 28, no. 6, pp. 502–510, 1998.
- [86] E. Keshavarzian, P. F. Ghalati, O. Abouali, G. Ahmadi, and M. H. Bagheri, "Micro/Nano-particle deposition in the airway of a 6-year-old child from nostril to the third generation," in *Proceedings of the Asme Fluids Engineering Division Summer Meeting*, vol. 1 of *Symposia, Parts A and B*, pp. 831–837, American Society of Mechanical Engineer, Rio Grande, Puerto Rico, USA, 2012.
- [87] P. A. Jaques and C. S. Kim, "Measurement of total lung deposition of inhaled ultrafine particles in healthy men and women," *Inhalation Toxicology*, vol. 12, no. 8, pp. 715–731, 2000.
- [88] J. S. Brown, K. L. Zeman, and W. D. Bennett, "Ultrafine particle deposition and clearance in the healthy and obstructed lung," *The American Journal of Respiratory and Critical Care Medicine*, vol. 166, no. 9, pp. 1240–1247, 2002.
- [89] C. C. Daigle, D. C. Chalupa, F. R. Gibb et al., "Ultrafine particle deposition in humans during rest and exercise," *Inhalation Toxicology*, vol. 15, no. 6, pp. 539–552, 2003.
- [90] J. Xi, P. W. Longest, and T. B. Martonen, "Effects of the laryngeal jet on nano- and microparticle transport and deposition in an approximate model of the upper tracheobronchial airways," *Journal of Applied Physiology*, vol. 104, no. 6, pp. 1761–1777, 2008.
- [91] K.-H. Cheng, Y.-S. Cheng, H.-C. Yen, and D. L. Swift, "Measurements of airway dimensions and calculation of mass transfer characteristics of the human oral passage," *Journal of Biomechanical Engineering*, vol. 119, no. 4, pp. 476–482, 1997.
- [92] B. Grgic, W. H. Finlay, and A. F. Heenan, "Regional aerosol deposition and flow measurements in an idealized mouth and throat," *Journal of Aerosol Science*, vol. 35, no. 1, pp. 21–32, 2004.
- [93] J. Xi and P. W. Longest, "Transport and deposition of micro-aerosols in realistic and simplified models of the oral airway," *Annals of Biomedical Engineering*, vol. 35, no. 4, pp. 560–581, 2007.
- [94] F. Rengier, A. Mehndiratta, H. von Tengg-Kobligk et al., "3D printing based on imaging data: review of medical applications," *International Journal of Computer Assisted Radiology and Surgery*, vol. 5, no. 4, pp. 335–341, 2010.
- [95] H. Chrystyn, "Methods to identify drug deposition in the lungs following inhalation," *British Journal of Clinical Pharmacology*, vol. 51, no. 4, pp. 289–299, 2001.
- [96] D. Yi, A. Price, A. Panoskaltsis-Mortari, A. Naqwi, and T. S. Wiedmann, "Measurement of the distribution of aerosols among mouse lobes by fluorescent imaging," *Analytical Biochemistry*, vol. 403, no. 1-2, pp. 88–93, 2010.
- [97] S. Eberl, H.-K. Chan, and E. Daviskas, "SPECT imaging for radioaerosol deposition and clearance studies," *Journal of Aerosol Medicine: Deposition, Clearance, and Effects in the Lung*, vol. 19, no. 1, pp. 8–20, 2006.
- [98] M. S. Berridge, Z. Lee, and D. L. Heald, "Pulmonary distribution and kinetics of inhaled [¹¹C]triamcinolone acetone," *Journal of Nuclear Medicine*, vol. 41, no. 10, pp. 1603–1611, 2000.
- [99] M. M. Bailey and C. J. Berkland, "Nanoparticle formulations in pulmonary drug delivery," *Medicinal Research Reviews*, vol. 29, no. 1, pp. 196–212, 2009.
- [100] P. A. Schulte, V. Murashov, R. Zumwalde, E. D. Kuempel, and C. L. Geraci, "Occupational exposure limits for nanomaterials: state of the art," *Journal of Nanoparticle Research*, vol. 12, no. 6, pp. 1971–1987, 2010.

Research Article

Clinical Effects of Novel Nanoscaled Core Decompression Rods Combined with Umbilical Cord Mesenchymal Stem Cells on the Treatment of Early Osteonecrosis of the Femoral Head

Hongyang Gao,¹ Guoping Zhang,¹ Jian Wang,¹ Feng Zhao,¹ Yuchen Zhang,¹ Wei Wang,¹ and Yang You²

¹Department of Orthopedics, The First Hospital of Hebei Medical University, Shijiazhuang 050031, China

²Department of Cardiovasculology III, The First Hospital of Hebei Medical University, Shijiazhuang 050031, China

Correspondence should be addressed to Yang You; ghy0618@yahoo.com.cn

Received 11 December 2014; Accepted 29 January 2015

Academic Editor: Shuming Zhang

Copyright © 2015 Hongyang Gao et al. This is an open access article distributed under the Creative Commons Attribution License, which permits unrestricted use, distribution, and reproduction in any medium, provided the original work is properly cited.

Osteonecrosis of the femoral head (ONFH) is one of the most common diseases in orthopedics. In this study, we investigated the clinical effects of novel nanoscaled core decompression rods combined with mesenchymal stem cells on the treatment of the ONFH. 12 adult patients with early ONFH (at the stage of Ficat II) received the treatment using the implantation of novel nanoscaled core decompression rods combined with umbilical cord mesenchymal stem cells. The grade of the patients' hip was scored by Harris marking system before and after the surgery, and then paired *t*-test was done. We assessed the curative efficiency based on the change of the patients before and after the surgery. In particular, the survival rate of femoral head was assessed at 12 months after the surgery. The results demonstrated that according to the standard of Harris Scoring, the average grade of hip joint before the surgery was 54.16 ± 4.23 points while average grade of hip joint at 12 months after the surgery was 85.28 ± 3.65 points. So, the implantation of the novel nanoscaled core decompression rods combined with mesenchymal stem cells had satisfactory clinical effects, suggesting that this implantation should be effective to treat early ONFH.

1. Introduction

Osteonecrosis of the femoral head (ONFH), which is caused by the interruption of blood supply [1], is one of the most common diseases in orthopedics [2], with an average age of occurrence accounts to be 38 years old, and highest incidence rates for young people. At present, total hip replacement is commonly used in the treatment of patients suffering from ONFH [3]. However, it has been reported that prosthetic replacement in young patients with ONFH has a poor durability [4]. Generally speaking, core decompression (CD), electrical stimulation, and vascularized bone grafting are the three most commonly used method for the treatment of early stage ONFH [5, 6]. According to the previous report, surgical core decompression has an excellent treatment effect on the osteonecrosis of hip and knee [7–13]. Core decompression

(CD) is employed in wide treatment of hip osteonecrosis in its early stages (before mechanical failure has occurred) [10, 14–17]. Owing to the incomplete reconstruction necrotic area by core decompression, the effect of core decompression is not always satisfactory [18]. Moreover, the deficiency of osteoprogenitor cells of the osteonecrotic hip also restricts its implication [19–21]. Owing to the incomplete reconstruction necrotic area by core decompression, its efficacy still remains to be controversial [10]. It has been reported that if the ONFH cannot be treated effectively and actively, the majority of patients' femoral head will collapse in 2–3 years [22, 23]. Ideal therapeutic procedure should include (1) cleaning the bone lesions as far as possible and (2) implant possessing adequate biological activity and mechanical supporting to avoid early collapse of the femoral head. Recently, bone marrow mesenchymal stem cells (BMSCs) have attracted great attention

[24–28]. Due to their ability to differentiate into multiple cell lineages including osteoprogenitor cells, a successful use of BMSC after making a single drill hole into the avascular area in patients who has atraumatic osteonecrosis has been reported [25–32].

In this work, we used the implantation of a novel nanoscaled core decompression rod combined with umbilical cord mesenchymal stem cells to cure 12 cases of early ONFH, with complete follow-up for all of them. Their period of follow-up was more than 12 months. The aim of the present study is to investigate the clinical effects of implantation with the novel nanoscaled core decompression rod combined with umbilical cord mesenchymal stem cells on the treatment of early ONFH.

2. Experimental Materials and Methods

2.1. Materials. The supporting material used in this study was porous nanoscaled core decompression bar from Guona Technology Co. Ltd in Sichuan. The cell therapy center in the first hospital of Hebei Medical University provided the stem cells required for the treatment. Under the situation of acquiring the consent of delivery woman and approval of the ethics committee, we got the umbilical cord mesenchymal stem cells from healthy pregnant women after caesarean in the Department of Obstetrics and Gynecology, the First Affiliated Hospital of Hebei Medical University.

2.2. Surgical Method. The patient lies on the hospital bed, and we anaesthetized patients using the injection of spinal canal. The channel of core decompression was determined under the guide of C-armed fluoroscopy. A 5 cm incision was obtained in the lateral femoral, making the lateral cortical bone exposed. Meanwhile, the hip at internal rotation of 15° was kept and the guide pin in the perspective along the direction of femoral neck was inserted. The far-end of guide needle reached the center of osteonecrosis of the femoral head, the length of nail was measured using depth gauge, and the dead tissue was removed by using rotary cutter after the reaming of hollow drill (with a diameter of 12 mm), and the taping treatment of the near-end of the pressure relief channel was conducted using tap. Fresh autogenous cancellous bone was collected from intertrochanteric region in the course of decompression process, mixed fresh autogenous cancellous bone, and prepared allogeneic mesenchymal stem cell suspension (5 mL) fully for later use. Nanoscaled core decompression rod was screwed in using a controller, and the tail of decompression rod was embedded in bone cortex slightly. Then, the rest of 5 mL cell suspension was injected into the hollow channel of the decompression rod. Finally, the hollow channel was sealed using gelatin sponge and bone wax in order to minimize the loss of the cells.

2.3. Treatment after the Surgery. The exercises of the patients after anesthesia recovery were guided by researchers. We encouraged patients to expand hip joint and make active flexion and extension and functional exercises. Moreover, there was no restriction on the movement of patients' hip

joint under the condition of nonweight bearing. Patients' hip joint was forbidden to load in 2 months after surgery. Some loading could be imposed on the patients' hip joint 3 months after surgery.

2.4. Observation and the Evaluation Standard. The observation was carried out 1, 2, 3, 6, and 12 months after the surgery, respectively. In order to check whether the supporting material had the sign of loosening or not and the improvement of radiological staging of the ONFH, the picture of front and frog leg position of pelvis was taken. The change of pain and the range of movement of patients' hip were recorded before and after the surgery and the grade of patients' hip was scored using Harris marking system. The evaluation standard of the treatment was collapse of the femoral head or final hip replacement.

2.5. Statistical Analysis. Paired *t*-test was conducted on the Harris score of patients' hip before and after the surgery using statistical software SPSS17.0. $P < 0.05$ indicated that there was a statistical difference.

3. Results

According to the standard of Harris Scoring, the average grade of hip joint before surgery was 54.16 ± 4.23 points while average grade of hip joint 12 months' follow-up after surgery was 85.28 ± 3.65 points. So the Harris Scoring raised distinctly ($P < 0.05$). On the basis of Harris Scoring, points from 91 to 100 was excellent level, points from 81 to 90 was relatively excellent level, points from 71 to 80 was good level, less than 70 points was bad level, and the excellent and good rate of points in this group was up to 92.2%.

According to the international osteonecrosis staging criteria of World Bone Circulation Research Association, we made a radiological evaluation on our results. With the obvious collapse of osteonecrosis of the femoral head or final joint replacement as the end point of study, the abscission had never occurred to all the 12 samples in this group over 12 months after surgery. Obvious collapse did not happen to any 12 cases; the survival rate of the femoral head was up to 100% in terms of 12 samples (patients' hip) 12 months after surgery. Of all the 8 patients whose follow-up periods exceed 12 months, the progress of the disease was discovered in only one case in 18 months after surgery, showing the phenomenon of collapse of femoral head, and dynamic observation was temporarily stopped without any other special treatment.

A typical case of patients' hip was analyzed. The patient was male (31 years old). The patients' left hip suffered from pain without any induction factor and his activity was restricted for 1 year. The patient came to see the doctor after his condition worsened for 3 months. The X-ray and CT pictures of patients' hip indicated that it indeed occurred to the left femoral head osteonecrosis (at the stage of Ficat II) (Figures 1 and 2). Moreover, no obvious osteonecrosis and collapse of femoral head happened after continuous follow-up of 12 months (Figure 3).

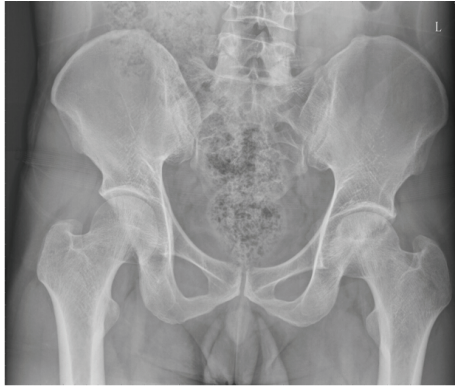


FIGURE 1: X-ray picture of normal position of pelvis (before surgery).

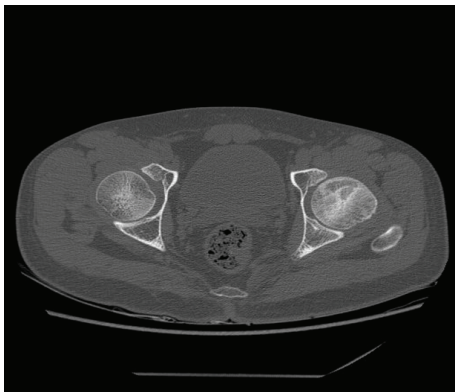


FIGURE 2: CT picture of normal position of pelvis (before surgery).

4. Discussion

4.1. The Application of Umbilical Cord Mesenchymal Stem Cells in the Treatment of ONFH. The technology of core decompression for femoral marrow could reduce the internal pressure in the femoral head, thus removing the sclerotic band, creating the new collateral circulations, relieving the pain of the hip joint, and, moreover, completing the repair of femoral head in the end. As with early osteonecrosis of the femoral head, core decompression has been widely recognized as a highly effective manner in surgical intervention. However, throughout all the earlier achievements, some clinical efficacy has been identified in the joint-preserving cure of early osteonecrosis of the femoral head after decades of constant efforts. The of joint-preserving treatment still has obvious limitations, such as poor treatment effect and low efficiency (only 60%–80% in case of short and mid-term treatment) for the majority of patients [33]. Through the analysis of the causes, the potential interpretation was that a simple core decompression may not thoroughly solve the problem of rising of bone marrow pressure [34]. It has been proved that stem cells owned multiple differentiation potential and could differentiate into other cells in certain direction under the action of specific cytokines, thus making a difference in the repair of damaged tissue. The application of stem cells provided an entirely new thought to

the joint-preserving treatment of early osteonecrosis of the femoral head. At present, transplantation of bone marrow mesenchymal stem cells which combined femoral marrow core decompression has been widely used in joint-preserving treatment of osteonecrosis of the femoral head [35]. Umbilical cord mesenchymal stem cells had the same biological characteristics as bone marrow mesenchymal stem cells and possessed the capability of totipotent differentiation potential in all directions; almost all tissue cells of human body could be differentiated from umbilical cord mesenchymal stem cells. It has been demonstrated that umbilical cord mesenchymal stem cells have excellent osteogenic ability, which is very useful to repair the large segmental bone defect [36]. What is more, umbilical cord mesenchymal stem cells could improve the local blood supply of osteonecrosis of the femoral head and initial effect in the treatment of early osteonecrosis of the femoral head [37]. In this study, umbilical cord mesenchymal stem cells were used as the seed cells in the reconstruction of the femoral head. On one hand, the strong differentiation and proliferation ability of umbilical cord mesenchymal stem cells could improve the bone microcirculation, promote the regeneration of vascular endothelial cells, and ameliorate venous reflux in lesions. On the other hand, intraosseous pressure will be decreased, and the blood supply of the femoral head will be restored and improved, creating favorable environment for newly born bone. In contrast to mesenchymal stem cells derived from bone marrow, the application of umbilical cord mesenchymal stem cells did not involve argument in ethical, social, legal, and other aspects; moreover, the source of umbilical cord mesenchymal stem cells is sufficient, the separation of cells is simple, and the cell viability of cells is powerful. Finally, in addition to lower probability of infectious diseases, umbilical cord mesenchymal stem cells are easier to amplification in vitro; all advantages mentioned above make them perfect for the clinical applications as seed cells.

4.2. The Selection of Supports after Core Decompression of ONFH. Experts and scholars from home and abroad hold the common view that an implant was needed for providing the mechanical support in the area of bone defect to avoid or delay the collapse of femoral head. Moreover, an ideal support should meet at least two key criteria: (1) biological factors, namely, good bone-induced and bone conduction activity are necessary for supports, and bone defect caused by the removal of the necrotic bone residue could be repaired by the implantation of the implant; moreover, the implant should offer the necessary mechanical support for bone formation; (2) biomechanical factors, the implant should provide some mechanical support for femoral head to avoid or delay the collapse of the articular surface of the femoral head [38]. On the basis of these two points, supports commonly used are impaction bone grafting with simple bone tunnel, vascular bone transplantation, implantation of tantalum rod, and so on. The pure impaction bone grafting has been proved to be failed to provide sufficient mechanical support for the cartilage of femoral head. Although vascularized bone grafts could improve local blood supply and promote

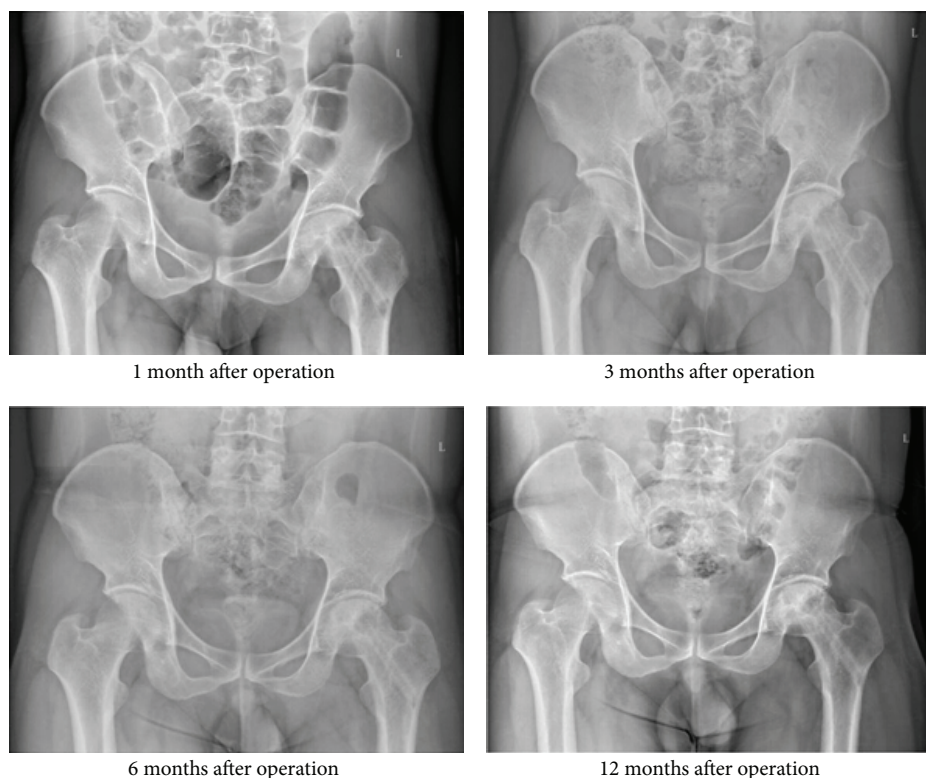


FIGURE 3: X-ray picture of normal position of pelvis at the 1th, 3rd, 6th, and 12th month after surgery.

the formation of new bone, the length of vascular pedicle restricted the movement of hip joint undoubtedly, giving rise to inevitable influence on the recovery of patients' hip after surgery. More importantly, vascularized bone grafts had higher requirements on the microsurgical technique and other disadvantages, such as the difficulty of surgery in the operation and relatively large trauma, limiting their clinical application.

In this study, we selected porous nanocore decompression rod as supporting material, with core decompression rod designed by Guona Technology Co. Ltd, Sichuan. The main components of supporting material are nanohydroxyapatite/polyamide 66 (nano-HA/PA66). Due to the good compatibility and biological activity of nano-HA/PA66, it has gained an excellent effect as a new type of bone substitute material [39–42]. In comparison with other supporting materials, the molecular and structural characteristics of nano-HA/PA66 not only ensured its good mechanical supporting capability, but also provided incomparable biological activity and bone conduction, which is the biggest advantage of novel nanocore decompression rod [43, 44]. Additionally, the unique design of hollow and porous nanocore decompression rod allows autogenous bone particles to fill in the hollow cavity, favoring the fusion of implant and the bone. Multiporosity of periporium could also increase the environmental channel for bone graft, creating excellent microenvironment for the growth of new bone.

4.3. The Application of Novel Nanocomposites Combined with Mesenchymal Stem Cells in the Treatment of ONFH. Seed cells

and bone scaffold materials are the two major elements of bone tissue engineering. In recent years, some researchers have attempted to form tantalum bars composites containing mesenchymal stem cells to promote the neovascularization of materials [45]. Compared with tantalum metal phase, nano-HA/PA66, as a nonmetal biomimetic material, possesses pore structure mimicking the structure and morphology of natural cancellous bone. The dual culture of external mesenchymal stem cells and nano-HA/PA66 showed that the cell proliferation and cell biological characteristics of mesenchymal stem cells cultured on the nano-HA/PA66 materials are similar to that of mesenchymal stem cells cultured alone, indicating that nano-HA/PA66 materials are beneficial to the growth, bone adhesion, and differentiation of mesenchymal stem cells [46]. More importantly, by means of promoting the formation of new vessels, accelerating the bone transformation, preventing chondrocytes' apoptosis, and finally serving the purpose of promoting the bone repair, the addition of mesenchymal stem cells into nano-HA/PA66 composites has an extremely important significance in treating early revascularization [47–50].

5. Conclusions

In our study, on the basis of core decompression, we organically combined two main elements in bone tissue engineering, cells (umbilical cord mesenchymal stem cells) and scaffolds (nanoscaled core decompression rods), to treat the early osteonecrosis of the femoral head. According to the standard of Harris Scoring, the average grade of hip joint

before surgery was 54.16 ± 4.23 points while average grade of hip joint 12 months' follow-up after surgery was 85.28 ± 3.65 points. The clinical effect was significant, suggesting that this implantation is effective to treat early osteonecrosis of the femoral head.

Conflict of Interests

The authors have no conflict of interests.

Authors' Contribution

Hongyang Gao and Guoping Zhang contributed equally to this work.

References

- [1] Y. Assouline-Dayana, C. Chang, A. Greenspan, Y. Shoenfeld, and M. E. Gershwin, "Pathogenesis and natural history of osteonecrosis," *Seminars in Arthritis and Rheumatism*, vol. 32, no. 2, pp. 94–124, 2002.
- [2] M. A. Mont, L. C. Jones, S. David et al., "Nontraumatic osteonecrosis of the femoral head: ten years later," *The Journal of Bone and Joint Surgery. American Volume*, vol. 88, pp. 1117–1132, 2006.
- [3] K. L. Lee, G. A. Ngai, S. C. Varghese, L. Duan, and J. A. Cooper, "Nanostructures for ligament and tendon regeneration," *Journal of Biomaterials and Tissue Engineering*, vol. 3, no. 4, pp. 409–425, 2013.
- [4] X. M. Li, Y. Yang, Y. B. Fan, Q. L. Feng, F.-Z. Cui, and F. Watari, "Biocomposites reinforced by fibers or tubes as scaffolds for tissue engineering or regenerative medicine," *Journal of Biomedical Materials Research Part A*, vol. 102, no. 5, pp. 1580–1594, 2014.
- [5] F. A. Petrigliano and J. R. Lieberman, "Osteonecrosis of the hip: novel approaches to evaluation and treatment," *Clinical Orthopaedics and Related Research*, no. 465, pp. 53–62, 2007.
- [6] M. A. Mont, L. C. Jones, and D. S. Hungerford, "Nontraumatic osteonecrosis of the femoral head: ten years later," *The Journal of Bone & Joint Surgery—American Volume*, vol. 88, no. 5, pp. 1117–1132, 2006.
- [7] F. P. Castro Jr. and R. L. Barrack, "Core decompression and conservative treatment for avascular necrosis of the femoral head: a meta-analysis," *American Journal of Orthopaedics*, vol. 29, no. 3, pp. 187–194, 2000.
- [8] C. G. Zalavras and J. R. Lieberman, "Osteonecrosis of the femoral head: evaluation and treatment," *Journal of the American Academy of Orthopaedic Surgeons*, vol. 22, no. 7, pp. 455–464, 2014.
- [9] M. A. Mont, P. S. Ragland, and G. Etienne, "Core decompression of the femoral head for osteonecrosis using percutaneous multiple small-diameter drilling," *Clinical Orthopaedics and Related Research*, no. 429, pp. 131–138, 2004.
- [10] J. R. Lieberman, "Core decompression for osteonecrosis of the hip," *Clinical Orthopaedics and Related Research*, no. 418, pp. 29–33, 2004.
- [11] F. Specchiulli, "Core decompression in the treatment of necrosis of the femoral head. Long-term results," *La Chirurgia Degli Organi di Movimento*, vol. 85, no. 4, pp. 395–402, 2000.
- [12] S. Patel, "Primary bone marrow oedema syndromes," *Rheumatology*, vol. 53, no. 5, Article ID ket324, pp. 785–792, 2014.
- [13] M. A. Mont, L. C. Schon, M. W. Hungerford, and D. S. Hungerford, "Avascular necrosis of the talus treated by core decompression," *The Journal of Bone and Joint Surgery Series B*, vol. 78, no. 5, pp. 827–830, 1996.
- [14] A. J. Marti-Carvajal, I. Sola, and L. H. Agreda-Perez, "Treatment for avascular necrosis of bone in people with sickle cell disease," *Cochrane Database of Systematic Reviews*, vol. 7, Article ID CD004344, 2014.
- [15] N. F. SooHoo, S. Vyas, J. Manunga, H. Sharifi, G. Kominski, and J. R. Lieberman, "Cost-effectiveness analysis of core decompression," *The Journal of Arthroplasty*, vol. 21, no. 5, pp. 670–681, 2006.
- [16] X. Li, Y. Huang, L. Zheng et al., "Effect of substrate stiffness on the functions of rat bone marrow and adipose tissue derived mesenchymal stem cells *in vitro*," *Journal of Biomedical Materials Research Part A*, vol. 102, no. 4, pp. 1092–1101, 2014.
- [17] D. S. Hungerford, "Treatment of osteonecrosis of the femoral head. Everything's new," *The Journal of Arthroplasty*, vol. 22, no. 4, pp. 91–94, 2007.
- [18] X. Liu, X. Li, Y. Fan et al., "Repairing goat tibia segmental bone defect using scaffold cultured with mesenchymal stem cells," *Journal of Biomedical Materials Research Part B: Applied Biomaterials*, vol. 94, no. 1, pp. 44–52, 2010.
- [19] P. Hernigou, A. Poignard, O. Manicom, G. Mathieu, and H. Rourd, "The use of percutaneous autologous bone marrow transplantation in nonunion and avascular necrosis of bone," *The Journal of Bone and Joint Surgery Series B*, vol. 87, no. 7, pp. 896–902, 2005.
- [20] P. Hernigou, F. Beaujean, and J. C. Lambotte, "Decrease in the mesenchymal stem-cell pool in the proximal femur in corticosteroid-induced osteonecrosis," *The Journal of Bone and Joint Surgery Series B*, vol. 81, no. 2, pp. 349–355, 1999.
- [21] C. Nelson, A. Magge, T. S. Bernard, Y. Khan, and C. T. Laurencin, "Nanostructured composites for bone repair," *Journal of Biomaterials and Tissue Engineering*, vol. 3, no. 4, pp. 426–439, 2013.
- [22] C. C. Chen, C. L. Lin, W. C. Chen, H. N. Shih, S. W. Ueng, and M. S. Lee, "Vascularized iliac bone-grafting for osteonecrosis with segmental collapse of the femoral head," *Journal of Bone and Joint Surgery*, vol. 91, no. 10, pp. 2390–2394, 2009.
- [23] A. I. Stavrakis, N. F. SooHoo, and J. R. Lieberman, "A comparison of the incidence of complications following total hip arthroplasty in patients with or without osteonecrosis," *The Journal of Arthroplasty*, vol. 30, no. 1, pp. 114–117, 2015.
- [24] X. Li, H. Liu, X. Niu et al., "The use of carbon nanotubes to induce osteogenic differentiation of human adipose-derived MSCs *in vitro* and ectopic bone formation *in vivo*," *Biomaterials*, vol. 33, no. 19, pp. 4818–4827, 2012.
- [25] G. C. Daltro, V. A. Fortuna, M. A. S. de Araújo, P. I. F. Lessa, U. D. A. B. Sobrinho, and R. Borojevic, "Femoral head necrosis treatment with autologous stem cells in sickle cell disease," *Acta Ortopedica Brasileira*, vol. 16, no. 1, pp. 23–27, 2008.
- [26] X. Li, H. Liu, X. Niu et al., "Osteogenic differentiation of human adipose-derived stem cells induced by osteoinductive calcium phosphate ceramics," *Journal of Biomedical Materials Research Part B: Applied Biomaterials*, vol. 97, no. 1, pp. 10–19, 2011.
- [27] P. Hernigou, "Autologous bone marrow grafting of avascular osteonecrosis before collapse," *Revue du Rhumatisme*, vol. 62, pp. 650–651, 1995.
- [28] P. Hernigou, "Growth factors released from bone marrow are promising tools in orthopedic surgery," *Revue du Rhumatisme*, vol. 65, no. 2, pp. 79–84, 1998.

- [29] P. Hernigou and F. Beaujean, "Treatment of osteonecrosis with autologous bone marrow grafting," *Clinical Orthopaedics and Related Research*, no. 405, pp. 14–23, 2002.
- [30] Z. Q. Yan, Y. S. Chen, W. J. Li et al., "Treatment of osteonecrosis of the femoral head by percutaneous decompression and autologous bone marrow mononuclear cell infusion," *Chinese Journal of Traumatology*, vol. 9, no. 1, pp. 3–7, 2006.
- [31] V. Gangji, J.-P. Hauzeur, C. Matos, V. de Maertelaer, M. Toungouz, and M. Lambermont, "Treatment of osteonecrosis of the femoral head with implantation of autologous bone-marrow cells: a pilot study," *The Journal of Bone and Joint Surgery Series A*, vol. 86, no. 6, pp. 1153–1160, 2004.
- [32] A. M. Cortizo, G. Ruderman, G. Correa, I. G. Mogilner, and E. J. Tolosa, "Effect of surface topography of collagen scaffolds on cytotoxicity and osteoblast differentiation," *Journal of Biomaterials and Tissue Engineering*, vol. 2, no. 2, pp. 125–132, 2012.
- [33] M. A. Mont, L. C. Jones, and D. S. Hungerford, "Nontraumatic osteonecrosis of the femoral head: ten years later," *The Journal of Bone and Joint Surgery—American Volume*, vol. 88, pp. 1117–1132, 2006.
- [34] X. Li, H. Gao, M. Uo et al., "Effect of carbon nanotubes on cellular functions *in vitro*," *Journal of Biomedical Materials Research Part A*, vol. 91, no. 1, pp. 132–139, 2009.
- [35] Z. Li, W. Liao, Q. Zhao et al., "Angiogenesis and bone regeneration by allogeneic mesenchymal stem cell intravenous transplantation in rabbit model of avascular necrotic femoral head," *Journal of Surgical Research*, vol. 183, no. 1, pp. 193–203, 2013.
- [36] M. Cuervas-Mons, J. Narbona, R. Laguna, and J. Vaquero, "Autologous concentrated bone marrow graft in the treatment of femoral head avascular necrosis: clinical outcome after two years of follow up in a non-controlled prospective study," *Revista Española de Cirugía Ortopédica y Traumatología*, vol. 57, no. 2, pp. 106–110, 2013.
- [37] G. E. Garrigues, J. M. Aldridge III, J. K. Friend, and J. R. Urbaniak, "Free vascularized fibular grafting for treatment of osteonecrosis of the femoral head secondary to hip dislocation," *Microsurgery*, vol. 29, no. 5, pp. 342–345, 2009.
- [38] J. K. Koper and J. Jakubowicz, "Correlation of wettability with surface structure and morphology of the anodically oxidized titanium implants," *Journal of Biomaterials and Tissue Engineering*, vol. 4, no. 6, pp. 459–464, 2014.
- [39] A. Palmquist, H. Engqvist, J. Lausmaa, and P. Thomsen, "Commercially available dental implants: review of their surface characteristics," *Journal of Biomaterials and Tissue Engineering*, vol. 2, no. 2, pp. 112–124, 2012.
- [40] L. I. Castelan-Velazco, J. Mendez-Nonell, S. Sanchez-Valdes, and L. F. Ramos-Devalle, "Morphology and osteogenetic characteristics of polyamide/nanohydroxyapatite biocomposites," *Polymer Bulletin*, vol. 62, no. 1, pp. 99–110, 2009.
- [41] H. Wang, Y. Li, Y. Zuo, J. Li, S. Ma, and L. Cheng, "Biocompatibility and osteogenesis of biomimetic nano-hydroxyapatite/polyamide composite scaffolds for bone tissue engineering," *Biomaterials*, vol. 28, no. 22, pp. 3338–3348, 2007.
- [42] F. Sun, H. Zhou, and J. Lee, "Various preparation methods of highly porous hydroxyapatite/polymer nanoscale biocomposites for bone regeneration," *Acta Biomaterialia*, vol. 7, no. 11, pp. 3813–3828, 2011.
- [43] S. Zhou, Y.-B. Li, Y.-Y. Wang et al., "The porous structure and mechanical properties of injection molded HA/PA66 scaffolds," *International Polymer Processing*, vol. 29, no. 4, pp. 454–460, 2014.
- [44] Y. Xiong, C. Ren, B. Zhang et al., "Analyzing the behavior of a porous nano-hydroxyapatite/polyamide 66 (n-HA/PA66) composite for healing of bone defects," *International Journal of Nanomedicine*, vol. 9, no. 1, pp. 485–494, 2014.
- [45] M. Xu and D. Peng, "Mesenchymal stem cells cultured on tantalum used in early-stage avascular necrosis of the femoral head," *Medical Hypotheses*, vol. 76, no. 2, pp. 199–200, 2011.
- [46] Q. Mengchun, D. Jiupeng, D. Wei et al., "The biological activity of co-culture of bone marrow mesenchymal stem cells and nHA/PA66 scaffold materials," *Journal of Oral Science Research*, vol. 26, pp. 805–808, 2010.
- [47] X. Li, L. Wang, Y. Fan, Q. Feng, F.-Z. Cui, and F. Watari, "Nanostructured scaffolds for bone tissue engineering," *Journal of Biomedical Materials Research Part A*, vol. 101, no. 8, pp. 2424–2435, 2013.
- [48] M. G. M. G. Penido and U. S. Alon, "Phosphate homeostasis and its role in bone health," *Pediatric Nephrology*, vol. 27, no. 11, pp. 2039–2048, 2012.
- [49] U. Saran, S. G. Piperni, and S. Chatterjee, "Role of angiogenesis in bone repair," *Archives of Biochemistry and Biophysics*, vol. 561, pp. 109–117, 2014.
- [50] S. M. Walzer, E. Cetin, R. Gröbl-Barabas et al., "Vascularization of primary and secondary ossification centres in the human growth plate," *BMC Developmental Biology*, vol. 14, article 36, 2014.

Review Article

Current Development of Silver Nanoparticle Preparation, Investigation, and Application in the Field of Medicine

Maxwell Murphy,¹ Kang Ting,^{1,2} Xinli Zhang,¹ Chia Soo,³ and Zhong Zheng^{1,3}

¹Dental and Craniofacial Research Institute and Division of Growth and Development, Section of Orthodontics, School of Dentistry, University of California, Los Angeles, CA 90095-1759, USA

²California NanoSystems Institute, University of California, Los Angeles, CA 90095, USA

³UCLA Department of Surgery and Department of Orthopaedic Surgery and the Orthopaedic Hospital Research Center, University of California, Los Angeles, CA 90095-1759, USA

Correspondence should be addressed to Chia Soo; scarlesslabs@earthlink.net and Zhong Zheng; zzheng@dentistry.ucla.edu

Received 15 September 2014; Accepted 14 October 2014

Academic Editor: Xiaoming Li

Copyright © 2015 Maxwell Murphy et al. This is an open access article distributed under the Creative Commons Attribution License, which permits unrestricted use, distribution, and reproduction in any medium, provided the original work is properly cited.

The invited review covers different research areas of silver nanoparticles (AgNPs), including the synthesis strategies of AgNPs, antimicrobial and anti-inflammatory properties of AgNPs, osteoconductive and osteoinductive activities of AgNP-based materials, and potential toxicity of AgNPs. The potential mechanisms of AgNP's biological efficacy as well as its potential toxicity are discussed as well. In addition, the current development of AgNP applications, especially in the area of therapeutics, is also summarized.

1. Introduction

Silver has been used as an antimicrobial agent for centuries. For example, the Phoenicians used silver vessels to preserve water and wine during their long voyages [1]. In addition, ancient Egyptians believed that silver powder provided beneficial healing and antidisease properties; thus silver compounds were used for prohibiting wound infection prior to antibiotics [1]. In 1884, German obstetrician Crede introduced 1% silver nitrate (AgNO_3) as an eye solution for prevention of gonococcal ophthalmia neonatorum, which is most likely the first scientifically documented medical use of silver [1]. In modern society, topically used silver sulfadiazine cream is the standard antibacterial treatment for serious burn wounds and is still widely used in burn units today [2]. However, inadequate local retention and severe cytotoxic effects limited the clinical use of these ionic reservoir forms of silver materials [3–5].

Due to recent advances in nanotechnology, it is now possible to produce silver at the nanoscale [6, 7]. In addition to their potential electronic and transparent conductor applications, the emergence of nanosilver materials in antimicrobial consumer goods and medical products is driving

the growth of the nanosilver market, which is expected to grow in value from US\$290 million in 2011 to around US\$1.2 billion by 2016 (http://www.merid.org/Content/News.Services/Nanotechnology_and_Development_News/Articles/2011/Sep/14/nanosilver.aspx). Among the different nanosilver preparations, silver nanoparticles (AgNPs) are made up of 20–15,000 silver atoms, generally range from 1 to 100 nm in diameter and present in one dimension [8]. These extremely small dimensions lead to a high surface area to volume ratio and, subsequently, change the physical, chemical, and biological properties of AgNPs [9, 10]. This review critically outlines recent developments in the synthesis, physicochemical properties, toxicity, and biomedical applications of AgNPs.

2. Synthesis of AgNPs

AgNPs can be synthesized in a variety of different ways, each with its own advantages and disadvantages. Till now, the most common methods of AgNPs synthesis are through chemical reduction of silver salt (e.g., AgNO_3) using a reducing agent (e.g., sodium borohydride) [11]. During chemical reduction, silver ion (Ag^+) receives an electron from the reducing

agent and reverts to its metallic form (Ag^0) eventually clustering to form AgNPs. AgNO_3 is the most often used silver salt for these chemical methods of AgNP synthesis due to its low cost and high stability [10]. Generally, a capping agent [e.g., poly(*N*-vinyl-2-pyrrolidone) (PVP)] is used during chemical reduction to stabilize the nanoparticles and prevent them from aggregating [11]. However, reducing agents and organic solvents used in chemical reduction, such as *N,N*-dimethylformamide, hydration hydrazine, and sodium borohydride, are highly reactive and pose potential environmental and biological risks [12]. Moreover, the inability to control the size of the AgNPs obtained by chemical reduction could result in a wide distribution of sizes of AgNPs obtained.

Photoreduction of silver salt in the presence of PVP or citrate by ultraviolet (UV) light is another simple and effective strategy to produce AgNPs [11, 13, 14]. However, most photoreduction methods still use organic solvents, such as PVP, and are unable to control the size of obtained AgNPs [11, 13, 14].

Recent efforts have been focused on developing new *green chemistry* methods of AgNPs synthesis with the advantage of using natural products and avoiding toxic reducing agents, organic solvents, and wasteful purifications with high cytotoxic residuals. With these methods, molecules produced by living organisms such as bacteria, fungi, or plants replace the reducing and capping agents [15–18]. For example, AgNO_3 is added to chitosan obtained from various species of bacteria and dissolved in acetic acid. The silver ions are then reduced through gamma radiation and stabilized by chitosan [19, 20]. There have also been efforts to synthesize AgNPs in the lamellar space of montmorillonite/chitosan by utilizing the UV irradiation reduction method in the absence of any reducing agent or heat treatment [21]. Additionally, AgNPs have been synthesized via photoreduction of AgNO_3 in layered inorganic clay suspensions, laponite, which serve as stabilizing agents that prevent nanoparticles from aggregating instead of using PVP [22]. The disadvantage to using these types of *green synthesis* is the potential of contamination due to the pathogenic bacteria created during the purification [10]. Consequently, herbal extracts and essential oils are gaining in popularity for methods of *green synthesis* due to their antioxidant and antimicrobial properties while avoiding the use of pathogenic bacteria [23–25]. However, the disadvantage of using herbal extracts is once again the wide distribution of particle sizes obtained.

In addition, there have also been novel developments by using *green physical* methods for AgNP synthesis avoiding the use of chemicals completely. One such method, laser ablation, can synthesize pure colloidal AgNPs in solutions without the use of chemical reagents [27, 28]. However, the concentration and morphology of these AgNPs are inconsistent since they are dependent on many parameters such as number of laser shots, wavelength of the laser, laser fluence, liquid medium, and ablation time duration [27, 28]. Another chemical-free method for AgNP synthesis involves the application of an electrical current between two silver wires in deionized water causing surface silver atoms to evaporate and condense back into aqueous AgNPs [29]. Without the use of chemicals, there are no toxic residuals or contaminations. However, since

no capping agents are used, agglomeration of AgNPs may pose a problem [30]. To date, perhaps the most effective method for AgNP synthesis is the production through a novel, nonchemically based proprietary process (USPTO 7,282,167). In this process, silver granules with a purity of 99.99% are distilled into silver vapor by heating on a ceramic conductive element. By controlling the generation rate of silver vapor, gas flow, and reactor pressure, the nucleation rate of silver nanoclusters can be designed to produce nanosilver liquid droplets, which are then condensed in a stream of flowing helium gas into solid crystalline spherical AgNPs of desired size. The hot nanoparticles are then attracted to a cooled chamber wall by thermophoresis where they are mechanically collected and packaged for use. Furthermore, the active surface of the obtained highly purified (>99.9% pure) 20–40 nm AgNPs ($15\text{--}25\text{ m}^2/\text{g}$) is much greater compared to commercial nonnanoscale silver powder ($1\text{--}2\text{ m}^2/\text{g}$) and previously reported AgNPs ($4\text{ m}^2/\text{g}$) [31, 32].

3. Biological Properties of AgNPs

Currently, the unique antimicrobial properties of AgNPs have led to their application in areas such as clothing manufacturing, food preservation, and water purification [33–36]. More importantly, AgNPs are being increasingly utilized in the medical industry due to their antibacterial, antifungal, antiviral, anti-inflammatory, and osteoinductive effects as well as their ability to enhance wound healing [32, 37–42].

3.1. Antibacterial Properties of AgNPs. Antibiotics are standard antimicrobials used in medicine that bind to specific chemical targets of bacteria not present in humans [41]. However, this binding specificity narrows the number of bacterial species that are vulnerable to a specific antibiotic and contributes to the antibiotic resistance developed by bacteria, ultimately creating multidrug resistant bacteria [43]. With the increasing number of infections due to multidrug resistant bacteria, there has been a need for effective antimicrobial alternatives. Thus, silver is a great alternative because it is an antiseptic that targets a broad spectrum of Gram⁺ and Gram[−] bacteria as well as vancomycin-resistant strains [7, 31, 36, 40, 43]. Moreover, silver-resistant bacteria are rarely observed in hospital microbial germ flora because silver resistance requires one generation of bacteria to undergo three separate mutations in three different bacterial systems [31, 44].

Mechanistically, silver-based materials are thought to release silver ions (Ag^+) in aqueous solution, which account for their antibacterial properties by attaching to specific thiol (–SH) groups containing sulfur and hydrogen found in a variety of structural and functional bacterial proteins [45–47]. It should be noted that the reservoir form of the active silver ions might differ [43]. For instance, the reservoir form of AgNO_3 is a chemical combination of Ag(I) and nitrate, but AgNO_3 is not suitable for sustained local application due to its high solubility as an ionic salt. Nonnanoscale elemental silver [$\text{Ag}(0)$] used in silverware and jewelry is relatively insoluble in most fluids, resulting in minimal oxidative Ag^+ release [43]. Thus, neither the *in vitro* antibacterial action nor the clinical behavior of nonnanoscale silver-coated stainless

steel cortical screws significantly differed from that of the uncoated ones [48]. Due to the greater surface-to-mass ratio, AgNPs offer greater active surface, higher solubility, and chemical reactivity. As a result, although the reservoir form for AgNPs is also elemental silver [Ag(0)], AgNPs have higher release of oxidative Ag⁺ and/or partially oxidized AgNP with chemisorbed (surface-bound) Ag(I) and thus have higher antibacterial activity compared with conventional silver repartitions [40, 49, 50].

However, a comparative study of AgNPs, AgNO₃, and silver chloride (AgCl) found that AgNPs have higher antibacterial properties than free silver ions (Ag⁺) [51]. This implies that AgNPs have intrinsic antibacterial properties not dependent on the release of silver ions (Ag⁺). One possible mechanism of Ag⁺ releasing-independent bactericidal effects of AgNPs is partly due to the ability of AgNPs to attach to the bacterial cell wall and penetrate it, thereby increasing its permeability and, ultimately, leading to cell death [52]. Another possible mechanism attempts to explain the antibacterial effect of positively charged silver atoms (Ag⁺) on the surface of AgNPs through the formation of free radicals and the subsequent free radical-induced membrane damage [53]. Furthermore, a recent study suggests a novel mechanism for the antibacterial effect of AgNPs, namely, the induction of a bacterial apoptosis-like response [54]. This new proposed mechanism involves an accumulation of reactive oxygen species (ROS), increased intracellular calcium levels, and phosphatidylserine exposure in the outer membrane, all hallmarks of early apoptosis. It also includes disruption of the membrane potential and DNA degradation, indicators of late apoptosis, in bacterial cells treated with AgNPs [54]. Collectively, it is believed that AgNPs are thought to interact with the bacterial DNA, the peptidoglycan cell wall and plasma membrane, and the bacterial proteins involved with the electron transport chain to produce their bactericidal effects [30, 47, 55–57]. Although it is not fully understood which mechanism provides the main antibacterial effect, a combined effect of each mechanism provides broad-spectrum antibacterial resistance.

It is worth noting that the size and shape of nanosilver influence its antibacterial efficacy. Previous studies have demonstrated that 5–50 nm sized AgNPs are bactericidal [31]. Further investigation suggested that the greater the surface area of AgNPs is, the greater the antibacterial activity is [58–60]. In addition, Sadeghi et al. reported that nanoscale silver plates demonstrated the best antimicrobial activity against *Staphylococcus aureus* and *Escherichia coli* compared with nanoscale silver rods and particles [61]. Antibacterial activity of nanosilver was found to be dependent on the surface area of nanosilver shapes with nanoscale silver plates showing the greatest surface area [61]. Thus, nanosilver with the greatest surface area exhibits better antibacterial properties at lower concentrations [61].

As discussed, the evidence supporting AgNPs as an effective antimicrobial agent is abundant with AgNPs showing broad-spectrum resistance to bacterial strains such as *S. aureus* (including methicillin resistant strains, known as MRSA), *Staphylococcus epidermidis* (including methicillin resistant strains, known as MRSE), *Enterococcus faecalis*,

Enterococcus faecium, *E. coli*, *Pseudomonas aeruginosa*, and *Klebsiella pneumonia* and even vancomycin-resistant strains [7, 31, 32, 36, 40, 42, 43].

3.2. Antifungal Properties of AgNPs. Long-term, repetitive administration of standard antifungal drugs leads to increased fungal resistance, especially by the *Candida* species [39]. Therefore, new antifungal agents are constantly being investigated. AgNPs have displayed many antifungal properties against common fungi and thus offer potential as an effective antifungal agent. A recent study found that a AgNP-coated reverse osmosis membrane, which is used in water purification systems, exhibited good antifungal activities against fungal strains such as *Candida tropicalis*, *Candida krusei*, *Candida glabrata*, and *Candida albicans* [36]. Additionally, Pulit et al. reported that AgNP suspensions created from aqueous raspberry extract acted as effective growth inhibition factors against two resistant fungal strains *Cladosporium cladosporioides* and *Aspergillus niger* [39]. Furthermore, a higher concentration of AgNPs induced stronger reduction of fungal growth in both cases. With the promising potential of AgNPs as a broad-spectrum antifungal agent, further investigation is warranted to elucidate the mechanisms concerning their antifungal properties.

3.3. Antiviral Properties of AgNPs. Various viruses, such as influenza, hepatitis, herpes simplex virus (HSV), and human immunodeficiency virus (HIV), can be life threatening [62]. Although many vaccines have been developed against various viruses, medicine has yet to develop a broad-spectrum antiviral vaccine. Furthermore, these viruses are developing antiviral resistance to current treatments and classical antiviral drugs, especially in immunocompromised patients [62]. In light of this, there is a pressing need for the development of new antiviral agents against a broad spectrum of viruses. AgNPs act as a broad-spectrum agent against a variety of viral strains and are not prone to developing resistance [10]. For example, studies have demonstrated antiviral activity of AgNPs against HSV-1, HSV-2, hepatitis B, and human immunodeficiency virus 1 (HIV-1) [63–66]. With regard to HSV-1, AgNPs are hypothesized to target the virus and to compete for its binding to cellular heparin sulfate through their sulfonate end groups, leading to the blockage of viral entry into the cell and the prevention of subsequent infection [63]. Additionally, a recent study demonstrated that 100 µg/mL of AgNPs could completely inhibit HSV-2 replication [66]. AgNPs at nontoxic concentrations were capable of inhibiting HSV-2 replication when administered prior to viral infection or soon after initial virus exposure. These findings suggest that the mode of action of AgNPs occurs during the early phases of viral replication [66]. Furthermore, there has been evidence of AgNP's antiviral activity against HIV-1 at noncytotoxic concentrations. AgNPs exerted anti-HIV activity at an early stage of viral replication, most likely as a virucidal agent or as an inhibitor of viral entry [65].

3.4. Anti-Inflammatory Properties of AgNPs. Despite the billions of dollars that have been spent on immunological

research, few effective anti-inflammatory drugs have emerged [72]. Thus, an urgent need for new drugs exists, as many inflammatory diseases are insufficiently responsive to current medications [72]. Recently, there has been increasing evidence that AgNPs are viable anti-inflammatory agents. Initially, anti-inflammatory properties of AgNPs were investigated by applying AgNP-coated, 0.5% silver nitrate (AgNO_3), or saline wound dressings to a porcine model of contact dermatitis [37]. AgNP-coated wound dressings outperformed other wound dressings as erythema, edema, and histological data showed that AgNP-treated pigs had near-normal skin after 72 hours, while other treatment groups remained inflamed [37]. Furthermore, AgNP-coated wound dressings decreased levels of proinflammatory cytokines transforming growth factor- (TGF-) β and tumor necrosis factor- (TNF-) α compared with other treatment groups. Similarly, another study evaluating the anti-inflammatory effects of AgNPs on an allergic rhinitis mouse model reported reduced nasal symptoms in sensitized mice and an inhibition of ovalbumin-specific immunoglobulin E, interleukin- (IL-) 4, and IL-10 [73]. Moreover, decreased inflammatory cell infiltration and goblet cell hyperplasia were also observed [73]. Further evidence of the anti-inflammatory effects of AgNPs has been demonstrated in a postoperative peritoneal adhesion model and through the use of AgNP-coated sutures [74, 75]. Wong et al. found that AgNPs are effective at decreasing inflammation in peritoneal adhesions without significant cytotoxic effects while Zhang et al. reported that using AgNP-coated sutures decreased inflammation and improved mechanical strength at intestinal anastomosis in mice [74, 75]. Our previous studies have also demonstrated that AgNP/poly(lactic-co-glycolic acid) (PLGA-) coated stainless steel alloy (SNPSA) materials significantly reduced bacterial infection and inflammatory cell infiltration in the intramedullary tissue in rat femoral canals (Figure 1) [76]. Mechanistically, the anti-inflammatory effects of AgNPs are not fully understood but are thought to be associated with the TNF- α pathway [74].

3.5. Osteoconductivity and Osteoinductivity of AgNP-Based Materials. Previously, by implanting AgNP/PLGA composite grafts for the healing of infected bone defects into grossly infected critical-sized bone segmental defects, we demonstrated that AgNP/PLGA composite grafts possess significant, antibacterial properties and osteoconductivity *in vivo* (Figure 2) [32]. AgNP/PLGA composite grafts displayed osteoconductive properties as they did not inhibit adherence, proliferation, alkaline phosphatase activity, or mineralization of ongrowth MC3T3-E1 preosteoblasts *in vivo* [32]. In a follow-up experiment, we unexpectedly found that SNPSA materials not only exhibited strong antibacterial activity *in vitro* and *ex vivo*, but also promoted MC3T3-E1 preosteoblast proliferation and maturation *in vitro* [42]. Furthermore, SNPSA implants induced osteogenesis while suppressing bacterial survival in contaminated rat femoral canals with no observed cytotoxicity (Figure 1) [42]. These findings require more research into the osteoconductive and osteoinductive properties of AgNP-based materials, but they offer promising therapeutic material for orthopedic surgery.

4. Toxicity of AgNPs

Applying silver as an antimicrobial agent has been hindered by its potential toxic effects, such as argyria, an irreversible pigmentation of the skin and eyes due to inappropriate silver deposition [3]. Thus, the toxicity of AgNPs must be investigated for commercial products and before widespread medical application. Also, environmental pollution must be considered to avoid ecological damage.

AgNPs enter the human body most often through the respiratory tract, gastrointestinal tract, skin, and female genital tract, as well as through systemic administration [77]. Recently, an *in vivo* oral toxicity study of AgNPs on Sprague-Dawley (SD) rats demonstrated the accumulation of AgNPs in the blood, liver, lungs, kidneys, stomach, testes, and brain, but showed no significant genotoxicity function after oral administration of AgNPs of 60 nm average size for 28 days at different doses [78]. Similarly, another *in vivo* 28-day inhalation toxicity study of 1.98–64.9 nm AgNPs on SD rats found no effects on respiratory function, hematology, or blood biochemical values [79]. In our previous studies, 3D porous graft and 43 μm thick PLGA coating composited by up to 2% 20–40 nm AgNPs and PLGA materials did not show significant cytotoxicity against preosteoblast MC3T3-C1 cells *in vitro* or toxicity during 8-week bone regeneration in SD rats *in vivo* [32, 42]. Other studies have shown that 20–25 nm AgNPs effectively inhibit microorganisms without causing significant cytotoxicity and that 10–20 nm AgNPs are nontoxic in mice and guinea pigs when administered by the oral, ocular, and dermal routes [32, 80]. In contrast, a 90-day whole body inhalation toxicity study of 18 nm AgNPs on SD rats reported that prolonged exposure to AgNPs elicited an inflammatory response within the alveoli and induced alterations in lung function at all particle concentrations [81]. Also, AgNPs have been reported to cross the blood-brain barrier in rats and induce neuronal degeneration and necrosis through accumulation in the brain over a long period of time [82]. Additionally, Vandebriel et al. and de Jong et al. found that intravenous administration of both 20 and 100 nm AgNPs in a 28-day repeated-dose toxicity study in SD rats induces suppression of the functional immune system [83, 84]. In the area of development, a study reported that AgNPs less than 12 nm in size affected early development of fish embryos, caused chromosomal aberrations and DNA damage, and induced proliferation arrest in cell lines of zebrafish indicating that AgNPs must be investigated for their potential teratogenic effects in humans [85]. *In vitro* studies have demonstrated that AgNPs are cytotoxic to various types of cells including neuroendocrine cells, mouse germ line cells, mouse fibroblasts, rat liver cells, human alveolar epithelial cell line, human peripheral blood mononuclear cells, normal human lung fibroblast cells, and human glioblastoma cells [86–91]. These conflicting results reveal the difficulty of pinpointing the overall toxicity of AgNPs to humans because the tremendous variation in particle size, particle aggregation, and concentration or coating thickness (in implants) of AgNPs has different profiles of silver release and bioactivity [43]. In short, much longer and detailed studies must be carried out to seriously consider AgNPs' potential toxicity in humans.

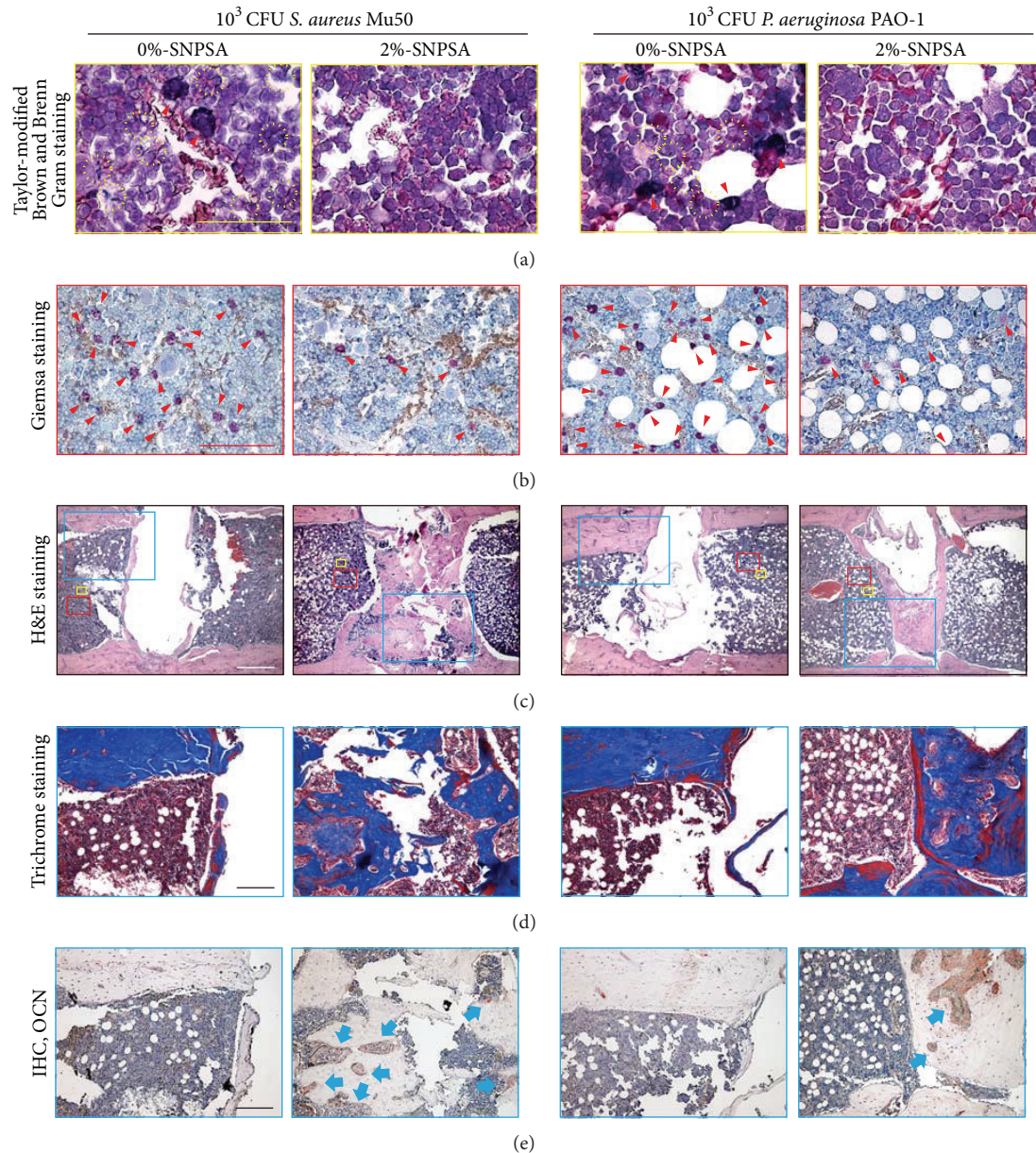


FIGURE 1: Histological and immunohistochemical staining of contaminated 0% and 2% AgNP/PLGA-coated 316L stainless steel alloy (SNPSA) implants in rat femoral canals (FCs) at 8 weeks after implantation. 10^3 colony forming units (CFU) *S. aureus* Mu50 or *P. aeruginosa* PAO-1 in $10 \mu\text{L}$ phosphate buffered saline (PBS) (10^5 CFU/mL, the typical criteria for invasive tissue infection [26]) were pipetted into the canal before implantation for bacterial invasion. Taylor-modified Brown and Brenn Gram staining (a) and Giemsa staining (b) revealed bacterial persistence (yellow dotted circles) with massive inflammatory cell infiltration (red arrowheads) in the intramedullary tissue around 0% SNPSA implants in rat FCs. In contrast, no bacterial survival was evident around 2% SNPSA implants in the same situation, and inflammatory cell infiltration in the intramedullary tissues around the implants was minimal. Moreover, only minimal bone formation around the 0% SNPSA groups was observed, whereas significant bone formation (blue arrows) was detected around 2% SNPSA implants, as shown by hematoxylin and eosin (H&E) staining (c), Masson's trichrome staining (d), and immunohistochemical staining of high-intensity osteocalcin signals (e). Yellow scale bar = $50 \mu\text{m}$; red scale bar = $100 \mu\text{m}$; white scale bar = $500 \mu\text{m}$; black scale bar = $200 \mu\text{m}$. Reprinted from *Biomaterials*, Vol. 33, Y. Liu and Z. Zheng et al., "The antimicrobial and osteoinductive properties of silver nanoparticle/poly (DL-lactic-co-glycolic acid)-coated stainless steel," pp. 8745–8756, 2012, with permission from Elsevier.

A potential contributing factor to AgNPs cytotoxicity is the oxidative stress caused by the creation of reactive oxygen species after AgNPs enter the cell [89]. AgNPs also damage cellular components leading to DNA damage, activation of antioxidant enzymes, depletion of antioxidant molecules

(e.g., glutathione), binding and disabling of proteins, and damage to the cell membrane [92]. However, an emerging study suggests that cellular oxidative stress may not be the main cause of toxicity and that it might be a different mechanism all together. Two widely used *in vitro* human cell lines

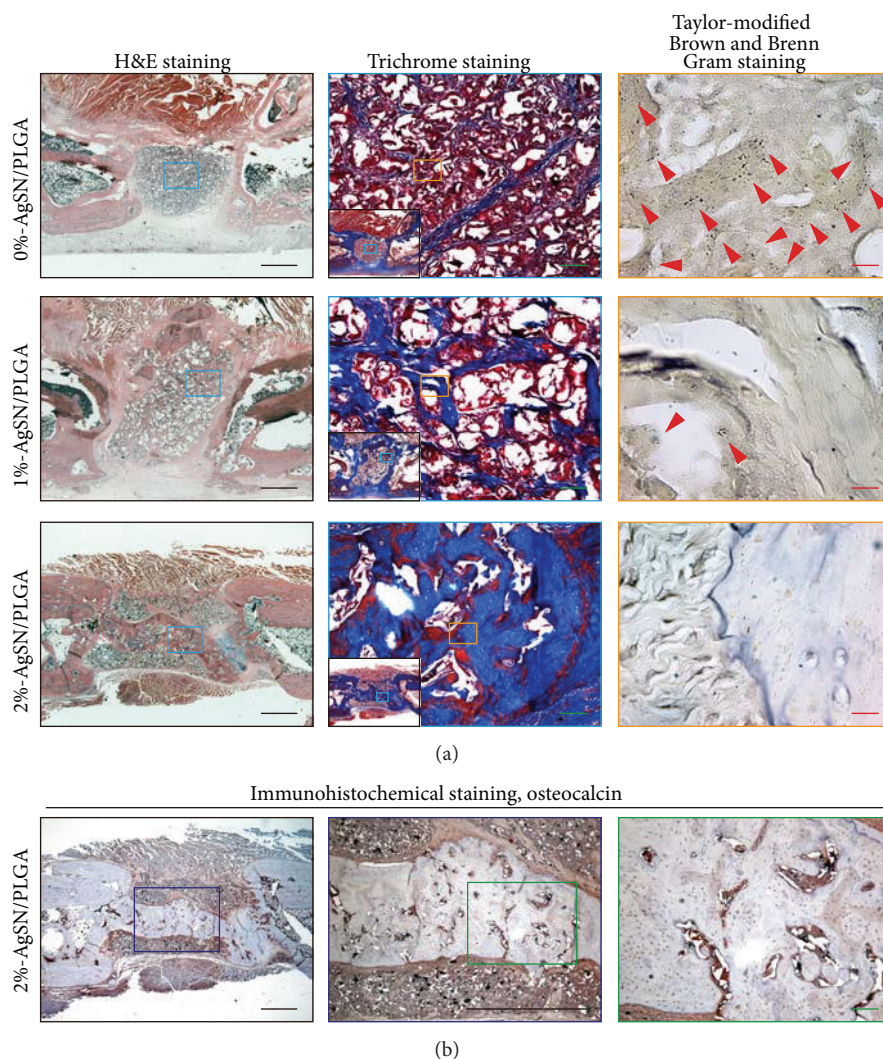


FIGURE 2: Histological and immunohistochemical staining of contaminated rat femoral segmental (FSD) defects implanted with 0.0%, 1.0%, and 2.0% AgNP/PLGA bone grafts coupled with 30 µg/mL bone morphogenetic protein 2 (BMP-2) at 12 weeks after implantation. With a small oscillating saw blade, a 6 mm critical-sized middiaphyseal defect was created in 16–18-week-old male SD rat femur. The volume of the defect was approximately 75 µL. 10^8 CFU *S. aureus* Mu50 in 75 µL 20% gelatin gel was implanted into the defect before implantation. H&E staining and Masson's trichrome staining (a) revealed no bone regeneration in BMP-2/0.0% AgNP/PLGA (control BMP-2 coupled control PLGA) implanted groups with obvious continued bacterial contamination evidenced by Taylor modified Brown and Brenn Gram stain (red arrows). However, BMP-2/2.0% NS/PLGA grafts promoted significantly greater bone formation to form a mineralized bony bridge between the two defect ends by eliminating bacteria in the defect area (a). Immunohistochemical staining against osteocalcin showed active bone regeneration around the mineralized bridge and in the marrow-like cavities in the bridge (b). Black scale bar = 2 mm; green scale bar = 100 µm; red scale bar = 10 µm. Reprinted from *Biomaterials*, Vol. 31, Z. Zheng et al. "The use of BMP-2 coupled—nanosilver-PLGA composite grafts to induce bone repair in grossly infected segmental defects," pp. 9293–9300, 2010, with permission from Elsevier.

for determining cytotoxicity in the liver and gastrointestinal tract, hepatoblastoma HepG2 and colon carcinoma Caco2, did not display any AgNP-induced oxidative stress when exposed to AgNPs at a concentration of 1–20 µg/mL [93]. These results suggest that cellular oxidative stress did not play a major role in the observed cytotoxicity of AgNPs in HepG2 and Caco2 cells and that a different mechanism of AgNP-induced mitochondrial injury leads to the cytotoxicity. The HepG2 and Caco2 cells appear to be targets for AgNPs, suggesting that the differences in the mechanisms of toxicity induced by AgNP may be largely a consequence of the type

of cells used [93]. Another study reported a correlation between AgNP size and inhibitory effects on mitochondria, with smaller AgNPs of 15 nm significantly more toxic than larger AgNPs of 55 nm [94]. Thus, oxidative stress, cell type, and preparation of AgNPs all play a role in the toxicity. With regard to the environment, a recent study found that AgNPs have a significant impact on the microbial community and severely disrupt the natural seasonal progression of tundra assemblages [95]. This effect was evidenced by levels of differential respiration in 0.066% AgNP-treated soil that were only half that of control soils, a decrease in signature

TABLE 1: Commonly used burn topical antimicrobials.

Agent	Advantages	Disadvantages
0.5% silver nitrate solution Introduced in 1964	(i) Bactericidal against most gram positive, gram negatives, and yeast (ii) Avoids mucopurulent exudate formation (pseudoeschar) (iii) Minimal pain after application (iv) No hypersensitivity	(i) No eschar penetration (ii) Electrolyte imbalance (hypotonic solution depletes wounds cations) (iii) Needs frequent application (iv) Discolors wound bed (v) Possible methemoglobinemia (vi) Rare silver toxicity
Mafenide acetate—historically 11.1% in water-soluble cream, but newer formulation is 8.5% First introduced in 1964	(i) Bacteriostatic against most gram positives, gram negatives; may be more effective for clostridial and pseudomonal infections than silver nitrate or SSD (ii) Good eschar penetration	(i) Potential loss of bacteriostatic action at high ($>10^6$) bacterial loads (ii) Effective concentration in eschar drops below therapeutic levels after 10 hours—needing twice daily application (iii) Metabolic acidosis [drug and metabolite (p-carboxybenzenesulfonamide) inhibit carbonic anhydrase—can worsen ventilation] (iv) Pain after application (v) Potential hypersensitivity
1% silver sulfadiazine (SSD) water-soluble cream Developed in 1968	(i) Bactericidal against most gram positives and some gram negatives (ii) Minimal pain after application	(i) Less activity against certain gram negatives (<i>Enterobacter</i> and <i>Pseudomonas</i>) and yeast (ii) Poor eschar penetration (iii) Forms pseudoeschar that requires daily washings (iv) Neutropenia ^A (v) Potential hypersensitivity to sulfa component (vi) Rare silver toxicity
Mafenide acetate—5% solution First introduced in 1971	(i) Similar to cream (ii) Less pain after application versus cream	(i) Similar to cream (ii) Effective concentration in eschar drops below therapeutic levels after 6–8 hours—needing 3x–4x daily application
Acticoat Rayon/polyester core encased in dense polyethylene mesh coated with nanocrystalline silver	(i) Bactericidal against most gram positives, gram negatives, and fungus (ii) Sustained silver release for 3–7 days (iii) Minimizes pain from daily dressings	(i) Poor eschar penetration (ii) Requires maintenance of moist dressings for silver release (iii) Rare silver toxicity

Table information modified and compiled from the following references: [67–71].

^ANeutropenia thought to be due to transient depression of granulocyte-macrophage progenitor cells in the marrow [67].

bacterial fatty acids, and changes in both richness and evenness in bacterial and fungal DNA sequence assemblages [95]. Similarly, Völker et al. investigated the effects of AgNPs on *Potamopyrgus antipodarum*, a freshwater mudsnail, and found that AgNPs decreased their reproduction [96]. Thus, further assessment of the environmental pollution and risks due to AgNP exposure is required to prevent damage to the environment.

5. Applications of AgNPs

AgNPs have been widely used as an antibacterial coat in medical applications such as wound dressings, cardiovascular implants, catheters, orthopedic implants, and dental composites.

5.1. Wound Dressings. Silver wound dressings have been used for over a decade to clinically treat various wounds, such as burns (Table 1), chronic ulcers, toxic epidermal necrolysis, and pemphigus [30]. Surprisingly, compared to standard silver sulfadiazine and gauze dressings, AgNP wound

dressings significantly decreased wound healing time by an average of 3.35 days while simultaneously increasing bacterial clearance from infected wounds with no adverse effects [38]. Meanwhile, AgNP wound dressings could enhance healing in superficial burn wounds compared with conventional 1% silver sulfadiazine cream or plain petrolatum gauze [97]. However, AgNP wound dressings made no difference in the healing of deep burn wounds, compared with 1% silver sulfadiazine, suggesting that AgNPs accelerate reepithelialization but not new tissue formation, such as angiogenesis and proliferation [97].

As research in this area continues, new ideas for AgNP wound dressings with the intention of further increasing wound healing and antibacterial efficacy are being investigated. For example, a recent chitosan-AgNP wound dressing demonstrated significantly improved wound healing compared with 1% silver sulfadiazine along with the deposition of less silver, which may lower the occurrence of argyria or skin discoloration [98]. Additionally, chitin-AgNP wound dressings possessed a strong antibacterial potential for wound healing applications [99, 100].

5.2. Cardiovascular Implants. In order to reduce the occurrence of endocarditis, a prosthetic silicone heart valve was the first cardiovascular device coated with silver element [101]. The use of silver was intended to prevent bacterial infection on the silicone valve thereby reducing the inflammation response of the heart. However, clinical trials testing the silver heart valve found that silver causes hypersensitivity, inhibits normal fibroblast function, and leads to paravalvular leakage in patients [101]. Thus, efforts turned towards incorporating AgNPs into medical devices as a potential for providing a safe, nontoxic antibacterial coating. The development of a new nanocomposite with AgNPs and diamond-like carbon as a surface coating for heart valves and stents demonstrated antithrombogenic and antibacterial properties [102]. Additionally, studies have also found that incorporation of nanostructured materials into the backbone of polymers in polymeric heart valves improves biocompatibility, resistance to calcification, and durability [103].

5.3. Catheters. Catheters used in the hospital setting have a high propensity for infection, which can lead to unwanted complications. Thus, AgNPs have been investigated as a method of reducing biofilm growth on catheters. Recently, polyurethane catheters have been modified with a coat of AgNPs to create effective antibacterial catheters [104]. Multiple studies have reported that AgNP-coated catheters can effectively reduce bacteria for up to 72 hours in animal models [105–108]. Furthermore, a follow-up 10-day *in vivo* study in mice confirmed that the AgNP-coated catheter was nontoxic [104]. Similarly, a clinical pilot study investigating the prevention of catheter-associated ventriculitis (CAV) found no incidence of CAV, and all cerebrospinal fluid cultures were negative in the 19 patients that received a AgNP-coated catheter [109]. On the contrary, in the control group of 20 patients, 5 were positive for CAV [109].

5.4. Dentistry. AgNPs have also been applied to dental instruments and bandages. Akhavan et al. demonstrated that incorporating AgNPs into orthodontic adhesives could increase or maintain the shear bond strength of an orthodontic adhesive while simultaneously increasing its resistance to bacteria [110]. A recent study by Chladek et al. found that incorporating AgNPs into dental composites could reduce the microbial colonization of lining materials, enhancing the antifungal efficiency [111]. Similarly, AgNPs incorporated into endodontic fillings displayed an increased antibacterial effect against *Streptococcus milleri*, *S. aureus*, and *E. faecalis* [112].

5.5. Orthopedic and Orthodontic Implants and Fixations. Implant associated and joint replacement bacterial infections are high at 1.0–4.0% and are one of the most serious complications in orthopedic surgery because they are extremely difficult to treat and result in increased morbidity and significantly worse outcomes [31, 32, 41, 42]. Thus, AgNPs have been incorporated into plain poly(methyl methacrylate) bone cement, used for the secure attachment of joint prostheses hip and knee replacement surgery, as a way to reduce bacterial resistance [31, 41]. Similarly, our lab investigated

incorporating AgNPs into PLGA grafts as a potential for implant and fixation material in orthopedic and orthodontic surgery [32, 42]. All studies reported markedly increased antibacterial activity without significant toxicity [31, 32, 41, 42]. Additionally, our results indicated that AgNP/PLGA coating is a practical process that is nontoxic, easy to operate, and free of AgNP aggregation (Figures 1 and 2) [32, 76], suggesting that AgNP/PLGA-coated implants have excellent clinical potential for use in orthopedics and orthodontics.

5.6. Other Applications. AgNPs are also available in many commercial products such as water filters and purification systems, deodorants, soaps, socks, food preservation, and room sprays [34–36, 57, 77], which contributes to the increasing market of AgNPs.

6. Future Outlook

The use of AgNPs is already established for many commercial applications and certain medical applications, such as wound dressings, while many new potential applications are being heavily investigated. AgNPs possess great potential due to their antibacterial, antifungal, antiviral, and anti-inflammatory properties while our recent research has revealed novel osteoinductive properties as well. However, the mechanisms and biological interactions behind these properties are not fully understood. For example, the relationship between the size and shape of AgNPs and their biological properties and toxicity is not clearly revealed and thus requires further investigation as AgNP use continues to increase. Therefore, there is a pressing need to fully elucidate the mechanisms concerning the efficacy and toxicity of AgNPs before widespread medical application can occur.

Conflict of Interests

Kang Ting, Chia Soo, and Zhong Zheng are inventors of silver nanoparticle-related patents filed from UCLA.

Acknowledgments

The authors would like to thank Nadia Barakat from the University of California, Berkeley, for assistance in the preparation of this paper. This research is supported by the National Center for Advancing Translational Sciences UCLA CTSI Grant UL1TR000124.

References

- [1] A. D. Russell and W. B. Hugo, “7 Antimicrobial activity and action of silver,” in *Progress in Medicinal Chemistry*, pp. 351–370, 1994.
- [2] B. S. Atiyeh, M. Costagliola, S. N. Hayek, and S. A. Dibo, “Effect of silver on burn wound infection control and healing: review of the literature,” *Burns*, vol. 33, no. 2, pp. 139–148, 2007.
- [3] K. Van De Voorde, T. Nijsten, K. Schelfhout, G. Moorkens, and J. Lambert, “Long term use of silver containing nose-drops resulting in systemic argyria,” *Acta Clinica Belgica*, vol. 60, no. 1, pp. 33–35, 2005.

- [4] H. Vik, K. J. Andersen, K. Julshamn, and K. Todnem, "Neuropathy caused by silver absorption from arthroplasty cement," *The Lancet*, vol. 1, no. 8433, p. 872, 1985.
- [5] E. Sudmann, H. Vik, M. Rait et al., "Systemic and local silver accumulation after total hip replacement using silver-impregnated bone cement," *Medical Progress through Technology*, vol. 20, no. 3-4, pp. 179-184, 1994.
- [6] Y. Sun, B. Mayers, and Y. Xia, "Transformation of silver nanospheres into nanobelts and triangular nanoplates through a thermal process," *Nano Letters*, vol. 3, no. 5, pp. 675-679, 2003.
- [7] A. Panáček, L. Kvítek, R. Prucek et al., "Silver colloid nanoparticles: synthesis, characterization, and their antibacterial activity," *The Journal of Physical Chemistry B*, vol. 110, no. 33, pp. 16248-16253, 2006.
- [8] D. Williams, "The relationship between biomaterials and nanotechnology," *Biomaterials*, vol. 29, no. 12, pp. 1737-1738, 2008.
- [9] K. M. M. Abou El-Nour, A. A. Eftaiha, A. Al-Warthan, and R. A. A. Ammar, "Synthesis and applications of silver nanoparticles," *Arabian Journal of Chemistry*, vol. 3, no. 3, pp. 135-140, 2010.
- [10] L. Ge, Q. Li, M. Wang, J. Ouyang, X. Li, and M. M. Q. Xing, "Nanosilver particles in medical applications: synthesis, performance, and toxicity," *International Journal of Nanomedicine*, vol. 9, no. 1, pp. 2399-2407, 2014.
- [11] R. Sato-Berfú, R. Redón, A. Vázquez-Olmos, and J. M. Saniger, "Silver nanoparticles synthesized by direct photoreduction of metal salts. Application in surface-enhanced Raman spectroscopy," *Journal of Raman Spectroscopy*, vol. 40, no. 4, pp. 376-380, 2009.
- [12] N. Vigneshwaran, R. P. Nachane, R. H. Balasubramanya, and P. V. Varadarajan, "A novel one-pot 'green' synthesis of stable silver nanoparticles using soluble starch," *Carbohydrate Research*, vol. 341, no. 12, pp. 2012-2018, 2006.
- [13] G.-N. Xu, X.-L. Qiao, X.-L. Qiu, and J.-G. Chen, "Preparation and characterization of stable monodisperse silver nanoparticles via photoreduction," *Colloids and Surfaces A: Physicochemical and Engineering Aspects*, vol. 320, no. 1-3, pp. 222-226, 2008.
- [14] A. J. Kora, R. Manjusha, and J. Arunachalam, "Superior bactericidal activity of SDS capped silver nanoparticles: synthesis and characterization," *Materials Science and Engineering C*, vol. 29, no. 7, pp. 2104-2109, 2009.
- [15] D. Mandal, M. E. Bolander, D. Mukhopadhyay, G. Sarkar, and P. Mukherjee, "The use of microorganisms for the formation of metal nanoparticles and their application," *Applied Microbiology and Biotechnology*, vol. 69, no. 5, pp. 485-492, 2006.
- [16] L. Sintubin, W. de Windt, J. Dick et al., "Lactic acid bacteria as reducing and capping agent for the fast and efficient production of silver nanoparticles," *Applied Microbiology and Biotechnology*, vol. 84, no. 4, pp. 741-749, 2009.
- [17] D. S. Balaji, S. Basavaraja, R. Deshpande, D. B. Mahesh, B. K. Prabhakar, and A. Venkataraman, "Extracellular biosynthesis of functionalized silver nanoparticles by strains of *Cladosporium cladosporioides* fungus," *Colloids and Surfaces B: Biointerfaces*, vol. 68, no. 1, pp. 88-92, 2009.
- [18] M. Solgi, "Evaluation of plant-mediated Silver nanoparticles synthesis and its application in postharvest physiology of cut Flowers," *Physiology and Molecular Biology of Plants*, vol. 20, no. 3, pp. 279-285, 2014.
- [19] F. M. Reicha, A. Sarhan, M. I. Abdel-Hamid, and I. M. El-Sherbiny, "Preparation of silver nanoparticles in the presence of chitosan by electrochemical method," *Carbohydrate Polymers*, vol. 89, no. 1, pp. 236-244, 2012.
- [20] V. Thomas, M. M. Yallapu, B. Sreedhar, and S. K. Bajpai, "Fabrication, characterization of chitosan/nanosilver film and its potential antibacterial application," *Journal of Biomaterials Science, Polymer Edition*, vol. 20, no. 14, pp. 2129-2144, 2009.
- [21] K. Shameli, M. B. Ahmad, W. M. Z. W. Yunus et al., "Green synthesis of silver/montmorillonite/chitosan bionanocomposites using the UV irradiation method and evaluation of antibacterial activity," *International Journal of Nanomedicine*, vol. 5, no. 1, pp. 875-887, 2010.
- [22] H. Huang and Y. Yang, "Preparation of silver nanoparticles in inorganic clay suspensions," *Composites Science and Technology*, vol. 68, no. 14, pp. 2948-2953, 2008.
- [23] H. Mighri, H. Hajlaoui, A. Akrou, H. Najjaa, and M. Neffati, "Antimicrobial and antioxidant activities of *Artemisia herba-alba* essential oil cultivated in Tunisian arid zone," *Comptes Rendus Chimie*, vol. 13, no. 3, pp. 380-386, 2010.
- [24] V. Vilas, D. Philip, and J. Mathew, "Catalytically and biologically active silver nanoparticles synthesized using essential oil," *Spectrochimica Acta Part A: Molecular and Biomolecular Spectroscopy*, vol. 132, pp. 743-750, 2014.
- [25] A. R. Vilchis-Nestor, V. Sánchez-Mendieta, M. A. Camacho-López, R. M. Gómez-Espinosa, M. A. Camacho-López, and J. A. Arenas-Alatorre, "Solventless synthesis and optical properties of Au and Ag nanoparticles using *Camellia sinensis* extract," *Materials Letters*, vol. 62, no. 17-18, pp. 3103-3105, 2008.
- [26] T. Calandra and J. Cohen, "The International Sepsis Forum Consensus Conference on definitions of infection in the intensive care unit," *Critical Care Medicine*, vol. 33, no. 7, pp. 1538-1548, 2005.
- [27] V. Amendola and M. Meneghetti, "Laser ablation synthesis in solution and size manipulation of noble metal nanoparticles," *Physical Chemistry Chemical Physics*, vol. 11, no. 20, pp. 3805-3821, 2009.
- [28] T. Tsuji, N. Watanabe, and M. Tsuji, "Laser induced morphology change of silver colloids: formation of nano-size wires," *Applied Surface Science*, vol. 211, no. 1-4, pp. 189-193, 2003.
- [29] D.-C. Tien, K.-H. Tseng, C.-Y. Liao, and T.-T. Tsung, "Colloidal silver fabrication using the spark discharge system and its antimicrobial effect on *Staphylococcus aureus*," *Medical Engineering and Physics*, vol. 30, no. 8, pp. 948-952, 2008.
- [30] K. Chaloupka, Y. Malam, and A. M. Seifalian, "Nanosilver as a new generation of nanoparticle in biomedical applications," *Trends in Biotechnology*, vol. 28, no. 11, pp. 580-588, 2010.
- [31] V. Alt, T. Bechert, P. Steinrücke et al., "An in vitro assessment of the antibacterial properties and cytotoxicity of nanoparticulate silver bone cement," *Biomaterials*, vol. 25, no. 18, pp. 4383-4391, 2004.
- [32] Z. Zheng, W. Yin, J. N. Zara et al., "The use of BMP-2 coupled—nanosilver-PLGA composite grafts to induce bone repair in grossly infected segmental defects," *Biomaterials*, vol. 31, no. 35, pp. 9293-9300, 2010.
- [33] G. Zhang, Y. Liu, X. Gao, and Y. Chen, "Synthesis of silver nanoparticles and antibacterial property of silk fabrics treated by silver nanoparticles," *Nanoscale Research Letters*, vol. 9, no. 1, p. 216, 2014.
- [34] Q. Chaudhry, M. Scotter, J. Blackburn et al., "Applications and implications of nanotechnologies for the food sector," *Food Additives and Contaminants A: Chemistry, Analysis, Control, Exposure and Risk Assessment*, vol. 25, no. 3, pp. 241-258, 2008.
- [35] T. M. Benn and P. Westerhoff, "Nanoparticle silver released into water from commercially available sock fabrics," *Environmental Science and Technology*, vol. 42, no. 11, pp. 4133-4139, 2008.

- [36] R. Manjumeena, D. Duraibabu, J. Sudha, and P. T. Kalaichelvan, "Biogenic nanosilver incorporated reverse osmosis membrane for antibacterial and antifungal activities against selected pathogenic strains: an enhanced eco-friendly water disinfection approach," *Journal of Environmental Science and Health—Part A Toxic/Hazardous Substances and Environmental Engineering*, vol. 49, no. 10, pp. 1125–1133, 2014.
- [37] P. L. Nadworny, J. Wang, E. E. Tredget, and R. E. Burrell, "Anti-inflammatory activity of nanocrystalline silver in a porcine contact dermatitis model," *Nanomedicine: Nanotechnology, Biology, and Medicine*, vol. 4, no. 3, pp. 241–251, 2008.
- [38] Y. Huang, X. Li, Z. Liao et al., "A randomized comparative trial between Acticoat and SD-Ag in the treatment of residual burn wounds, including safety analysis," *Burns*, vol. 33, no. 2, pp. 161–166, 2007.
- [39] J. Pulit, M. Banach, R. Szczygłowska, and M. Bryk, "Nanosilver against fungi. Silver nanoparticles as an effective biocidal factor," *Acta Biochimica Polonica*, vol. 60, no. 4, pp. 795–798, 2013.
- [40] C.-N. Lok, C.-M. Ho, R. Chen et al., "Silver nanoparticles: partial oxidation and antibacterial activities," *Journal of Biological Inorganic Chemistry*, vol. 12, no. 4, pp. 527–534, 2007.
- [41] H. van de Belt, D. Neut, W. Schenk, J. R. van Horn, H. C. van der Mei, and H. J. Busscher, "Infection of orthopedic implants and the use of antibiotic-loaded bone cements," *Acta Orthopaedica Scandinavica*, vol. 72, no. 6, pp. 557–571, 2001.
- [42] Y. Liu, Z. Zheng, J. N. Zara et al., "The antimicrobial and osteoinductive properties of silver nanoparticle/poly (dl-lactico-glycolic acid)-coated stainless steel," *Biomaterials*, vol. 33, no. 34, pp. 8745–8756, 2012.
- [43] L. G. Ovington, "The truth about silver," *Ostomy Wound Management*, vol. 50, no. 9, supplement, pp. 1s–10s, 2004.
- [44] S. Silver, L. T. Phung, and G. Silver, "Silver as biocides in burn and wound dressings and bacterial resistance to silver compounds," *Journal of Industrial Microbiology and Biotechnology*, vol. 33, no. 7, pp. 627–634, 2006.
- [45] P. Sanpui, A. Murugadoss, P. V. D. Prasad, S. S. Ghosh, and A. Chattopadhyay, "The antibacterial properties of a novel chitosan-Ag-nanoparticle composite," *International Journal of Food Microbiology*, vol. 124, no. 2, pp. 142–146, 2008.
- [46] J. R. Morones, J. L. Elechiguerra, A. Camacho et al., "The bactericidal effect of silver nanoparticles," *Nanotechnology*, vol. 16, no. 10, pp. 2346–2353, 2005.
- [47] S. Shrivastava, T. Bera, S. K. Singh, G. Singh, P. Ramachandrarao, and D. Dash, "Characterization of antiplatelet properties of silver nanoparticles," *ACS Nano*, vol. 3, no. 6, pp. 1357–1364, 2009.
- [48] A. Masse, A. Bruno, M. Bosetti, A. Biasibetti, M. Cannas, and P. Gallinaro, "Prevention of pin track infection in external fixation with silver coated pins: clinical and microbiological results," *Journal of Biomedical Materials Research*, vol. 53, no. 5, pp. 600–604, 2000.
- [49] G. A. Martinez-Castanon, N. Niño-Martínez, F. Martínez-Gutierrez, J. R. Martínez-Mendoza, and F. Ruiz, "Synthesis and antibacterial activity of silver nanoparticles with different sizes," *Journal of Nanoparticle Research*, vol. 10, no. 8, pp. 1343–1348, 2008.
- [50] G. A. Sotiriou and S. E. Pratsinis, "Antibacterial activity of nano-silver ions and particles," *Environmental Science and Technology*, vol. 44, no. 14, pp. 5649–5654, 2010.
- [51] O. Choi, K. K. Deng, N.-J. Kim, L. Ross Jr., R. Y. Surampalli, and Z. Hu, "The inhibitory effects of silver nanoparticles, silver ions, and silver chloride colloids on microbial growth," *Water Research*, vol. 42, no. 12, pp. 3066–3074, 2008.
- [52] C.-N. Lok, C.-M. Ho, R. Chen et al., "Proteomic analysis of the mode of antibacterial action of silver nanoparticles," *Journal of Proteome Research*, vol. 5, no. 4, pp. 916–924, 2006.
- [53] J. S. Kim, E. Kuk, K. N. Yu et al., "Antimicrobial effects of silver nanoparticles," *Nanomedicine: Nanotechnology, Biology, and Medicine*, vol. 3, no. 1, pp. 95–101, 2007.
- [54] W. Lee, K. J. Kim, and D. G. Lee, "A novel mechanism for the antibacterial effect of silver nanoparticles on *Escherichia coli*," *Biometals*, vol. 27, no. 6, pp. 1191–1201, 2014.
- [55] M. Yamanaka, K. Hara, and J. Kudo, "Bactericidal actions of a silver ion solution on *Escherichia coli*, studied by energy-filtering transmission electron microscopy and proteomic analysis," *Applied and Environmental Microbiology*, vol. 71, no. 11, pp. 7589–7593, 2005.
- [56] K. J. Woo, C. K. Hye, W. K. Ki, S. Shin, H. K. So, and H. P. Yong, "Antibacterial activity and mechanism of action of the silver ion in *Staphylococcus aureus* and *Escherichia coli*," *Applied and Environmental Microbiology*, vol. 74, no. 7, pp. 2171–2178, 2008.
- [57] W. Yang, C. Shen, Q. Ji et al., "Food storage material silver nanoparticles interfere with DNA replication fidelity and bind with DNA," *Nanotechnology*, vol. 20, no. 8, Article ID 085102, 2009.
- [58] S. H. Jeong, S. Y. Yeo, and S. C. Yi, "The effect of filler particle size on the antibacterial properties of compounded polymer/silver fibers," *Journal of Materials Science*, vol. 40, no. 20, pp. 5407–5411, 2005.
- [59] G. A. Martinez-Castanon, N. Niño-Martínez, F. Martínez-Gutierrez, J. R. Martínez-Mendoza, and F. Ruiz, "Synthesis and antibacterial activity of silver nanoparticles with different sizes," *Journal of Nanoparticle Research*, vol. 10, no. 8, pp. 1343–1348, 2008.
- [60] F. Martinez-Gutierrez, P. L. Olive, A. Banuelos et al., "Synthesis, characterization, and evaluation of antimicrobial and cytotoxic effect of silver and titanium nanoparticles," *Nanomedicine: Nanotechnology, Biology, and Medicine*, vol. 6, no. 5, pp. 681–688, 2010.
- [61] B. Sadeghi, F. S. Garmaoui, M. Hashemi, H. R. Nezhad, A. Nasrollahi, and S. Ardalan, "Comparison of the anti-bacterial activity on the nanosilver shapes: nanoparticles, nanorods and nanoplates," *Advanced Powder Technology*, vol. 23, no. 1, pp. 22–26, 2012.
- [62] S. Gaikwad, A. Ingle, A. Gade et al., "Antiviral activity of mycosynthesized silver nanoparticles against herpes simplex virus and human parainfluenza virus type 3," *International Journal of Nanomedicine*, vol. 8, pp. 4303–4314, 2013.
- [63] D. Baram-Pinto, S. Shukla, N. Perkash, A. Gedanken, and R. Sarid, "Inhibition of herpes simplex virus type 1 infection by silver nanoparticles capped with mercaptoethane sulfonate," *Bioconjugate Chemistry*, vol. 20, no. 8, pp. 1497–1502, 2009.
- [64] L. Lu, R. W.-Y. Sun, R. Chen et al., "Silver nanoparticles inhibit hepatitis B virus replication," *Antiviral Therapy*, vol. 13, no. 2, pp. 253–262, 2008.
- [65] H. H. Lara, N. V. Ayala-Núñez, L. Ixtapan-Turrent, and C. Rodríguez-Padilla, "Mode of antiviral action of silver nanoparticles against HIV-1," *Journal of Nanobiotechnology*, vol. 8, article 1, 2010.
- [66] R. L. Hu, S. R. Li, F. J. Kong, R. J. Hou, X. L. Guan, and F. Guo, "Inhibition effect of silver nanoparticles on herpes simplex virus 2," *Genetics and Molecular Research*, vol. 13, no. 3, pp. 7022–7028, 2014.

- [67] L. C. D'Avignon, J. R. Saffle, K. K. Chung, and L. C. Cancio, "Prevention and management of infections associated with burns in the combat casualty," *Journal of Trauma—Injury, Infection and Critical Care*, vol. 64, no. 3, pp. S277–S286, 2008.
- [68] E. E. Tredget, H. A. Shankowsky, R. Rennie, R. E. Burrell, and S. Logsetty, "Pseudomonas infections in the thermally injured patient," *Burns*, vol. 30, no. 1, pp. 3–26, 2004.
- [69] L. Martineau, S. C. Davis, H. T. Peng, and A. Hung, "Controlling methicillin resistant *Staphylococcus aureus* and pseudomonas aeruginosa wound infections with a novel biomaterial," *Journal of Investigative Surgery*, vol. 20, no. 4, pp. 217–227, 2007.
- [70] D. J. Barillo, "Topical antimicrobials in burn wound care: a recent history," *Wounds*, vol. 20, no. 7, pp. 192–198, 2008.
- [71] W. G. Cioffi, "Conventional warfare: ballistic, blast, and burn injuries," in *Textbook of Military Medicine: Part 1-Warfare, Weaponry, and the Casualty*, pp. 349–377, 1989.
- [72] C. R. Mackay, "Moving targets: cell migration inhibitors as new anti-inflammatory therapies," *Nature Immunology*, vol. 9, no. 9, pp. 988–998, 2008.
- [73] S.-H. Shin and M.-K. Ye, "The effect of nano-silver on allergic rhinitis model in mice," *Clinical and Experimental Otorhinolaryngology*, vol. 5, no. 4, pp. 222–227, 2012.
- [74] K. K. Y. Wong, S. O. F. Cheung, L. Huang et al., "Further evidence of the anti-inflammatory effects of silver nanoparticles," *ChemMedChem*, vol. 4, no. 7, pp. 1129–1135, 2009.
- [75] S. Zhang, X. Liu, H. Wang, J. Peng, and K. K. Y. Wong, "Silver nanoparticle-coated suture effectively reduces inflammation and improves mechanical strength at intestinal anastomosis in mice," *Journal of Pediatric Surgery*, vol. 49, no. 4, pp. 606–613, 2014.
- [76] Y. Liu, Z. Zheng, J. N. Zara et al., "The antimicrobial and osteoinductive properties of silver nanoparticle/poly (DL-lactic-co-glycolic acid)-coated stainless steel," *Biomaterials*, vol. 33, no. 34, pp. 8745–8756, 2012.
- [77] X. Chen and H. J. Schluesener, "Nanosilver: a nanoproduct in medical application," *Toxicology Letters*, vol. 176, no. 1, pp. 1–12, 2008.
- [78] Y. S. Kim, J. S. Kim, H. S. Cho et al., "Twenty-eight-day oral toxicity, genotoxicity, and gender-related tissue distribution of silver nanoparticles in Sprague-Dawley rats," *Inhalation Toxicology*, vol. 20, no. 6, pp. 575–583, 2008.
- [79] J. H. Ji, J. H. Jung, S. S. Kim et al., "Twenty-eight-day inhalation toxicity study of silver nanoparticles in Sprague-Dawley rats," *Inhalation Toxicology*, vol. 19, no. 10, pp. 857–871, 2007.
- [80] P. Maneewattanapinyo, W. Banlunara, C. Thammacharoen, S. Ekasit, and T. Kaewamatawong, "An evaluation of acute toxicity of colloidal silver nanoparticles," *Journal of Veterinary Medical Science*, vol. 73, no. 11, pp. 1417–1423, 2011.
- [81] J. H. Sung, J. H. Ji, J. D. Park et al., "Subchronic inhalation toxicity of silver nanoparticles," *Toxicological Sciences*, vol. 108, no. 2, pp. 452–461, 2009.
- [82] J. Tang, L. Xiong, S. Wang et al., "Influence of silver nanoparticles on neurons and blood-brain barrier via subcutaneous injection in rats," *Applied Surface Science*, vol. 255, no. 2, pp. 502–504, 2008.
- [83] R. J. Vandebriel, E. C. M. Tonk, L. J. de la Fonteyne-Blankestijn et al., "Immunotoxicity of silver nanoparticles in an intravenous 28-day repeated-dose toxicity study in rats," *Acta Veterinaria Scandinavica*, vol. 11, article 21, 2014.
- [84] W. H. de Jong, L. T. M. van der ven, A. Sleijffers et al., "Systemic and immunotoxicity of silver nanoparticles in an intravenous 28 days repeated dose toxicity study in rats," *Biomaterials*, vol. 34, no. 33, pp. 8333–8343, 2013.
- [85] K. J. Lee, P. D. Nallathamby, L. M. Browning, C. J. Osgood, and X.-H. Nancy Xu, "In vivo imaging of transport and biocompatibility of single silver nanoparticles in early development of zebrafish embryos," *ACS Nano*, vol. 1, no. 2, pp. 133–143, 2007.
- [86] P. V. AshaRani, G. L. K. Mun, M. P. Hande, and S. Valiyaveetil, "Cytotoxicity and genotoxicity of silver nanoparticles in human cells," *ACS Nano*, vol. 3, no. 2, pp. 279–290, 2009.
- [87] S.-H. Shin, M.-K. Ye, H.-S. Kim, and H.-S. Kang, "The effects of nano-silver on the proliferation and cytokine expression by peripheral blood mononuclear cells," *International Immunopharmacology*, vol. 7, no. 13, pp. 1813–1818, 2007.
- [88] S. M. Hussain, A. K. Javorina, A. M. Schrand, H. M. H. M. Duhart, S. F. Ali, and J. J. Schlager, "The interaction of manganese nanoparticles with PC-12 cells induces dopamine depletion," *Toxicological Sciences*, vol. 92, no. 2, pp. 456–463, 2006.
- [89] S. M. Hussain, K. L. Hess, J. M. Gearhart, K. T. Geiss, and J. J. Schlager, "In vitro toxicity of nanoparticles in BRL 3A rat liver cells," *Toxicology in Vitro*, vol. 19, no. 7, pp. 975–983, 2005.
- [90] Y. H. Hsin, C. F. Chen, S. Huang, T. S. Shih, P. S. Lai, and P. J. Chueh, "The apoptotic effect of nanosilver is mediated by a ROS- and JNK-dependent mechanism involving the mitochondrial pathway in NIH3T3 cells," *Toxicology Letters*, vol. 179, no. 3, pp. 130–139, 2008.
- [91] S. Park, Y. K. Lee, M. Jung et al., "Cellular toxicity of various inhalable metal nanoparticles on human alveolar epithelial cells," *Inhalation Toxicology*, vol. 19, no. 1, pp. 59–65, 2007.
- [92] D. McShan, P. C. Ray, and H. Yu, "Molecular toxicity mechanism of nanosilver," *Journal of Food and Drug Analysis*, vol. 22, no. 1, pp. 116–127, 2014.
- [93] S. C. Sahu, J. Zheng, L. Graham et al., "Comparative cytotoxicity of nanosilver in human liver HepG2 and colon Caco2 cells in culture," *Journal of Applied Toxicology*, vol. 34, no. 11, pp. 1155–1166, 2014.
- [94] C. Carlson, S. M. Hussein, A. M. Schrand et al., "Unique cellular interaction of silver nanoparticles: size-dependent generation of reactive oxygen species," *Journal of Physical Chemistry B*, vol. 112, no. 43, pp. 13608–13619, 2008.
- [95] N. Kumar, G. R. Palmer, V. Shah, and V. K. Walker, "The effect of silver nanoparticles on seasonal change in arctic tundra bacterial and fungal assemblages," *PLoS ONE*, vol. 9, no. 6, Article ID e99953, 2014.
- [96] C. Völker, T. Gräf, I. Schneider, M. Oetken, and J. Oehlmann, "Combined effects of silver nanoparticles and 17 α -ethinylestradiol on the freshwater mudsnail *Potamopyrgus antipodarum*," *Environmental Science and Pollution Research*, vol. 21, no. 18, pp. 10661–10670, 2014.
- [97] J. Chen, C.-M. Han, X.-W. Lin, Z.-J. Tang, and S.-J. Su, "Effect of silver nanoparticle dressing on second degree burn wound," *Zhonghua Wai Ke Za Zhi/Chinese Journal of Surgery*, vol. 44, no. 1, pp. 50–52, 2006.
- [98] S. Lu, W. Gao, and H. Y. Gu, "Construction, application and biosafety of silver nanocrystalline chitosan wound dressing," *Burns*, vol. 34, no. 5, pp. 623–628, 2008.
- [99] R. Singh and D. Singh, "Chitin membranes containing silver nanoparticles for wound dressing application," *International Wound Journal*, vol. 11, no. 3, pp. 264–268, 2014.
- [100] K. Madhumathi, P. T. S. Kumar, S. Abhilash et al., "Development of novel chitin/nanosilver composite scaffolds for wound

- dressings applications,” *Journal of Materials Science: Materials in Medicine*, vol. 21, no. 2, pp. 807–813, 2010.
- [101] G. L. Grunkemeier, R. Jin, and A. Starr, “Prosthetic heart valves: objective performance criteria versus randomized clinical trial,” *Annals of Thoracic Surgery*, vol. 82, no. 3, pp. 776–780, 2006.
- [102] M. Andara, A. Agarwal, D. Scholvin et al., “Hemocompatibility of diamondlike carbon-metal composite thin films,” *Diamond and Related Materials*, vol. 15, no. 11-12, pp. 1941–1948, 2006.
- [103] H. Ghanbari, H. Viatge, A. G. Kidane, G. Burrieschi, M. Tavakoli, and A. M. Seifalian, “Polymeric heart valves: new materials, emerging hopes,” *Trends in Biotechnology*, vol. 27, no. 6, pp. 359–367, 2009.
- [104] D. Roe, B. Karandikar, N. Bonn-Savage, B. Gibbins, and J.-B. Roulet, “Antimicrobial surface functionalization of plastic catheters by silver nanoparticles,” *Journal of Antimicrobial Chemotherapy*, vol. 61, no. 4, pp. 869–876, 2008.
- [105] S.-H. Hsu, H.-J. Tseng, and Y.-C. Lin, “The biocompatibility and antibacterial properties of waterborne polyurethane-silver nanocomposites,” *Biomaterials*, vol. 31, no. 26, pp. 6796–6808, 2010.
- [106] A. de Mel, K. Chaloupka, Y. Malam, A. Darbyshire, B. Cousins, and A. M. Seifalian, “A silver nanocomposite biomaterial for blood-contacting implants,” *Journal of Biomedical Materials Research—Part A*, vol. 100, no. 9, pp. 2348–2357, 2012.
- [107] F. Paladini, M. Pollini, D. Deponti, A. di Giancamillo, G. Peretti, and A. Sannino, “Effect of silver nanocoatings on catheters for haemodialysis in terms of cell viability, proliferation, morphology and antibacterial activity,” *Journal of Materials Science: Materials in Medicine*, vol. 24, no. 4, pp. 1105–1112, 2013.
- [108] C.-W. Chou, S.-H. Hsu, and P.-H. Wang, “Biostability and biocompatibility of poly(ether)urethane containing gold or silver nanoparticles in a porcine model,” *Journal of Biomedical Materials Research Part A*, vol. 84, no. 3, pp. 785–794, 2008.
- [109] P. Lackner, R. Beer, G. Broessner et al., “Efficacy of silver nanoparticles-impregnated external ventricular drain catheters in patients with acute occlusive hydrocephalus,” *Neurocritical Care*, vol. 8, no. 3, pp. 360–365, 2008.
- [110] A. Akhavan, A. Sodagar, F. Mojtahedzadeh, and K. Sodagar, “Investigating the effect of incorporating nanosilver/nanohydroxyapatite particles on the shear bond strength of orthodontic adhesives,” *Acta Odontologica Scandinavica*, vol. 71, no. 5, pp. 1038–1042, 2013.
- [111] G. Chladek, J. Kasperski, I. Barszczewska-Rybarek, and J. Zmudzki, “Sorption, solubility, bond strength and hardness of denture soft lining incorporated with silver nanoparticles,” *International Journal of Molecular Sciences*, vol. 14, no. 1, pp. 563–574, 2013.
- [112] A. P. R. Magalhães, L. B. Santos, L. G. Lopes et al., “Nanosilver application in dental cements,” *ISRN Nanotechnology*, vol. 2012, Article ID 365438, 6 pages, 2012.

Review Article

Recent Applications of Nanomaterials in Prosthodontics

Wei Wang,¹ Susan Liao,² Yuhe Zhu,¹ Ming Liu,¹ Qian Zhao,¹ and Yating Fu¹

¹Department of Prosthodontics, School of Stomatology, China Medical University, Shenyang 110002, China

²School of Materials Science and Engineering, Nanyang Technological University, Singapore 639798

Correspondence should be addressed to Wei Wang; yuhe740442@hotmail.com

Received 8 January 2015; Revised 30 March 2015; Accepted 30 March 2015

Academic Editor: Sang C. Lee

Copyright © 2015 Wei Wang et al. This is an open access article distributed under the Creative Commons Attribution License, which permits unrestricted use, distribution, and reproduction in any medium, provided the original work is properly cited.

In recent years, lots of researches have been launched on nanomaterials for biomedical applications. It has been shown that the performances of many biomaterials used in prosthodontics have been significantly enhanced after their scales were reduced by nanotechnology, from micron-size into nanosize. On the other hand, many nanocomposites composed of nanomaterials and traditional metals, ceramics, resin, or other matrix materials have been widely used in prosthodontics because their properties, such as modulus elasticity, surface hardness, polymerization shrinkage, and filler loading, were significantly increased after the addition of the nanomaterials. In this paper, the latest research progress on the applications of nanometals, nanoceramic materials, nanoresin materials, and other nanomaterials in prosthodontics was reviewed, which not only gives a detailed description of the new related investigations, but also hopefully provides important elicitation for future researches in this field.

1. Introduction

Prosthodontics is an important branch of the oral medicine. With the improvement of people's living standards and the promotion of oral health knowledge, prosthodontics increasingly received widespread attention. Prosthodontics is mainly for dental defects, treatment after tooth loss, such as lays, crowns, and dentures, also including the use of artificial prostheses for periodontal disease, temporomandibular joint disease, and maxillofacial tissue defects [1–4]. The main purposes of dentures are to restore dental function and facial appearance and maintain the wearer's health. Dental materials of dentures can be divided into mainly three categories: resin, ceramic, and metal. They are important to fabricate dental prosthesis, which directly contacts with the oral mucosa and is under long-term use in the oral environment, so the dental materials must have comprehensive properties and good biological activity to function properly. Dental materials should have certain mechanical strength, hardness, higher fatigue strength, high elastic modulus, low thermal and electrical conductivity, good castability, and less shrinkage deformation. Chemical stability is also required, such as corrosion resistance, being not easily broken, and aging. The colors of dental materials can be formulated and

maintain long-term stability. As a good oral material, it should have good biocompatibility and safety and be biofunctional [2–4]. However, due to the nature of the material itself, continued use for long period in moist environment, a variety of problems will occur during wear dentures, such as pigment adhesion, color change, and aging fracture.

In recent years, nanomaterials have captured more and more attention because of their unique structures and properties. The concept of “nanomaterials” formed in the early 1980s, referring to zero-dimensional, one-dimensional, two-dimensional, and three-dimensional materials with a size of less than 100 nm [5, 6]. Nanomaterials can be divided into four categories of nanopowder, nanofiber, nanomembrane, and nanoblock, in which development of nanopowder is longest, and its technology is most mature [6]. Nanomaterials have small size, large surface area, high surface energy, a large proportion of surface atoms, and four unique effects: small size effect, quantum size effect, quantum tunneling effect, and surface effect [7]. Development of nanomaterials has greatly enriched the field of research in materials science including biomaterials. As people understanding of natural biological material properties and microstructure at nanoscale is gradually deepening, the role of nanomaterials in biomedical material science is more important [7, 8]. Studies showed that

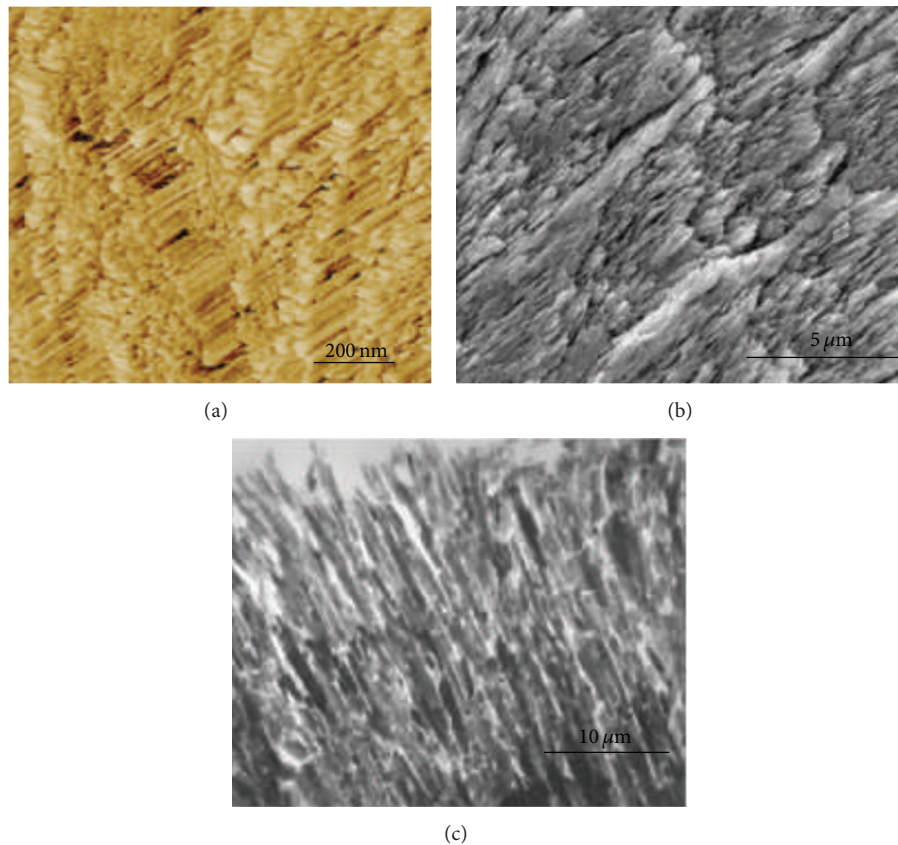


FIGURE 1: Hierarchical structure of the dental enamel. The enamel is composed of three-dimensionally organized nanosized hydroxyl apatite crystallites. (a) Atomic force microscope, (b) scanning electron microscope images of the enamel surface, and (c) transmission electron microscope [9].

a natural tooth is biological nanomaterial, which is composed of enamel, dentin, and cementum with nanoscale particles.

Dental enamel comprises 80–90% volume of calcium-deficient carbonate hydroxyl apatite. Mature-human-enamel crystallites are 26.3 ± 2.2 nm thick, 68.3 ± 13.4 nm wide, and between 100 and 1,000 nm long (Figure 1) [9, 10]. Dentine is a hydrated tissue made up of approximately 50 vol.% mineral, 30 vol.% collagenous and noncollagenous proteins, and 20 vol.% fluids. The dentinal matrix is mainly composed of type I collagen fibrils forming a three-dimensional scaffold matrix, reinforced by hydroxyl apatite crystallites, measuring approximately 20 nm in size [11, 12]. This natural dental hard tissue structure provides a foundation platform for biological research of nanomaterials with biomimetic manners.

Nanomaterials have been developed promptly and some researches of nanomaterials have been carried out on prosthodontics. Many of the current dental materials are available through nanocrystallization to improve their original performance and play continuously key role in oral applications. Research of nanotechnology in dental materials is mainly focused on two ways: one is the preparation of new inorganic nanoparticles, and the other is to modify the surface with inorganic nanofillers and thereby to develop ultralow shrinkage rate of repair resin [13]. Through the development of nanocomposites, properties such as modulus

of elasticity, surface hardness, polymerization shrinkage, and filler loading were enhanced by the addition of nanomaterials [14, 15]. Nanocomposite denture base has higher interfacial shear bond strength between the resin matrix and nanomaterials, compared to the conventional resin matrix. It is because that this supermolecular bonding covers or shields the nanomaterials and creates thick interface, which enhances the bond between the resin molecules and creates higher molecular weight polymers [16]. Nanomaterials are mainly used in ceramic, resin, and metal, providing a huge space for the improvement and innovation of dental material. Nanoceramic material has small grain size and the inherent porosity of materials greatly reduced, on one hand improving the flexibility, strength, and plasticity and on the other hand making its elastic modulus similar to natural bone, greatly improving the mechanical compatibility and biocompatibility [15–17]. The emergence of nanoresin may change the nature of the resin that is easy to be aging and increase its strength [16–19]. Studies of nanometal showed that it might have better antibacterial property [20].

In this paper, we briefly reviewed the development history of prosthodontics materials including metals, ceramics, and resin and evaluated the research and application of nanomaterials in prosthodontics. The properties of those prosthodontic materials were summarized in Table 1.

TABLE 1: Properties of prosthodontics materials.

Dental materials	PMMA	Ceramics			Metal		
		ZrO ₂	Al ₂ O ₃	glass ceramic	Ti6Al4V	CoCrMo	CoCr
Advantage	Good biocompatibility, aesthetics processability, and reparability [3]	High strength, suitable color, and low thermal and electrical conductivity [21]			Titanium alloy has high strength, low density, light weight, low shrinkage, nonmagnetic, good mechanical properties and corrosion resistance, and nonallergic, teratogenic, and carcinogenic. CoCr alloy has high strength, wear resistance, and less tooth tissue cutting, with good biological safety CoCrMo has good corrosion resistance, wear resistance, ductility, gloss, anti-plaque adhesion and biosafety		
Disadvantage	Poor strength, low fracture resistance radiopacity behavior, and microbial adhesion [2, 4, 18, 20]	Low ductility and brittleness [21]			Further improvement is desired to improve the corrosion resistance and biocompatibility of the Ti and CoCrMo alloy CoCr alloy easily leads to sensitive symptoms		
Nanoresearch	TiO ₂ nanoparticle reinforced the mechanical behavior of PMMA [17] Well-dispersion nano-ZrO ₂ particles can improve the modulus and strength and maintain or even improve ductility [17] Ag TiO ₂ and Fe ₂ O ₃ particles significantly reduce adherence of <i>C. albicans</i> of PMMA and do not affect metabolism or proliferation [22–24]	The hardness and fracture toughness increased of nanozirconia ceramics [25] Glass ceramics with nanosized grains showed excellent corrosion resistance, high fracture toughness, and translucency [26]			Nanophase metals (specifically, Ti, Ti6Al4V, and CoCrMo alloys) promote osteoblast adhesion, proliferation, differentiation, and mineralization [27–29]		

2. Nanomaterials Applied in Prosthodontics

2.1. Nanometal Materials in Prosthodontics. Currently, most metal stents of partial denture are applying cobalt-chromium alloy or cobalt-chromium-molybdenum alloy and titanium alloy [27–29]. The initial cobalt-based alloy is cobalt-chromium binary alloy and is then developed into cobalt-chromium-tungsten alloy and later developed into cobalt-chromium-molybdenum alloy [27]. Its mechanical properties and corrosion resistance are better than stainless steel or gold alloy [28, 29]. Another metal material that is often used in prosthodontics is titanium alloys because of its outstanding properties which are close to natural human bones, such as high specific strength, good biological security, high corrosion resistance, and elastic modulus. Although those metal prosthodontics materials have excellent mechanical properties, less tooth tissue cutting, and good biological security, biological integration is usually unsatisfactory, and some patients are prone to allergies, causing skin, mucous membrane inflammation [22, 30, 31]. Satisfactory biological integration of the implant surfaces with the surrounding host tissues is one of the most important elements for long-term success of dental implants. Modification of titanium implant surfaces into nanostructures has been found to be able to improve their biological integration with surrounding

soft tissues. Dorkhan et al. modified the surface of titanium implant by anodic oxidation into nanoscales with pores in the 50 nm range and found that both the vitality and the adherence level of soft-tissue cells, such as keratinocytes and fibroblasts, on the nanostructured surfaces were similar to those on pure titanium, while the attachment of oral streptococci on the nanostructured surfaces was significantly lower than on the pure titanium [32, 33], suggesting that the nanostructured surfaces of metal implants might be capable of improving surrounding host tissue cell adherence while minimizing bacterial attachment.

Another nonnegligible disadvantage for titanium alloy as oral implant material is its relatively poor wear resistance. To overcome the drawback, nanostructured ceramic coatings such as TiN, ZrO₂/Al₂O₃, Si₃N₄/TiO₂, and ZrO₂/SiO₂ are being used [23, 24, 34–37]. Sathish et al. coated a novel nanostructured bilayered ZrO₂/Al₂O₃-13TiO₂ on biomedical Ti-13Nb-13Zr alloy. The bilayered coating was shown to exhibit 200- and 500-fold increase in the wear resistance, compared to the monolayer Al₂O₃-13TiO₂ and ZrO₂, respectively, because of its higher adhesion strength and lower porosity [38]. Many studies have demonstrated increased functions of osteoblasts on nanophase compared to conventional materials such as ceramics, polymers, carbon nanofibers or nanotubes, and their composites. For example, Li et al. investigated

the functions of human adipose-derived stem cells cultured on carbon nanotubes, compared to those of the cells cultured on microstructured graphite that have the same composition and layered structure with carbon nanotubes. The cells attached and proliferated better on carbon nanotubes. Moreover, the cells synthesized more alkaline phosphatase and deposited more extracellular calcium on carbon nanotubes [39]. So whether nanometal possesses better biological activity than traditional metal attracted researchers' attention. At present, many studies have shown that titanium and titanium alloy with nanosizes have better biocompatibility than traditional titanium and titanium alloy. Researchers have fabricated metal surface nanocrystallization by different methods for improving biological activity of the metal. Lan et al. [40] prepared a nanotextured titanium surface using a chemical etching technique and studied the effects of a nanotextured titanium surface on murine preosteoblastic cells adherence, proliferation, differentiation, and mineralization *in vitro*, setting rough and smooth surfaces of pure titanium as controls. A characteristic nanotexture was formed on the titanium surface according to the result of SEM. The number of cells attached to the nanotextured titanium surface was higher than that of the cells attached to smooth surfaces of pure titanium after the incubation of 30, 60, and 120 minutes, respectively. Under SEM for the nanotextured surface, more adherent cells and larger spreading areas were observed. The proliferation of cells, after 3 and 5 days, was significantly higher on the nanotextured surface than controls according to the results of CCK-8 test. The alkaline phosphatase activity of the cells on the nanotextured titanium surface was higher at 7 days than 3 and 5 days. In addition, a larger amount of calcified nodules could be observed on the nanotextured titanium surface 14 days later. The results above suggest that it should be better to further consider nanotechnologies for prosthodontic implant applications.

Yao et al. [41] created nanometer surface features on titanium and Ti6Al4V implants by anodization, which was a quick and relatively inexpensive electrochemical method. The results showed that the anodized surfaces had higher root-mean-square roughness at nanoscale dimensions than the unanodized Ti-based surfaces. Most important of all, as compared to respective unanodized counterparts, osteoblast adhesion was enhanced on the anodized metal substrates according to the results of *in vitro* studies. Thus, it demonstrated that anodization of Ti-based metals might create nanometer surface features that could promote osteoblast adhesion.

Webster and Eijofor further provided the evidence of increased osteoblast adhesion on Ti, Ti₆Al₄V, and CoCrMo compacts with nanometer compared to conventionally sized metals [20]. In their study, each respective group of nanophase and conventional metals possessed the same material properties (chemistry and shape) and altered only in dimension. Human osteoblasts were seeded and placed in standard cell culture conditions for either 1 or 3 h. As expected, the dimensions of nanometer surface features gave rise to larger amounts of interparticulate voids in nanophase Ti and Ti₆Al₄V. Osteoblast adhesion was significantly greater on nanophase Ti, Ti₆Al₄V, and CoCrMo

when compared to their conventional counterparts after 1 and 3 h and osteoblast adhesion occurred primarily at particle boundaries (Figure 2). Since nanophase materials possess increased particle boundaries at the surface (due to smaller particle size), this may be an explanation for the increased osteoblast adhesion measured on nanophase formulations. This study implies further enhanced adhesion of osteoblasts on nanophase Ti, Ti₆Al₄V, and CoCrMo. The result suggests that nanophase metals may be a kind of potential materials in prosthodontics or implant applications.

2.2. Nanoceramics Materials in Prosthodontics. Ceramics have been used in manufacture of dental dentures because of their high strength, suitable color, and low thermal and electrical conductivity [21]. At present, ceramic dental crown is mainly including alumina ceramic and zirconia ceramic. Traditional ceramics are made of clay and other natural occurring materials, while modern high-tech ceramics use silicon carbide, alumina, and zirconia. The development of ceramic crown experienced long essence of ceramic materials: hydroxyapatite (HA) ceramic, glass ceramic, alumina ceramic, and zirconia ceramic. Alumina ceramics have good aesthetics, high gloss, chemical stability, wear resistance, high hardness, good biocompatibility, no allergies, and no effect on the MRI, but the biggest drawback is crisp, and it is likely to porcelain crack [42]. ZrO₂ has a good abrasion resistance, physiological corrosion resistance, and biocompatibility, whose modulus of elasticity, flexural strength, and hardness are higher, compared to those of HA and titanium alloys. The strength and bending resistance of zirconia ceramics through computer aided design/computer aided manufacture are significantly higher than alumina ceramic, but they still lack toughness and high sintering temperature [43].

Because the low ductility and brittleness of ceramics directly influence and limit the development of the traditional ceramic materials, we hope that nanostructured ceramics may offer some specific improvements. In addition, dental applications of ceramic materials add aesthetic requirements (colour, translucency) to the mechanical specifications. Nanostructured ceramics may meet the need for translucency of dental restoration. Examples of transparent or highly translucent ceramics (alumina, YAG, etc.) are already published but not dedicated to the clinical application [44, 45]. Nanoceramic refers to the ceramic material with nanoscale dimensions in the microstructures phase. Compared with the conventional ceramics, nanoceramics have unique properties, which make it become the hot topics in the study of material science. Firstly, nanoceramics have superplasticity. Ceramic is essentially a kind of brittle material; however, nanoceramic shows good toughness and ductility. As far as the arrangement of atoms in nanoceramics interface is quite confusing, the atoms are very easy to migrate under the conditions of force deformation. Secondly, compared to the conventional ceramics, nanoceramic has the superior mechanical properties, such as strength and hardness increasing significantly. The hardness and strength of many nanoceramics are four to five times higher than those of the traditional materials. For example, at 100°C the microhardness of nano-TiO₂ ceramics is 13,000 kN/mm², while

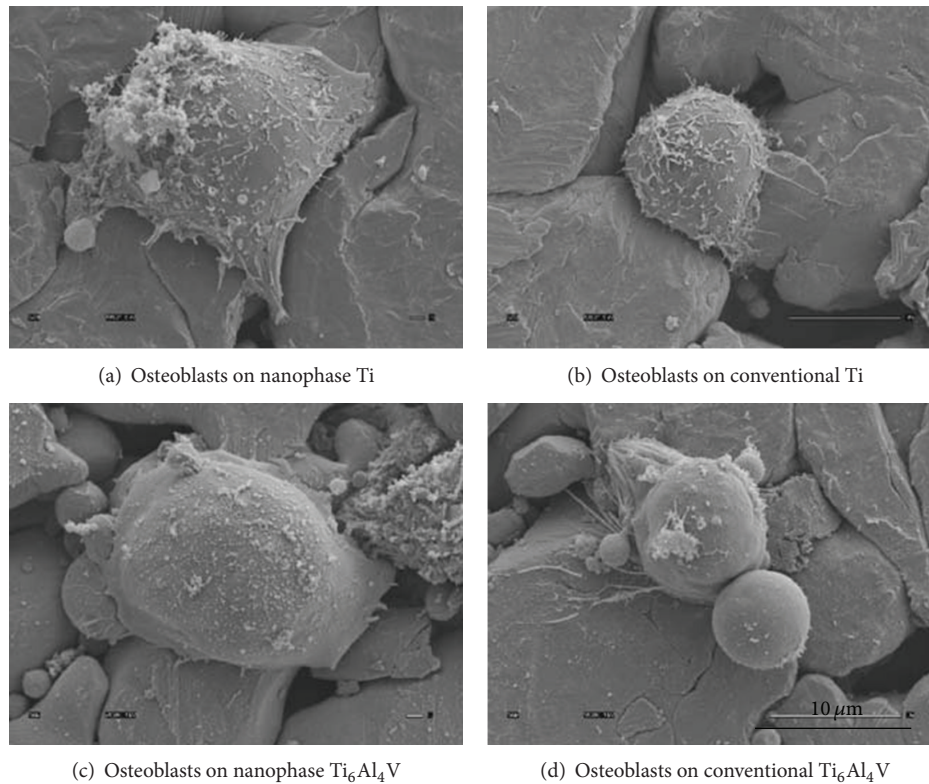


FIGURE 2: SEM images of osteoblasts on Ti and Ti₆Al₄V compacts, respectively [20].

that of ordinary TiO₂ ceramics is lower than 2,000 kN/mm². Most importantly, toughness of nanoceramics is much higher than that of traditional ceramics. At room temperature, nano-TiO₂ ceramic exhibits very high toughness. When compressed to 1/4 of the original length, it was still intact without being broken [46].

Li et al. reported the different physical properties of nano-ZrO₂ ceramic materials from the traditional ones. The hardness of traditional ZrO₂ was generally around 1,500, and its fracture toughness was very low, so breakage or crack might easily occur in the processing. However, the hardness of nanozirconia ceramics could reach more than 1,750, increased by about 20%. Not only does its hardness increase, but also the fracture toughness also increased accordingly [47]. Wang et al. reported the influence of nano-ZrO₂ content on the mechanical properties and microstructure of nano-ZrO₂ toughened Al₂O₃ and found that the composite had better toughness with 20% nano-ZrO₂, very suitable as dental all-ceramic restoratives [25].

Glass ceramics based on lithium disilicate with lack of mechanical properties are commonly used in dental veneers and crowns. Due to insufficient mechanical properties of glass ceramics, failure clinical cases have been often reported. To improve mechanical properties of glass ceramics based on lithium disilicate, Persson et al. used a sol-gel method to produce glass ceramics in the zirconia-silica system with nanosized grains, which was found to be translucent, with a transmittance of over 70%, and possessed excellent corrosion resistance. It also presented a somewhat lower elastic

modulus but higher hardness than the conventional lithium disilicate [26].

Carbon nanotubes (CNTs) have attracted remarkable attention as reinforcements of materials because of their exceptional mechanical and electronic properties. Furthermore, CNTs have been considered as reinforcing elements in ceramic matrix composites due to their unique mechanical properties [48, 49]. An et al. produced alumina-CNT composites by hot-pressing and investigated the mechanical and tribological properties of alumina-CNT composites (Figure 3) [50]. The results showed that wear and mechanical properties were enhanced in the range of 0–4% CNT content and the addition of CNTs up to 4% has a positive influence on the reinforcement effect, increased about 30%.

2.3. Nanoresin Based Materials in Prosthodontics. Currently, resin used in prosthodontics is mainly including polymethyl methacrylate (PMMA) and its modified products. PMMA is obtained by the polymerization of acrylic acid and its esters and is dating back over one hundred years of history. In 1937, the methyl acid lipid began to enter scale manufacturing and was applied to the denture base processing. The wide range of clinical applications of PMMA was successfully developed by the Kulzer Company in Germany in 1930. The main component of PMMA is polymethyl methacrylate, also containing small amounts of ethylene glycol dimethacrylate [51]. PMMA has good mechanical properties such as high hardness, rigidity, discontinuity deformation, biological properties, aesthetic properties, and easy processing

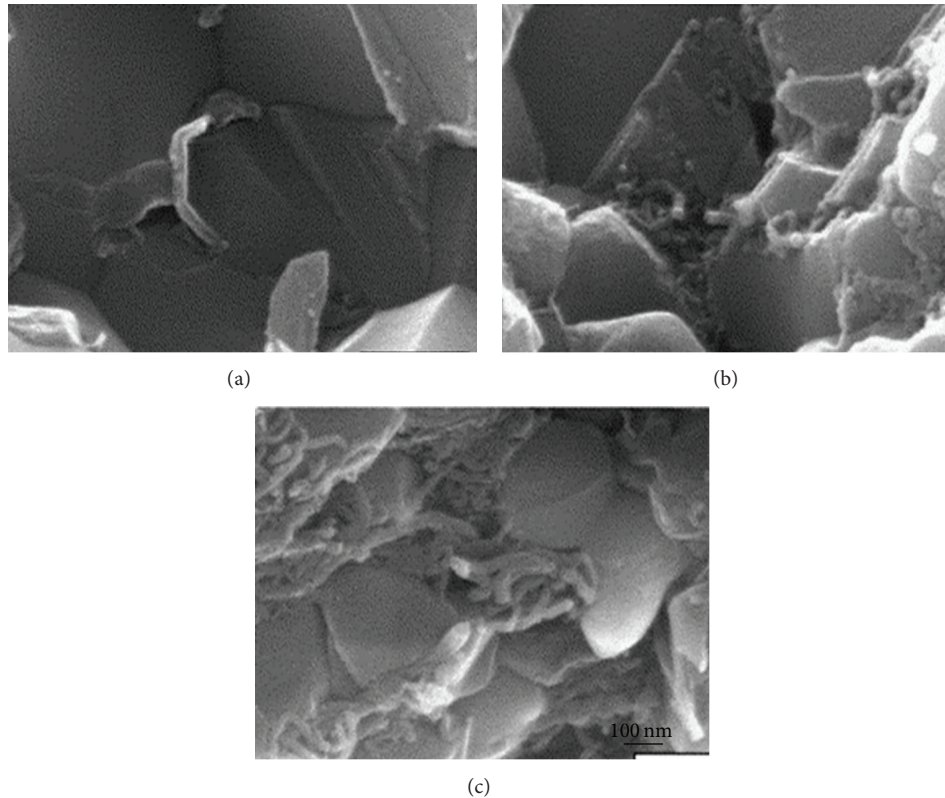


FIGURE 3: The fractured surface morphologies of the hot-pressed alumina composites: (a) with 2.7 wt% CNT content, (b) with 4.1 wt% CNT content, and (c) with 12.5 wt% CNT content [50].

characteristics. Its main disadvantages are the instability of color, poor resistance to wear and tear, volume shrinkage after the polymerization, oral mucosa irritation, and aging, and staining or discoloration relatively easily occurs [3].

Nowadays, most products for dental restoration have been produced from acrylic resins based on heat-cured PMMA, due to its optical properties, biocompatibility, and aesthetics [52, 53]. However, it has a long-standing drawback that is lack of strength particularly under fatigue failure inside the mouth and also shows low abrasion resistance and microbial adhesion onto PMMA to long-term PMMA wearers. Therefore, some studies are still ongoing in order to solve these problems and improve acrylic polymers properties for artificial dentures [54]. Recently, much attention has been directed toward the incorporation of inorganic nanoparticles into PMMA to improve its properties. Various nanoparticles such as ZrO_2 , TiO_2 , and CNT have been used to improve the performance of PMMA, and the results showed that desired mechanical property enhancement can be achieved in those composites with small amounts of nanoparticles [16–19].

The mechanical behaviors of TiO_2 nanoparticle-reinforced resin-based dental composites were characterized in the paper of Hua et al., using a three-dimensional nano-scale representative volume element [16]. The results clearly showed that, to achieve the same reinforcing effect with microcomposites, nanocomposites needed much lower volume fraction of reinforcing media because nanoparticles with

aspect ratio larger than 30 could nearly make the reinforcing effect reach saturation. For example, the reinforcing effect of the nanoparticle with 3% volume fraction on the stiffness is the same as that of the glass fiber with 6% volume fraction. These results might provide us with valuable inspiration to optimize the compositions of dental composites. Mohammed and Mudhaffar [17] designed and evaluated the addition of modified ZrO_2 nanomaterials in different percentage (2 wt%, 3 wt%, and 5 wt%) to heat-cured acrylic resin PMMA materials. Abrasive wear resistance and tensile and fatigue strength showed highly significant increase with 3 wt% and 5 wt% of nanofillers, compared to pure PMMA materials. The same results were showed in the study of Hong et al. where methacryloxypropyltrimethoxysilane- (MPS-) modified colloidal silica nanoparticles were added to PMMA, which caused a significant increase in tensile strength and tensile modulus [18].

CNTs and carbon nanofibrils have been used as reinforcements or additives in various materials to improve the properties of the matrix materials. Cooper et al. prepared the composites consisting of different quantities of CNTs or carbon nanofibrils in a PMMA matrix using a dry powder mixing method (Figure 4). The results showed that the impact strength of the composites was significantly improved by even small amounts of single-wall nanotubes [19].

In dentistry, adhesion and plaque formation onto PMMA-based resins is a common source of oral cavity infections and

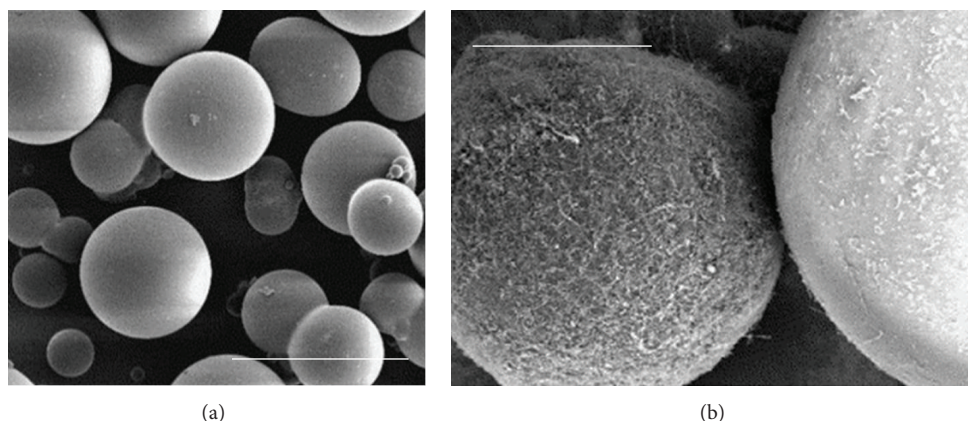


FIGURE 4: (a) SEM micrograph of as-received PMMA particles (scale bar: 200 μm); (b) SEM micrograph of PMMA particles with nanofibrils spread over the surface (4 wt% nanofibrils) (scale bar: 50 μm).

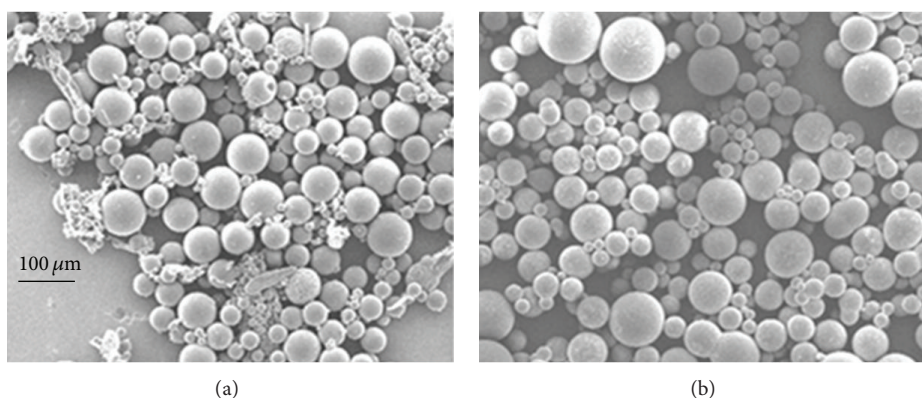


FIGURE 5: SEM of standard (a) and nanopigmented PMMA (b) at $\times 100$ magnification [62].

stomatitis [55, 56]. Some researchers showed that the addition of metal nanoparticles such as TiO_2 , Fe_2O_3 , and silver to PMMA materials could increase the surface hydrophobicity to reduce bimolecular adherence [57–59].

In recent years, metal oxide nanoparticles (e.g., TiO_2 , silver) have been largely investigated for their performances as antimicrobial additives. In particular, TiO_2 is now considered as a low-cost, clean photocatalyst with chemical stability and nontoxicity [60, 61]. Laura et al. prepared the PMMA composites, adding TiO_2 and Fe_3O_2 nanoparticles, for simultaneously coloring and/or improving the antimicrobial properties of PMMA (Figure 5). PMMA containing nanoparticles showed a lowered *Candida albicans* (*C. albicans*) cells adhesion and a lower porosity, compared to standard PMMA. Because high porosities have been considered a critical drawback for PMMA in prosthodontics applications, metal oxide nanoparticles might be suitable additives for the improvement of PMMA formulations [62]. These results indicated that nanostructured metal coloring additives are a promising means for producing nontoxic hybrid materials with antimicrobial properties for dentistry applications.

Silver (Ag) has been well known for its antimicrobial properties and has a long history of application in medicine with well-tolerated tissue response and low toxicity profile.

The antimicrobial action of Ag may be proportional to the amount of released bioactive silver ions (Ag^+) and their interaction with bacterial cell membranes [63–66]. Silver nanoparticles can kill all pathogenic microorganisms, and no report as yet has shown that any organism can readily build up resistance to them. In dentistry, some studies of the antibacterial effect of dental materials incorporating silver were made [67–69]. Yoshida et al. showed that a resin composite incorporated with silver-containing nanomaterials had a long-term inhibitory effect against *S. mutans* [70]. Laura et al. formulated PMMA-silver nanocomposites, with fairly good dispersion of silver nanoparticles in the polymer matrix. And the results showed that PMMA-silver nanocomposites significantly reduced adherence of *C. albicans* and did not affect metabolism or proliferation. They also did not appear to cause genotoxic damage to cells. These results demonstrated that PMMA-silver nanoparticles might be a kind of suitable candidates to produce nontoxic materials with antimicrobial properties for use in dentistry [71]. The same results were demonstrated in the study of Monteiro et al., where silver nanoparticles were incorporated in the PMMA denture resin to attain an effective antimicrobial material to help control common infections involving oral mucosal tissues in complete denture wearers, because the nanocomposites had good

efficacy against *C. albicans* [59]. Silver has been shown to be a biocompatible material being used for a range of medical devices. Recently, Ag nanoparticles with a high surface area were incorporated into resins to reduce the Ag particle concentration necessary for efficacy, without compromising the composite color and mechanical properties. Regarding the durability, Ag-containing nanocomposites showed long-term antibacterial effects and inhibited *S. mutans* growth for more than 6 months [72–74].

However, although there are a lot of the studies on nanoresins, most of them belong to basic researches. We hope in the near future that nanoresin can be widely used in the field of clinical prosthodontics.

3. Brief Description of Nanomaterials' Applications in Other Aspects of Dentistry

Nanotechnology and nanomaterials are widely carried out not only in the field of prosthodontics, but also in other areas of dentistry, such as oral medicine, oral surgery, and preventive dentistry, and so forth. We believe that with the study of nanotechnology and nanomaterials research dental medicine will be able to make great progress and open up new ways to benefit patients.

3.1. The Application of Nanocomposites for Oral Medicine.

Currently, the main material of oral medicine is composite resin filling materials, and composite resin repairing dental defects has been of more than 40 years of history. The properties of composite resin have some shortcomings such as polymerization shrinkage being easy to form microleakage, low wear resistance, and low mechanical strength. Because nanoparticles have unique properties, such as many unpaired atoms, less surface defects, and large surface area, combined with polymer with the occurrence of strong chemical or physical binding, thus they have higher strength and toughness. Many kinds of nanoparticles have been widely used in oral medicine composite resin, such as nanosilica, nanozirconia, nanohydroxyapatite, and nanotitanium oxide, and so forth [51]. Addition of nanoparticles in composite resin can increase strength and toughness of the composite resin. Due to small particle size, composite resins with nanoparticles significantly reduce the effect of polymerization shrinkage and dramatically improve physical properties [75]. In addition, composites containing nanofillers resulted in smooth surfaces with their ease of polish ability, increased abrasion resistance, and surface hardness [76].

3.2. The Application of Nanocomposites for Oral Surgery.

Mandibular bone defects caused by the cyst are a kind of common diseases in oral surgery. Facial deformities caused by the bone defects seriously affect the appearance of the patients. Exogenous bone implants have been commonly used to repair this kind of bone defects, which, however, have poor biocompatibility, higher probability of postoperative infection. Some nanomaterials such as nanohydroxyapatite have excellent biocompatibility, which have been shown to have high potential as repair materials to treat the oral

diseases caused by bone defects. They not only can be used as scaffolds for new bone formation, but also have the ability to promote the osteogenic differentiation and biomineralization of cells, which play very important roles in the bone defect repair. For example, the addition of nanohydroxyapatite, a simple operation, can not only fill the bone defects and avoid the infection problems, but also obviously induce new bone induction, which suggests that it should have high potential to be widely used in oral surgery.

At another important aspect, the oral cancer has become a serious threat to human life. The biggest problem of the oral cancer chemotherapy is currently low local concentration of the drug and large systemic toxicity. Precise dose delivery to malignant tissue in radiotherapy is of great importance for effectively treating the cancer efficacy while minimizing morbidity of surrounding normal tissues. Several researches have showed that some nanoparticles such as magnetic nanoparticles could be used for tumor targeted therapy. Due to the small diameter of the nanoparticles, they can be directly with the bloodshed to evenly penetrate into the tumor site and tumor tissue, improving the therapeutic index of drugs, reducing the toxicity of drugs, and getting the desired effect of complete tumor regression [77–79]. Therefore, the use of nanomaterials is one of promising means to accurately highlight tumor cells and deliver therapeutics specifically to the tumor to maximize tumor cell killing and normal tissue sparing.

3.3. The Application of Nanocomposites for Preventive Dentistry.

The purpose of preventive dentistry is the early prevention of tooth decay rather than invasive restorative therapy. However, the prevention of early caries lesions is still challenge for dental research. Recent studies show that nanotechnology might provide novel strategies in preventive dentistry. Biomimetic approaches have been used to develop nanomaterials for inclusion in a variety of oral health-care products, such as liquids and pastes that contain nanoapatites for biofilm management at the tooth surface and products that contain nanomaterials for the remineralization of early submicrometre-sized enamel lesions. Dental caries is caused by bacterial biofilms on the tooth surface. Nanocomposite surface coatings can make the tooth surface easy to clean, prevent the pathogenic consequences, and reduce bacterial adherence [80–82]. The toothpastes that contain the apatite nanoparticles can be used for biofilm management nanomaterials and can be used as an approach for remineralization of submicrometre-sized enamel lesions [9, 83, 84]. However, currently these oral prevention products with nanoparticles are also still in the research stage and intensive study is necessary for clinical application in the future.

4. Concluding Remarks

Future development of prosthodontics technology has been recognized to be dependent on the progress of materials science. Nanomaterials have been playing a significant role in basic scientific innovation and clinical technological change of prosthodontics. In this paper, the latest research progress on the applications of nanometals, nanoceramic, nanoresin,

and other nanomaterials in prosthodontics was reviewed, which clearly shows that many properties, such as modulus elasticity, surface hardness, polymerization shrinkage, and filler loading, of materials used in prosthodontics can be significantly improved after their scales were reduced from micron-size into nanosize by nanotechnology and that the performances of composites can be also enhanced by adding appropriate nanomaterials. We hope that this review article could provide some valuable elicitation for the future scientific and technological innovations in the related field.

Conflict of Interests

The authors declare that there is no conflict of interests regarding the publication of this paper.

Acknowledgments

The authors acknowledge the financial support from the Shenyang city science and technology project (F14-158-9-37). The authors acknowledge the graduate students in Department of Prosthodontics, School of Stomatology, China Medical University, for their kind help.

References

- [1] C. S. Petrie, M. P. Walker, and K. Williams, "A survey of U.S. prosthodontists and dental schools on the current materials and methods for final impressions for complete denture prosthodontics," *Journal of Prosthodontics*, vol. 14, no. 4, pp. 253–262, 2005.
- [2] M. Mehra, V. Farhad, and W. Robert, "A complete denture impression technique survey of postdoctoral prosthodontic programs in the United States," *Journal of Prosthodontics*, vol. 23, pp. 320–327, 2014.
- [3] G. Saavedra, L. F. Valandro, F. P. P. Leite et al., "Bond strength of acrylic teeth to denture base resin after various surface conditioning methods before and after thermocycling," *International Journal of Prosthodontics*, vol. 20, no. 2, pp. 199–201, 2007.
- [4] J. L. Cuy, A. B. Mann, K. J. Livi, M. F. Teaford, and T. P. Weihs, "Nanoindentation mapping of the mechanical properties of human molar tooth enamel," *Archives of Oral Biology*, vol. 47, no. 4, pp. 281–291, 2002.
- [5] M. S. Soh, A. Sellinger, and A. U. J. Yap, "Dental nanocomposites," *Current Nanoscience*, vol. 2, no. 4, pp. 373–381, 2006.
- [6] I. Roy, M. K. Stachowiak, and E. J. Bergey, "Nonviral gene transfection nanoparticles: function and applications in the brain," *Nanomedicine: Nanotechnology, Biology, and Medicine*, vol. 4, no. 2, pp. 89–97, 2008.
- [7] X. M. Li, Q. Feng, R. Cui et al., "The use of nanoscaled fibers or tubes to improve biocompatibility and bioactivity of biomedical materials," *Journal of Nanomaterials*, vol. 2013, Article ID 728130, 16 pages, 2013.
- [8] X. M. Li, L. Wang, Y. B. Fan, Q. L. Feng, and F.-Z. Cui, "Biocompatibility and toxicity of nanoparticles and nanotubes," *Journal of Nanomaterials*, vol. 2012, Article ID 548389, 19 pages, 2012.
- [9] M. Hannig and C. Hannig, "Nanomaterials in preventive dentistry," *Nature Nanotechnology*, vol. 5, no. 8, pp. 565–569, 2010.
- [10] L. Wang, X. Guan, H. Yin, J. Moradian-Oldak, and G. H. Nancollas, "Mimicking the self-organized microstructure of tooth enamel," *Journal of Physical Chemistry C*, vol. 112, no. 15, pp. 5892–5899, 2008.
- [11] L. E. Bertassoni, S. Habelitz, J. H. Kinney, S. J. Marshall, and G. W. Marshall Jr., "Biomechanical perspective on the remineralization of dentin," *Caries Research*, vol. 43, no. 1, pp. 70–77, 2009.
- [12] V. Imbeni, J. J. Kruzic, G. W. Marshall, S. J. Marshall, and R. O. Ritchie, "The dentin-enamel junction and the fracture of human teeth," *Nature Materials*, vol. 4, no. 3, pp. 229–232, 2005.
- [13] C. C. Trapalis, P. Keivanidis, G. Kordas et al., "TiO₂(Fe³⁺) nanostructured thin films with antibacterial properties," *Thin Solid Films*, vol. 433, no. 1–2, pp. 186–190, 2003.
- [14] R. B. Huang, S. Mocherla, M. J. Heslinga, P. Charoenphol, and O. Eniola-Adefeso, "Dynamic and cellular interactions of nanoparticles in vascular-targeted drug delivery (review)," *Molecular Membrane Biology*, vol. 27, no. 4–6, pp. 190–205, 2010.
- [15] S. K. Kim, S. J. Heo, J. Y. Koak et al., "A biocompatibility study of a reinforced acrylic-based hybrid denture composite resin with polyhedraloligosilsesquioxane," *Journal of Oral Rehabilitation*, vol. 34, no. 5, pp. 389–395, 2007.
- [16] Y. Hua, L. Gu, and H. Watanabe, "Micromechanical analysis of nanoparticle-reinforced dental composites," *International Journal of Engineering Science*, vol. 69, pp. 69–76, 2013.
- [17] B. D. S. D. Mohammed and B. D. S. M. Mudhaffar, "Effect of modified zirconium oxide nano-fillers addition on some properties of heat cure acrylic denture base material," *Journal of Baghdad College of Dentistry*, vol. 24, no. 4, pp. 1–7, 2012.
- [18] X. Y. Hong, L. Wei, and Q. Wei, "Nano technology: basic concepts and definition," *Clinical Chemistry*, vol. 40, p. 1400, 2003.
- [19] C. A. Cooper, D. Ravich, D. Lips, J. J. Mayer, and H. D. Wagner, "Distribution and alignment of carbon nanotubes and nanofibrils in a polymer matrix," *Composites Science and Technology*, vol. 62, no. 7–8, pp. 1105–1112, 2002.
- [20] T. J. Webster and J. U. Ejirofor, "Increased osteoblast adhesion on nanophase metals: Ti, Ti6Al4V, and CoCrMo," *Biomaterials*, vol. 25, no. 19, pp. 4731–4739, 2004.
- [21] H. W. Roberts, D. W. Berzins, B. K. Moore, and D. G. Charlton, "Metal-ceramic alloys in dentistry: a review," *Journal of Prosthodontics*, vol. 18, no. 2, pp. 188–194, 2009.
- [22] J. G. dos Santos, R. G. Fonseca, G. L. Adabo, and C. A. dos Santos Cruz, "Shear bond strength of metal-ceramic repair systems," *Journal of Prosthetic Dentistry*, vol. 96, no. 3, pp. 165–173, 2006.
- [23] S. van Bael, G. Kerckhofs, M. Moesen, G. Pyka, J. Schrooten, and J. P. Kruth, "Micro-CT-based improvement of geometrical and mechanical controllability of selective laser melted Ti6Al4V porous structures," *Materials Science and Engineering A*, vol. 528, no. 24, pp. 7423–7431, 2011.
- [24] Z. D. Liu, X. C. Zhang, F. Z. Xuan, Z. Wang, and S. Tu, "Effect of laser power on the microstructure and mechanical properties of TiN/Ti₃Al composite coatings on Ti6Al4V," *Chinese Journal of Mechanical Engineering*, vol. 26, no. 4, pp. 714–721, 2013.
- [25] G. K. Wang, H. Kong, K. J. Bao, J. J. Lv, and F. Gao, "Influence on mechanical properties and microstructure of nano-zirconia toughened alumina ceramics with nano-zirconia content," *West China Journal of Stomatology*, vol. 24, no. 5, 2006.
- [26] C. Persson, E. Onosson, I. Ajaxon, J. Engstrand, H. Engqvist, and W. Xia, "Nano grain sized zirconia-silica glass ceramics for dental applications," *Journal of the European Ceramic Society*, vol. 32, no. 16, pp. 4105–4110, 2012.

- [27] N. Tang, Y. P. Li, S. Kurosu, H. Matsumoto, Y. Koizumi, and A. Chiba, "Interfacial reactions between molten Al and a Co-Cr-Mo alloy with and without oxidation treatment," *Corrosion Science*, vol. 53, no. 12, pp. 4324–4326, 2011.
- [28] N. Tang, Y. P. Li, Y. Koizumi, S. Kurosu, and A. Chiba, "Interfacial reaction between Co-Cr-Mo alloy and liquid Al," *Corrosion Science*, vol. 75, pp. 262–268, 2013.
- [29] N. Tang, Y. Li, Y. Koizumi, and A. Chiba, "Nitridding of Co-Cr-Mo alloy in nitrogen," *Materials Chemistry and Physics*, vol. 145, no. 3, pp. 350–356, 2014.
- [30] G. H. L. Lombardo, R. S. Nishioka, R. O. A. Souza et al., "Influence of surface treatment on the shear bond strength of ceramics fused to cobalt-chromium," *Journal of Prosthodontics*, vol. 19, no. 2, pp. 103–111, 2010.
- [31] M. Pretti, E. Hilgert, M. A. Bottino, and R. P. Avelar, "Evaluation of the shear bond strength of the union between two CoCr-alloys and a dental ceramic," *Journal of Applied Oral Science*, vol. 12, no. 4, pp. 280–284, 2004.
- [32] M. Dorkhan, T. Yücel-Lindberg, J. Hall, G. Svensäter, and J. R. Davies, "Adherence of human oral keratinocytes and gingival fibroblasts to nano-structured titanium surfaces," *BMC Oral Health*, vol. 14, no. 1, article 75, 2014.
- [33] M. Dorkhan, J. Hall, P. Uvdal, A. Sandell, G. Svensäter, and J. R. Davies, "Crystalline anatase-rich titanium can reduce adherence of oral streptococci," *Biofouling*, 2014.
- [34] B. Liang, G. Zhang, H. Liao, C. Coddet, and C. Ding, "Friction and wear behavior of $\text{ZrO}_2\text{-Al}_2\text{O}_3$ composite coatings deposited by air plasma spraying: Correlation with physical and mechanical properties," *Surface and Coatings Technology*, vol. 203, no. 20–21, pp. 3235–3242, 2009.
- [35] M. Aliofkhazraei, A. S. Rouhaghdam, and T. Shahrabi, "Abrasive wear behaviour of $\text{Si}_3\text{N}_4/\text{TiO}_2$ nanocomposite coatings fabricated by plasma electrolytic oxidation," *Surface and Coatings Technology*, vol. 205, pp. S41–S46, 2010.
- [36] M. F. Morks and A. Kobayashi, "Development of $\text{ZrO}_2/\text{SiO}_2$ bioinert ceramic coatings for biomedical application," *Journal of the Mechanical Behavior of Biomedical Materials*, vol. 1, no. 2, pp. 165–171, 2008.
- [37] M. F. Morks, N. F. Fahim, and A. Kobayashi, "Structure, mechanical performance and electrochemical characterization of plasma sprayed SiO_2/Ti -reinforced hydroxyapatite biomedical coatings," *Applied Surface Science*, vol. 255, no. 5, pp. 3426–3433, 2008.
- [38] S. Sathish, M. Geetha, S. T. Aruna, N. Balaji, K. S. Rajam, and R. Asokamani, "Sliding wear behavior of plasma sprayed nanoceramic coatings for biomedical applications," *Wear*, vol. 271, no. 5, pp. 934–941, 2011.
- [39] X. Li, H. Liu, X. Niu et al., "The use of carbon nanotubes to induce osteogenic differentiation of human adipose-derived MSCs in vitro and ectopic bone formation in vivo," *Biomaterials*, vol. 33, no. 19, pp. 4818–4827, 2012.
- [40] G. B. Lan, M. Li, and Y. Zhang, "Effects of a nano-textured titanium surface on murine preosteoblasts," *Orthopedic Journal of China*, vol. 21, no. 23, 2013.
- [41] C. Yao, V. Perla, J. L. McKenzie, E. B. Slamovich, and T. J. Webster, "Anodized Ti and $\text{Ti}_6\text{Al}_4\text{V}$ possessing nanometer surface features enhances osteoblast adhesion," *Journal of Biomedical Nanotechnology*, vol. 1, no. 1, pp. 68–73, 2005.
- [42] T. Akova, Y. Ucar, A. Tukay, M. C. Balkaya, and W. A. Brantley, "Comparison of the bond strength of laser-sintered and cast base metal dental alloys to porcelain," *Dental Materials*, vol. 24, no. 10, pp. 1400–1404, 2008.
- [43] T. Miyazaki, Y. Hotta, J. Kunii, S. Kuriyama, and Y. Tamaki, "A review of dental CAD/CAM: current status and future perspectives from 20 years of experience," *Dental Materials Journal*, vol. 28, no. 1, pp. 44–56, 2009.
- [44] J. Lemons and F. Misch-Dietsh, "Biomaterials for dental implants," in *Contemporary Implant Dentistry*, C. E. Misch, Ed., pp. 511–542, Mosby, St. Louis, Mo, USA, 3rd edition, 2008.
- [45] A. Krell, T. Hutzler, and J. Klimke, "Transparent ceramics for structural applications," *CFI Ceramic Forum International*, vol. 84, no. 6, pp. E50–E56, 2007.
- [46] V. Raj and M. S. Mumjitha, "Formation and surface characterization of nanostructured $\text{Al}_2\text{O}_3\text{-TiO}_2$ coatings," *Bulletin of Materials Science*, vol. 37, no. 6, pp. 1411–1418, 2014.
- [47] C. H. Li, Y. L. Hou, Z. R. Liu, and Y. C. Ding, "Investigation into temperature field of nano-zirconia ceramics precision grinding," *International Journal of Abrasive Technology*, vol. 4, no. 1, pp. 77–89, 2011.
- [48] E. T. Thostenson, Z. Ren, and T.-W. Chou, "Advances in the science and technology of carbon nanotubes and their composites: a review," *Composites Science and Technology*, vol. 61, no. 13, pp. 1899–1912, 2001.
- [49] A. Peigney, C. Laurent, E. Flahaut, and A. Rousset, "Carbon nanotubes in novel ceramic matrix nanocomposites," *Ceramics International*, vol. 26, no. 6, pp. 677–683, 2000.
- [50] J. W. An, D. H. You, and D. S. Lim, "Tribological properties of hot-pressed alumina-CNT composites," *Wear*, vol. 255, no. 1–6, pp. 677–681, 2003.
- [51] Y. Xia, F. Zhang, H. Xie, and N. Gu, "Nanoparticle-reinforced resin-based dental composites," *Journal of Dentistry*, vol. 36, no. 6, pp. 450–455, 2008.
- [52] M. Tanoglu and Y. Ergün, "Porous nanocomposites prepared from layered clay and PMMA [poly(methyl methacrylate)]," *Composites Part A: Applied Science and Manufacturing*, vol. 38, no. 2, pp. 318–322, 2007.
- [53] O. Gurbuz, F. Unalan, and I. Dikbas, "Comparative study of the fatigue strength of five acrylic denture resins," *Journal of the Mechanical Behavior of Biomedical Materials*, vol. 3, pp. 636–639, 2010.
- [54] D. C. Jagger, A. Harrison, R. G. Jagger, and P. Milward, "The effect of the addition of poly(methyl methacrylate) fibres on some properties of high strength heat-cured acrylic resin denture base material," *Journal of Oral Rehabilitation*, vol. 30, no. 3, pp. 231–235, 2003.
- [55] L. Gendreau and Z. G. Loewy, "Epidemiology and etiology of denture stomatitis," *Journal of Prosthodontics*, vol. 20, no. 4, pp. 251–260, 2011.
- [56] M. Yamauchi, K. Yamamoto, M. Wakabayashi, and J. Kawano, "In vitro adherence of microorganisms to denture base resin with different surface texture," *Dental Materials Journal*, vol. 9, no. 1, pp. 19–24, 1990.
- [57] L. S. Acosta-Torres, L. M. Lopez-Marín, R. E. Núñez-Anita, G. Hernández-Padrón, and V. M. Castaño, "Biocompatible metal-oxide nanoparticles: nanotechnology improvement of conventional prosthetic acrylic resins," *Journal of Nanomaterials*, vol. 2011, Article ID 941561, 12 pages, 2011.
- [58] L. S. Acosta-Torres, I. Mendieta, R. E. Núñez-Anita, M. Cajero-Juárez, and V. M. Castaño, "Cytocompatible antifungal acrylic resin containing silver nanoparticles for dentures," *International Journal of Nanomedicine*, vol. 7, pp. 4777–4786, 2012.
- [59] D. R. Monteiro, L. F. Gorup, A. S. Takamiya, E. R. de Camargo, A. C. R. Filho, and D. B. Barbosa, "Silver distribution and

- release from an antimicrobial denture base resin containing silver colloidal nanoparticles,” *Journal of Prosthodontics*, vol. 21, no. 1, pp. 7–15, 2012.
- [60] M. R. Hoffmann, S. T. Martin, W. Choi, and D. W. Bahnemann, “Environmental applications of semiconductor photocatalysis,” *Chemical Reviews*, vol. 95, no. 1, pp. 69–96, 1995.
- [61] A. Fujishima, T. N. Rao, and D. A. Tryk, “Titanium dioxide photocatalysis,” *Journal of Photochemistry and Photobiology C: Photochemistry Reviews*, vol. 1, no. 1, pp. 1–21, 2000.
- [62] L. S. Acosta-Torres, L. M. Lpez-Marín, R. E. Núñez-Anita, G. Hernández-Padrón, and V. M. Castaño, “Biocompatible metal-oxide nanoparticles: nanotechnology improvement of conventional prosthetic acrylic resins,” *Journal of Nanomaterials*, vol. 2011, Article ID 941561, 8 pages, 2011.
- [63] M. Rai, A. Yadav, and A. Gade, “Silver nanoparticles as a new generation of antimicrobials,” *Biotechnology Advances*, vol. 27, no. 1, pp. 76–83, 2009.
- [64] T. V. Slenters, I. Hauser-Gerspach, A. U. Daniels, and K. M. Fromm, “Silver coordination compounds as light-stable, nanostructured and anti-bacterial coatings for dental implant and restorative materials,” *Journal of Materials Chemistry*, vol. 18, no. 44, pp. 5359–5362, 2008.
- [65] C. Damm, H. Münstedt, and A. Rösch, “Long-term antimicrobial polyamide 6/silver-nanocomposites,” *Journal of Materials Science*, vol. 42, no. 15, pp. 6067–6073, 2007.
- [66] J. J.-Y. Peng, M. G. Botelho, and J. P. Matinlinna, “Silver compounds used in dentistry for caries management: a review,” *Journal of Dentistry*, vol. 40, no. 7, pp. 531–541, 2012.
- [67] Ç. Çınar, T. Uluşu, B. Özçelik, N. Karamüftüoğlu, and H. Yücel, “Antibacterial effect of silver-zeolite containing root-canal filling material,” *Journal of Biomedical Materials Research Part B: Applied Biomaterials*, vol. 90, no. 2, pp. 592–595, 2009.
- [68] M. E. Odabaş, Ç. Çınar, G. Akça, I. Araz, T. Uluşu, and H. Yücel, “Short-term antimicrobial properties of mineral trioxide aggregate with incorporated silver-zeolite,” *Dental Traumatology*, vol. 27, no. 3, pp. 189–194, 2011.
- [69] R. Bürgers, A. Eidt, R. Frankenberger et al., “The anti-adherence activity and bactericidal effect of microparticulate silver additives in composite resin materials,” *Archives of Oral Biology*, vol. 54, no. 6, pp. 595–601, 2009.
- [70] K. Yoshida, M. Tanagawa, S. Matsumoto, T. Yamada, and M. Atsuta, “Antibacterial activity of resin composites with silver-containing materials,” *European Journal of Oral Sciences*, vol. 107, no. 4, pp. 290–296, 1999.
- [71] A. P. R. Magalhães, L. B. Santos, L. G. Lopes et al., “Nanosilver application in dental cements,” *ISRN Nanotechnology*, vol. 2012, Article ID 365438, 6 pages, 2012.
- [72] K. Yoshida, M. Tanagawa, and M. Atsuta, “Characterization and inhibitory effect of antibacterial dental resin composites incorporating silver-supported materials,” *Journal of Biomedical Materials Research*, vol. 47, no. 4, pp. 516–522, 1999.
- [73] L. Cheng, M. D. Weir, H. H. K. Xu et al., “Antibacterial amorphous calcium phosphate nanocomposites with a quaternary ammonium dimethacrylate and silver nanoparticles,” *Dental Materials*, vol. 28, no. 5, pp. 561–572, 2012.
- [74] M. A. S. Melo, L. Cheng, K. Zhang, M. D. Weir, L. K. A. Rodrigues, and H. H. K. Xu, “Novel dental adhesives containing nanoparticles of silver and amorphous calcium phosphate,” *Dental Materials*, vol. 29, no. 2, pp. 199–210, 2013.
- [75] M. S. Soh, A. U. J. Yap, and A. Sellinger, “Physicomechanical evaluation of low-shrinkage dental nanocomposites based on silsesquioxane cores,” *European Journal of Oral Sciences*, vol. 115, no. 3, pp. 230–238, 2007.
- [76] H. H. K. Xu, L. Sun, M. D. Weir et al., “Nano DCPA-whisker composites with high strength and Ca and PO₄ release,” *Journal of Dental Research*, vol. 85, no. 8, pp. 722–727, 2006.
- [77] Z. I. Xu and J. Sun, “Application of nanotechnology and nanomaterials in oral medicine,” *Dental Materials and Devices*, vol. 18, no. 4, pp. 186–191, 2009.
- [78] F.-X. Huber, O. Belyaev, J. Hillmeier et al., “First histological observations on the incorporation of a novel nanocrystalline hydroxyapatite paste OSTIM in human cancellous bone,” *BMC Musculoskeletal Disorders*, vol. 7, article 50, 5 pages, 2006.
- [79] S. J. Kalita, A. Bhardwaj, and H. A. Bhatt, “Nanocrystalline calcium phosphate ceramics in biomedical engineering,” *Materials Science and Engineering C*, vol. 27, no. 3, pp. 441–449, 2007.
- [80] M. Hannig, L. Kriener, W. Hoth-Hannig, C. Becker-Willinger, and H. Schmidt, “Influence of nanocomposite surface coating on biofilm formation in situ,” *Journal of Nanoscience and Nanotechnology*, vol. 7, no. 12, pp. 4642–4648, 2007.
- [81] K. J. Cross, N. L. Huq, and E. C. Reynolds, “Casein phosphopeptides in oral health—chemistry and clinical applications,” *Current Pharmaceutical Design*, vol. 13, no. 8, pp. 793–800, 2007.
- [82] R. K. Rose, “Binding characteristics of streptococcus mutans for calcium and casein phosphopeptide,” *Caries Research*, vol. 34, no. 5, pp. 427–431, 2000.
- [83] C. Rahiotis, G. Vougiouklakis, and G. Eliades, “Characterization of oral films formed in the presence of a CPP-ACP agent: an in situ study,” *Journal of Dentistry*, vol. 36, no. 4, pp. 272–280, 2008.
- [84] E. C. Reynolds, F. Cai, P. Shen, and G. D. Walker, “Retention in plaque and remineralization of enamel lesions by various forms of calcium in a mouthrinse or sugar-free chewing gum,” *Journal of Dental Research*, vol. 82, no. 3, pp. 206–211, 2003.